Plasma Physics

Edited by
B. KADOMTSEV, Mem. USSR Acad. Sc.

Advances
in
Science
and
Technology
in
the USSR

Physics Series

MIR Publishers
Moscow

Mir Publishers Moscow

Advances
in
Science
and
Technology
in
the USSR

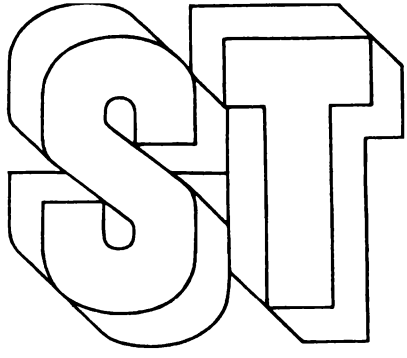

Physics Series

Plasma Physics

Edited by
B. B. KADOMTSEV,
Mem. USSR Acad. Sc.

Translated from the Russian by
Oleg Glebov

MIR Publishers
Moscow

Физика плазмы
Под редакцией акад.
Б. Б. Кадомцева
Издательство «Мир»
Москва

First published 1981

На английском языке

Printed in the Union of Soviet Socialist Republics

Contents

Preface

This book consists of the review papers written by the specialists in high-temperature plasma physics working in the Kurchatov Atomic Energy Institute. These papers are mainly related to or stimulated by the studies of controlled thermonuclear synthesis. But, as always, the ideas and concepts developed in the field prove to be of a wider, more general, interest for the theory.

In the last ten years plasma confinement in the tokamak systems has been extensively studied. A kilovolt plasma temperature has been obtained in tokamaks with the plasma density about 10^{20} m^{-3} and a sufficiently good confinement time (up to 100 μs). Extrapolation of the obtained regularities indicates a definite feasibility of the thermonuclear reactor based on tokamak. The focus of the relevant studies is increasingly shifted from the plasma physics proper to the engineering and technological problems of the reactor design. This does not mean that everything is now known about the physics of plasma in tokamaks. The problem of optimization of discharge in the reactor tokamak necessitates simulation of plasma processes which should be more accurate than under the experimental conditions. A primary problem is controlling of the stability and equilibrium of the tokamak plasma.

Variation of the parameters of the equilibrium configuration (plasma pressure, current distribution, and external magnetic fields) results in variation of the shape of the cross section of the magnetic surfaces, which can lead to breakdown of thermal insulation. To predict such variation and control the plasma shape we have to perform numerical simulation of the equilibrium evolution process. The paper by Zakharov and Shafranov discusses a solution of this problem under the conditions of two-dimensional distribution of the configuration parameters.

The paper by Pogutse and Yurchenko deals with some problems of the linear theory of hydromagnetic plasma stability, which were not quite clear until recently and which are of a certain interest both theoretically and experimentally. The discussion is focussed on two most important hydromagnetic instabilities, namely, the kink instability and the flute instability (the ballooning modes).

The theory of kink instability was developed primarily for the cylindrical plasma column as the toroidal effects were assumed to be inessential for it. The authors have shown for the first time that the inclusion of toroidality results in a splitting of the spectrum of oscillations of the plasma column, similar to the splitting of the electronic spectrum in crystals. This effect leads to closing of the stability "gaps" in which the modern tokamaks operate. The magnitude of splitting is proportional to the plasma pressure and the curvature of the torus so that the stability in tokamak deteriorates with increasing pressure (the ballooning effect).

The above picture is typical of the lowest (large-scale) oscillation modes. The role of the current decreases with the mode number and the instability acquires a purely ballooning-type form when the source of generation of the oscillations is

the thermal energy of the plasma. In the recent years there has been a considerable advance in our understanding of the mechanism of development of the flute oscillations of plasma in the torus (the bollooning modes). For instance, it has been found that these oscillations are less stable than the perturbations that are constant along the field lines, which were studied earlier. The authors are the first to derive the analytical criterion of stability for the ballooning modes and to identify the physical mechanisms responsible for the higher instability of the plasma in torus. They used this criterion to calculate the thresholds for the plasma pressure in the tokamaks with the circular and D-shaped cross section of the plasma column.

The paper also discussed the effect of dissipation on the kink and ballooning modes. The authors show that the peripheral plasma even of a relatively low conductivity has a stabilizing effect on the large-scale kink perturbations. When dissipation is taken into account, the ballooning oscillations are found to develop from the zero pressure gradient, that is, to have no threshold. Though the growth rate of these oscillations is considerably lower then the ideal growth rate, it can be suggested that their existence is a fairly universal property of the toroidal plasma and they may be responsible for the so-called Alcator scaling.

The relationship of the kink instability with the current disruptions in the discharge observed under certain conditions is discussed in the paper by Zakharov. In his unconventional approach to the analysis of the kink instabilities he considers the balance of the forces determining the geometry of the configuration with the helical symmetry. This makes it possible to identify explicitly the cause of the kink instabilities related to the interaction between the plasma current and the longitudinal field, which under certain conditions results in increasing deformation of the plasma column. The approach based on the theory of kink instability makes it possible to obtain a new necessary criterion of stability of the kink modes, to describe the nonlinear dynamics of the kink instabilities and to evaluate the consequences of their development. In particular, the theory gives a sufficiently good explanation of the experimentally observed features of the disruptive instability in tokamaks, such as the existence of large-scale and small-scale disruptions, the order of appearance of modes with different spatial structures, and the increase in the total plasma current during disruption.

The paper by Petviashvili deals with a new rapidly developing field of the theory of nonlinear oscillations— the theory of solitary waves (solitons). It has been shown in recent years that depending on the relation between the signs of the dispersive and nonlinear terms in the wave equation either there can occur synchronization of the waves producing separate wave packets, that is, solitons, or the individual waves remain independent of each other and we are dealing with the wave turbulence. Thus, solitons are a fairly common phenomenon (they are close to such effects as self-focussing and collapse). The study of nonlinear waves in plasma can be especially gratifying since a large number of oscillation branches exist in plasma.

The theory of one-dimensional solitons is sufficiently well developed. In his paper Petviashvili analyzes a much more complicated and interesting problem of

existence and stability of two- and three-dimensional solitons. He is the first to obtain solutions for a wide class of non-one-dimensional nonlinear wave equations using both the numerical methods and the analytical methods. Petviashvili has analyzed the non-one-dimensional forms of the Korteweg-de Vries equation and the equation for the Langmuir oscillations, the Langmuir solitons in the magnetic field and the solitons (vortexes) in non-one-dimensional plasma which are nonlinear solutions for the drift waves. He has used his results to explain the high-intensity scattering of electromagnetic waves from the ionosphere and the radiation of the plasma in a stellator.

The paper "Observation of the Langmuir Solitons" by Nezlin reviews the Soviet experimental studies of the Langmuir solitons formed from the large-amplitude plasma waves. These studies differ essentially in their approach from the experiments conducted by foreign (American and Japanese) scientists. The main differences are due to the fact that the Langmuir solitons are studied for the first time in the following new conditions: a) in a strong magnetic field, b) in a collisionless plasma, c) under the free-path conditions (which makes it possible to observe solitons in the absence of external wave pumping), d) in a plasma confined perpendicularly to the magnetic field. The pumping of the Langmuir waves is carried out with the external high-frequency fields and electron beams.

These experiments have yielded the following main results. Solitons have been shown to be produced owing to the modulational instability of the large-amplitude Langmuir waves. This is the same instability which, for instance, determines the nonuniform spatial distribution of the wave energy over the sea surface or separation of a laser beam in a dispersive medium into a series of travelling "focuses", that is, solitons. The principal parameters of solitons have been studied. The soliton size proves to be the smaller the higher is the wave energy density (that is, the deeper is the plasma density "well"). The minimum observed size of solitons is 5 to 6 Debye radiuses and, apparently, corresponds to the boundary of strong absorption by the plasma particles (the Landau damping). The Langmuir solitons are shown to be sufficiently stable despite the fact that the plasma is radially limited and nonuniform, they propagate without spreading and exist for not less than tens of thousands of the Langmuir periods in the absence of external pumping. The mean free path of solitons is about 10^2 cm (about 3×10^3 Debye radiuses). The experimentally observed soliton properties on the whole are in good agreement with the theoretical predictions.

These experimental results indicate that solitons are a characteristic state of strong Langmuir turbulence. They have a general physical interest and can be used in the studies of plasma heating with waves and beams of charged particles.

The paper by Timofeev et al. deals with the measurement of the electron temperature in the open-ended traps. The paper reviews the results and analyzes the diagnostic techniques based on the measurement of the absorption coefficient for the probe beam of electromagnetic waves with the frequency close to the cyclotron frequency (or its harmonics). The resonance interaction between such oscillations is entirely due to the effects of thermal motion, and the absorption coefficient is a sharply varying function of the electron temperature. This technique makes possible in many cases to measure temperature on a smaller spatial

scale than other techniques. In particular, the electron temperature in the Ogra-3B trap was measured with this technique. The measurement of the absorption coefficient makes it possible simultaneously to find the spatial distribution of the plasma density. The paper presents the derivation and detailed analysis of the expressions for the absorption coefficients for the electromagnetic wave near the cyclotron frequency harmonics, discusses various modification of the technique and gives some results of its application in experiments.

B. B. Kadomtsev

February, 1981

1. Evolution of Equilibrium of Toroidal Plasma

L. E. Zakharov, *Cand. Sc. (Phys. and Math.)*, **and**
V. D. Shafranov, *D. Sc. (Phys. and Math.)*

1.1 General Statement of the Problem

Alongside with the conventional tokamaks with circular cross section and constant major radius of the plasma torus, a well-established modern system is the tokamak with complex geometry of magnetic configuration that varies with time. This class of systems includes tokamaks with adiabatic compression, "Doublet" tokamak, finger-ring tokamaks, tokamaks with divertors and expanding magnetic diaphragm which programs the current density profile at the initial stage of discharge, as well as tokamaks with high heating power and, respectively, extremely high pressure.

In connection with development of the reactor tokamaks it is interesting to study some new possibilities for manipulating the toroidal plasma, such as mixing of several plasma columns into one for rapid plasma heating, exhaust of the plasma column from the working chamber into the evacuation chamber, and stripping of the external magnetic surfaces with the confining field varying with time. Especially many problems of this type are encountered in the reactor tokamaks operating in the cyclic regime.

The primary problem for the system of these types is that of two-dimensional evolution of the equlibrium of the toroidal plasma column, and this paper deals with its statement and methods of solution. In contrast to the problems in simulation of the transport processes, which are solved with the use of one-dimensional codes, the main question here is the evolution of the geometry of plasma configuration.

In the simplest case of tokamak with a circular cross section, large aspect ratio R/b (where R is the major radius and b is the minor radius of the plasma) and intermediate pressure $\beta = 8\pi\langle p\rangle/B_s^2 \sim b^2/R^2q_b^2$ (where $\langle p\rangle$ is the mean pressure, B_s is the longitudinal magnetic field, and q_b is the stability safety factor at the plasma boundary) the variation of the geometry amounts only to a small ($\sim b\beta q_b^2 R/b$) displacement of the centres of the cross sections of the magnetic surfaces while their circular shape remains unchanged (see Fig. 1.1*a*). For high plasma pressure $\beta \sim b/Rq_b^2$ the variation of the shape of the magnetic surface is comparatively small but their displacements ($\sim b/2$) are large (Fig. 1.1*b*), and for very high pressure $\beta \sim 1/q_b^2$ the shape of the cross section of the magnetic surfaces is changed significantly (Fig. 1.1*c*). The external fields needed to maintain the equilibrium must vary accordingly.

The variation of the equilibrium during discharge is especially large in the toroidal systems with noncircular, for instance, elongated, plasma cross section

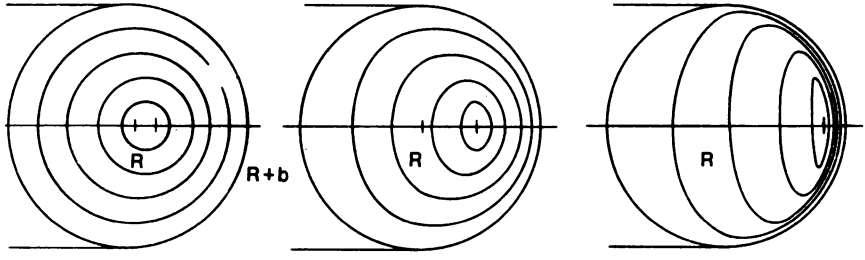

Fig. 1.1. Deformations of the cross sections of magnetic surfaces in the shell with the circular cross section owing to increasing plasma pressure. (*a*) $\beta \equiv 8\pi\, p\, /B_s^2 \sim b^2/R^2 q_b^2$, $\beta_J \equiv 2c^2 \int pdS/J^2 \sim 1$; (*b*) $\beta \sim b/Rq_b^2, \beta_J \sim R/b$; (*c*) $\beta \sim 1/q_b^2$.

(see Fig. 1.2), such as the Doublet, finger-ring and belt-pinch devices and those with a poloidal divertor. Since plasma quality is very sensitive to the contacts with the constructional components of the device, it is, clearly, very important to develop precise techniques for calculating the plasma shape and controlling it in such systems, particularly, for parameters close to the thermonuclear conditions.

In principle, we can trace the variation of the plasma torus with time using the motion equations, that is, the MHD equations including inertia terms. However, in these calculations on the short-time scale, of the order of the transit time, there can appear oscillations (Alfven, sound) constituting a "noise" which is inessential on the longer time scale we are interested in but which greatly complicates that calculations. Introduction of artificially strong dissipation [1.1] in this calculation scheme did not yield successful results. On a time scale longer than the fast or inertial scale it is natural to regard the plasma as a quasistatic system satisfying the equilibrium equations at any moment (that is, we can ignore the inertia terms):

$$\nabla p = \frac{1}{c}[\mathbf{j} \times \mathbf{B}] \tag{1.1}$$

$$\text{curl}\, \mathbf{B} = \frac{4\pi}{c}\mathbf{j} \tag{1.2}$$

$$\text{div}\, \mathbf{B} = 0 \tag{1.3}$$

To describe the evolution of the equilibrium we must add to this system the equations describing variations of the current and the pressure of the plasma. Apart from the Maxwell equation for the electric field **E**

$$\text{curl}\, \mathbf{E} = -\frac{1}{c}\frac{\partial \mathbf{B}}{\partial t} \tag{1.4}$$

we can take the balance equations for the energy and the number of particles (to

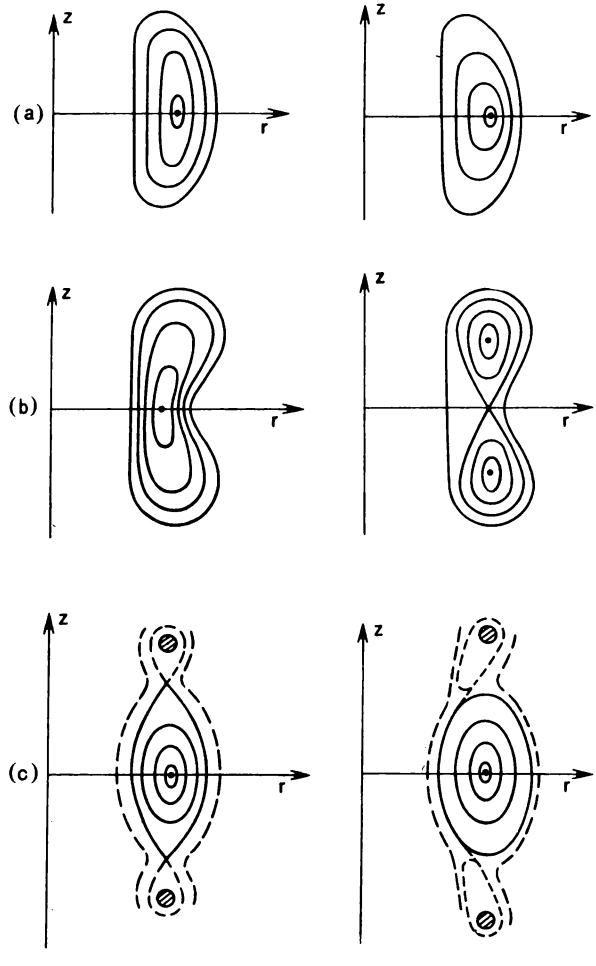

Fig. 1.2. Evolution of configurations with noncircular cross sections. (*a*) The decrease in elongation of the cross sections of the magnetic surfaces in the D-shaped shell with contraction of the current. (*b*) Formation of a split configuration with three axes in the "doublet"-shaped shell with contraction of the current. (*c*) Variation of the shape of the magnetic surfaces of the plasma configuration with the poloidal divertor with a sharp increase in the pressure; the displacement along the major radius is assumed to be compensated by the increase in the transverse magnetic field.

determine the pressure) and the generalized Ohm's law in the form of the motion equation for the electron fluid

$$\mathbf{E} + \frac{1}{c}[\mathbf{v}_e \times \mathbf{B}] = \frac{\mathbf{j}_\parallel}{\sigma_\parallel} + \frac{\mathbf{j}_\perp}{\sigma_\perp} + \frac{\mathbf{R} - \operatorname{div} \overleftrightarrow{\pi}}{en} \tag{1.5}$$

Here $\mathbf{R}$ is the drag force with the exception of the explicit terms $\mathbf{j}_\parallel/\sigma_\parallel$ and $\mathbf{j}_\perp/\sigma_\perp$, and $\overleftrightarrow{\pi}$ is the tensor of the electron momentum flux. In the hydrodynamic limit tensor $\overleftrightarrow{\pi}$ is isotropic and $\operatorname{div} \overleftrightarrow{\pi} = \nabla p_e$. If the collision frequency is low, the difference $\operatorname{div} \overleftrightarrow{\pi} - \mathbf{R} - \nabla p_e$ gives rise to "neoclassical" effects.

Thus, the system of equations (1.1)–(1.5) with the addition of the equations of energy and particle balance, in principle, fully describes the evolution of the equilibrium plasma configuration (if the right-hand side in Eq. (1.5) is written in terms of the plasma parameters) so that it can be calculated on the time scale related to the transport processes, rather than inertial oscillations in the plasma. Though such calculations can lead to configurations which are, in reality, unstable, the use of a longer time scale provides for essential simplification of the problem. The analysis of stability of equilibrium configurations can be regarded as an independent problem to be optimized separately.

However, we encounter two difficulties here. One is a technical difficulty related to the two-dimensional character of the problem. It can be overcome by selecting the optimal approach to the development of numerical codes for evolution calculations. The other difficulty has a fundamental character. As it has been shown by many years of experimental work on the controlled thermonuclear fusion, the coefficients of particle and energy transport in the high-temperature plasma are, typically, anomalous so that in fact we have no reliable two-dimensional transport equations for calculating the density, temperature and pressure of the plasma. But cumbersome calculations based on unreal classical and neoclassical transport concepts seem to be unreasonable. This difficulty has greatly inhibited the development of methods for calculating the evolution of the equilibrium including the dissipative processes.

The importance of development of methods for calculating the evolution of the equilibrium was repeatedly emphasized by Grad [1.2–4] and Taylor [1.5]. Connor [1.6] developed Taylor's theoretical concepts concerning the methods for solving the "neoclassical" evolution problems. For the dissipation-free processes (tokamak with frozen-in fluxes) the Oak Ridge group [1.7] solved the technical problem of realizing the process of determination of the two-dimensional evolution. The problem of adiabatic (dissipation-free) evolution of the equilibrium with the varying topology of magnetic surfaces (splitting and merging of magnetic surfaces) was formulated and partially solved in [1.3, 1.4]. At present there have been developed numerical codes in which the problem of evolution of the two-dimensional configuration is an integral part of the programme for simulating transport processes in tokamaks [1.8].

In paper [1.9] and in preprint [1.10] which serves as a basis for the present paper the problem of evolution of equilibrium was treated independently of the transport processes. This made it possible to identify the contribution of this problem to the general simulation of the processes in tokamaks and largely eliminated the above-mentioned difficulty.

It has been shown there that, despite the apparent dependence of the magnetic field on the velocity of the diffusion of the plasma according to the equation of the type of

$$\frac{\partial \mathbf{B}}{\partial t} = \operatorname{curl}[\mathbf{v} \times \mathbf{B}] - \operatorname{curl}\left(\frac{c^2}{4\pi\sigma} \times \operatorname{curl} \mathbf{B}\right) \quad (1.6)$$

which follows from eqs. (1.4) and (1.5), in reality, the field diffusion and the plasma diffusion are, in a sense, unrelated. Let us now analyze the use of the Ohm's law in the evolution problems according to the ideas of [1.9, 1.10].

Take the projections of the vector equation (1.5) on the normal to the magnetic surface, on the vector **B** and on the perpendicular to them.

1. The projection on the normal to the magnetic surface

$$\mathbf{E} \cdot \nabla p + \frac{\mathbf{v}}{c} \cdot [\mathbf{B} \times \nabla p] = \frac{1}{en}(\mathbf{R} - \operatorname{div} \overline{\pi}) \cdot \nabla p \quad (1.7)$$

relates the "radial" electric field of the plasma column $\mathbf{E} \cdot \nabla p / |\nabla p|$ to the rotation speed. These quantities do not enter into the equilibrium equation and, hence, this projection is not needed for solving the evolution problem.

2. The projection on the magnetic surface perpendicular to the vector **B**

$$|\mathbf{B}|^2 \mathbf{v} \cdot \nabla p = [\mathbf{E} \times \mathbf{B}] \cdot \nabla p + \frac{1}{en}[(\operatorname{div} \overline{\pi} - \mathbf{R}) \times \mathbf{B}] \cdot \nabla p \quad (1.8)$$

serves, in principle, for determination of the "radial" plasma velocity $\mathbf{v} \cdot \nabla p / |\nabla p|$. In its turn, this diffusion velocity enters into the transport equations for particles and heat. But in fact, heat transport is anomalous and there are reasons to believe that particle's diffusion is also anomalous. Therefore, the pressure and temperature are calculated from various models with adjustable parameters. Thus, at present we have no adequate expressions for the quantities on the right-hand side of eq. (1.8), and it can be largely regarded as being symbolic.

Hence, the vector equation (1.5) yields only one equation for describing the evolution of the magnetic configuration:

3. The projection of the generalized Ohm's law on the magnetic field is

$$\mathbf{E} \cdot \mathbf{B} = \frac{\mathbf{j} \cdot \mathbf{B}}{\sigma_\parallel} + \frac{\mathbf{R} - \operatorname{div} \overline{\pi}}{en} \cdot \mathbf{B} \quad (1.9)$$

In the collisional hydrodynamic limit the last term in eq. (1.9) vanishes, $(\mathbf{R} - \operatorname{div} \overline{\pi}) \cdot \mathbf{B} = 0$. Fortunately, the experimental results on the plasma conductivity largely confirm this theoretical prediction for the available plasma parameters. Therefore, we can employ (within certain limits) the "classical" expression

$$\mathbf{E} \cdot \mathbf{B} = \mathbf{j} \cdot \mathbf{B}/\sigma_\parallel \quad (1.10)$$

as the longitudinal projection of the Ohm's law.

Equation (1.10), taken together with the equilibrium equations (1.1)–(1.3), is sufficient for describing evolution of the magnetic configuration under the

assumption that we know the time dependences of the pressure p and the longitudinal conductivity $\sigma_\parallel$. Since we lack an adequate transport model, it is reasonable to assume that these p and $\sigma_\parallel$ are given. We shall refer to the approach based on eqs. (1.1)–(1.3) and (1.10) as the "method of given pressure".

The method of given pressure allows us to divide the entire problem of describing the plasma evolution into two more specific problems, namely, (i) evolution of the equilibrium, and (ii) simulation of the transport processes. The first problem deals with the geometry and the conditions of the equilibrium of the plasma configuration and to solve it we must know only the functions $p(t)$ and $\sigma_\parallel(t)$. Other parameters can be needed only if the longitudinal Ohm's law differs from eq. (1.10). In the second problem we employ the results of solution of the first problems as the coefficients in the equations for the fluxes of heat and particles. Even if the last term in the Ohm's law (1.9) makes a significant contributions so that these two problems are combined, the identification of the equilibrium evolution is a methodologically useful approach for the development of solution algorithms. This gives rise to individual units (packets) in the code which can be independently debugged.

It should be stressed once more that, though this approach employs the "classical" expression for the longitudinal projection of Ohm's law, eq. (1.10), it is, by no means, dependent on its classical formulation

$$\mathbf{E} + \frac{1}{c}[\mathbf{v} \times \mathbf{B}] = \frac{\mathbf{j}}{\sigma_\parallel} \tag{1.11}$$

which yields a comparatively low diffusion speed of the plasma. If diffusion does not correspond to the simple Ohm's law (1.11) but if the longitudinal projection (1.10) is valid, the Ohm's law can be expressed phenomenologically as

$$\mathbf{E} + \frac{1}{c}[(\mathbf{v} - \mathbf{v}^*) \times \mathbf{B}] = \frac{\mathbf{j}}{\sigma_\parallel} \tag{1.12}$$

where $\mathbf{v}^*$ is the anomalous diffusion velocity. In the simplest cylindrical case one of the two components of this equation ($v = v_\varrho$)

$$E_\theta - \frac{1}{c}(v - v^*) B_s = j_\theta/\sigma_\parallel \tag{1.13}$$

$$E_s + \frac{1}{c}(v - v^*) B_\theta = j_s/\sigma_\parallel \tag{1.14}$$

for instance, the first one can be used for determining the speed of the plasma motion

$$v = c\frac{E_\theta}{B_s} - \frac{cj_\theta}{\sigma_\parallel B_s} + v^* \tag{1.15}$$

Here we denote the cylindrical coordinates by ϱ, θ and s.

After we have eliminated the speed from eq. (1.14), we have only eq. (1.10) left. As it will be shown below, eq. (1.10) describes the mutual diffusion of the

poloidal and longitudinal magnetic fields, which always proceeds with the skin time $\tau_{sk} = \pi\sigma b^2/c^2$ (where b is the minor radius) irrespective of the anomalous diffusion speed v^*. Here we can even assume that, for instance, the plasma is ideally conducting, $\sigma_\parallel = \infty$ ($\mathbf{E} \cdot \mathbf{B} = 0$, mutually frozen fluxes), irrespective of the value of v^*.

If the term $\sim(\mathbf{R} - \operatorname{div}\overline{\pi})$ is significant in the Ohm's law (1.5) and, in particular, in eq. (1.9) for its longitudinal component, then we encounter some qualitative peculiarities in the evolution problem. For instance, in the axially symmetric systems ($\partial/\partial s = 0$, s is taken along the major axis of the torus) we can sometimes assume that $(\mathbf{R} - \operatorname{div}\overline{\pi})_s = 0$ but, at the same time, the poloidal component of this term (along the minor axis of the torus) differs from zero. Then the right-hand side of eq. (1.13) acquires the additional term $(\mathbf{R} - \operatorname{div}\overline{\pi})_\theta/en$ which is not related to the current density j_θ. Introducing a convection velocity v_c, we can write it as $(1/c)v_cB_s$ [1.11]. Then eqs. (1.13) and (1.14) can be written as the following system:

$$E_\theta - \frac{1}{c}(v_c + v - v^*)B_s = j_\theta/\sigma_\parallel \tag{1.13*}$$

$$E_s + \frac{1}{c}(v - v^*)B_\theta = j_s/\sigma_\parallel \tag{1.14*}$$

The difference between the speeds determining the convention of the magnetic fields relative to the plasma in eqs. (1.13) and (1.14), as noted in [1.12], results in convective transfer of the poloidal magnetic flux with respect to the longitudinal flux. In this paper with its emphasis on the methodology of solution of the evolution problems we shall neglect the effects of mutual convection of the magnetic fields for the sake of simplicity and assume $v_c = 0$.

Thus, the solution of the entire problem of evolution of the toroidal plasma column is divided into two stages:

1) The solution of the two-dimensional system of equations (1.1)–(1.3), (1.9) and (1.10) with the given p and $\sigma_\parallel$.

2) A more or less standard calculation of the density and temperature of the plasma using the heat and particle transport equations and various models for finding p and $\sigma_\parallel$.

Owing to the lack of reliable transport equations in the first stage of the study of evolution of the magnetic configuration the natural approach is to take reasonable distributions of p and $\sigma_\parallel$ on the magnetic surfaces and to focus attention at solving the first problem. Then it will not be difficult to add equations for calculating n and T and, respectively, p and $\sigma_\parallel$.

1.2. Evolution Equations

To explain the statement of the problem in our method of given pressure let us apply eq. (1.10) to the current-carrying plasma with cylindrical geometry in the longitudinal magnetic field. The case of strong and almost constant longitudinal

fields $B_z \gg B_\theta$ with $\partial B_z/\partial t$ is trivial. In this case eq. (1.10) yields

$$j_z = \sigma_\parallel E_z \tag{1.16}$$

and we come just to the problem of skin effect for the poloidal component B_θ in a medium with the given $\sigma_\parallel(\varrho, t)$ profile:

$$\frac{\partial B_\theta}{\partial t} = \frac{\partial}{\partial \varrho}\frac{c^2}{4\pi\sigma_\parallel}\frac{1}{\varrho}\frac{\partial}{\partial \varrho}(\varrho B_\theta) \tag{1.17}$$

The longitudinal magnetic field acts as though a framework of the system, adjusting owing to small changes $\partial B_z/\partial \varrho = -\frac{4\pi}{c} j_\theta$ to the equilibrium equation

$$\frac{\partial p}{\partial \varrho} = \frac{1}{c}(j_\theta B_z - j_z B_\theta) \tag{1.18}$$

so that this equation does not affect the evolution of B_θ. The situation is quite different if $B_z \lesssim B_\theta$ (stabilized pinch) or the variation of B_z is large (for instance, with adiabatic compression of the plasma in tokamak). In this case the poloidal projection j_θ of the current can also make a significant contribution to $\mathbf{j} \cdot \mathbf{B}$. Obtaining from the equilibrium equation (1.18)

$$j_\theta = j_z\frac{B_\theta}{B_z} + \frac{c}{B_z}\frac{\partial p}{\partial \varrho} \tag{1.19}$$

and eliminating it from eq. (1.10), we have

$$E_z B_z + E_\theta B_\theta = \frac{B^2}{\sigma_\parallel B_z^2}\left(j_z + c\frac{B_\theta}{B_z^2}\frac{\partial p}{\partial \varrho}\right) \tag{1.20}$$

Let us introduce the "toroidal" (longitudinal) flux Φ and the external "poloidal" flux Ψ by

$$B_\theta = -\frac{\partial \Psi}{\partial \varrho}, \qquad B_z = \frac{1}{2\pi\varrho}\frac{\partial \Phi}{\partial \varrho} \tag{1.21}$$

$$E_z = -\frac{1}{c}\frac{\partial \Psi}{\partial t}, \qquad E_\theta = -\frac{1}{2\pi\varrho c}\frac{\partial \Phi}{\partial t} \tag{1.22}$$

Then the system of equilibrium equations (1.1)–(1.3) and the Ohm's law (1.10) can be written as

$$\frac{\partial \Psi}{\partial t} + \frac{B_\theta}{2\pi\varrho B_z}\frac{\partial \Phi}{\partial t} = \frac{c^2}{4\pi\sigma_\parallel}\frac{B^2}{B_z^2}\frac{1}{\varrho}\frac{\partial}{\partial \varrho}\varrho\frac{\partial \Psi}{\partial \varrho} - \frac{c^2}{\sigma_\parallel}\frac{B_\theta}{B_z^2}\frac{\partial p}{\partial \varrho} \tag{1.23}$$

$$\frac{B_\theta}{\varrho}\frac{\partial}{\partial \varrho}\varrho B_\theta + B_z\frac{\partial B_z}{\partial \varrho} = -4\pi\frac{\partial p}{\partial \varrho} \tag{1.24}$$

when $B_z \gg B_\theta$, even if the variation of the longitudinal field with time is great its

gradient remains close to zero, according to the equilibrium equation (1.24), for low plasma pressure $8\pi p \ll B_z^2$ (owing to high heat conductivity or strong cooling by radiation, high diffusion of particles, etc.). Then eq. (1.23) has the form of the equation of diffusion with convection:

$$\frac{\partial \Psi}{\partial t} - \frac{\varrho}{2}\frac{\dot{B}_z}{B_z}\frac{\partial \Psi}{\partial \varrho} = \frac{c^2}{4\pi\sigma_1}\frac{1}{\varrho}\frac{\partial}{\partial \varrho}\varrho\frac{\partial \Psi}{\partial \varrho} \quad (\dot{B}_z \equiv \partial B_z/\partial t) \tag{1.25}$$

Here the rate v_{con} of convection of the poloidal flux Ψ is determined by the rate of variation of the longitudinal magnetic field as if it were in the motion of the plasma with frozen toroidal flux:

$$v_{\text{con}} = -\frac{\varrho}{2}\frac{\dot{B}_z}{B_z} \tag{1.26}$$

in fact, $v_{\text{con}} = v - v^*$ (see eq. (1.12)) has nothing in common with the plasma speed v which can even have the opposite direction (that is, diffusion can overcome the pinching of the plasma by the compressing magnetic flux, $| v^* | > v_{\text{con}}$).

Below, as an illustration, we shall solve eqs. (1.23) and (1.24) for the cylinder.

Let us now modify the system of equations (1.23) and (1.24) describing the evolution with time for the two-dimensional case.

In the case of cylindrical symmetry the magnetic surfaces automatically coincide with the coordinate surfaces ϱ = const, significantly facilitating the solution of the problem. In the case of toroidal geometry the current lines $\mathbf{j}$ and the constant-pressure levels $\mathbf{p(r, t)}$ = const lie on the magnetic surfaces which are, typically, taken as the coordinate surfaces [1.13–15]. We shall assign to each of them a scalar parameter a which monotonically increases with increasing distance from the magnetic axis. In principle, the "radial" coordinate a in such a coordinate system may be any "surface quantity", for instance, the volume V bounded by the magnetic surface. We can also identify a with one of the magnetic fluxes of the magnetic field which are to be determined providing thus for the "reversal" of variables so that the normal coordinates r and z are to be found.

Our formulation of the evolution problems does not depend on the choice of the surface function a but this choice is important for the solution of specific problems. We believe that the treatment here should be based on the minimization of convection across the surfaces $a(t)$ = const. From this viewpoint it is definitely a suboptimal approach to use, as it is frequently done, as the radial coordinate the poloidal flux Ψ which is the main varying function of time in the process of evolution. A more convenient approach, both physically and computationally, is to relate the radial coordinate a either to the flux Φ of the longitudinal field, or to the normalized volume V/V_0, or cross-sectional area S/S_0 of the magnetic surfaces (here V_0 and S_0 are the volume and the cross-sectional area of the boundary magnetic surface). It is convenient here to identify a with the effective minor radius which is related to the above quantities and tends to ϱ in the limit of the straight plasma column with the circular cross section. Then all the equations will have a quasicylindrical form and can be easily made

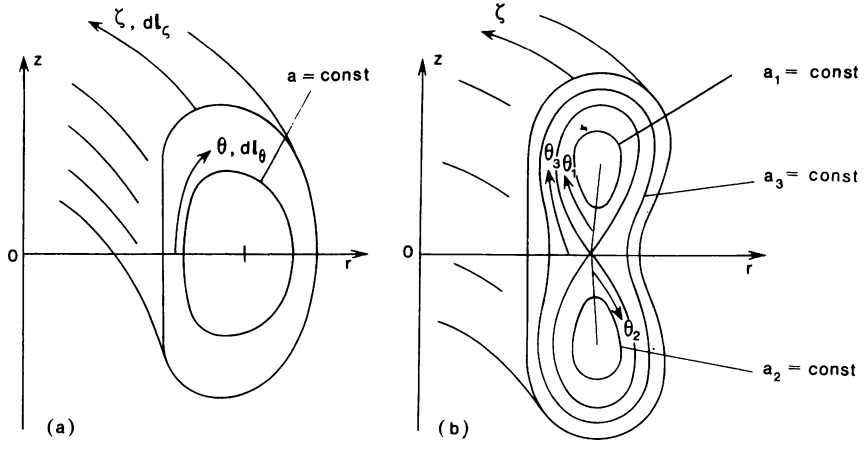

Fig. 1.3. The use of the magnetic surfaces as natural coordinates for simply connected configuration (*a*) and for the triaxial configuration (*b*); (a_1, θ_1, ζ), (a_2, θ_2, ζ)—the coordinates in the region of separated poloidal fluxes, (a_3, θ_3, ζ)—the coordinates in the common flux region.

consistent with the conventional quasicylindrical formulation of the transport processes.

Apart from a, two cyclic coordinates θ and ζ are used; they vary from 0 to 2π along the minor and major circuits of the torus respectively (see Fig. 1.3). Of course, this coordinate system is applicable whithin the simply connected system of the magnetic surfaces, that is, only up to the separatrix. In the presence of an island structure (multiply connected configurations) we must take into account the conditions for matching the solutions for the constituent simply connected regions.

In the theory of equilibrium of the toroidal plasma the electric currents and the magnetic fields are described by integral characteristics, namely, the currents and magnetic fluxes across two independent contours on a given magnetic surface. The longitudinal (toroidal) current $J(a)$ flux Φ (a) are related to the contour encircling the magnetic axis. When $a \to 0$, the contour is contracted to a point and hence $J(0) = \Phi(0) = 0$. The poloidal current and flux are related to the contour encircling the major axis of the torus. It should be noted that they can be taken either from the major axis of the torus or from the magnetic axis. In different papers an equilibrium and stability these parameters are defined and designated in different ways, which results sometimes in confusion. In our opinion, it is reasonable to denote the poloidal current and the flux across the hole of the torus by F and Ψ (see Fig. 1.4). At the major axis F and Ψ are zero. The parameters reckoned from the magnitic axis will be denoted by $I(a)$ and $\varkappa(a)$; $I(0) = 0$, $\varkappa(0) = 0$. The relationship between them is given by

$$F(a, t) = F_0(t) - I(a, t),$$
$$\Psi(a, t) = \Psi_0(t) - \varkappa(a, t) \qquad (1.27)$$

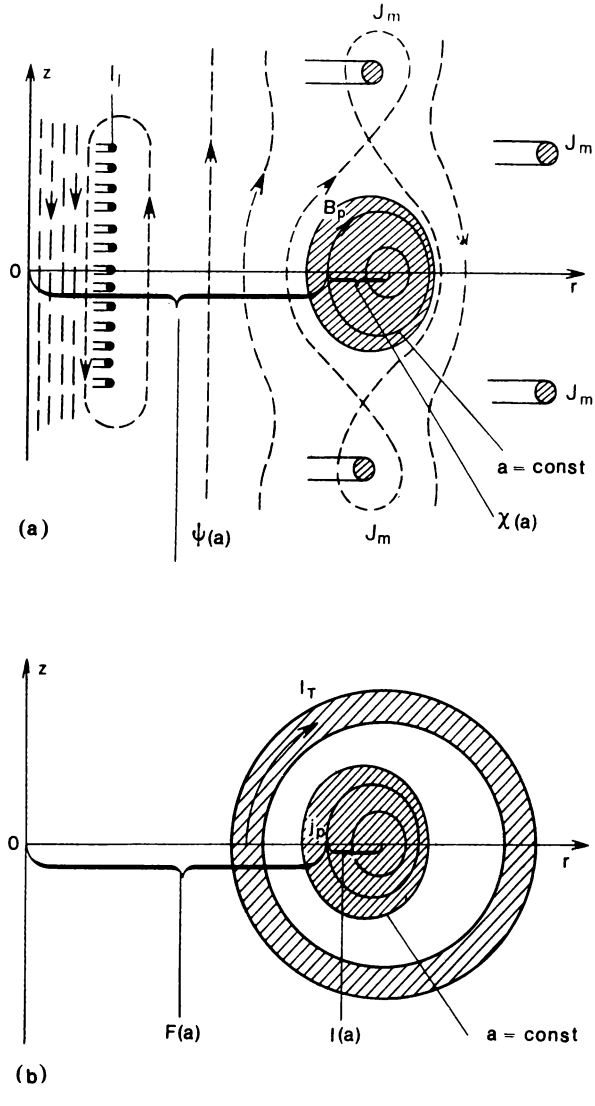

Fig. 1.4. Convention for the poloidal fluxes $\psi(a)$, $\chi(a)$ and the poloidal currents $F(a)$, $I(a)$ in the equilibrium configuration. (*a*) $\psi(a)$ is the flux between the symmetry axis and the magnetic surfaces including the flux of the inductor with the current I_I, the external part of the flux of the plasma and the equilibrium windings with the currents J_m; $\chi(a)$ is the flux between the magnetic axis and the surface. (*b*) $F(a)$ is the poloidal current between the symmetry axis and the magnetic surface including the current I_T of the coils of the longitudinal field; $I(a)$ is the poloidal current between the magnetic axis and the magnetic surface.

where F_0 and Ψ_0 are the total poloidal current and flux encircling the magnetic axis. The functions $I(a)$ and $\varkappa(a)$, naturally, enter into the expression for the poloidal current density and the poloidal field if only the region of plasma in the equilibrium configuration is considered (for instance, in the analysis of internal instabilities).

Let us compare our notation with that of some other papers. In [1.16] the coordinate system was a, ζ, θ, rather than a, θ, ζ, and therefore I and $\varkappa$ denoted in [1.16] by J_3 and Ψ_3 [see eqs. (3.19) and (3.20)] enter into eq. (1.27) with the plus sign. In later papers on stability and equilibrium in the toroidal systems [1.17, 1.18] the equivalent of our notation $\varkappa$ was used but the poloidal current I was denoted by $-F$.

The quantities Ψ, Φ, F and J are simply related to the circulations of the vector potential $\mathbf{A}$ and the magnetic field $\mathbf{B}$, which can be found from the equations $\mathbf{B} = \operatorname{curl} \mathbf{A}$ and $(4\pi/c)\mathbf{j} = \operatorname{curl} \mathbf{B}$:

$$\begin{aligned}
&\Psi \equiv \int \mathbf{B} \cdot d\mathbf{S}_\theta = \oint \mathbf{A} \cdot d\mathbf{l}_\zeta \\
&\Phi \equiv \int \mathbf{B} \cdot d\mathbf{S}_\zeta = \oint \mathbf{A} \cdot d\mathbf{l}_\theta \\
&\frac{4\pi}{c} F \equiv \frac{4\pi}{c} \int \mathbf{j} \cdot d\mathbf{S}_\theta = \oint \mathbf{B} \cdot d\mathbf{l}_\zeta \\
&\frac{4\pi}{c} J \equiv \frac{4\pi}{c} \int \mathbf{j} \cdot d\mathbf{S}_\zeta = \oint \mathbf{B} \cdot d\mathbf{l}_\theta
\end{aligned} \tag{1.28}$$

In these case of axial symmetry eq. (1.28) yields

$$\Psi = 2\pi r A_\zeta, \qquad \frac{4\pi}{c} F = 2\pi r B_\zeta \tag{1.29}$$

and, in particular, at the magnetic axis we have $(4\pi/c)F_0 = 2\pi R B_\zeta$ and $E_\zeta = -\dot{\Psi}_0/(2\pi R c)$. For the poloidal components $\mathbf{B}_p$ and $\mathbf{j}_p$ we obtain

$$\begin{aligned}
\mathbf{B}_p &= \frac{1}{2\pi} [\nabla\Psi \times \nabla\zeta] = \frac{1}{2\pi} [\nabla\zeta \times \nabla\varkappa] \\
\mathbf{j}_p &= \frac{1}{2\pi} [\nabla F \times \nabla\zeta] = \frac{1}{2\pi} [\nabla\zeta \times \nabla I]
\end{aligned} \tag{1.30}$$

where ζ is chosen according to the symmetry; $\partial/\partial\zeta = 0$. Substitution of eq. (1.30) into eq. (1.1) and the use of $p = p(\Psi)$ and $F = F(\Psi)$ lead to

$$j_\zeta = 2\pi c r \left(p' + \frac{FF'}{4\pi^2 r^2} \cdot \frac{4\pi}{c^2} \right) \tag{1.31}$$

and the equilibrium equation acquires the form

$$r^2 \operatorname{div} \frac{\nabla\Psi}{r^2} = \frac{\partial^2\Psi}{\partial r^2} - \frac{1}{r}\frac{\partial\Psi}{\partial r} + \frac{\partial^2\Psi}{\partial z^2} = -\frac{4\pi}{c} \cdot c \cdot 4\pi^2 \left(r^2 p' + \frac{FF'}{4\pi^2} \cdot \frac{4\pi}{c^2} \right) \tag{1.32}$$

The factors $4\pi/c$ and c are shown explicitly here to facilitate conversion to another system of units.

The geometry of the chosen coordinate system in the evolution problems, as in the problems of hydromagnetic stability, can be usefully described by the metric tensor determining the element of length

$$dl^2 = g_{11}da^2 + 2g_{12}dad\theta + g_{22}d\theta^2 + g_{33}d\zeta^2 \qquad (1.33)$$

(in the case of axial symmetry $g_{33} = r^2$).

The contravariant magnetic field components B^i and the contravariant current density components j^i ($B^i \equiv \mathbf{B} \cdot \nabla x^i$, $x^i = a, \theta, \zeta$) in these coordinates are expressed in terms of the integral quantities in the following form ($g = \det g_{ik}$):

$$\begin{aligned} B^i &= \left\{0, \frac{-\Psi'(a)}{2\pi\sqrt{g}}, \frac{\Phi'(a) + \partial\eta/\partial\theta}{2\pi\sqrt{g}}\right\} \\ j^i &= \left\{0, \frac{-F'(a)}{2\pi\sqrt{g}}, \frac{J'(a) + \partial\nu/\partial\theta}{2\pi\sqrt{g}}\right\} \end{aligned} \qquad (1.34)$$

The equations of equilibrium and magnetostatics (1.17)–(1.3) now have the form

$$c \cdot 4\pi^2 p'\sqrt{g} = -F'\left(\Phi' + \frac{\partial\eta}{\partial\theta}\right) + \left(J' + \frac{\partial\nu}{\partial\theta}\right) \cdot \Psi' \qquad (1.35)$$

$$\frac{4\pi}{c}\left(J' + \frac{\partial\nu}{\partial\theta}\right) = -\frac{\partial}{\partial a}\frac{g_{22}}{\sqrt{g}}\Psi' + \frac{\partial}{\partial\theta}\frac{g_{12}}{\sqrt{g}}\Psi' \qquad (1.36)$$

$$\frac{4\pi}{c}F = \frac{g_{33}}{\sqrt{g}}\left(\Phi' + \frac{\partial\eta}{\partial\theta}\right) \qquad (1.37)$$

Note that we can choose the angle θ so that the field lines in the θ, ζ coordinates be straight, $B^2/B^3 = f(a)$. This can be done if $g_{33}/\sqrt{g}$ is a function of only a (then $\eta = 0$). In some cases θ is chosen according to the condition of orthogonality of the coordinates or some other considerations.

In the equilibrium configuration with the parameters varying with time our coordinate system is moving in space. Therefore, the longitudinal Ohm's law (1.10) together with eq. (1.4) must be written in the moving coordinate system. As shown in Appendix, these equations averaged over the magnetic surfaces yield the following equation of evolution for the most general form of $a(\mathbf{r}, t)$:

$$\Phi'\frac{\partial\Psi}{\partial t} - \Psi'\frac{\partial\Phi}{\partial t} = \frac{4\pi}{\sigma_\parallel}(JF' - FJ') \qquad (1.38)$$

Now introduce the notation

$$b_\theta = -\frac{\Psi'}{2\pi R}, \qquad b_z = \frac{\Phi'}{2\pi a} \qquad (1.39)$$

where R = const is a characteristic major radius of the configuration. Equation (1.38) together with the averaged equilibrium equation (1.35) comprise a system of two equations describing the evolution of the fluxes Ψ and Φ and having the

quasicylindrical form (eqs. (1.23) and (1.24)):

$$\frac{\partial \Psi}{\partial t} + \frac{R}{a}\frac{b_\theta}{b_z}\frac{\partial \Phi}{\partial t} = \frac{c^2}{\sigma_\parallel}\left\langle \frac{R}{a}\frac{g_{22}}{\sqrt{g}}\right\rangle \left\langle \frac{\sqrt{g}}{aR}\right\rangle \frac{p'}{b_z^2}\Psi'$$

$$+ \frac{c^2}{4\pi\sigma_\parallel}\frac{\left\langle \frac{R}{a}\frac{g_{22}}{\sqrt{g}}\right\rangle b_\theta^2 + b_z^2\left/\left\langle \frac{R}{a}\frac{\sqrt{g}}{g_{33}}\right\rangle\right.}{b_z^2}\frac{1}{a}\frac{\partial}{\partial a}\left\langle \frac{R}{a}\frac{g_{22}}{\sqrt{g}}\right\rangle a\frac{\partial \Psi}{\partial a} \tag{1.40}$$

$$4\pi p'\left\langle \frac{\sqrt{g}}{aR}\right\rangle + \frac{b_\theta}{a}\frac{\partial}{\partial a}\left\langle \frac{R}{a}\frac{g_{22}}{\sqrt{g}}\right\rangle ab_\theta + b_z\frac{\partial}{\partial a}\frac{b_z}{\left\langle \frac{R}{a}\frac{\sqrt{g}}{g_{33}}\right\rangle} = 0 \tag{1.41}$$

The coefficients averaged over the angle θ (denoted by the angle brackets) should be calculated using the solution of the two-dimensional equilibrium equation (1.32) or the variable part of eq. (1.36) which is equivalent to it:

$$-\frac{4\pi}{c}FF'\left(\frac{\tilde{\sqrt{g}}}{g_{33}}\right) - 4\pi^2 p'\cdot c\cdot(\tilde{\sqrt{g}}) = \Psi'\frac{\partial}{\partial a}\left(\frac{\tilde{g}_{22}}{\sqrt{g}}\right)\Psi' - \Psi'^2\frac{\partial}{\partial \theta}\frac{g_{12}}{\sqrt{g}} \tag{1.42}$$

Here $(\tilde{\ })$ denotes the oscillating part: $(\tilde{\sqrt{g}}) \equiv \sqrt{g} - \langle\sqrt{g}\rangle$.

In the closed system of equations (1.40)–(1.42) the first two equations describe redistribution of fluxes over the magnetic surfaces and eq. (1.42) describes the evolution of the geometry of the system of magnetic surfaces.

In the tokamak, when we have $a/R \ll 1$, $B_\theta/B_z \ll 1$, $a\beta_J/R \ll 1$ (here $\beta_J \equiv 2c^2\int p\,dS/J^2$) and a stationary longitudinal field ($\partial B_z/\partial t = 0$), eq. (1.40) is simplified and, to the first order in the above parameters, has the form

$$\frac{\partial \Psi}{\partial t} = \frac{c^2}{4\pi\sigma_\parallel}\frac{1}{\left\langle \frac{R}{a}\frac{\sqrt{g}}{g_{33}}\right\rangle}\frac{1}{a}\frac{\partial}{\partial a}\left\langle \frac{R}{a}\frac{g_{22}}{\sqrt{g}}\right\rangle a\frac{\partial \Psi}{\partial a} \tag{1.43}$$

This equation, together with eq. (1.32) or eqs. (1.41) and (1.42), can be used for describing evolution, for instance, in the tokamaks with noncircular cross section.

Let us discuss the boundary conditions for eqs. (1.40)–(1.42). The main question here is how to choose the plasma boundary, which is equivalent to choosing $\sigma_\parallel(a, t)$. Within the framework of the method of given pressure we can take any surface of the radius $a_0(t)$ as the plasma boundary outside of which $\sigma_\parallel$ is assumed to be zero. It should be borne in mind, however, that in fact this boundary is determined by plasma diffusion and therefore, we must have additional reasons for choosing $a_0(t)$.

Let us first consider the plasma bounded by an ideally conducting shell. The shell is a magnetic surface with $a = a_0$ fixed in space, and it is natural to take the boundary conditions on it. Regarding the first of the system of equations (1.40) as the diffusion equation for the poloidal flux Ψ, we can either stipulate at

the boundary the emf

$$\mathcal{E}(t) = -\frac{1}{c}\frac{\partial \Psi}{\partial t}\Bigg|_{a = a_0} \tag{1.44}$$

or the total plasma current

$$J_0(t) = J(a_0, t) = -\left\langle \frac{g_{22}}{\sqrt{g}} \right\rangle \Psi' \Bigg|_{a = a_0} \tag{1.45}$$

as functions of time.

If matching with the primary circuit of current generation is required, then we have to identify in eq. (1.44) the emf of self-induction of the plasma column:

$$\mathcal{E}_{\mathrm{pl}} = -\frac{1}{c} L_{22} \frac{dJ_0}{dt} \tag{1.46}$$

Here L_{22} is the inductance which is equal to that for the superconducting torus whose shape coincides with the shell. For the simplest primary circuit comprising capacitance C_{I}, resistance R_{I}, inductance L_{11} and a power source with the emf $\mathcal{E}_{\mathrm{I}}$, whose mutual inductance for the plasma is L_{12}, we obtain the following boundary condition:

$$-\frac{1}{c}\frac{d\Psi_0}{dt} = -\frac{1}{c} L_{22} \frac{dJ_0}{dt} - \frac{1}{c} L_{12} \frac{dI_{\mathrm{I}}}{dt} \tag{1.47}$$

$$\frac{\int I_{\mathrm{I}} dt}{C_{\mathrm{I}}} + R_{\mathrm{I}} I_{\mathrm{I}} + \frac{1}{c} L_{11} \frac{dI_{\mathrm{I}}}{dt} = \mathcal{E}_{\mathrm{I}} - \frac{1}{c} L_{12} \frac{dJ_0}{dt} \tag{1.48}$$

Here I_{I} has the sense of the current in the primary circuit.

The averaged equation (1.41) should be regarded in the evolution problem as the equation for determination of the longitudinal flux. It has the following formal solution:

$$\frac{b_z^2}{\left\langle \frac{R}{a}\frac{\sqrt{g}}{g_{33}} \right\rangle^2} = b_{z0}^2 - \int_0^a \left[4\pi p' \left\langle \frac{\sqrt{g}}{aR} \right\rangle + \frac{b_\theta}{a}\frac{d}{da}\left\langle \frac{R}{a}\frac{g_{22}}{\sqrt{g}} \right\rangle ab_\theta \right] \frac{da}{\left\langle \frac{R}{a}\frac{\sqrt{g}}{g_{33}} \right\rangle} \tag{1.49}$$

The constant b_{z_0} is chosen so that to provide either the given total longitudinal flux in the plasma

$$\Phi_0(t) = \Phi(a_0, t) = 2\pi \int_0^{a_0} ab_z da \tag{1.50}$$

or the given poloidal current $F_0(t)$ in the windings producing the longitudinal field,

$$\frac{4\pi}{c} F_0(t) = \frac{2\pi a b_z}{\left\langle \frac{\sqrt{g}}{g_{33}} \right\rangle}\Bigg|_{a = a_0} \tag{1.51}$$

The equilibrium equation (1.32) with the known right-hand side is solved with the conventional boundary condition on the shell

$$\Psi \mid_{a=a_0} = \text{const} \tag{1.52}$$

where the constant is found from the solution of eq. (1.40).

If the plasma equilibrium is maintained by the external maintaining fields, then the boundary conditions should be taken at some surface $a = a_0(t)$ moving in space. The first- and second-kind conditions (1.44) and (1.45) for eq. (1.40) and the conditions (1.50)–(1.52) for eqs. (1.41) and (1.42) have the same form as in the case of the shell. If matching to the primary circuit is required, we must bear in mind the following fact. The surface of the plasma column becomes a magnetic surface only in the presence of currents producing definite maintaining fields related to the plasma current by the equilibrium conditions. Therefore, we should regard as the secondary circuit the entire system of the plasma current J_0 and the equilibrium currents J_m^i ($i = 1, 2, \ldots$) in the shaping coils.

The emf of the secondary circuit at the plasma boundary is determined by the flux $\Psi_{eq,\,0}$ of the equilibrium field comprising the own flux Ψ_{pl} of the current in the plasma column and the flux Ψ_{ext} of the maintaining fields:

$$\mathcal{E}_{22} = -\frac{1}{c}\frac{d\Psi_{eq,\,0}}{dt} = -\frac{1}{c}\frac{d}{dt}(\Psi_{pl} + \Psi_{ext}) \tag{1.53}$$

The emf induced by the secondary circuit in the primary circuit is determined in a similar way:

$$\mathcal{E}_{12} = -\frac{1}{c}\frac{d\Psi_{eq,\,12}}{dt} \tag{1.54}$$

Here $\Psi_{eq,\,12}$ is the flux of the equilibrium configuration across the circuit that generates the current. If we use eqs. (1.53) and (1.54) instead of the similar expressions for the emf, $(1/c)d(L_{22}J_0)/dt$ and $(1/c)d(L_{12}J_0)/dt$, then boundary conditions (1.47) and (1.48) are also applicable to the plasma whose equilibrium is maintained by external confining fields.

Of course, there can be used other "electrotechnical" systems for current generation and maintenance of equilibrium. But since it is necessary to control the position of the plasma column, the system should include currents strictly related to the plasma current by the equilibrium conditions, which, as noted above, together with the plasma current should comprise an integral secondary circuit. Then all the other external currents are automatically regarded as the primary circuit which differs, to a greater or lesser degree, from the circuit used in derivation of eqs. (1.46) and (1.47).

Now let us discuss the frequently used formulation of the problem in which the plasma is assumed to be ideally conducting ($\sigma_1 = \infty$), that is, in which all the processes occur in a time which is small in comparison with the skin time. Equation (1.40) indicates the mutual frozenness of the fluxes, $\Psi = \Psi(\Phi)$. If we assume that the plasma have the frozen longitudinal flux (no diffusion), then eq. (1.41) gives the dependence $\Phi(a)$, and, moreover, the radius of the boundary magnetic surface. In these conditions the poloidal surface current $i_p(\theta)$ and the

longitudinal surface current $i_s(\theta)$ can flow along the plasma boundary; in the absence of pressure jump these currents are related by

$$\left(B_{pi} + \frac{4\pi}{c} i_s\right)^2 - B_{pi}^2 + \left(B_{si} - \frac{4\pi}{c} i_p\right)^2 - B_{si}^2 = 0 \qquad (1.55)$$

The subscript i in eq. (1.55) indicates that the values are taken at the inside of the plasma boundary. The amplitudes of the surface currents are determined by the primary circuit which gives, for instance, the total longitudinal current J_0 and the poloidal current $I_0 = I(a_0)$ in the plasma column. Since the distributions $B_{pi}(\theta)$ and $B_{si}(\theta)$ are found from the condition of frozeness and the solution of the internal equilibrium problem and the distribution $i_p(\theta) \sim 1/r$ is known, eq. (1.55) is sufficient for determination of the function $i_s(\theta)$. It should be borne in mind, however, that eq. (1.55) should be solved together with the two-dimensional internal equilibrium equation.

Thus, even in the simplified approach using given functions $p(a, t)$ and $\sigma_1(a, t)$ the problem of evolution reduces to solving several simultaneous equations (1.32) and (1.40)–(1.42), and since they are two-dimensional, the calculations seem to be rather cumbersome. We must understand, at least qualitatively, the main features and trends of evolution of the equilibrium of plasma configuration in order to develop numerical methods of solution selecting the optimal procedures and providing for reliability of the calculated results.

Therefore, we believe it will be useful to discuss first some simple typical cases illustrating the specific features of the problem.

1.3. Cylindrical Plasma Column with Circular Cross Section

The evolution of this simplest configuration is described by two one-dimensional equations (1.23) and (1.24) the first of which is similar to the equation of diffusion of the magnetic field in a solid conductor. This similarity is highly useful for the development of solution methods but it is entirely valid only in the special case (though it is practically the most important one currently) of the strong stationary longitudinal field $B_z \gg B_\theta$, low plasma pressure $\beta \ll 1$ and in the absence of noticeable plasma diffusion. Let us show for the case of the straight plasma column with circular cross section the difference between the evolution problem in the simplest one-dimensional formulation and the conventional diffusion equation.

Consider a plasma column enclosed by a shell of radius b and assume that a negligibly low plasma pressure is maintained, for instance, owing to strong radiation, $p = 0$. This configuration is force-free and the magnetic fields are related by the equilibrium expression $j_\theta B_z = j_z B_\theta$. In a strong field with $B_z \gg B_\theta$ this expression is satisfied owing to the weak poloidal current $\frac{4\pi}{c} j_\theta = -dB_z/d\varrho$ so that we can ignore the variation of the longitudinal flux in eq. (1.23).

The equilibrium equation starts to play a significant role for $B_\theta > B_z$. If the current growth time t is shorter than the skin time $\tau_{sk} = \pi\sigma_1 b^2/c^2$ and the

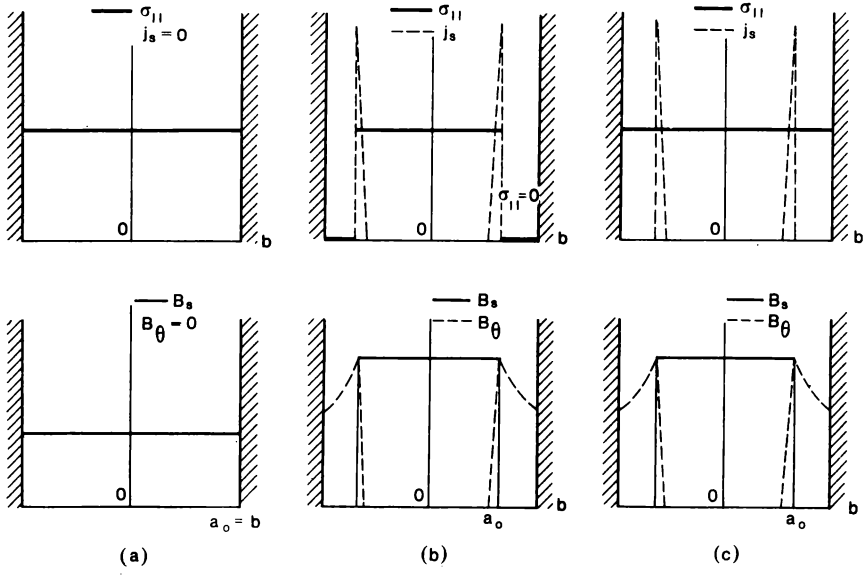

Fig. 1.5. The distributions of the conductivity $\sigma_{\parallel}$, current density j_s and the magnetic fields B_s and B_θ along the radius for fast current growth; $t < \tau_{sk}$, $B_\theta > B_s$ for $t = 0$. (*a*) The initial distributions (t = 0), no longitudinal current. (*b*) Compressed state in the case of weak plasma diffusion, $\tau_{dif} > t$. (*c*) Compression of the longitudinal flux by the poloidal field in the absence of plasma constriction for the case of high diffusion, $\tau_{dif} < t$.

plasma diffusion time τ_{dif}, then eqs. (1.23) and (1.24) describe the conventional case of the pinch effect with magnetic fluxes frozen into the plasma. Denote the initial plasma radius by $a_0(0)$ and assume that the region between the plasma and the shell has the zero conductivity $\sigma_{\parallel}$ (see Fig. 1.5). When the current increases, the plasma, naturally, does not behave as solid conductor but is compressed owing to the pinch effect. The plasma radius $a_0(t)$ is determined from the conditions of frozenness and the equilibrium equation

$$B_{si}^2 = B_{se}^2 + (2J/ca_0)^2; \qquad B_{si}a_0^2(t) = B_{s0}a_0^2(0)$$
$$B_{se}[b^2 - a_0^2(t)] = B_{s0}[b^2 - a_0^2(0)] \tag{1.56}$$

Here B_{si} and B_{se} are the longitudinal fields inside and outside of the plasma and B_{s0} is the initial longitudinal field. The solution of eq. (1.56) has the simplest form if $a_0(0) = b$. Then $a_0(t) = b$ for $B_\theta < B_s$ and $a_0(t) = bB_{s0}/B_\theta$ for $B_\theta > B_s$.

In the above case with $t < \tau_{dif}$ the boundary of the plasma conductivity and the current shell coincided.

Now let us treat the unconventional case in which the diffusion is so high that $t > \tau_{dif}$ but, as above, $t < \tau_{sk}$. Under such conditions plasma does not sense the

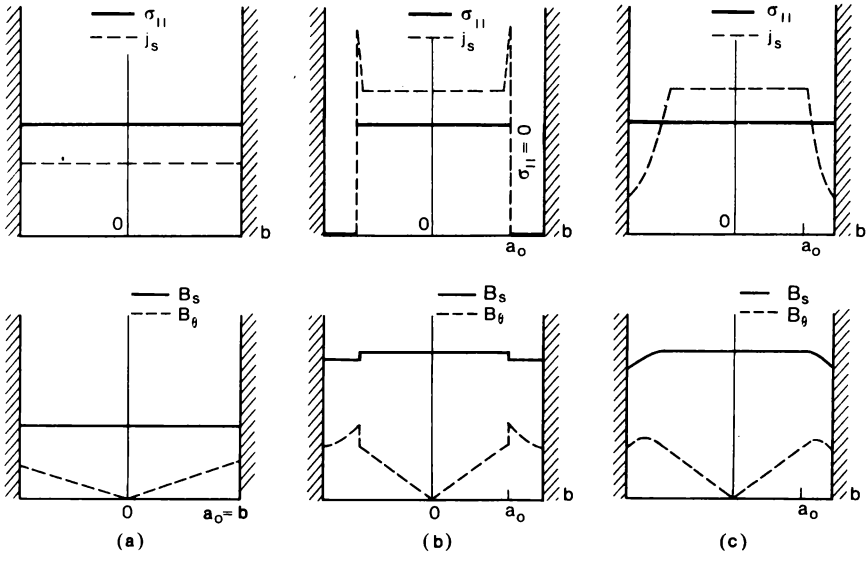

Fig. 1.6. The adiabatic compression of the cylindrical plasma column by the longitudinal field with simultaneous current growth, $p = 0$. (*a*) The initial distribution ($t = 0$), the longitudinal current is uniform. (*b*) Compressed state in the case of weak diffusion $\tau_{dif} > t$, the additional current has the surface character. (*c*) Compression of the poloidal flux by the longitudinal flux in the absence of plasma constriction for the case of high diffusion, $\tau_{dif} < t$, the additional current is distributed over the volume between a_0 and b. The plasma is paramagnetic, the declining profile B_z is related to the assumption that the pressure is negligible, $p = 0$.

magnetic field and the conductivity may be regarded as being uniform up to the shell.

How will the current increase under such conditions? In contrast to the concept of current diffusion in solid conductors, the current increase will proceed in the same way as in the above case (see Fig. 1.5). In particular, the radius $a_0(t)$, which now has the meaning of only the radius of the current shell, can be determined from eqs. (1.56). Outside the current shell where the longitudinal field is zero the current density is also zero in accordance with the "force-free" model.

The fact that eq. (1.23) of the type of the diffusion equation can describe "nondiffusive" current penetration is due to the nonlinearity of the diffusion coefficient $[c^2/(4\pi\sigma_\parallel)]$ (B^2/B_z^2) which tends to infinity for $B_z \to 0$, in spite of the high conductivity.

The possible independence of the plasma diffusion from the diffusion of magnetic fields should also be taken into account for so-called adiabatic compression of the plasma column by a strong longitudinal field. If the process time

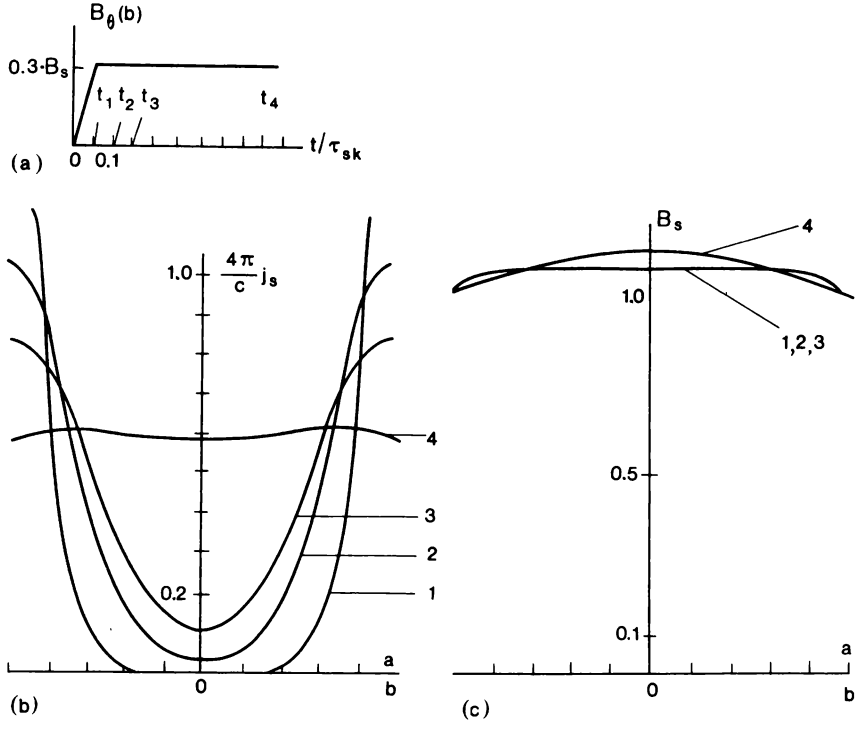

Fig. 1.7. The skin effect in the cylindrical plasma column in the case of a high longitudinal field, $B_\theta/B_z = 0.3$, $\sigma_\parallel = \text{const}$, $p = 0$. (*a*) Variation of the current with time. (*b*) Evolution of the current density distribution j_z. (*c*) Evolution of the longitudinal field B_z. (*1*) $t/\tau_{sk} = 0.1$; (*2*) $t/\tau_{sk} = 0.2$; (*3*) $t/\tau_{sk} = 0.3$; (*4*) $t/\tau_{sk} = 1.0$.

t is shorter than the skin time τ_{sk}, then the conditions of mutual frozenness of the fluxes $\Psi(\Phi)$ yields, in particular, the frozenness of the safety factor $q = q(\Phi) = -d\Phi/d\Psi$. In a strong longitudinal field when

$$q = \frac{aB_z}{RB_\theta} = \frac{c}{2\pi R}\frac{\Phi}{J} \tag{1.57}$$

this frozenness reduces to the frozenness of the current $J(\Phi)$.

If $t < \tau_{dif}$, the course of the process is trivial and the plasma is compressed according to the growth of the field:

$$\frac{a_0^2(t)}{a_0^2(0)} = \frac{B_z(0)}{B_z(t)} \tag{1.58}$$

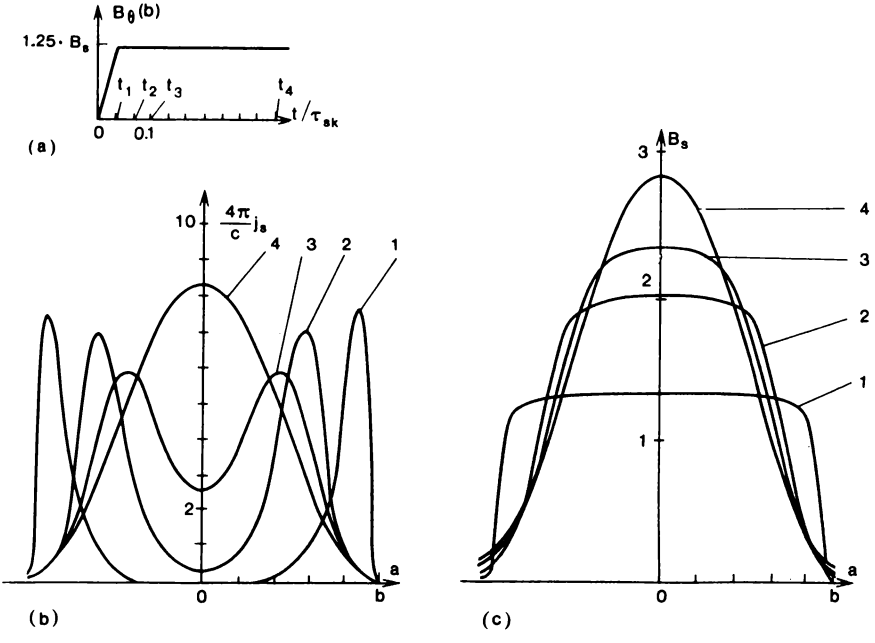

Fig. 1.8. The process of current increase in a weak longitudinal field, $B_\theta/B_s = 1.25$ (stabilized pinch), $\sigma_\parallel = \text{const}$, $p = 0$. (*a*) Variation of the current with time. (*b*) Evolution of the current density distribution j_s. (*c*) Evolution of the longitudinal field B_s. (*1*) $t/\tau_{sk} = 0.1$. (*2*) $t/\tau_{sk} = 0.2$. (*3*) $t/\tau_{sk} = 0.4$. (*4*) $t/\tau_{sk} = 1.0$.

If the external circuit determines the total current as a function of time, then the surface current J_s can appear at the plasma boundary (see Fig. 1.6). This results in the formation of a configuration with a smaller radius, constant bulk current and some surface current.

If for $t > \tau_{dif}$ and the plasma has time to diffuse across the field, the resulting configuration will differ from the above one in that the current J_s, which was a surface current, will be distributed over the external region. The current distribution can be found from the condition (1.57) of frozenness of the current, if we know the mutual matching between the inducing circuit and the growth of the longitudinal field, that is, $J(\Phi)$, and from the condition that the fields outside the compressed flux is "force-free".

Note that though the picture of compression of the magnetic fluxes in the internal region is the same, irrespective of the ratio between t and τ_{dif}, the heating of the plasma will, naturally, depend on this ratio.

The above case of compression of the cylindrical plasma column by the longitudinal fields is close to the case of displacement of the toroidal column

along the major radius in the stationary longitudinal field. If the time of compression is shorter than the skin time, then the condition of conservation of the fluxes yields the following relations for the variation of the radius $a_0(t)$ bounding the initial flux and the variation of the bulk current:

$$\frac{a_0^2(t)}{a_0^2(0)} = \frac{R(t)}{R(0)}, \qquad \frac{J(t)}{J(0)} = \frac{R(0)}{R(t)} \tag{1.59}$$

Since the flux of the field of the plasma current is

$$\Psi_{\text{pl}} = \frac{2\pi R}{c} J \left[\ln \frac{8R}{a_0} - 2 + O\left(\frac{a_0^2}{R^2}\right) \right] \tag{1.60}$$

the variation of the bulk current, to a logarithmic accuracy, corresponds to the conservation of this flux. However, the flux due to external sources enclosed by the column can change significantly in the process of compression, giving rise to an additional current J_*. In this case, too, this additional current can be distributed either at the survace or over a layer into which the plasma had time to diffuse, depending on the relationship between the compression time t and the diffusion time τ_{dif}. When $t < \tau_{\text{dif}}$, the current distribution along the minor radius is determined by the frozenness conditions.

Figures 1.7 and 1.8 illustrate the growth of current for the cylindrical column [1.9] under the conditions of finite conductivity for $\sigma_1 = \text{const}$ and $p = 0$. When $B_\phi(b) \ll B_*$ (Fig. 1.7), we encounter the normal skin effect; when $B_\phi(b) = 1.25B_*$ (Fig. 1.8), the compression of the longitudinal field determined by the equilibrium conditions becomes significant, effectively enhancing penetration of the longitudinal field into the plasma.

1.4. Evolution of High-Pressure Toroidal Configurations

Let us now analyze the two-dimensional effects in evolution of the equilibrium. The main such effect is the ballooning of the plasma column along the major radius due to the toroidality of the configuration. The ballooning necessitates application of external confining fields to maintain the equilibrium and results in toroidal displacement of the magnetic surfaces. This effect should make an important contribution to the evolution of equilibrium in high-pressure tokamaks.

Detailed analysis of the fast heating of plasma in tokamaks due to neutral injection gave rise to the concept of the so-called flux-conserving tokamak [1.19]. The underlying idea of this concept is that if the plasma is heated in a time shorter than the skin time, then the plasma configuration changes according to the condition of frozenness of the fluxes. Therefore, the topology of the configuration cannot change, making it possible to reach arbitrarily high pressures without violating the equilibrium conditions. For instance, numerical calculations [1.7] have demonstrated the existence of equilibrium configurations with $\beta = 8\pi \langle p \rangle / B_*^2 \gtrsim 20\%$ ($q_b \approx 3$).

We should note here that though the formulation of this concept implies fluxes frozen into the plasma, the mutual frozenness of the fluxes is sufficient for conservation of the topology. In particular, the relationship between the plasma heating time and the plasma diffusion time is insignificant. The rate of diffusion can be as high as desired without violating the topology (naturally, necessitating a respective increase in the heating power).

The configuration produced as a result of fast heating may change its topology owing to mutual diffusion of the fluxes so that it can even become non-equilibrium. The analysis of this situation should be based on the evolution equation (1.40) and the averaged equilibrium equation (1.41), and it is essential that the two-dimensional character of the configuration and the conditions of solvability the equilibrium equation (1.42) be taken into account. Let us analyze qualitatively the process of decay of a high-pressure configuration without going into details.

The possibility of decay can be explained in the following way. Let a plasma column with a small toroidality $a/R \ll 1$ and the uniform conductivity $\sigma_\parallel = \text{const}$ be in a strong longitudinal field. The stationary state (that is, the state with stationary fields) is the state described by the evolution equation (1.40) the left-hand side of which is replaced with the emf $\mathcal{E}$. The current density averaged over

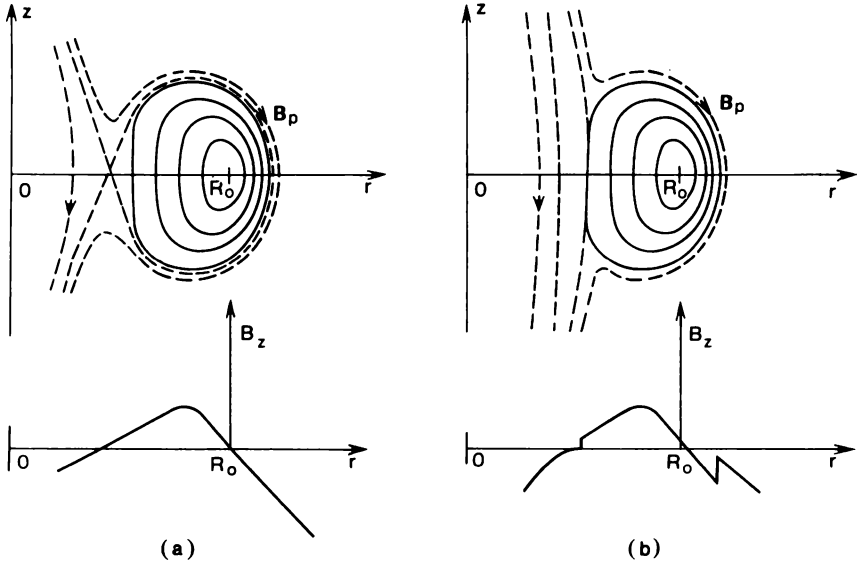

Fig. 1.9. The topology of the high-pressure configuration with frozen fluxes. (*a*) No surface current at the plasma boundary. (*b*) Configuration with uncompensated surface current; despite the frozennes of the fluxes the separatrix is at the plasma boundary.

the magnetic surface is approximately uniform and the total current is approximately $\pi a^2 \sigma_1 \mathcal{E}$. We know from the theory of equilibrium that for a given current there is a limiting pressure owing to the appearance on the inner side of the torus of a point with the zero poloidal field (the maintaining transverse field becomes equal to the plasma-generated field). For a given plasma current the pressure cannot exceed this limiting value which corresponds to $\beta \approx a/(Rq)^2$ (where $q \approx ca^2 B_z/2(RJ)$).

The configuration obtained unter the condition of flux conservation is nonstationary. Let us discuss the processes accompanying its evolution to the stationary state. Consider a high-pressure plasma column whose equilibrium is maintained by external fields. When the pressure increases while the fluxes are conserved the bulk current increases and special measures should be taken to eliminate the generated surface current. Otherwise, the x points of the separatrix will appear just in the process of pressure growth on the inner surface of the column (see Fig. 1.9) and this will immediately disturb the topology of the configuration. If the surface current is eliminated (by means of variation of the external poloidal magnetic flux), then the separatrix surface will be outside the plasma but with time it will approach the plasma boundary owing to the decrease in the total current and its redistribution due to the finite conductivity.

At a certain moment the x point of the separatrix will reach the boundary, as a result an analogue to the divertor layer will be formed and the plasma will begin to spread out along the open field lines with the speed of sound, exposing the internal magnetic surfaces. This process of stripping of the external envelope depending on the pressure distribution may prove to be unrelated to the skin effect (a peculiar instability of the equilibrium). The process will be terminated if the pressure after some decrease in the column size satisfies the stationarity conditions.

Though the time in which the separatrix reaches the plasma boundary is determined by the diffusion of the magnetic fields, it can be considerably shorter than the skin time.

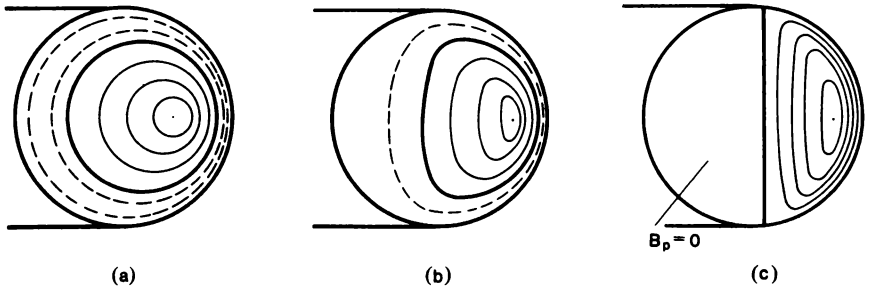

Fig. 1.10. Evolution of the high-pressure plasma with a finite conductivity maintained at equilibrium by the ideally conducting shell. (*a*) Initial configuration. (*b*) Configuration with the decreased poloidal flux between the plasma and the shell. (*c*) Limiting configuration without any flux between the plasma and the shell.

Thus, in the case of high-pressure plasma column maintained at equilibrium by external fields we should expect that the decay of the configuration will be due to the appearance of the x point of the separatrix at the plasma boundary. This leads to the question whether we can prevent the decay by specially choosing the maintaining fields or, for instance, enclosing the plasma by a high-conductivity shell which, at first sight, would not allow the separatrix to appear in the configuration.

However, even under these conditions the decay can occur. Assume that the plasma column with the radius a is enclosed in a shell of the radius b with a circular cross section (see Fig. 1.10). If the pressure is low, $\beta_J \sim 1$, the displacement of the plasma column is described by the well-known equation

$$\Delta = \frac{b^2}{2R}\left[\ln\frac{b}{a} + \left(1 - \frac{a^2}{b^2}\right)\left(\beta_J + \frac{l_i}{2} + \frac{1}{2}\right)\right] \tag{1.61}$$

where R is the major radius of the shell, and l_i is the internal inductance of the plasma column. Formally, according to eq. (1.61), the plasma starts to touch the wall ($\Delta = b - a$) for

$$\beta_J = \frac{2R/b - \dfrac{\ln(b/a)}{1 - a/b}}{1 + a/b} - \frac{l_i}{2} + \frac{1}{2} \tag{1.62}$$

In fact, whether the plasma touches the wall or not depends on the method by which pressure is increased. If the fluxes are conserved in the process, the poloidal flux between the plasma and the wall must be conserved. This prevents the contact between the plasma and the wall so that equilibrium is possible at any pressure. Then the current should be raised and, as a result, β_J determining the position of the column in the shell will be limited by $\sim R/b$ despite the increase in the total β. After violation of the frozenness conditions the total current starts to decline (we assume that a high pressure is maintained) tending to the stationary value $\sim \pi a^2 \sigma_1 \mathcal{E}$. The value of β_J starts to increase and the plasma column will be displaced toward the shell with its cross section matching its shape to that of the shell (see Fig. 1.10*b*). The loops of the field lines of the poloidal field enter the plasma during this process, clearing the vacuum region. At a certain moment the external surface of the plasma touches the wall and the shape of the column cross section becomes close to the segment. The poloidal field along the "straight" part of the segment is zero and the pressure gradient is compensated owing to the interaction between the longitudinal field B_z and the poloidal current; this is similar to the confinement of the currentless plasma with a limiter. On the external part of the column both the longitudinal field and the poloidal field contribute to confinement.

There is no poloidal field in the vacuum cavity between the plasma boundary and the shell. We may say that this cavity is an analogue of the x point of the separatrix, which appeared when the equilibrium was maintained by the external maintaining fields. In other words, though the hyperbolic magnetic axis does not penetrate inside the shell, the x point of the separatrix spreads out to fill the entire space between the plasma and the shell.

After touching the wall the plasma starts to be stripped off from the external magnetic surfaces until the stationary equilibrium is established for reduced column dimensions. In this case, depending on the current and pressure distributions, the transition to the stationary state or even the disappearance of the column can be unrelated to the field diffusion processes and occur on the inertial time scale (the equilibrium instability).

It should be noted that, though we have employed here the concepts based on the equation of evolution up to the critical state when the poloidal field vanishes, it is still unclear how to describe evolution of the transitional state between the configurations with different topologies. For instance, we do not know how the configuration would be changed if certain factors did not result in the reduction of pressure on the magnetic surfaces touching the wall of the shell.

1.5. Methods for Solving the Evolution Problems

The recent interest to the problems of equilibrium evolution was stimulated by the work on tokamaks with noncircular cross sections and, especially, high-pressure configurations. The first results have been reported and solution methods are being developed.

First, let us consider the process of solution of the simplest one-dimensional problem in which evolution is described only by two equations (1.23) and (1.24). Even in this case the iterative method must be used owing to the non-linearity of the problem. The fields B_θ and B_z, the plasma pressure p and the derivative $\partial\Phi/\partial t$ of the longitudinal flux entering into eq. (1.23) are taken with each previous step in time or iteration, while eq. (1.23) is regarded as a linear diffusion equation for determination of the poloidal flux Ψ:

$$\frac{\partial\Psi^{(n+1)}}{\partial t} + \left(\frac{B_\theta}{aB_z}\frac{\partial\Phi}{\partial t}\right)^{(n)} = \frac{c^2}{4\pi\sigma_\parallel}\left(\frac{B^2}{B_z^2}\right)^{(n)}\frac{\partial}{\partial a}\,a\,\frac{\partial\Psi^{(n+1)}}{\partial a} - \left(\frac{B_\theta}{\sigma_\parallel B_z^2}\frac{\partial p}{\partial a}\right)^{(n)} \tag{1.63}$$

Here (n) denotes the iteration number.

After eq. (1.63) with the given boundary conditions has been solved, for instance, by the predictor method, we can find the current distribution $j_z^{(n+1)}$ and the poloidal field distribution $B_\theta^{(n+1)}$ which are used to determine the longitudinal field distribution $B_z^{(n+1)}$ from eq. (1.24):

$$(B_z^2)^{n+1} = (B_{z0}^2)^{(n+1)} - \int_0^a \left[4\pi p' + \frac{4\pi}{c}B_\theta j_z\right]^{(n+1)} da \tag{1.64}$$

Then the quantities entering into eq. (1.63) are corrected. This solution procedure is repeated for eqs. (1.63) and (1.64) and when a sufficient accuracy is obtained, the following step in time is made. Such calculations for the plasma column with a finite conductivity have been illustrated above (se Figs. 1.7 and 1.8).

In the two-dimensional configurations the averaged equations (1.40) and (1.41) determining the diffusion of the fluxes contain such coefficients which can be

calculated only from the known solution $\Psi(r, z) = \Psi(a)$ of the two-dimensional equilibrium equation (1.32). Then we have

$$\langle \sqrt{g} \rangle = -\frac{\Psi'}{4\pi^2} \oint \frac{dl}{rB_p} \tag{1.65}$$

$$\left\langle \frac{g_{22}}{\sqrt{g}} \right\rangle = -\frac{1}{\Psi'} \oint B_p dl \tag{1.66}$$

$$\left\langle \frac{\sqrt{g}}{g_{33}} \right\rangle = -\frac{\Psi'}{4\pi^2} \oint \frac{dl}{r^2 B_p} \tag{1.67}$$

where $\Psi' = d\Psi/da$, and a is a specially chosen characteristic of the magnetic surfaces (see Sec. 1.2.). The integrals in the above equations are taken along the contour of the meridional cross section of the magnetic surfaces.

Numerous methods have been developed for solving various forms of eq. (1.32). For instance, in the analysis of the equilibrium with the shell the typical approach is to use the difference approximation of the differential operator in the equilibrium equation (1.32) [1.20–1.22]. However, a disadvantage of this method is the need to match the difference net to the shell for which the boundary conditions are specified. Expansions in special functions providing for regularity of the solutions at infinity are used for simulation of equilibrium in external fields. For instance, the popular method suggested by Lackner [1.23] uses the spherical system of coordinates and expansion in the Legendre functions. The method of integral equations based on the Green's functions offers certain advantages as it is flexible enough to allow unified approach to the equilibrium problems both in the shell and in the external fields as well as various combinations of these problems [1.24]. All methods employ a simple iteration procedure for solving the equilibrium equation

$$\frac{\partial^2 \Psi^{(n+1)}}{\partial r^2} - \frac{1}{r}\frac{\partial \Psi^{(n+1)}}{\partial r} + \frac{\partial^2 \Psi^{(n+1)}}{\partial z^2} = -\frac{4\pi}{c} \cdot c \cdot 4\pi^2 [r^2 p'(\Psi^{(n)}) + \frac{4\pi}{c^2} \cdot F(\Psi^{(n)}) \cdot F'(\Psi^{(n)})/4\pi^2] \tag{1.68}$$

and a grid fixed in space.

In the conventional approach to equilibrium analysis the functions $p'(\Psi)$ and $F'(\Psi)$ are assumed to be known. In the evolution problem the function $F(\Psi)$ (or $F(a)$) itself is determined by the evolution equations (1.40) and (1.41). Moreover, it is more natural to specify the pressure p as a function $p(a)$ of the coordinate a which determines $p(\Psi)$ in only an implicit form. Since the right-hand side of the equilibrium equation (1.68) is now determined by the averaged evolution equation (1.40) and the averaged equilibrium equation (1.41), they must be solved at every iteration step. To do this, we have to add to the conventional procedure for solving the two-dimensional equation (1.68) a cumbersome procedure of searching for the magnetic surfaces, that is, the contours $\Psi(r, z) = \text{const}$, corresponding to the fixed grid in a and averaging eqs. (1.65)–(1.67) over them. The

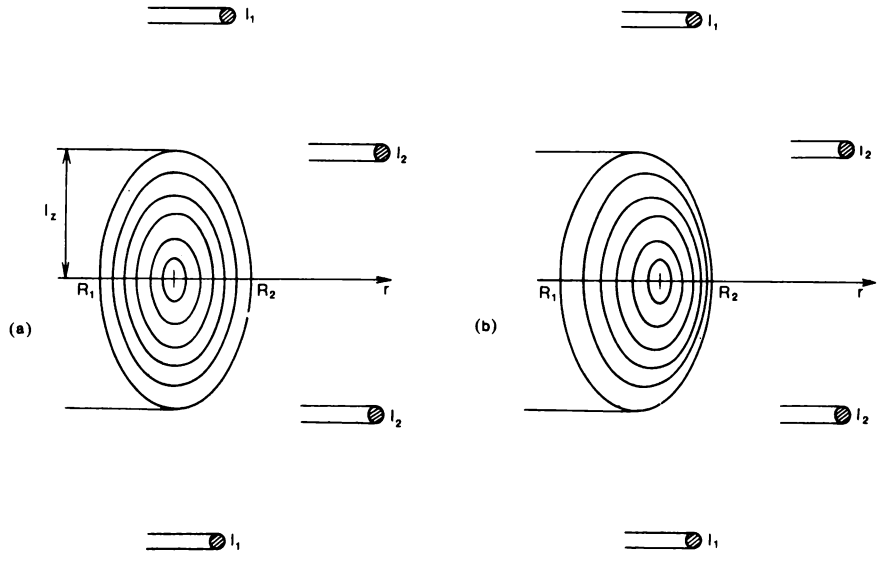

Fig. 1.11. Calculation of the equilibrium of the configuration with frozen fluxes in the external fields using the expansions in toroidal functions (reported by N. V. Chudin); $q = 1 + 2\Phi/\Phi_0, p = p_0(1 - \Phi/\Phi_0)$. (*a*) $\beta_J = 0$, $R/l_r = 3.7$, $l_z/l_r = 1.6$, $I_1 = 0.8$, $I_2 = -0.475$. (*b*) $\beta_J = 2.3$, $I_1 = 0.8, I_2 = -0.743, R/l_r = 3.8, l_z/l_r = 1.65\,(l_r = (R_2 - R_1)/2)$.

need for frequent averaging distinguishes the methods of solving the two-dimensional equilibrium equation applied in the evolution problems.

The most universal, though suboptimal, approach is to use the conventional methods for solving eq. (1.68) and to perform direct averaging over the magnetic surfaces using the values of Ψ at the nodes of the fixed grid. This approach has been used in the Princeton PEST code [1.25] (though only for the stability problems) and also in [1.7] for calculating the successive states of the configurations with frozen fluxes.

One of the authors of this paper together with N.V. Chudin employed a similar approach based on a fixed grid using the expansion of Ψ in toroidal functions for calculating the equilibrium with conserved fluxes but now in external fields. The coordinate a was the longitudinal magnetic flux and q varied along the plasma column from 1 at the magnetic axis to 3 at the plasma boundary. The pressure was assumed to be a linear function of the flux Φ, $p = p_0(1 - \Phi/\Phi_0)$. An external current I_2 producing principally the maintaining field perpendicular to the torus plane was chosen in the process of solution from the condition that two points selected in the equatorial plane be always in a common magnetic surface. This prevented displacement of the column as a whole with growing pressure and simulated the control of the plasma position. For the sake of

simplicity, no surface current was included. Figure 1.11 shows the calculated results for two pressures: $\beta_J = 0$, and $\beta_J = 2.3$.

This approach based on the fixed grid still allows only a limited number of averaging procedures. A natural approach in the equilibrium problems is to analyze the equilibrium itself in a moving grid corresponding to the coordinates a, θ, and ζ (see Sec. 1.2) related to the magnetic surfaces. The sought functions in this case are, actually, the magnetic surface coordinates $\mathbf{r}(a, \theta, \zeta)$. In the case of axial symmetry it is convenient to take orthogonal a, θ, and ζ, that is, with $g_{12} = 0$. Since $g_{ik} = (\partial \mathbf{r}/\partial x^i) \times (\partial \mathbf{r}/\partial x^k)$ (see Appendix), we can write the orthogonality condition in the form

$$\frac{\partial r}{\partial a}\frac{\partial r}{\partial \theta} + \frac{\partial z}{\partial a}\frac{\partial z}{\partial \theta} = 0 \tag{1.69}$$

or

$$\frac{\partial z}{\partial \theta} \Big/ \frac{\partial z}{\partial a} = -\frac{\partial r}{\partial \theta} \Big/ \frac{\partial r}{\partial a} = \alpha(a, \theta) \tag{1.70}$$

Here we have

$$g_{11} = \left(\frac{\partial r}{\partial a}\right)^2 + \left(\frac{\partial z}{\partial a}\right)^2, \qquad g_{22} = \alpha^2 g_{11}, \qquad \sqrt{g} = \alpha r g_{11} \tag{1.71}$$

Equation (1.70) together with the equilibrium equation (1.42) comprise a system of three equations for the unknown functions $r(a, \theta)$, $z(a, \theta)$ and $\alpha(a, \theta)$ [1.26]:

$$\frac{\partial}{\partial a}\alpha\frac{\partial z}{\partial a} + \frac{\partial}{\partial \theta}\frac{1}{\alpha}\frac{\partial z}{\partial \theta} = 0 \tag{1.72}$$

$$\frac{\partial}{\partial a}\alpha\frac{\partial r}{\partial a} + \frac{\partial}{\partial \theta}\frac{1}{\alpha}\frac{\partial r}{\partial \theta} = 0 \tag{1.73}$$

$$\frac{\partial}{\partial a}\frac{\alpha}{r}\frac{\partial \Psi}{\partial a} = -\frac{4\pi^2}{\Psi'}\frac{\alpha}{r}\left[\left(\frac{\partial r}{\partial a}\right)^2 + \left(\frac{\partial z}{\partial a}\right)^2\right]\left(c \cdot r^2 p' + \frac{FF'}{4\pi^2}\cdot\frac{4\pi}{c}\right) \tag{1.74}$$

The boundary conditions for eqs. (1.72)–(1.74) are the condition of periodicity in θ and the condition that the external magnetic surface coincide with the shell. We should specify an additional boundary condition for the value of a corresponding to the magnetic axis whose position in space is generally unknown. The common feature of all the methods using the natural coordinates is that the coefficients $\alpha(a, \theta)$ of eqs. (1.72)–(1.74) vanish at the magnetic axis. Therefore, an equivalent boundary condition at the magnetic axis is the condition of regularity of the solution which, in particular, implicitly determines also the spatial position of the magnetic axis. This property of the equations in the natural coordinates leads to certain procedural difficulties, and the methods for solving eqs. (1.72)–(1.74) are still being developed. Figure 1.12 shows the first calculated results for straight plasma column with a noncircular cross section enclosed in an ideally conducting shell [1.26].

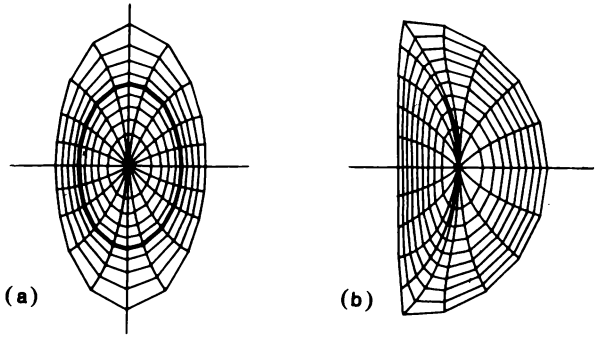

Fig. 1.12. Calculation of the equilibrium of the plasma in the shell using the natural coordinates [1.26]. (*a*) The shell with the elliptical cross section; the plasma-vacuum boundary is shown. (*b*) The shell with a segment-shaped cross section; plasma spreads to the shell.

Along with further optimization of the calculation methods, the method of reversal of the variables is currently applied for simulation of some physical processes. Figure 1.13 shows the calculated results for the limiting magnetic configurations in the so-called two-stroke tokamak [1.27] in which the plasma column is exhausted from the working chamber to the evacuated chamber. The calculation problem can be described as follows. We have an ideally conducting toroidal shell comprising two linked chambers (the cross section see in Fig. 1.13). The chamber which is closer to the symmetry axis is regarded as the working chamber in which the discharge occurs. After the reaction products or impurities have accumulated in this chamber the plasma column must be transferred to another chamber from which the plasma is pumped off. This can be done by using the loss of equilibrium along the major radius in the working chamber with increasing parameters $\beta_J = 2c^2 \int p\, dS/J^2$, for instance, owing to a decrease in the plasma current J or the natural increase in the pressure during the thermonuclear fusion reaction. When β_J exceeds the limiting value, equilibrium in the working chamber becomes impossible and the plasma column as a whole or in

Fig. 1.13. The limiting equilibrium configurations for the tokamaks with different widths d of the channel between the working chamber and the evacuated chamber. The pressure $p(\psi) = p_0(\psi - \psi_s)/(\psi_0 - \psi_s)$, where ψ_s and ψ_0 are the values of ψ at the plasma boundary and the magnetic axis; $\psi_0 = 1$, $\psi_s = 0.65$. At the shell wall $\psi = 0$. The safety factor $q = 1$. The plasma boundary is shown by the thick line and the orthogonal coordinates related to the magnetic surfaces, by the thin lines. (a) $\beta_J^* = 8\pi\langle p\rangle/\langle B_p^2\rangle = 2.0$, $p_0 = 0.34$, $d/2r_0 = 0.3$, r_0 is the minor radius of the chamber. (*b*) $\beta_J^* = 3.3$, $p_0 = 0.40$, $d/2r_0 = 0.25$. (*c*) $\beta_J^* = 4.1$, $p_0 = 0.67$, $d/2r_0 = 0.2$. (*d*) $\beta_J^* = 5.1$, $p_0 = 5.1$, $p_0 = 0.90$, $d/2r_0 = 0.15$.

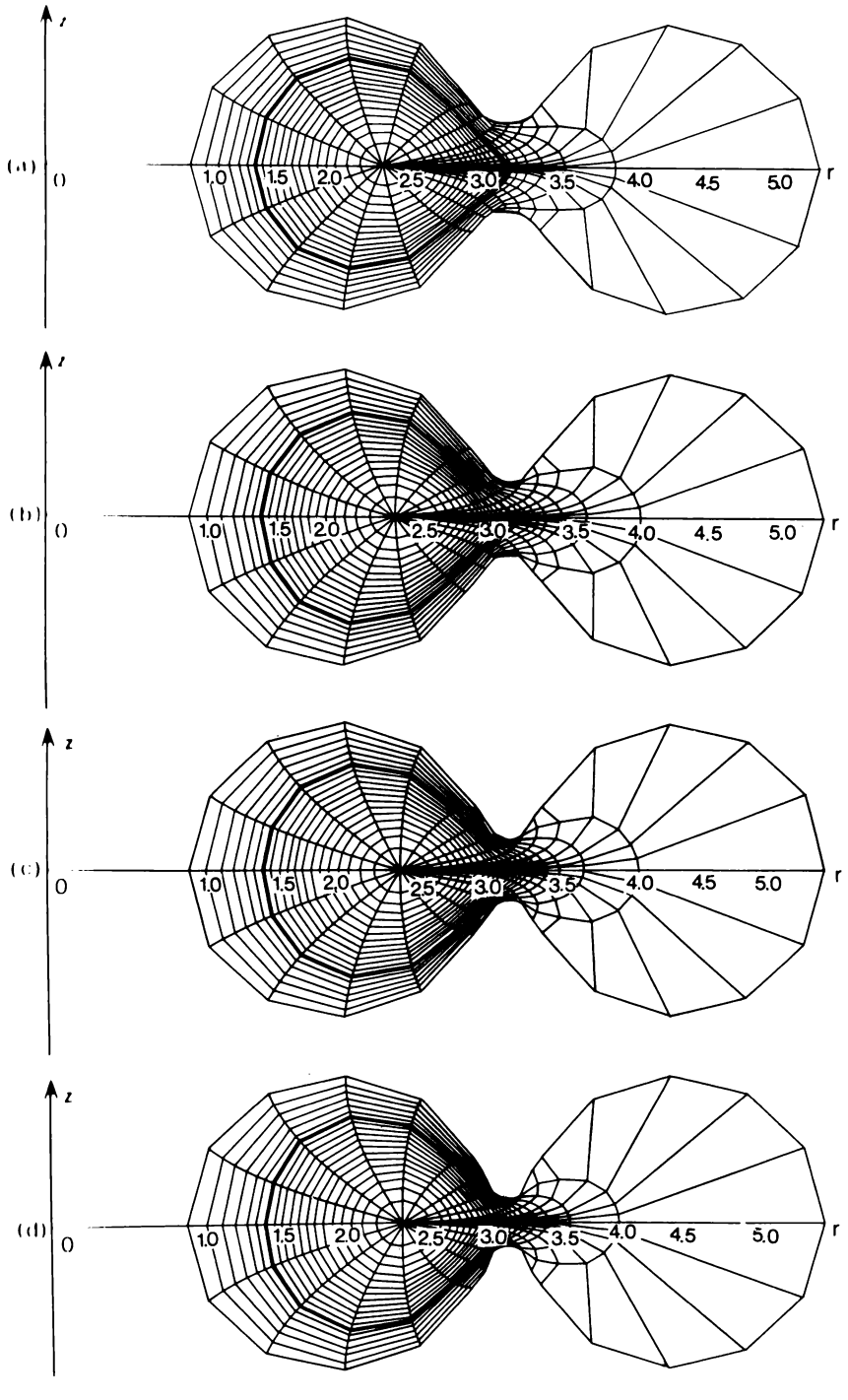
(a)
z
0
1.0
1.5
2.0
2.5
3.0
3.5
4.0
4.5
5.0
r
(b)
z
0
1.0
1.5
2.0
2.5
3.0
3.5
4.0
4.5
5.0
r
(c)
z
0
1.0
1.5
2.0
2.5
3.0
3.5
4.0
4.5
5.0
r
(d)
z
0
1.0
1.5
2.0
2.5
3.0
3.5
4.0
4.5
5.0
r

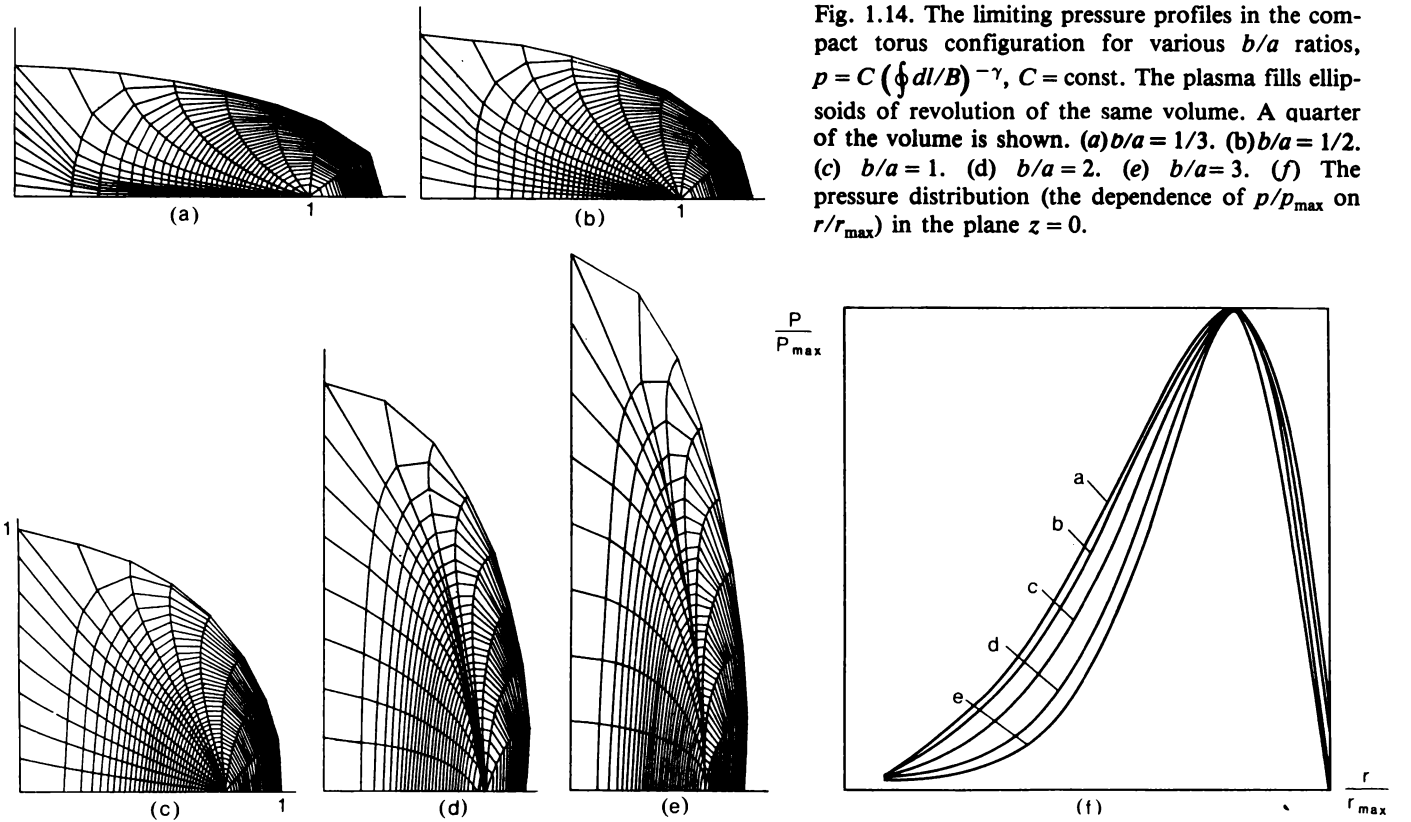

Fig. 1.14. The limiting pressure profiles in the compact torus configuration for various b/a ratios, $p = C\left(\oint dl/B\right)^{-\gamma}$, $C = \text{const}$. The plasma fills ellipsoids of revolution of the same volume. A quarter of the volume is shown. (*a*) $b/a = 1/3$. (b) $b/a = 1/2$. (*c*) $b/a = 1$. (d) $b/a = 2$. (*e*) $b/a = 3$. (*f*) The pressure distribution (the dependence of p/p_{max} on r/r_{max}) in the plane $z = 0$.

parts flows over the evacuated chamber. Figure 1.13 shows a series of limiting equilibria corresponding to various sizes of the channel between the chambers. To describe the process of plasma evacuation we have to find the solution of the problems of variation in time taking into account the inertial terms.

The method of reversal of the variables is also useful for solving the problem of the limiting pressure profile in the so-called compact toruses. These are the systems with closed magnetic surfaces in the absence of the longitudinal field: that is, toroidal z pinch devices, traps and θ pinch devices with reversed field. A characteristic feature of such systems is that the field lines are closed. Therefore, a dangerous instability for them is the interchange mode [1.28]. The necessary criterion of stability for it is the inequality

$$-\frac{p'}{p} \leq \gamma \frac{V''}{V'} \tag{1.75}$$

where $V' = \oint dl/B$, and $\gamma = 5/3$. In accordance with this criterion there is a limiting pressure profile

$$p = C\gamma/(\oint dl/B) \tag{1.76}$$

corresponding to the marginal stability. The constant C determines the current distribution in the configuration. To calculate the limiting pressure profile we have just to solve the equilibrium equation (1.32) in which $F = 0$ and p' is given by eq. (1.76) which yields an implicit dependence on the averaged characteristics of the magnetic configuration. Figure 1.14 illustrates calculation of the limiting pressure (1.76) by the method of reversal of variables for the toroidal configurations in which plasma has the shape of the ellipsoid of revolution. Note that the ratio p_{max}/p_{min} between the pressures at the plasma column axis and at the plasma boundary in these calculations was more than 100.

The method based on eqs. (1.72)–(1.74) and using directly the coordinates a, θ and ζ is a general one and, in principle, it can be applied to multiply connected configurations; its clear advantage in comparison with the conventional method is the convenience of averaging over the magnetic surfaces.

It should be borne in mind, however, that both of the above methods employ equations in partial derivatives, which are noticeably more difficult to solve than, for instance, the equilibrium equations (1.40) and (1.41) themselves or the one-dimensional transport equations. Therefore, it is natural to try to simplify the process of finding the two-dimensional equilibrium to make it no more difficult than the solution of other equations. Such a simplification is feasible because the equilibrium plasma configurations possess a fairly smooth system of magnetic surfaces which, in principle, can be described by simple approximation functions.

Let us specify the shape of the magnetic surfaces analytically with several parameters. Then the calculation of the metric coefficients and averaging procedures are performed explicitly. The parameters are determined not from the exact differential equation but from its averaged modification — the ordinary differential equations for the moments. The number of such equations should correspond to the number of the selected parameters.

The use of the method of moments has been suggested earlier [1.29] for obtaining the integral characteristics of the plasma column with a noncircular cross section. Following [1.29], a natural approach is to obtain the equation for the moments from the relationship

$$\frac{4\pi}{c}\int j_z f\,ds = \oint B_n f\,dl \tag{1.77}$$

where the integral on the left-hand side is taken over the meridional cross section of the magnetic surface and the integral on the right is taken over the contour of this cross section. The function $f(r, z)$ is the flux of an arbitrary noncircuital field and satisfies the equation

$$\operatorname{div}\frac{\nabla f}{r^2} = 0 \tag{1.78}$$

for instance, $f_0 = 1$, $f_1 = r^2$, $f_2 = r^4 - 4r^2z^2$, and so on.

Writing down eq. (1.77) in the coordinates a and θ, using eqs. (1.34)–(1.37) and differentiating eq. (1.77) with respect to a, we obtain the equation for the moments

$$-\frac{4\pi}{c}FF'\left\langle f_k\frac{\sqrt{g}}{g_{33}}\right\rangle - 4\pi^2\cdot c\cdot p'\langle f_k\sqrt{g}\rangle = \frac{c}{4\pi}\cdot\Psi'\frac{d}{da}\left\langle f_k\frac{g_{22}}{\sqrt{g}}\Psi'\right\rangle \tag{1.79}$$

When $k = 0$, eq. (1.79) reduces to the averaged equilibrium equation (1.41). Using eq. (1.41) to eliminate the function FF' from eq. (1.79), we obtain the equation describing the geometry of the magnetic configuration:

$$\begin{aligned}&\frac{4\pi}{c}\cdot 4\pi^2\cdot c\cdot p'\left\langle f_k\left[\frac{\sqrt{g}/g_{33}}{\langle\sqrt{g}/g_{33}\rangle}\langle\sqrt{g}\rangle - \sqrt{g}\right]\right\rangle\\ &= \Psi'\frac{d}{da}\left\langle f_k\frac{g_{22}}{\sqrt{g}}\Psi'\right\rangle - \Psi'\left\langle f_k\frac{\sqrt{g}}{g_{33}}\right\rangle\frac{1}{\langle\sqrt{g}/g_{33}\rangle}\frac{d}{da}\left\langle\frac{g_{22}}{\sqrt{g}}\Psi'\right\rangle\end{aligned} \tag{1.80}$$

Let us apply the method of moments for calculating the evolution of the configuration with a high β. Assume that the magnetic surfaces are toruses with circular cross sections. This assumption is valid up to the pressures of the order of $\beta \sim a/Rq^2$. The equation of the magnetic surfaces has the simple form:

$$r = R - \Delta(a) + a\cos\theta, \quad z = a\sin\theta \tag{1.81}$$

Here the displacement $\Delta(a)$ is the only parameter of the configuration. The metrics can be easily found:

$$\begin{aligned}&g_{11} = 1 - 2\Delta'\cos\theta + \Delta'^2, \quad g_{22} = a^2\\ &g_{12} = a\Delta'\sin\theta, \ \sqrt{g} = ar(1 - \Delta'\cos\theta), \ g_{33} = r^2\end{aligned} \tag{1.82}$$

Ignoring the small corrections of the order of a/R, we obtain the following

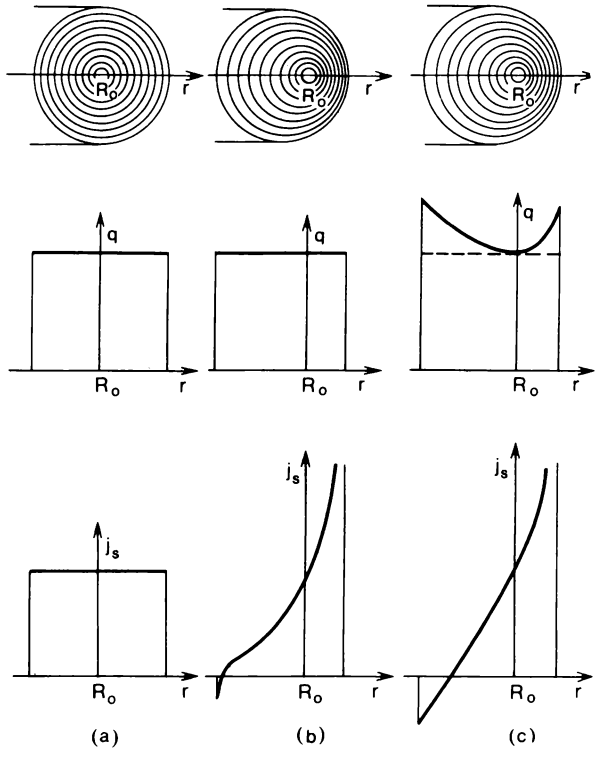

Fig. 1.15. Calculation of the evolution of a model with the circular magnetic surfaces and finite conductivity (results obtained by the authors of this paper); $a_0/R \ll 1$, $\sigma_\parallel = \text{const}$. (*a*) The initial state, $t = -0$, $\beta_J = 0$, $q = \text{const}$, $j_s = \text{const}$, (*b*) High-pressure configuration, $t = +0$, $\beta_{J_{st}} = 1.0(R/a_0)$, with flux conservation, $q = \text{const}$, $\beta_{J_{st}} \equiv 2c^2 \int pdS/(\sigma_\parallel \pi a_0^2 \varepsilon)^2$. (*c*) The stationary configuration, $t = 2.4\tau_{sk}$. The pressure level, $\beta_{J_{st}} = 1.0R/a_0$ made possible the stationary field distribution.

equation for Δ:

$$-8\pi^2 \cdot \frac{c^2}{4\pi} \cdot p \; \frac{a^4}{R} \frac{1 - \Delta^2/2}{\sqrt{1 - \Delta^2}} = J^2 a\xi + J^2\left(\frac{2aJ}{J} - 1\right)\xi - \frac{a}{R}J^2$$
$$+ aJJ \; \frac{\Delta^3}{(1 + \sqrt{1 - \Delta^2})^2} - \frac{2\Delta^3}{(1 + \sqrt{1 - \Delta^2})^2} J^2 \qquad (1.83)$$

Here $\xi = -2\Delta/(1 + \sqrt{1 - \Delta^2})$. For small Δ eq. (1.83) reduces to the well-known linear equation for the displacement.

Thus, the evolution problem reduces to the solution of three ordinary differential equations. Figures 1.15 and 1.16 illustrate the evolution of such configura-

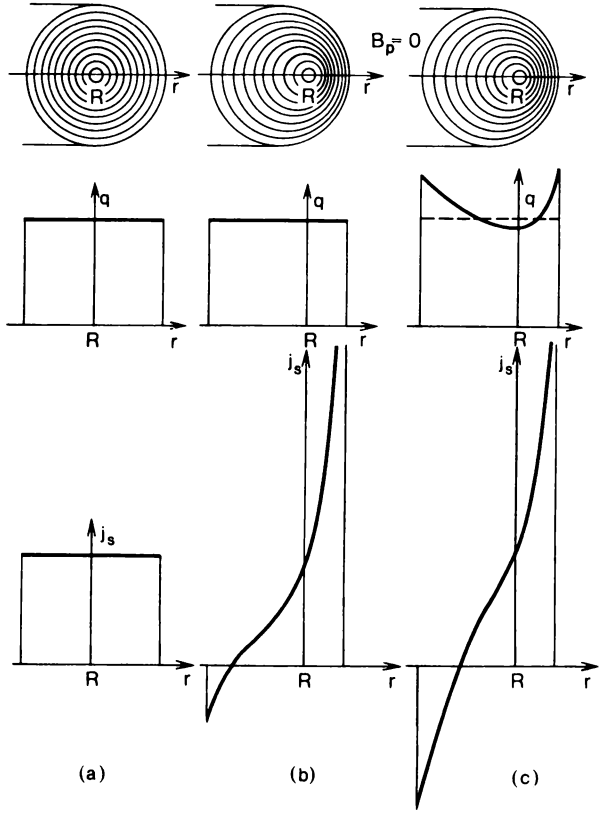

Fig. 1.16. Calculation of the evolution for a model with circular magnetic surfaces and a higher pressure, $a_0/R \ll \sigma_j = \text{const}$. (*a*) The initial state, $t = -0$, $\beta_J = 0$, $q = \text{const}$ $j_s = \text{const}$. (*b*) The high-pressure equilibrium, $t = +0$, $\beta_{J_{st}} = 1.5R/a_0$, watch frozen fluxes, $q = \text{const}$. (*c*) The equilibrium at the moment $t = 0.4\tau_{sk}$ when the poloidal field on the inner surface of the torus is zero. The pressure level does not allow a stationary configuration to be established and for $t > 0.4_{sk}$ the configuration must decay.

tion. At the initial moment the pressure is increased without changing the fluxes, and then relaxation occurs under conditions of finite conductivity. Depending on the pressure the plasma column either goes over to the stationary state (Fig. 1.15) or the stationary state cannot be reached owing to the appearance of the poloidal field on the inner surface of the torus after which the configuration should start to decay.

The method of moments have been used so far only for the simplest cases (torus with circular cross section, straight column with the elliptical cross section) in which the magnetic surfaces can be described with just one parameter. The use of additional two or three parameters will make this method sufficiently universal, fully retaining its advantages in the fast rate of calculations. In particular, this approach will make it possible to take into account, in a natural way, the geometry of the configuration in simulation of the transport processes in the real devices.

1.6 Mixing of Plasma Columns

The above discussion was concerned with the equilibrium evolution whose characteristic time scale was the skin time $\tau_{sk} = \pi\sigma a^2/c^2$. In fact, the equilibrium evolution can be regarded as a wider concept since eqs. (1.1)–(1.3) and (1.10) are valid also for shorter characteristic times down to the inertial time τ_{in}. The typical processes occurring in the intermediate characteristic times, $\tau_{in} < t < \tau_{sk}$, are the so-called processes of reconnection of the field lines resulting in variation of the topology of the magnetic configuration [1.30, 1.31]. The main features of such processes can be illustrated by the case of mixing of two plasma columns [1.32].

Let us consider two straight plasma columns of a small radius a carrying positive parallel currents I_{pl} in a strong longitudinal field (see Fig. 1.17). We have to apply respective transverse maintaining magnetic fields to compensate for the attraction between the columns and provide for the equilibrium. If these maintaining fields are removed the two columns will approach each other with the Alfven speeds until they touch and the magnetic surfaces are essentially deformed (see Fig. 1.18). This will result in generation of negative currents concentrated along the boundary between the plasma columns in the so-called neutral layer. At a certain moment these currents producing a repulsive force acting on the columns will be sufficiently large to compensate fully the attractive force acting between the columns. Thus, an equilibrium will be established in the direction of the attractive force and a quasi-equilibrium configuration will be formed. The speed $v_\perp$ with which the columns approach each other will become lower than the Alfven speed, $v_\perp \ll v_A$.

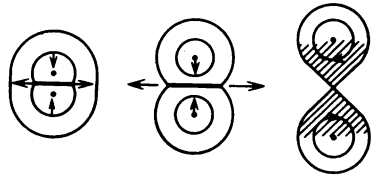

Fig. 1.17. The process of mixing of two plasma columns into one. The fields have opposite directions in the shaded region. The thick lines show the positions of the current layers; the arrows indicate the direction of motion of the plasma.

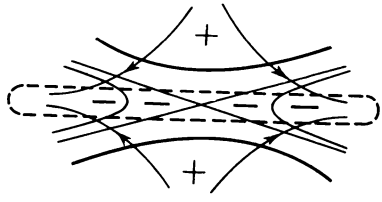

Fig. 1.18. The structure of the equilibrium configuration in the vicinity of the neutral layer in the process of mixing of the plasma columns with parallel currents. The dashed line shows the arbitrary boundary of the neutral current layer. The arrow shows the direction of motion of the plasma during the process. The plus and minus signs indicate the directions of the current density.

The negative current I_s concentrated in a narrow layer with the thickness h and the width about $2a$ in a high-conductivity plasma is determined only by the equilibrium conditions and is approximately equal to the total current of one plasma column, $I_s \approx I_{pl}$. We can estimate the layer thickness h by equating the convective transfer of the magnetic flux with the speed $v_\perp$ to its diffusive spreading:

$$v_\perp \frac{\partial \Psi}{\partial n} = \frac{c^2}{4\pi\sigma} \frac{\partial^2 \Psi}{\partial n^2} \tag{1.84}$$

Here the derivatives are taken along the direction $\mathbf{n}$ perpendicular to the current-carrying layer. Equation (1.84) yields

$$\frac{v_\perp}{h} = \frac{c^2}{4\pi\sigma h^2}$$

However, such configuration does not provide for the equilibrium along the neutral layer and the plasma spread in this direction under the effect of the force $(1/c)I_s B_n$. To estimate the speed of spreading v_τ (where τ is the direction along the layer) we have to equate the inertia force $\varrho v \nabla v \simeq \varrho v^2/a$ and the Lorentz force $(1/c)(I_s/ha)B_n$. The quantity B_n is approximately equal to $(h/a)B_\tau$ and B_τ is of the order of the field of the current, $2I_{pl}/ca$. Hence, v_τ is of the order of the Alfven speed v_A calculated from the field of the plasma current:

$$v_\tau \simeq v_A = \sqrt{\frac{I_{pl}^2}{\pi c^2 a^2 \varrho}}, \qquad \varrho = m_i n \tag{1.85}$$

The continuity condition for the plasma flux div $\mathbf{v} = 0$ due to the frozenness of the longitudinal field yields

$$v_\perp = \frac{h}{a} v_A \tag{1.86}$$

Using eq. (1.84), we obtain the layer thickness

$$h = \sqrt{c^2 a/(4\pi\sigma v_A)} \tag{1.87}$$

and the time of complete mixing of the plasma columns

$$t = a/v_{\perp} = \sqrt{\tau_{sk} a/v_A} \tag{1.88}$$

We see that the time of the process $\sqrt{\tau_{sk}\tau_{in}}$ lies between the skin time and the inertial time.

It can be easily seen that in the above process and in the similar processes there exists a large-scale equilibrium of the plasma configuration. Equilibrium is lacking only in the thin neutral layer where the plasma inertia plays a significant part. Using the fact that the thickness of this layer, h, is small, we can employ a simplified two-dimensional treatment of these processes and obtain in this way some effective boundary conditions for the quasi-equilibrium problem of the evolution of such configurations.

1.7 Combination of the Evolution Problems with Simulation of the Transport Processes

The philosophy of the above discussion rests entirely on the independence of the evolution of the equilibrium magnetic configuration with respect to the transport processes in the plasma, as noted in [1.9]. Therefore, we have taken from the whole system of transport equations only such rough characteristics as the pressure and the longitudinal conductivity. In a sense, this independence of the evolution problems from the transport phenomena is reciprocal since the indeterminacy of the transport coefficients and, in some cases, the generally determined losses are much greater than the corrections due to the configuration geometry varying with time. Therefore, it is a quite justified approach to employ the one-dimensional cylindrically symmetric model of the plasma column for simulation of the transport phenomena. At the same time, in some cases it would be useful to take into consideration simultaneously the equilibrium evolution and the transport processes in view of the noticeable recent progress in the understanding of the transport phenomena and the experiments to be carried out in the nearest future for obtaining the highest possible pressures in the tokamaks. Therefore, we present here a brief scheme of such approach without going into details.

The evolution equations (1.40) and the averaged equilibrium equation and (1.41) determining the evolution of the magnetic fluxes have already been written in the form suitable for this approach. We have to add to them the two-dimensional equilibrium equation (1.32) or (1.42) for determining the configuration geometry. Proceeding from the discussion of Sec. 1.5, we can expect that, owing to the improvement of the methods for the analysis of the equilibrium, this addition will be actually reduced to one or several ordinary differential equations (the method of moments). The system of the transport equations will consist of the conventional averaged equations of continuity and heat conduction, whose form is somewhat modified owing to the fact that the system of the natural coordinates a, θ and ζ is curvilinear and moving in space:

$$\frac{Dn}{Dt} + \frac{\partial}{\partial V} nv = \Gamma \tag{1.89}$$

$$\frac{3}{2} n_i \left(\frac{DT_i}{Dt} + v \frac{\partial T}{\partial V} \right) + n_i T_i \frac{\partial v}{\partial V} + \frac{\partial q_i}{\partial V} = Q_\Gamma^i + \frac{3m}{M} \frac{n_e}{\tau_e} (T_e - T_i) \tag{1.90}$$

$$\frac{3}{2} n_e \left(\frac{DT_e}{Dt} + v \frac{\partial T}{\partial V} \right) + n_e T_e \frac{\partial v}{\partial V} + \frac{\partial q_e}{\partial V} = Q_\Gamma^e + \langle j^2 \rangle / \sigma_\parallel - \frac{3m}{M} \frac{n_e}{\tau} (T_e - T_i) \tag{1.91}$$

The densities n_i and n_e and the temperatures T_i and T_e are the surface functions, that is, $n = n(a, t)$. The quantities V and $q_{i,e}$ are the "radial" contravariant components of the velocity and the heat fluxes averaged with the weight $\sqrt{g}$ over θ and ζ:

$$v \equiv \langle \sqrt{g}\, \mathbf{v} \cdot \nabla a \rangle_{\theta, \zeta}, \quad q \equiv \langle \sqrt{g}\, \mathbf{q} \cdot \nabla a \rangle_{\theta, \zeta} \tag{1.92}$$

The quantities Γ, Q_Γ^i and Q_Γ^e are the additional sources of heat averaged over the magnetic surfaces:

$$\Gamma = \frac{1}{\langle \sqrt{g} \rangle} \langle \Gamma \sqrt{g} \rangle_{\theta, \zeta}, \qquad Q_\Gamma^{i,e} = \frac{1}{\langle \sqrt{g} \rangle} \langle Q_\Gamma^{i,e} \sqrt{g} \rangle_{\theta, \zeta} \tag{1.93}$$

The derivatives D/Dt and $\partial/\partial V$ are the operators

$$\frac{D}{Dt} \equiv \left. \frac{\partial}{\partial t} \right|_a + \frac{1}{\langle \sqrt{g} \rangle} \left\langle \left. \frac{\partial a}{\partial t} \right|_\Gamma \sqrt{g} \right\rangle \frac{\partial}{\partial a}; \quad \frac{\partial}{\partial V} = \frac{1}{\langle \sqrt{g} \rangle} \frac{\partial}{\partial a} \tag{1.94}$$

Here $(\partial a/\partial t)_\Gamma$ has the sense of the contravariant component of the velocity v_a of the motion of the coordinate surface:

$$\left. \frac{\partial a}{\partial t} \right|_\Gamma = - v_a \cdot \nabla a$$

We have to add to this system an equation describing the normal projection of the plasma volocity, for instance, the respective projection (1.8) of Ohm's law.

Until now in our treatment the evolution equation (1.38) corresponded to the simplest form of the longitudinal projection of Ohm's law, $\mathbf{j} \cdot \mathbf{B} = \sigma_\parallel \mathbf{E} \cdot \mathbf{B}$. In the case of low collision frequency we should take into account other terms of generalized Ohm's law (1.9), too, namely, $\mathbf{B} \cdot \operatorname{div} \overleftrightarrow{\pi}$ and $\mathbf{R} \cdot \mathbf{B}$. The respective quantities averaged over the magnetic field line, $\langle f \rangle = (\oint f\, dl/B_p)/(\oint dl/B_p)$, have been calculated in [1.33]:

$$\frac{\langle \mathbf{R} \cdot \mathbf{B} \rangle}{en} = - \frac{5.24}{\sigma_\parallel} F[\beta_1 n'(T_e + T_i) - \beta_2 n T_e' - \beta_3 n T_i'] \cdot (1 - H) - \beta_4 \langle \mathbf{E} \cdot \mathbf{B} \rangle (1 - H) \tag{1.95}$$

$$- \frac{\langle \mathbf{B} \cdot \operatorname{div} \overleftrightarrow{\pi} \rangle}{en} = - \frac{5.24}{\sigma_\parallel} F[\alpha_1 n'(T_e + T_i) - \alpha_2 n T_e' - \alpha_3 n T_i'] \cdot (1 - H) + \alpha_4 \langle \mathbf{E} \cdot \mathbf{B} \rangle (1 - H) \tag{1.96}$$

where

$$\alpha_1 = 1.153, \quad \beta_1 = 0.513$$
$$\alpha_2 = 0.383, \quad \beta_2 = 0.624$$
$$\alpha_3 = 0.175, \quad \beta_3 = 0.09$$
$$\alpha_4 = 1.672, \quad \beta_4 = 0.362$$

$$H = \frac{3}{4} \langle B^2 \rangle \int_0^{1/B_{\max}} \frac{\lambda d\lambda}{\langle \sqrt{1 - \lambda \mid B \mid} \rangle} \tag{1.97}$$

For a torus with a circular cross section and a small aspect ratio we have $1 - H \approx 1.48 \sqrt{a/R}$.

The resulting evolution equation for the case of low collision frequency has the form

$$\sigma_\parallel [1 - (\alpha_4 - \beta_4)(1 - H)] \left(\Phi' \frac{\partial \Psi}{\partial t} - \Psi' \frac{\partial \Phi}{\partial t} \right)$$

$$+ \frac{5.24}{\Psi'} F \langle \sqrt{g} \rangle C[(\alpha_1 + \beta_1) n'(T_e + T_i) - (\alpha_2 + \beta_2) n T_e'$$

$$- (\alpha_3 + \beta_3) n T_i'] (1 - H) = 4\pi (JF' - FJ') \tag{1.98}$$

We can see that Eq. (1.98) differs from Eq. (1.38) only in an additional factor and an additional term on the left-hand side, which provides for a simple way for including the neoclassical effects in the general scheme of the evolution problems.

Conclusion

In fact, the theory of evolution of the plasma equilibrium in toroidal systems has just made its first steps. This paper summarizes the emerging approaches to the solution of the simplest problem of the equilibrium evolution, essentially, without changing the connectedness of the system of magnetic surfaces. The further work in this field must include, in particular, the development of the code for transport phenomena taking into account the changing geometry of the system. However, it should be emphasized that the analysis of the evolution of configurations is needed primarily for maintaining the equilibrium conditions and controlling the shape and position of the plasma column, rather than for accurate determination of the energy balance related to the geometry of the system.

The evolution of high-pressure configurations has a great importance for the reactor tokamaks. In this paper we have put forward only the qualitative considerations on a possible evolution process and illustrated them with model calculations. As the increase of pressure in tokamaks is an important problem, the details of this evolution should be analyzed including the aspects related to the variation of the configuration topology.

The reconstruction of the topology of the magnetic surfaces (namely, splitting into multiply connected regions or, on the contrary, amalgamation of split systems into one) is a fairly general problem in the plasma physics. It has been discussed [1.4] in connection with the experiments performed in the Doublet device. The problem of mixing appears to be the most interesting one since this process has been estimated to lead to a noticeable liberation of the magnetic field energy and a heating of the plasma. This process can occur via various pathways:

1. The diffusion mechanism is realized with slow variation of the external conditions during the time $\Delta t > \tau_{\text{dif}}$. In this case heating is not significant owing to its slow rate.

2. In the opposite case $\Delta t \ll \tau_{\text{dif}}$ and $\Delta t \lesssim \sqrt{\tau_{\text{sk}}\,\tau_{\text{in}}}$, where $\tau_{\text{sk}} = \pi\sigma_{\parallel}a^2/c^2$ and $\tau_{\text{in}} \approx a/\sqrt{B_p^2/4\pi\varrho + \gamma p/\varrho}$ is the inertial time. In this case (as in the case with $\Delta t \lesssim \tau_{\text{in}}$ which is difficult to realize) a neutral layer (see Sec. 1.6) is formed in the course of the process. According to estimates, the energy liberated in the neutral current layer is comparable with the energy of the poloidal magnetic field in the plasma. This process attracts great attention because of its high power (due to the short duration).

3. The adiabatic mechanism with $\sqrt{\tau_{\text{sk}}\,\tau_{\text{in}}} < \Delta t < \tau_{\text{sk}}$. The problem of adiabatic evolution has been analyzed by Grad et al. [1.3, 1.4]. Since the process involves a change of the topology, that is, it is irreversible while the losses are small owing to the adiabaticity, we encounter the problem of the energy dissipated in the plasma.

The processes of adiabatic and diffusive mixing and splitting are closely related to the nonlinear development of the helical tearing instability. Both processes involve changes of the topology of the system of magnetic surfaces and are, essentially, inertialess. Therefore, they can be treated within the framework of the theory of evolution of the equilibrium.

The problems discussed for tokamaks are wholly relevant for the stellarator-type systems. The analysis of the evolution problems for such systems will yield information on the limiting pressures, generation of the longitudinal current, and so on. Practically nothing has been done in this field yet.

Appendix

It is reasonable to describe the three-dimensional magnetohydrodynamic equilibria consistently using the coordinate system a, θ and ζ, whose coordinate surfaces a = const coincide with the magnetic surfaces and the cyclic coordinates (θ along the minor circuit of the torus and ζ along the major circuit) are chosen in a special way. The coordinates are not orthogonal. Below we present the relevant data on the curvilinear coordinates for those readers who have an insufficient knowledge of them.

a) Basis

The curvilinear coordinates $a = x^1$, $\theta = x^2$ and $\zeta = x^3$ can be defined either

by the transformation

$$\mathbf{r} = \mathbf{r}(x^1, x^2, x^3) \tag{1.A.1}$$

or by the equation of the coordinate surfaces

$$x^i(\mathbf{r}) = \text{const} \tag{1.A.2}$$

Accordingly, we can introduce two systems of the basis and supplementary vectors. The basis vectors (with subscripts)

$$\mathbf{e}_i = \partial \mathbf{r}/\partial x^i \tag{1.A.3}$$

give the direction of the variation of coordinates x^i in accordance with the expression for the oriented element of length

$$d\mathbf{l} = \frac{\partial \mathbf{r}}{\partial x^i}\, dx^i \tag{1.A.4}$$

(summation is implied over the superscript i repeated twice). Thus, vectors $\mathbf{e}_2$ and $\mathbf{e}_3$ are tangent to the coordinate surface $x^1 = \text{const}$, and so on.

The supplementary vectors (with the superscript)

$$\mathbf{e}^k = \nabla x^k \tag{1.A.5}$$

by definition are directed along the normals to the respective coordinate surfaces $x^k = \text{const}$. Thus, vector $\mathbf{e}^1$ is orthogonal to vectors $\mathbf{e}_2$, $\mathbf{e}_3$, and so on.

Accordingly, vector $\mathbf{e}_1$ which is tangent to the line of intersection of the surfaces $x^2 = \text{const}$ and $x^3 = \text{const}$ is orthogonal to the vectors $\mathbf{e}^2$ and $\mathbf{e}^3$. Therefore, we can write

$$\begin{aligned} &\mathbf{e}_1 = c_1 [\mathbf{e}^2 \times \mathbf{e}^3],\ \mathbf{e}_2 = c_2 [\mathbf{e}^3 \times \mathbf{e}^1],\ \mathbf{e}_3 = c_3 [\mathbf{e}^1 \times \mathbf{e}^2] \\ &\mathbf{e}^1 = c^1 [\mathbf{e}_2 \times \mathbf{e}_3],\ \mathbf{e}^2 = c^2 [\mathbf{e}_3 \times \mathbf{e}_1],\ \mathbf{e}^3 = c^3 [\mathbf{e}_1 \times \mathbf{e}_2] \end{aligned} \tag{1.A.6}$$

Note that the expression for the increment of any scalar function

$$d\varphi = \nabla\varphi \cdot d\mathbf{l} = \left(\frac{\partial \varphi}{\partial x^k}\, \nabla x^k\right) \cdot \left(\frac{\partial \mathbf{r}}{\partial x^i}\, dx^i\right) = \frac{\partial \varphi}{\partial x^k}\, \mathbf{e}^k \mathbf{e}^k\, dx^i \tag{1.A.7}$$

yields

$$\mathbf{e}_i \cdot \mathbf{e}^k = \delta_i^k \tag{1.A.8}$$

Hence, we can easily obtain

$$c_1 = c_2 = c_3 = \frac{1}{c_1} = \frac{1}{c_2} = \frac{1}{c_3} = \sqrt{g} \tag{1.A.9}$$

where

$$\sqrt{g} = \mathbf{e}_1 \cdot \mathbf{e}_2 \cdot \mathbf{e}_3 = \frac{1}{\mathbf{e}_1 \cdot \mathbf{e}_2 \cdot \mathbf{e}_3} \tag{1.A.10}$$

is, according to the definition of the vectors $\mathbf{e}_i$, the Jacobian for the transforma-

tion $\mathbf{r} = \mathbf{r}(x^1, x^2, x^3)$:

$$\sqrt{g} = \frac{\partial \mathbf{r}}{\partial x^1} \cdot \frac{\partial \mathbf{r}}{\partial x^2} \cdot \frac{\partial \mathbf{r}}{\partial x^3} = \frac{1}{\nabla x^1 \cdot \nabla x^2 \cdot \nabla x^3} \tag{1.A.11}$$

b) The metric tensor.

All the geometric properties of the coordinate system are determined by the expression for the squared element of length:

$$dl^2 = g_{ik} dx^i dx^k \tag{1.A.12}$$

The coefficients g_{ik} make up the fundamental metric tensor. The expression for dl yields

$$g_{ik} = \mathbf{e}_i \cdot \mathbf{e}_k \tag{1.A.13}$$

The squared gradient is expressed in terms of another tensor g^{ik}:

$$(\nabla \varphi)^2 = g^{ik} \frac{\partial \varphi}{\partial x^i} \frac{\partial \varphi}{\partial x^k} \tag{1.A.14}$$

where

$$g^{ik} = \mathbf{e}^i \cdot \mathbf{e}^k \tag{1.A.15}$$

Denote the cofactors for the elements g_{ik} and g^{ik} by G_{ik} and G^{ik}, respectively. Using eq. (1.A.3) for $\mathbf{e}_i$ and eqs. (1.A.6) and (1.A.8) we can readily find

$$g_{ik} = gG^{ik} \tag{1.A.16}$$

Accordingly, using eq. (1.A.5) for $\mathbf{e}^i$ we obtain

$$g^{ik} = \frac{1}{g} G_{ik} \tag{1.A.17}$$

Squaring $\sqrt{g} = \mathbf{e}_1 \cdot \mathbf{e}_2 \cdot \mathbf{e}_3$ and using the rule of multiplication of determinants, we obtain

$$g = \begin{vmatrix} \mathbf{e}_1 \cdot \mathbf{e}_1 & \mathbf{e}_1 \cdot \mathbf{e}_2 & \mathbf{e}_1 \cdot \mathbf{e}_3 \\ \mathbf{e}_2 \cdot \mathbf{e}_1 & \mathbf{e}_2 \cdot \mathbf{e}_2 & \mathbf{e}_2 \cdot \mathbf{e}_3 \\ \mathbf{e}_3 \cdot \mathbf{e}_1 & \mathbf{e}_3 \cdot \mathbf{e}_2 & \mathbf{e}_3 \cdot \mathbf{e}_3 \end{vmatrix} = \begin{vmatrix} g_{11} & g_{12} & g_{13} \\ g_{21} & g_{22} & g_{23} \\ g_{31} & g_{32} & g_{33} \end{vmatrix} \tag{1.A.18}$$

that is, $g = \text{Det}\, g_{ik}$. Similarly, squaring $(\sqrt{g})^{-1} = \mathbf{e}^1 \cdot \mathbf{e}^2 \cdot \mathbf{e}^3$, we obtain $\text{Det}\, g^{ik} = 1/g$.

c) Vector components

Any physical vector $\mathbf{A}$ (the magnetic field strength $\mathbf{B}$, the velocity $\mathbf{v}$, etc.) can be expanded either in the basis vectors or in the supplementary vectors:

$$\mathbf{A} = A^i \mathbf{e}_i = A_i \mathbf{e}^i \tag{1.A.19}$$

Here A_i is the covariant projection and A^i is the contravariant projection.

Using eq. (1.A.18), we obtain

$$A^i = \mathbf{A} \cdot \mathbf{e}^i = \mathbf{A} \cdot \nabla x^i$$

$$A_i = \mathbf{A} \cdot \mathbf{e}_i = \mathbf{A} \frac{\partial \mathbf{r}}{\partial x^i} \tag{1.A.20}$$

The scalar product of two vectors is

$$\mathbf{A} \cdot \mathbf{B} = A^i \mathbf{e}_i \cdot \mathbf{e}^k B_k = A^i B_i = A_i B^i \tag{1.A.21}$$

The square of the vector length is

$$|\mathbf{A}|^2 = A_i A^i \tag{1.A.22}$$

The vector product of $\mathbf{A} = A_1\mathbf{e}^1 + A_2\mathbf{e}^2 + A_3\mathbf{e}^3$ and $\mathbf{B} = B_1\mathbf{e}^1 + B_2\mathbf{e}^2 + B_3\mathbf{e}^3$ is

$$[\mathbf{A} \times \mathbf{B}]^1 = [\mathbf{AB}] \cdot \mathbf{e}^1 = (A_2B_3 - A_3B_2)\,[\mathbf{e}^2 \times \mathbf{e}^3] \cdot \mathbf{e}^1 = \frac{1}{\sqrt{g}}(A_2B_3 - A_3B_2) \tag{1.A.23}$$

Respectively, we have

$$[\mathbf{A} \times \mathbf{B}]_1 = [\mathbf{A} \times \mathbf{B}] \cdot \mathbf{e}_1 = (A^2B^3 - A^3B^2)\,[\mathbf{e}_2 \times \mathbf{e}_3] \cdot \mathbf{e}_1 = \sqrt{g}\,(A^2B^3 - A^3B^2) \tag{1.A.24}$$

The expressions for other components of the vector product can be obtained by cyclic permutation of the subscripts and superscripts.

If we substitute $\mathbf{A} = A_k\mathbf{e}^k$ and $\mathbf{A} = A^k\mathbf{e}_k$ into $A^i = \mathbf{A} \cdot \mathbf{e}^i$ and $A_i = \mathbf{A} \cdot \mathbf{e}_i$, then we obtain the relationship between the contravariant and covariant components:

$$A^i = g^{ik}A_k, \qquad A_i = g_{ik}A^k \tag{1.A.25}$$

so that we have, for instance,

$$|\mathbf{A}|^2 = g_{ik}A^iA^k = g^{ik}A_iA_k \tag{1.A.26}$$

In the orthogonal system of coordinates we have

$$|\mathbf{A}|^2 = g_{11}A^1A^1 + g_{22}A^2A^2 + g_{33}A^3A^3 = g^{11}A_1A_1 + g^{22}A_2A_2 + g^{33}A_3A_3 \tag{1.A.27}$$

Hence, we obtain the following expression for the "physical" components of the vector in terms of the contravariant and covariant components:

$$A_1^{\text{phys}} = \sqrt{g_{11}}\,A^1 = \sqrt{g^{11}}\,A_1, \tag{1.A.28}$$

and so on.

d) Differential operators

To treat physical problems in the given coordinate system we need expressions for the widely used operators, such as ∇, div, curl and ∇^2. These expressions can be written in different forms owing to the difference between the covariant and contravariant vector components but it is better to employ the simplest forms. For some operations the covariant vector representation is more convenient and

for other operations the contravariant representation is better. The expression

$$\nabla\varphi = \frac{\partial\varphi}{\partial x^i}\nabla x^i \equiv \frac{\partial\varphi}{\partial x^i}\mathbf{e}^i$$

shows that the *covariant* components of the gradient just coincide with the derivatives in the respective coordinates:

$$(\nabla\varphi)_i = \frac{\partial\varphi}{\partial x^i} \tag{1.A.29}$$

The contravariant components are expressed in terms of $\partial\varphi/\partial x^i$ according to the general rules and have rather complicated forms. Therefore, the covariant respresentation is more suitable for writing down the components of a vector equations containing gradients. For instance, the first component of the equilibrium equation is

$$c\frac{\partial P}{\partial x^1} = \sqrt{g}(j^2B^3 - j^3B^2) \tag{1.A.30}$$

Let us now apply the operator div to vector $\mathbf{A} = A^i\mathbf{e}_i$:

$$\operatorname{div}\mathbf{A} = \mathbf{e}_i \cdot \nabla A^i + A^i \operatorname{div}\mathbf{e}_i \tag{1.A.31}$$

Since $\mathbf{e}^i \cdot \nabla A^i = \partial A^i/\partial x^i$ and

$$\operatorname{div}\mathbf{e}_1 = \operatorname{div}\sqrt{g}[\nabla x^2 \times \nabla x^3] = [\nabla x^2 \times \nabla x^3]\cdot\nabla\sqrt{g} = [\nabla x^2 \times \nabla x^3]\cdot\nabla x^1\frac{\partial\sqrt{g}}{\partial x^1} = \frac{1}{\sqrt{g}}\frac{\partial\sqrt{g}}{\partial x^1}$$

we obtain

$$\operatorname{div}\mathbf{A} = \frac{1}{\sqrt{g}}\frac{\partial}{\partial x^i}(\sqrt{g}\,A^i) \tag{1.A.32}$$

Now let us apply the operator curl to vector $\mathbf{A} = A_i\mathbf{e}^i = A_i\nabla x^i$:

$$\operatorname{curl}\mathbf{A} = [\nabla A_i \times \nabla x^i] \tag{1.A.33}$$

Using the rule of vector multiplication, we obtain

$$(\operatorname{curl}\mathbf{A})^1 = \frac{1}{\sqrt{g}}\left(\frac{\partial A_3}{\partial x^2} - \frac{\partial A_2}{\partial x^3}\right) \tag{1.A.34}$$

Hence, according to the equation $(4\pi/c)\mathbf{j} = \operatorname{curl}\mathbf{B}$, the contravariant components of the current density are expressed in terms of the covariant components of the magnetic field.

Let us write down the expressions for the field components B^i and the current density components j^i in the system of coordinates a, θ and ζ, where a labels

the magnetic surfaces. The conditions $\mathbf{B} = \operatorname{curl} \mathbf{A}$ and $(4\pi/c)\mathbf{j} = \operatorname{curl} \mathbf{B}$ yield

$$B^i = \left\{0, -\frac{\Psi' a + \partial\eta/\partial\zeta}{2\pi\sqrt{g}}, \frac{\Phi'(a) + \partial\eta/\partial\theta}{2\pi\sqrt{g}}\right\} \tag{1.A.35}$$

$$j^i = \left\{0, -\frac{F'(a) + \partial\nu/\partial\zeta}{2\pi\sqrt{g}}, \frac{J'(a) + \partial\nu/\partial\theta}{2\pi\sqrt{g}}\right\}$$

$$B_i = \left\{\frac{\partial\varphi}{\partial a} - \nu, J + \frac{\partial\varphi}{\partial\theta}, F + \frac{\partial\varphi}{\partial\zeta}\right\} \frac{1}{2\pi} \cdot \frac{4\pi}{c} \tag{1.A.36}$$

where $\Psi = 2\pi A_3$, $\Phi = 2\pi A_2$, etc. have the same meaning as in Sec. 1.2. The equation of equilibrium and magnetostatics have the form

$$4\pi^2 \cdot c \cdot p' \sqrt{g} = -\left(F' + \frac{\partial\nu}{\partial\zeta}\right)\left(\Phi' + \frac{\partial\eta}{\partial\theta}\right) + \left(J' + \frac{\partial\nu}{\partial\theta}\right)\left(\Psi' + \frac{\partial\eta}{\partial\zeta}\right) \tag{1.A.37}$$

$$\frac{4\pi}{c}\left(-\nu + \frac{\partial\varphi}{\partial a}\right) = -\frac{g_{12}}{\sqrt{g}}\left(\Psi' + \frac{\partial\eta}{\partial\zeta}\right) + \frac{g_{13}}{\sqrt{g}}\left(\Phi' + \frac{\partial\eta}{\partial\theta}\right) \tag{1.A.38}$$

$$\frac{4\pi}{c}\left(F + \frac{\partial\varphi}{\partial\theta}\right) = -\frac{g_{22}}{\sqrt{g}}\left(\Psi' + \frac{\partial\eta}{\partial\zeta}\right) + \frac{g_{23}}{\sqrt{g}}\left(\Phi' + \frac{\partial\eta}{\partial\theta}\right) \tag{1.A.39}$$

$$\frac{4\pi}{c}\left(F + \frac{\partial\varphi}{\partial\zeta}\right) = -\frac{g_{23}}{\sqrt{g}}\left(\Psi' + \frac{\partial\eta}{\partial\zeta}\right) + \frac{g_{33}}{\sqrt{g}}\left(\Phi' + \frac{\partial\eta}{\partial\theta}\right) \tag{1.A.40}$$

and yeild, in particular, eqs. (1.35)–(1.37). The right-hand sides of eqs. (1.A.38)–(1.A.40) include the covariant components B_i multiplied by 2π, and the function $(2/c)\varphi$ has the meaning of the scalar potential of a noncircuital magnetic field.

Using the circulations $\oint \mathbf{E} \cdot d\mathbf{l}$ along the contours $a = \text{const}$, $\zeta = \text{const}$ and $a = \text{const}$, $\theta = \text{const}$,

$$\oint E_2 d\theta = -\frac{1}{c}\frac{\partial\Phi}{\partial t}, \quad \oint E_3 d\zeta = -\frac{1}{c}\frac{\partial\Psi}{\partial t} \tag{1.A.41}$$

we obtain the relationship between the electric field and the fluxes in the moving coordinate system a, θ, ζ:

$$E_2 = -\frac{1}{2\pi c}\frac{\partial\Phi}{\partial t} - \frac{\partial\varphi^E}{\partial\theta}$$

$$E_3 = -\frac{1}{2\pi c}\frac{\partial\Psi}{\partial t} - \frac{\partial\varphi^E}{\partial\zeta} \tag{1.A.42}$$

where φ^E is the scalar potential of the vector $\mathbf{E}$.

Now taking the expression $\sigma_\parallel E_i B^i \sqrt{g} = j^i B_i \sqrt{g}$ averaged over θ and ζ, where B_i is found from eqs. (1.A.39) and (1.A.40), we obtain the evolution equation in the invariant form:

$$\Phi' \frac{\partial\Psi}{\partial t} - \Psi' \frac{\partial\Phi}{\partial t} = \frac{4\pi}{\sigma_\parallel}(JF' - FJ') \tag{1.A.43}$$

References

1.1. Yu. N. Dnestrovsky, D. P. Kostomarov, A. M. Popov, *ZhTF*, **42**, 2255 (1972).
1.2. H. Grad, *Problems of the Plasma Theory* (Proceedings of the Conf. on Plasma Theory, Kiev, 1971), Kiev, 1972, p. 216.
1.3. H. Grad, P. N. Hu. D. C. Stevens, *Proc. US Nat. Acad. Sci.*, **72**, 3789 (1975).
1.4. H. Grad, P. N. Hu, D. C. Stevens, E. Turkel, *Plasma Phys. and Contr. Nucl. Fusion Res.*, Vienna, IAEA, vol. II, 1977, p. 355.
1.5. J. B. Taylor, Preprint Calam Lab., PP N10/75.
1.6. J. W. Connor, Preprint Calam Lab., PP N29/75.
1.7. R. A. Dory, Y.-K. M. Peng, *Nucl. Fusion*, **17**, 21 (1977).
1.8. J. Hogan, *Nucl. Fusion*, 20 (1980).
1.9. G. V. Pereversev, V. D. Shafranov, L. E. Zakharov, *Theoretical and Computational Plasma Physics*, IAEA, Vienna, 1978, p. 469.
1.10. L. E. Zakharov, V. D. Shafranov, Kurchatov Institute Preprint, IAE-3075, 1978.
1.11. B. B. Kadomtsev, V. D. Shafranov, *Plasma Phys. and Contr. Nucl. Fusion Res.*, 1971, IAEA, Vienna, 1972, vol. 2, p. 479.
1.12. G. V. Pereversev, P. N. Yushmanov, *Fizika plazmy*, **6**, 993 (1980).
1.13. S. Hamada, *Nucl. Fusion*, **1–2**, 23 (1962).
1.14. J. M. Greene, J. L. Johnson, *Phys. Fluids.* **5**, 510 (1962).
1.15. L. S. Soloviev, V. D. Shafranov, *Questions in Plasma Theory*, vol. 5, Atomizdat, Moscow, 1967.
1.16. V. D. Shafranov, *Questions in Plasma Theory*, vol. 2, Atomizdat, Moscow, 1963.
1.17. V. D. Shafranov, *Nucl. Fusion*, **8**, 253 (1968).
1.18. L. S. Soloviev, *Questions in Plasma Theory*, vol. 6, Atomizdat, Moscow, 1972.
1.19. J. F. Clark, D. J. Sigmar, *Phys. Rev. Lett.*, **38**, 70 (1977).
1.20. K. V. Hagenow, K. Lakner, *III Intern. Symposium on Toroidal Plasma Confinement*, Garching, March 1973, p 1/2, B-5.
1.21. J. D. Callen, R. A. Dory, *Phys. Fluids*, **15**, 1523 (1972).
1.22. D. Dobrott, F. J. Helton, *Nucl. Fusion*, **16**, 491 (1976).
1.23. W. Feneberg, K. Lackner, *Nucl. Fusion,* **13**, 549 (1973).
1.24. L. E. Zakharov, *ZhTF*, **44**, 1608 (1974).
1.25. R. C. Grimm, J. M. Greene, J. L. Johnson, *Methods in Computational Physics*, Acad. Press, N.-Y., **16**, 253 (1976).
1.26. P. N. Babishevich, L. M. Degtyarev, A. P. Favorsky, *Fizika plazmy*, **4**, 995 (1978).
1.27. L. M. Degtyarev, V. L. Pistunovich, V. D. Shafranov, *Nucl. Fusion*, 20, 102 (1980).
1.28. B. B. Kadomtsev, *Questions in Plasma Theory*, vol. 2, Atomizdat, Moscow, 1963.

1.29. L. E. Zakharov, V. D. Shafranov, *ZhTF*, **43**, 225 (1973).
1.30. S. I. Syrovatsky, *ZhTF*, **60**, 1727, (1971).
1.31. B. B. Kadomtsev, *Fizika plazmy*, **1**, 710 (1975).
1.32. V. D. Shafranov, *Nucl. Fusion*, **19**, 187 (1979).
1.33. D. K. Morozov, *Fizika plazmy*, **4**, 987 (1978).

2. Some Problems of Hydromagnetic Instability of Plasma

O. P. Pogutse, D. Sc. (Phys. and Math.), and
E. I. Yurchenko, Cand. Sc. (Phys. and Math.)

Introduction

This paper reviews the current problems of the linear theory of hydromagnetic instability of the plasma. Though these studies have been carried out for more than 20 years, there still remain some unclear problems which are of practical importance. Some of these problems are discussed in this review. We shall start with the large-scale and rapid instabilities and go over to smaller-scale and slow instabilities, that is, from the more dangerous to the less dangerous ones from the experimental viewpoint.

The first section deals with the ideal kink instability of the toroidal column. The main effect of toroidality consists in deterioration of stability and appearance of restrictions on permissible plasma pressure. The second section analyzes dissipation of the plasma outside the current channel and its contribution to evolution of the kink disturbances. It is shown that the peripheral plasma has a stabilizing effect even if the plasma density is low.

The flute oscillations can play the primary part if the kink instabilities have been suppressed. In this connection, the third section discusses the analytical criteria of plasma stability with respect to the balooning modes of the flute oscillations. The critical pressures are calculated for the tokamaks with the circular and D-shaped cross sections of the plasma column.

Similarly to the development of the tearing instability due to dissipation with stabilization of the ideal kink instability, suppression of the ideal flute oscillations leaves dissipative flute modes which can develop starting from the zero pressure gradient. These threshold-free dissipative ballooning modes are analyzed in section four.

This review aims primarily at presenting the physical meaning of the new results, and therefore the discussion is mainly qualitative. Some mathematical details are given in the Appendix and the reader is referred to the original papers for more detailed mathematics.

2.1. Kink Instability of the Toroidal Plasma Column

The kink instability of the cylindric plasma column was analyzed in detail by Shafranov [2.1]. Figure 2.1 shows the stability diagram (the oscillation spectrum) in the case of the uniform current. The oscillations are unstable for $\gamma^2 > 0$ and stable for $\gamma^2 < 0$. Different branches of the oscillations can be seen to intersect; for instance, the branches with $m = 2$ and $m = 3$ intersect at $nq = 2$. It can be

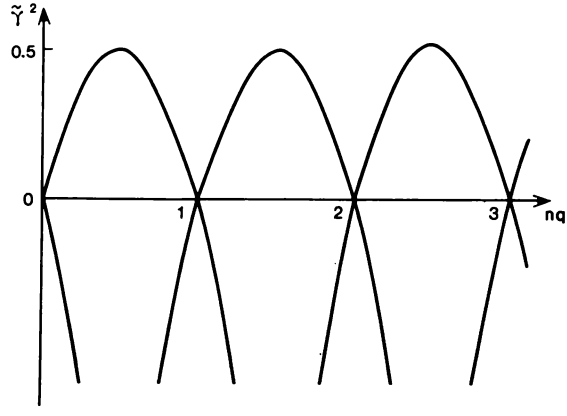

Fig. 2.1. Spectrum of oscillations of the cylindrical plasma column without shell.

expected that when a toroidal perturbation is introduced, these crossovers disappear as is the case in the band structure of the electronic spectrum of solids, and the oscillation spectrum will have the form illustrated in Fig. 2.2. The oscillation spectrum will have gaps where oscillations cannot propagate, and the growth rate γ^2 will increase on the average in the instability region.

Simple estimates indicate that the branch splitting is an effect proportional to $e = a/R$, that is, the inverse aspect ratio of the plasma column, rather than the quantity ϵ^2 which describes the frequency corrections outside the region of branch intersection.

Now let us make quantitative computation of this effect. Consider a toroidal plasma column carrying uniform current of the radius a in the shell of the radius b. At first, we consider $b \gg a$ and neglect the effect of the conducting wall on the oscillation spectrum, and then we shall analyze the results of its inclusion.

To analyze the stability we shall make use of the energy principle. It can be shown that the expression for the energy principle can be considerably simplified in the case of plasma in a strong magnetic field ($B_\theta^2/B_z^2 \gg 1$) by replacing the vector function ξ (the plasma displacement from the equilibrium position) with the perturbation of the scalar potential φ (see Appendix) [2.3]. We shall write the dependence of the potential φ on the variables ϱ, θ and s in the form

$$\varphi = \varphi(\varrho) \sum_m e^{i(m\theta - ns/k)} \tag{2.1}$$

since under axial symmetry the harmonics in s are independent and the nth harmonic can be treated separately. Owing to toroidal curvature the harmonics in θ are linked. The potential energy W and the kinetic energy T in the given approx-

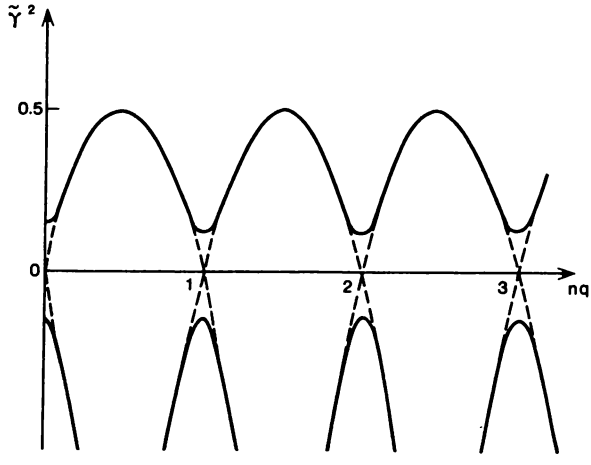

Fig. 2.2. Spectrum of oscillations of the toroidal plasma column without shell.

imation have the form

$$W = \frac{1}{2}\int\limits_{V_i+V_e} \varrho d\varrho d\theta ds \left\{\left[\frac{1}{4\pi}\left(\frac{1}{\varrho}\frac{\partial}{\partial\theta}\frac{\mathbf{B}\cdot\nabla}{B^s}\varphi\right)^2 + \frac{1}{4\pi}\left(\frac{\partial}{\partial\varrho}\frac{\mathbf{B}\cdot\nabla}{B^s}\varphi\right)^2\right]\right.$$
$$\left. - \frac{1}{\varrho B_0}\frac{\partial\varphi}{\partial\theta}\frac{dp}{d\varrho}\frac{1}{\varrho}\frac{D(\varphi, 1/B^s)}{D(\varrho,\theta)} + \frac{j^s}{C\varrho B^s}\frac{D(\varphi\ \mathbf{B}\cdot\nabla/B^s\varphi)}{D(\varrho,\theta)}\right\} \tag{2.2}$$

$$T = \frac{1}{2}\int\limits_{V_i} \varrho d\varrho d\theta ds' \left\{\left(\frac{\varrho_0}{\varrho B_0}\frac{\partial\varphi}{\partial\theta}\right)^2 + \left(\frac{\varrho_0}{B_0}\frac{\partial\varphi}{\partial\varrho}\right)^2\right\} \tag{2.3}$$

The expressions for the potential and kinetic energies are written in fact in the cylindrical approximation, that is the metric tensor coefficients are replaced with their values for the cylinder. Toroidality is taken into account only in the term describing drift in the nonuniform magnetic field (the coefficient at $dp_0/d\varrho$) and in the coefficient at the longitudinal current. The operator $(\mathbf{B}\cdot\nabla B^s) = (B^\theta/B^s)(\partial/\partial\theta - inq)$ acting along the field line yields a quantity independent of θ for any harmonic $(\mathbf{B}\cdot\nabla/B^s) = (i/qR)(m - nq)$. Expression (2.2) for the potential energy can be readily interpreted as follows. The first term in the brackets is the energy of the magnetic field in a vacuum and in the plasma. It should be noted that all the field components are proportional to the operator $\mathbf{B}\cdot\nabla/B^s = k_\parallel$. Thus, near the resonance surfaces, where $k_\parallel = 0$, the magnetic field does not affect the stability. The second term is proportional to $dp_0/d\varrho$; it is of the order of ϵ, that is, it appears only in the toroidal geometry and describes "squeezing out"

of the kink instability (it increases with increasing β_J). The last term describes the effect of the current, and the toroidal corrections to it are purely geometric in character.

The integral of the magnetic field energy is taken both in plasma and in a vacuum since, according to Shafranov [2.1], we formally introduced the "displasement" in a vacuum by the relation $\mathbf{B} = \text{curl}\,[\xi \times \mathbf{B}]$. Of course, only the combination $[\xi \times \mathbf{B}]$, which is the vector potential, has the physical meaning, rather than each term separately. However, this displacement is very convenient since it allows us to write the field in a vacuum in the same form as in plasma. Shafranov [2.1] took the magnetic field in a vacuum as $\mathbf{B}$ in the vacuum region. As shown by the expression for the fields, a more convenient form of $\mathbf{B}$ is such that the operator $k_\parallel$ yields a constant when acting on the Fourier components. This can be obtained just by continuing the field B^φ into a vacuum so that the combination $(\mathbf{B}\cdot\nabla/B^\varphi)\varphi = i\,[(B^\varphi/B^\varphi)m - (n/R)]\varphi$ be constant, that is $B^\varphi \sim B^\varphi$. The calculations are considerably simplified in this way. Note that this fictitious magnetic field is not related at all to the magnetic field in a vacuum.

A well-known fact is that to calculate the first-order corrections to the energy we have to know the eigenfunctions in the zero approximation. We shall take the eigenfunctions $\varrho^m\exp(im\theta)$ and $\varrho^{-m}\exp(im\theta)$ as the zero-approximation eigenfunctions. Since we deal with degenerate levels, we must take a combination of the neighbouring eigenfunctions Φ_m and Φ_{m+1}. We shall use the real combination

$$\Phi = c_m\exp(im\theta) + c_{m+1}\exp\,[i(m+1)\theta] + \text{c.c} \qquad (2.4)$$

where $c_m \sim \varrho^m$ in the inner region and $c_m \sim \varrho^{-m}$ in a vacuum.

Calculations indicate that the terms of the order of ϵ are due only to the terms proportional to $dp_0/d\varrho$ and j^s, and that the current term has a purely geometric effect since it is related only to the dependence of B^φ on θ.

A function of the type of (2.4) should be substituted into the variational relationship $\delta\int(T - W)dt = 0$. Averaging over θ and s and integration over ϱ yield a functional depending on c_m, c_m^*, c_{m+1}, c_{m+1}^*. After variation in c_m^* and c_{m+1}^* we obtain the following system of equation for determining c_m and c_{m+1}:

$$(\gamma_0^2 - 2k_m + 2k_m^2)\,C_m + \epsilon(\beta_s + 1)\,c_{m+1} = 0 \qquad (2.5)$$

$$(\gamma_0^2 - 2k_{m+1} + 2k_{m+1}^2)\,c_{m+1} + \epsilon(\beta_J + 1)\frac{m}{m+1}\,c_m = 0 \qquad (2.6)$$

Here

$$\gamma_0^2 = \frac{\gamma^2 a^2}{C_s^2},\quad C_s^2 = \frac{B_J^2}{4\pi\varrho_0},\quad k_m = m - nq \qquad (2.7)$$

The condition of solubility of this system of equations is the following dispersion relation:

$$\begin{vmatrix} \gamma_0^2 - 2k_m + 2k_m^2 & \epsilon(\beta_J + 1) \\ \epsilon(\beta_J + 1)\dfrac{m}{m+1} & \gamma_0^2 - 2k_{m+1} + 2k_m^2 \end{vmatrix} = 0 \qquad (2.8)$$

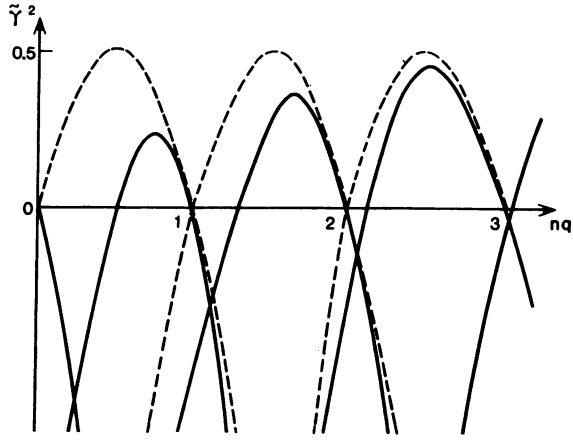

Fig. 2.3. Spectrum of oscillations of cylindrical plasma column with shell.

When $\epsilon \to 0$, eq. (2.8) is resolved into two independent equations for m and $m + 1$ modes. When $\epsilon \neq 0$, at the intersection point $k_m = 0$, $k_{m+1} = 1$, and we have the maximum resolution of the branches

$$\gamma_0^2 = \pm \epsilon(\beta_J + 1)\sqrt{\frac{m}{m+1}} \tag{2.9}$$

Far from the intersection point the effect of toroidality yields the corrections to γ_0^2 which are of the second order of smallness in e and since the terms of this order have been ignored, we cannot find a quantitative estimate of this effect outside the splitting region.

Figure 2.2 gives a qualitative illustration of resolution.

It is significant that the splitting value grows with increasing β_J. Note that the term proportional to β_J in eq. (2.9) is related to the term $dp_0/d\varrho$ in the expression (2.4) for the potential energy W, while the unity in the parentheses is due to the current term. The effects caused by the dependence of the resolution magnitude on the plasma density will be demonstrated below for the case of the toroidal plasma column in the ideally conducting shell.

In this case the stability diagram of the cylindrical plasma column contains the intervals in nq (the stability gaps, see Fig. 2.3), where oscillations are not amplified. The modern tokamaks are known to operate just in these stability gaps.

When we include toroidality, the degeneracy is again eliminated but now in the real region ($\gamma_0^2 < 0$), as can be seen in Fig. 2.4. The respective effects are

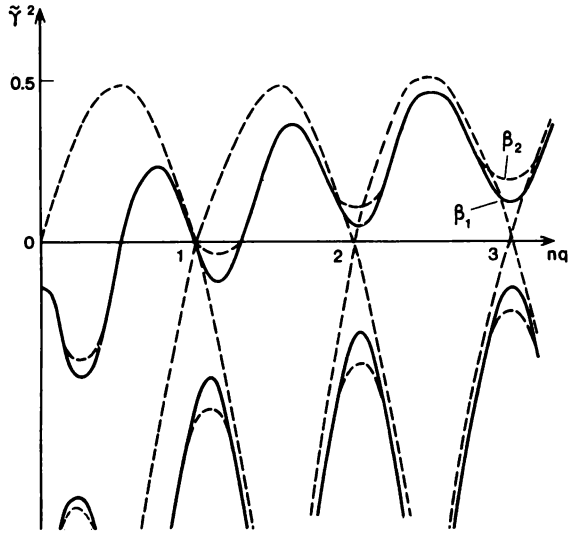

Fig. 2.4. Spectrum of oscillations of toroidal plasma column with shell.

described by the following dispersion equation:

$$\begin{vmatrix} \gamma_0^2 - 2k_m + \dfrac{2k_m^2}{1-(a/b)^{2m}} & \epsilon(\beta_y+1) \\ \epsilon(\beta_y+1)\dfrac{m}{m+1} & \gamma_0^2 - 2k_{m+1} + \dfrac{2k_{m+1}^2}{1-(a/b)^{2m}} \end{vmatrix} = 0 \qquad (2.10)$$

Equation (2.10) differs from eq. (2.8) in that its stabilizing terms contain denominators which are due to the inclusion of the shell; the eigenfunctions in the vacuum region $a \lesssim \rho < b$ now have the form $\rho^{-m} - \rho^m/b^{2m}$, rather than ρ^{-m}. Note that the stabilizing effect of the shell in the off-diagonal terms is insignificant in this approximation.

Assuming that the width of the gap is sufficiently small, we find the following approximate solution of the dispersion equation (2.10):

$$\gamma_0^2 = \pm(\beta_J+1)\epsilon\sqrt{\frac{m}{m+1}} - \left(\frac{a}{b}\right)^{2m+2} \qquad (2.11)$$

Thus, the stability gaps are closed with increasing β_J. The condition of stable operation of the tokamak in the mth gap has the form

$$\beta_J \le \frac{1}{\epsilon}\sqrt{\frac{m+1}{m}}\left(\frac{a}{b}\right)^{2m+2} - 1 \qquad (2.12)$$

If the plasma pressure is lower than the critical value given by criterion (2.12), the plasma column is stable for the declining current profile in the column cross section. If the plasma pressure is higher than the critical value, the stability depends on the form of the current profile. Sharper profiles are known to have a stabilizing effect, particularly on the high modes [2.1].

Note that though the effect of gap closure in the case of nonuniform current density must be calculated for specific conditions, this model readily yields its qualitative explanation.

2.2. Kink Instability of Nonideally Conducting Plasma

The theory of the kink instability of the current-carrying plasma column in the longitudinal magnetic field has been extensively developed for the following two limiting cases. In the first case the vacuum region with the zero conductivity is outside the current-carrying plasma (the case of free boundary) [2.1]; in the second case the high-conductivity plasma is outside the current channel (the case of fixed boundary—the tearing mode) [2.4]. For the plasma with the free boundary the growth rate of the kink instability is of the order of $\gamma_b \sim c_\theta/a$, where c_θ is the Afven velocity found from the current field, and a is the radius of the current channel. In the case of the tearing instability the growth rate is much lower than γ_0 : $\gamma_t = \gamma_b(\tau_\theta/\tau_s)^{3/5}$ since $\tau_\theta/\tau_s \ll 1$, where τ_θ and τ_s are the Alfven time and the skin time, respectively. Thus, the kink instability can continuously go over to the tearing instability in a wide interval of the parameters of the plasma outside the current channel. This continuous transition has not been identified before.

However, this is just the situation which is the most interesting one for experimental work. In modern tokamaks the temperature of the current channel is sufficiently high, so that the central part of the plasma column can easily be regarded as ideally conducting. It is well known that if the ideally conducting plasma extends to the shell, then the theory does not permit evolution of the kink instability (with the exception of the so-called internal mode with $m = 1$) but it is usually found in experiments. A qualitative explanation of this fact is well known and sufficiently simple.

The kink instability occurs when the resonance surface [$q(\varrho_0) = m/n$, where q is the safety coefficient and m and n are integers] is at the periphery of the plasma column, where the plasma density is small and the conductivity is lower (owing to the lower temperature). In a first approximation this plasma can be regarded as a vacuum, the field lines are not frozen in and the kink instability can develop. However, this explanation does not answer the question on the parameters of plasma which would allow us to treat the plasma as a vacuum. Moreover, the primary question remains unanswered: what growth rate of the kink instability can be expected under real experimental conditions?

The modern theory of plasma of finite conductivity, namely the theory of the tearing instability, cannot provide answers to these questions since it is asymptotic in the parameter τ_θ/τ_s and the growth rate in it is assumed to be

much lower than the growth rate of the kink instability. But we wish to find the parameters of the plasma column periphery for which the growth rate of the kink instability starts to differ from the growth rate of the kink instability, as well as the respective difference.

To analyze this problem we shall treat here a simple analytic model allowing us to trace the continuous transition from the kink instability to the tearing instability.

We think that, despite its simplicity, this model is sufficiently realistic and reflects the main features of experiments.

If the current field B_θ is much lower than the longitudinal field B_0 and the plasma pressure $\beta = 8\pi p/B_0^2$ is low, the equations of two-fluid hydrodynamics and the Maxwell equations can be expanded in the powers of the small parameters B_θ/B_0. This results in a considerable simplification of the equations, since we totally eliminate the magnetoacoustic oscillations. This procedure is described in detail in [2.5], and a more rigorous treatment is given in [2.6]. The simplified equations have the most symmetric form being written for the electric field potential φ and the longitudinal component of the vector potential A:

$$\frac{\omega c^2}{B_0^2}\,\mathrm{div}_\perp(\varrho_0\nabla_\perp\varphi) + \frac{m}{\varrho B_0}\frac{dj^0}{d\varrho}A = ik_\parallel\sigma\left(k_\parallel\varphi - \frac{\omega}{c}A\right) \tag{2.13}$$

$$\Delta_\perp A = i\frac{4\pi}{c}\sigma\left(k_\parallel\varphi - \frac{\omega}{c}A\right) \tag{2.14}$$

Here we have used the cylindrical geometry of the plasma column with the identical conditions at the ends ($L = 2\pi R$) and the equilibrium magnetic field of the form $\mathbf{B}\ (0,\ B_\theta(\rho),\ B_0)$. The perturbed quantities are written in the form $\varphi = \varphi(\rho)\exp(-i\omega t + im\beta + ins/R)$, ρ_0 is the unperturbed plasma density, $j^0 = (c/4\pi)\,(1/\varrho)\,(d/d\varrho)\,\varrho B_\theta$, σ is the plasma conductivity, $\Delta_\perp$ and $\nabla_\perp$ are the operators acting only on the transverse coordinates [for instance, $\Delta_\perp = (1/\varrho)\,(\partial/\partial\varrho)\,\varrho(\partial/\partial\varrho) - (m^2/\varrho^2)$, $k_\parallel = \mathbf{k}\cdot\mathbf{B}/B = (B_\theta/B_0)\,(1/\varrho)(m - nq)$ is the projection of the wave vector on the magnetic field, and $q(\varrho) = \varrho B_0/RB_\theta$ is the safety factor.

Equations (2.13) and (2.14) comprise a system of two second-order equations with variable coefficients, which is difficult to solve in the general form. Let us recall briefly how we can go over to the limiting case of the kink instability and the tearing instability in eqs. (2.13) and (2.14). First, let us write down a relationship between A and φ, which does not contain the conductivity. Expressing the combination $k_\parallel\varphi - \omega A/c$ from eq. (2.14) and substituting the result in eq. (2.13), we obtain

$$\frac{\omega c^2}{B_0^2}\,\mathrm{div}_\perp(\varrho_0\nabla_\perp\varphi) + \frac{m}{\varrho B_0}\frac{dj^0}{d\varrho}A = \frac{c}{4\pi}k_\parallel\Delta_\perp A \tag{2.15}$$

Take the cylindrical plasma column with distributed current, high-temperature central region and conductivity declining towards the periphery of the current channel.

Let us analyze the following simple model to trace the continuous transition from the kink instability to the tearing instability. Assume that a uniform current flows in the central part of radius a of the plasma column and the conductivity in this region is infinite. When $\varrho > a$, the current density is zero and the plasma has an arbitrary conductivity.

Generally, no analytic solution for the arbitrary conductivity outside the current channel can be obtained even in this model. But if we introduce another small parameter, namely, the ratio between the concentration outside the current channel and the concentration in the current channel, $\hbar = n_e/n_i$, proceeding from the experimental observation that the peripheral concentration of plasma is lower than the concentration at the centre, then we can obtain an analytical solution for an arbitrary conductivity at the plasma periphery for reasonable $\hbar$ values.

Within the framework of this model we can also introduce the conducting wall at $\varrho = b$ but this will merely give us an additional parameter and not make any essential difference, and since the effect of the wall has been analyzed in detail in [2.1], we shall ignore the wall for the sake of simplicity.

Thus, at $\varrho < a$ we shall analyze the equations for the ideal plasma and at $\varrho > a$, the equations for finite conductivity using the procedures developed in the studies of tearing instability [2.4]. The inclusion of the small parameter $\hbar$ allows us always to make the singular region, where eq. (2.17) is not valid, sufficiently narrow so that the theory remains applicable.

Now let us write down the equations for our model and solve them. For $\varrho < a$ eq. (2.14) implies that in this region (the superscript "i" will denote the values of all parameters in this region) the condition of frozenness relates φ and A:

$$\varphi^i = \frac{\omega}{k_\parallel^i c} A^i \tag{2.19}$$

It should be noted that for $j^0 = \text{const}$ we have $k_\parallel^i = \text{const}$. Now, substituting φ^i into eq. (2.15), we obtain the equation for A^i:

$$\left(1 - \frac{\omega^2}{k_\parallel^2 (c_A^i)^2}\right) \Delta_\perp A^i = 0 \tag{2.20}$$

Here $(c_A^i)^2 = B_0^2/4\pi\varrho_0$ and the fact that $dj^0/dr = 0$ has been used. Below it will be shown that $\omega \neq k_\parallel c_A$, and therefore eq. (2.20) can be reduced to $\Delta_\perp A^i = 0$. In the region $\varrho > a$, that is, outside the current channel, all the parameters will be denoted by the superscript "e". Assuming that ϱ_e and σ are constant, we obtain in this region

$$\frac{\omega c^2}{B_0^2} \varrho_e \Delta_\perp \varphi^e = i\sigma k_\parallel^2 \left(k_\parallel^2 \varphi - \frac{\omega}{c} A^e\right) \tag{2.21}$$

$$\Delta_\perp A^e = i \frac{4\pi}{c} \sigma \left(k_\parallel^2 \varphi - \frac{\omega}{c} A^e\right) \tag{2.22}$$

It is well known [2.4] that the kink instability can develop when the singularity $k_\parallel(\varrho_0) = 0$ is at the periphery of the plasma column; then in the whole region of high conductivity where $\sigma \to \infty$ we can assume

$$\varphi = \frac{\omega}{k_\parallel c} A \tag{2.16}$$

which follows from eqs. (2.13) and (2.14). This is just the condition of frozenness of the plasma $\mathbf{E} + (1/c)[\mathbf{v} \times \mathbf{B}] = 0$ rewritten in the terms of φ and A.

Substituting $\varphi = (\omega/k_\parallel c)A$ into eq. (2.15), we obtain the equation for the high-conductivity part of the plasma column:

$$\frac{\omega c^0}{B_0^2} \operatorname{div}_\perp \left(\varrho_0 \nabla_\perp \frac{\omega}{k_\parallel c} A \right) + \frac{m}{\varrho B_0} \frac{dj^0}{d\varrho} A = \frac{c}{4\pi} k_\parallel \Delta_\perp A \tag{2.17}$$

In the peripheral plasma region the conductivity is small, $\sigma \to 0$, and A can be described by the simple equation

$$\Delta_\perp A = 0 \tag{2.18}$$

Equations (2.17) and (2.18) describe evolution of the kink instability of the plasma column carrying current in a strong longitudinal magnetic field.

When we analyze the helical instability of plasma with the fixed boundary, that is, the tearing instability, we assume that the conductivity is high in the entire plasma region. Dissipation proves to be significant only in the vicinity of the singularity $k_\parallel(\varrho_0) = 0$ and the plasma density in this vicinity is typically assumed not to differ significantly from the plasma density at the centre of the current channel.

Under such conditions we should employ eq. (2.17) in the entire region with the exception of the vicinity of the point ϱ_0 and assume $\omega^2 \approx 0$. In the vicinity of the singularity high conductivity [as it follows from eq. (2.13)] is compensated with $k_\parallel \to 0$, and here we have to solve the full system of equations (2.13) and (2.14). Since the width of the region where eq. (2.17) is inapplicable tends to zero with increasing σ and is much smaller than the characteristic plasma size, we can regard the macroscopic quantities as being constant in the vicinity of ϱ_0. This results in such a simplification of the equations that the solution [2.4] for the singular region becomes universal, and the dependence on the specific distribution types is expressed only via the solution of eq. (2.17) for the region outside of the singularity.

The solution for the tearing mode corresponds for almost totally frozen plasma [almost everywhere $\varphi = (\omega/k_\parallel c)A$] and the growth rate for it is, naturally, much smaller than in the case when the singularity is in a vacuum and the condition of frozenness is absent.

Thus, if we gradually decrease conductivity near the singularity, this leads to the transition to the kink instability. But we cannot employ the solution for the tearing mode in the case of this transition since the width of the singular region increases with decreasing conductivity, and we can no longer distinguish between the inner and outer regions, while the solution in the vicinity of the singularity loses its universality.

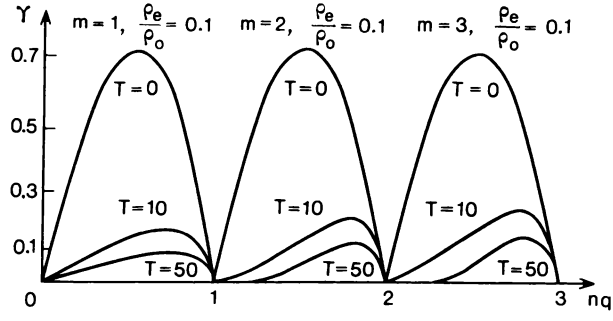

Fig. 2.5. Dimensionless growth rate as a function of nq for various plasma temperatures at the column periphery.

in the singular region $\varrho_0 - \delta < \varrho < \varrho_0 + \delta$. This difference is

$$\Delta = 2\frac{m}{\varrho_0}\frac{c_2 - 1}{[1 - c_2[1 - (a/\varrho_0)^{2m}]]} \tag{2.29}$$

where

$$c_2 = \frac{1}{m - nq}\left(1 - \frac{\gamma^2}{\frac{2c_\theta^2}{a^2}(m - nq)}\right), \quad \omega = i\gamma$$

In contrast to the conventional tearing mode, we have retained here the terms of the order of γ^2 since the resulting growth rates can be of the order of the growth rate of the kink instability, $\gamma_B \sim c_\theta/a$.

Another relationship between Δ and γ can be found from the solutions of eqs. (2.21) and (2.22) in the dissipative layer [2.4]. We obtain then

$$\Delta = 4\frac{m}{a}\frac{(\varrho_0/2ms_0)^{3/2}}{(c_\theta/a)^{1/2}}\frac{\gamma^{5/4}\tilde{n}^{1/4}}{\gamma^{3/4}} \tag{2.30}$$

where $s_0 = c/\omega_{pe}$ is the width of the collisionless skin. Equating eqs. (2.29) and (2.30), we obtain the dispersion equation for our model [2.7]:

$$\gamma_0^2 = 2k_m - 2k_m^2\frac{1 + Q_m}{1 + Q_m\left[1 - \left(1 - \frac{k_m}{m}\right)^m\right]} \tag{2.31}$$

Here $\gamma_0 = \gamma_a/c_\theta$, $Q_m = (2^{-1/2}\, m^{-3/2})\,(\varrho_0/a)^{5/2}\,\Pi e^{3/4}\gamma_0^{5/4}\tilde{n}(1/\nu_0^{3/4})$, $\nu_0 = \nu a/c_\theta$, and $\Pi e = a^2\omega_{pe}^2/c^2$ is the number of electrons per unit length in the current channel. The plasma of finite conductivity and finite concentration around the current channel always has a stabilizing effect owing to frozenness of the magnetic field (the factor at k_m^2 is smaller than unity).

We shall solve these equations using the tearing mode technique. In other words, we shall assume that the region of localization of the rapidly varying solution of the system of equations (2.21) and (2.22) is sufficiently small, so that we can retain only the linear term in the expansion of $k_\parallel^e = (k_\parallel^e)'(\varrho - \varrho_0)$.

Equation (2.17) for the ideal plasma can be employed in the external region, with the exception of the narrow layer near the resonance point ϱ_0 and for a sufficiently low ratio $\tilde{n} = n_e/n_i$ eq. (2.17) is reduced simply to

$$\Delta_\perp + A^e = 0 \tag{2.23}$$

In the immediate vicinity of the point ϱ_0 (where $k_\parallel^e = (k_\parallel^e)'(\varrho - \varrho_0)$; we shall estimate the width of this region below) we must use the entire system of equations (2.21) and (2.22) with the replacement $k_\parallel^e = (k_\parallel^e)'(\varrho - \varrho_0)$.

Now we can easily write down the solutions. In the region $\varrho < a$ we have

$$A^i = (\varrho/a)^m \tag{2.24}$$

The second solution is ignored owing to finiteness of A^i at the zero, and φ^i is related to A^i by $\varphi^i = \omega A^i/k_\parallel^i c$. In the interval $a < \varrho < \varrho_0 - \delta$ the solution of eq. (2.23) is A^e (here δ is the width of the region where dissipation is significant):

$$A_1^e = c_1\left(\frac{\varrho}{a}\right)^m + c_2\left(\frac{\varrho}{a}\right)^{-m} \tag{2.25}$$

In the region $\varrho_0 + \delta < \varrho < \infty$ it is sufficient to include only the decreasing solution

$$A_2^e = c_3\left(\frac{\varrho}{a}\right)^{-m} \tag{2.26}$$

In the entire nonresonance region, where dissipation can be ignored, we have

$$\varphi^e = \frac{\omega}{k_\parallel^e c} A^e$$

At the boundary of the current channel at $\varrho = a$ we have the condition of matching which follows from eq. (2.15)

$$\left(1 - \frac{\omega^2}{k_\parallel^{e2} c_A^2}\right)\frac{dA^i}{dr} - \frac{dA_1^e}{dr} - 2\frac{m}{k_\parallel^e a^2}\frac{c_\delta^2}{c_A^2}A = 0 \tag{2.27}$$

When we derived this condition, we used the fact that $\tilde{n} = n_e/n_i \ll 1$ and that $A^i = A_1^e$ and $\varphi^i = \varphi^e$ are continuous at the boundary of the current channel. Using the matching condition (2.27) we can find the relationship between the coefficients in the solutions (2.24) and (2.25) and the difference between the logarithmic derivative at the boundary of the region of localization of the dissipative solution:

$$\Delta = \frac{1}{A}\frac{dA}{d\varrho}\bigg|_{\varrho_0 - \delta}^{\varrho_0 + \delta} \tag{2.28}$$

It is well known [2.4] that we need only this difference to determine the solution

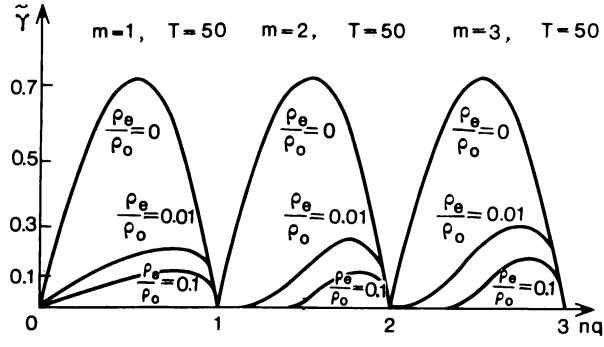

Fig. 2.6. Dimensionless growth rate as a function of nq for various ratios between the concentrations at periphery and at the centre of the plasma column.

When the plasma concentration outside the current channel tends to zero, eq. (2.31) reduces to the dispersion equation for the kink instability. We can find the growth rate of the tearing instability from eq. (2.31), assuming $\gamma_0^2 \to 0$.

The numerical solution of the dispersion equation (2.31) for the modes with $m = 1, 2, 3$ is shown in Figs. 2.5 and 2.6. The following values of the parameters were used in these calculations: $a = 20$ cm, $n_i = 5 \times 10^{13}$ cm^{-3}, and $J = 200$ kA. The temperature is given in electron-volts. Figure 2.5 shows that when the temperature of the peripheral plasma is higher than 10 eV and the relative concentration is $\tilde{n} = 0.1$, the instability regions for the second and third modes narrow down (the first mode is unstable at any temperature), that is, if we take into account the peripheral plasma, the stability gaps appear. Figure 2.6 shows these growth rates as functions of the relative plasma concentration at the column periphery.

The calculated results indicate that under real experimental conditions it is feasible to operate with low safety factor values $q(a) \lesssim 3$ since the temperature at the periphery of the plasma column is of the order of 10 eV. Note that an increase in dimensions of the current channel is accompanied with a decrease in the instability growth rate and extension of the range of the stable values of $q(a)$.

2.3. Influence of the Ballooning Effects on the Plasma Stability (Flute Oscillations)

Apart from the helical instability, in the plasma-carrying current in tokamaks there can develop the flute instability related to the curvature of the field lines.

The theoretical treatment of this instability is, typically, started from higher modes ($m \approx nq \gg 1$). Initially, the aim of such a treatment was to obtain general results independent of specific equilibrium configurations. But recently the results of numerical calculations have shown that it is just the higher modes that are most unstable, so that this approach is not of only an academic interest.

Saydom [2.8] was the first to derive the necessary criterion of stability of the current-carrying plasma for the cylindrical geometry (in a sense, the limiting case for tokamaks for $R \to \infty$);

$$\frac{1}{4} s^2 + \frac{2p'\varrho}{B_\theta^2} > 0 \tag{2.32}$$

Here $s' = q'\varrho/q$ is the parameter describing the shear.

It was clear, however, that to apply this criterion to torus we must alter it [2.6]. Firstly, when the cylinder is bent into a torus, this gives rise to an uncompensated force which is similar to the force expanding the car tire (clearly, this force increases with increasing plasma pressure and is a destabilizing factor). Secondly, a so-called magnetic well playing a stabilizing role is formed owing to the magnetic surfaces being pressed to the external contour [2.9].

Careful calculations of these effects for the tokamaks with circular magnetic surfaces yielded a somewhat unexpected result, namely, that the stabilization criterion converted into [2.10]

$$\frac{1}{4} s^2 + \frac{2p'\varrho}{B_\theta^2} (1 - q^2) > 0 \tag{2.33}$$

The terms responsible for the ballooning effect and the terms proportional to the pressure and corresponding to the magnetic well concelled out. And though this criterion was derived from the general geometric criterion of Mercier [2.11], there was something wrong here. The attempts to include higher terms in the expansion in curvature and pressure were unsuccessful in clarifying the situation.

It should be recalled that the standard technique universally employed in that period took into account, apart from the basic mode with the number m, two neighbouring satellites with $m + 1$ and $m - 1$ which were regarded as small (this was assumed to be natural since the toroidal curvature was small).

Criterion (2.33) indicates that when $q(\varrho) > 1$ the tokamak plasma is always stable with respect to the flute oscillations. The things had not been changed for a long time until the Prinston theorists [2.12] demonstrated by numerical calculations that the plasma stability deteriorated with increasing pressure, though criterion (2.33) completely ignores this effect. Moreover, the computer calculations gave such a mode structure for a moderate shear which had nothing in common with the theoretical predictions according to which the basic mode had to dominate and the other modes had to serve just as small additions. All the modes proved to occur equivalently and, moreover, to overlap.

A significant new contribution to the theory of the flute instability based on a very simple primary idea was made in [2.13].

Let us consider the Fourier expansion of a certain function describing the plasma oscillations, for instance, the potential $\varphi(\varrho, \theta, s)$:

$$\varphi = \sum_m \varphi_{mn}(\varrho)\, e^{i(m\theta - ks/R)} \tag{2.34}$$

For the sake of simplicity, we shall omit below the coordinate s with respect to which the tokamak is homogeneous. Assume that all harmonics in θ behave

equivalently. Then we shall take

$$\varphi_{mn}(\varrho) = \varphi_n[(m - nq(\varrho)] \tag{2.35}$$

Here any harmonic can be obtained from a certain harmonic by simple displacement along the radius ϱ. This can be easily seen if we replace $q(\varrho)$ with a linear function of ϱ, $q(\varrho) = q'\varrho$. Then for the mode m we have $m = nq'\varrho_m$ and for the mode $m + 1$ we have $m + 1 = nq'(\varrho_m + \Delta\varrho)$, that is, the next mode is displaced by $\Delta\varrho = 1/(nq') = \varrho_m/nqs$.

When we substitute the potential (2.34) with the coefficients of the type of eq. (2.35) into the equation of the flute oscillations (see Appendix), we obtain a system of coupled equations for the functions $\varphi_n[m - nq(a)]$. Since all these functions differ only in m which is equivalent to simple displacement along ϱ, then the natural approach to solving this system of equations is to expand the functions φ_n into the Fourier integral in $[m - nq(\varrho)]$:

$$\varphi_n[m - nq(\varrho)] = \int_{-\infty}^{\infty} F(y)\, e^{i[n - nq(\varrho)]y} dy \tag{2.36}$$

Then we obtain the transformation found in [2.13]. Now we have a differential equation for the Fourier transform $F(y)$, which is easier to analyze than an infinite system of coupled differential equations for $\varphi_n[m - nq(\varrho)]$.

The method of equivalent harmonics makes possible the asymptotically correct (for $nq \to \infty$) analysis of stability. This, naturally, leads to the question how to find an analytical criterion without using old approximate methods.

To illustrate the method of equivalent harmonics and the analytic procedure for solving the resulting differential equation let us treat a simple model equation describing the flute oscillations in the toroidal plasma. A comparison with the exact equation (see Appendix) shows that the model equation, though it is relatively simple, describes the essential features of the real situation eliminating the complications due to the aspects of secondary significance.

Let us illustrate in brief the derivation of the model equation. If we consider the boundary of the plasma stability, then practically all the information can be obtained from the equilibrium equation.

$$\nabla p = \frac{1}{c}[\mathbf{j} \times \mathbf{B}] \tag{2.37}$$

which yields $\mathbf{j}_\perp = (c/B^2)\,[\mathbf{B} \times \nabla p]$. The longitudinal current component $\mathbf{j}_\parallel$ can be found from the projection of $(4\pi/c)\mathbf{j} = \text{curl } \mathbf{B}$ on $\mathbf{B}$. In a low-pressure plasma the perturbed magnetic field is related only to the longitudinal component of the vector potential $\mathbf{B} = \text{curl } (\mathbf{B}_0/b)A_\parallel = -[(\mathbf{B}_0/\mathbf{B}) \times \nabla A_\parallel] = -[\mathbf{b} \times \nabla A_\parallel]$. Then we have $(4\pi/c)\tilde{j}^{\sim} = -\Delta A_\parallel$. Substitution of $\tilde{j}_\parallel$ and $\tilde{j}_\perp$ into $\text{div } \mathbf{j} = 0$ yields

$$(\mathbf{b} \cdot \nabla)\Delta_\perp \frac{c}{4\pi} A_\parallel + c[\mathbf{B} \times \nabla\tilde{p}] \cdot \nabla \frac{1}{B_0^2} = 0 \tag{2.38}$$

Another relation between $\tilde{p}$ and $A_\parallel$ follows from the longitudinal projection of eq. (2.37) $(\mathbf{B} \cdot \nabla p) = 0$, that is, $\mathbf{B} \cdot \nabla p_0 + \mathbf{B}^0 \cdot \nabla p = 0$. If we take $A_\parallel = (\mathbf{b} \cdot \nabla)\varphi$, then this equation can be integrated in the general form: $\tilde{p} = (dp_0/d\varrho)\varphi$. Substituting this equation into eq. (2.38), we obtain

$$(\mathbf{b} \cdot \nabla)\Delta_\perp(\mathbf{b} \cdot \nabla)\varphi + c\frac{dp_0}{d\varrho}[\mathbf{B}^0 \times \nabla\varphi] \cdot \nabla \frac{1}{B_0^2} = 0 \tag{2.39}$$

If we had not assumed the frequency to be zero, we would obtain, instead of eq. (2.39)

$$\omega^2\Delta\varphi + (\mathbf{b} \cdot \nabla)\Delta_\perp(\mathbf{b} \cdot \nabla)\varphi + c\frac{dp_0}{d\varrho}[\mathbf{B}^0 \times \nabla\varphi] \cdot \nabla \frac{1}{B_0^2} = 0 \tag{2.40}$$

Now it is quite clear that the first two terms describe the Alfven oscillations and the last term is due to the toroidal curvature.

Appendix presents a more rigorous and consistent derivation of the equation for the flute oscillations, based on the variational principle. In the simplified equation we shall take into account the fact that the metric differs from the cylindrical metric when we write the operator $(\mathbf{b} \cdot \nabla)$, and we shall retain only the term proportional to $\cos\theta$ among the terms due to the curvature (of course, we shall lose the effect of the mean magnetic well in this way).

If we expand the function φ into the Fourier series $(\varphi = \sum_m \varphi_{mn} \exp(im\theta))$, we obtain the following system of coupled equations for the harmonics:

$$\nabla_\perp(\gamma^2 + k_m^2) \cdot \nabla_\perp\varphi_{mn} + \frac{1}{2}\frac{m^2}{\varrho^2}\epsilon\beta_J(\varphi_{m+1} + \varphi_{m-1}) = 0 \tag{2.41}$$

Here $k_m = m - nq$ is proportional to the longitudinal component of the wave vector, and $\gamma^2 = -\omega^2$. This will be our primary model equation.

Substituting $\varphi_{mn} = \varphi_n(m - nq)$ and performing the Fourier transformation in the variable $(m - nq)$, we obtain

$$\frac{d}{dy}(1 + s'y^2)\frac{dF}{dy} + (\gamma^2 + \alpha\cos y)F = 0 \tag{2.42}$$

where $\alpha = 4\epsilon\beta_J$ and $s' = q'\varrho/q$. Clearly, eq. (2.42) is much simpler than the infinite system of linked equations (2.41). A special asymptotic method of solution of the ordinary differential equations with periodic or nonperiodic coefficients has been designed for solving equations of the type of eq. (2.42) (see [2.14]).

The method can be described as follows. Write down the variational principle for eq. (2.42). Since eq. (2.42) contains two scales $y \sim 1$ and $y \sim 1/s$ which greatly differ when $s \ll 1$ (this is just the case in reality), this equation can be solved by averaging (the method of van der Paul and Bogoliubov). The resulting eigenfunctions of the form of $F = F_1(sy) + F_2(sy)\cos y$ should be substituted into the equation for the variational principle. This makes it possible to include the terms of the form of $\exp(-1/|s|)$ (which are not analytic in s) that cannot be taken into account by the conventional averaging method.

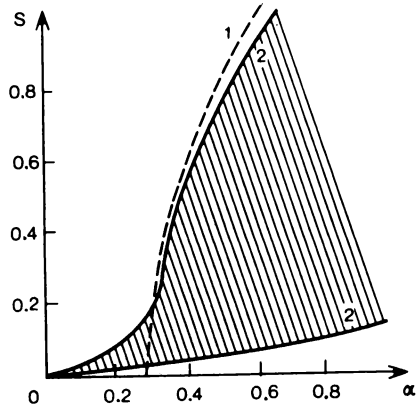

Fig. 2.7. Numerical solution of the equation from [2.13] (curve *1*); analytical solution of this equation by means of the asymptotic variational method (curves *2*). The instability region is shaded.

We can see how highly effective is the variational asymptotic method from the results of [2.13], for instance, curve *1* in Fig. 2.7 calculated by numerical integration (the region of instability is to the right of this curve). We have solved this equation analytically showing that, in fact, there are two curves starting at the origin (the curves *2* in Fig. 2.7; the region of instability is between them).

The equation of the flute oscillations of the plasma, which is applicable to an arbitrary cross section of the plasma column, can be written in the form [2.14] (see Appendix):

$$\frac{d}{dy}\left[\frac{g_{11}}{\sqrt{g}} - 2\frac{g_{12}}{\sqrt{g}}\frac{sy}{\varrho} + \frac{g_{22}}{\sqrt{g}}\frac{s^2y^2}{\varrho^2}\right]\frac{dF}{dy} - \frac{4\pi p_0' R^2 q^2}{\sqrt{g}B^*}\left(\frac{\partial}{\partial\varrho}\frac{1}{B^*} - \frac{sy}{\varrho}\frac{\partial}{\partial y}\frac{1}{B^*}\right)F = 0 \quad (2.43)$$

Here the specific form of the expression for g_{ik} is determined by the cross section of the magnetic surfaces. These metric coefficients for the circular magnetic surfaces are given in [2.7].

If we apply the variational asymptotic method to eq. (2.43), we can obtain the analytical criterion for the ballooning modes of the flute instability in the tokamaks with circular magnetic surfaces [2.7]:

$$\frac{1}{2}s^2 + \alpha\epsilon\left(1 - \frac{1}{q^2} - \frac{7}{4\epsilon}e^{-1/|s|}\right) - \frac{3}{4}s\alpha^2 > 0 \quad (2.44)$$

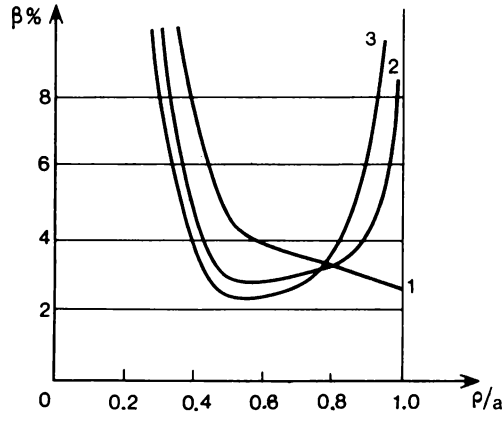

Fig. 2.8. Dependence of β^* on the relative radius for the toroidal plasma column ($R/a = 4.6$) with the circular cross section for the given current profile ($q_0 = 1$, $q(a) = 1.6$) and various pressure profiles ($p = p_0(1 - \varrho^2/a^2)^l$). 1) $l = 1$; 2) $l = 1.5$; 3) $l = 2$.

Let us analyze the individual terms in criterion (2.44). We have already met some of the terms, namely, the first three terms in criterion (2.33). The most strange term is, apparently, the term proportional to $\exp(-1/|s|)$. To understand the origin of this term, we shall analyze eqs. (2.41) retaining in them only two neighbouring harmonics with m and $m + 1$. Equation (2.41) shows that for $m \gg 1$ these harmonics satisfy the same equation [as in the case of helical instability; see eq. (2.9)] at the midpoint between the points $\varrho_m[m = nq(\varrho_m)]$ and ϱ_{m+1} $[m + 1 = nq(\varrho_{m+1})]$. Thus, we once more have the case of intersection of branches. In the case of the helical instability the eigenfunctions φ_m and φ_{m+1} in fact overlapped entirely; in this case the eigenfunction are localized near the resonance points and only their tails overlap so that, since φ_{mn} decline exponentially, the intersection gives $\exp(-1/|s|)$. Such a dependence on s is clear: since the distance between the singular points $\varrho_{m+1} - \varrho_m \sim 1/|s|$, then the distance increases with decreasing $|s|$, and overlapping is reduced. Obviously, if we included three harmonics, rather than two, we would obtain the terms with $\exp(-2|s|)$, and so on. However, they contain the additional factor $\epsilon\beta_J \ll 1$ and are, therefore, insignificant.

The last term in criterion (2.44) describes the ballooning effect associated with the shear ($s\epsilon^2\beta\mathfrak{z}$), and is destabilizing for declining current density. Now we can see that the concelling out of the ballooning effects in criterion (2.33) would, in fact, occur only for $s \sim \epsilon^2 \ll 1$.

Criterion (2.44) is local in character and therefore it makes it possible to determine at which point along the plasma column radius the ballooning instability starts to develop at first. Figure 2.8 shows the plots of the critical pressure

$\beta^* = 8\pi\langle p^{-2}\rangle^{1/2}/B_0^2$ as a function of the relative radius for three pressure profiles. The plots indicate the pressure for which at a given point of the plasma column there appears the ballooning instability for given distributions of the pressure and the current density. Since the ballooning effect is associated with the shear, the flattening of the current profile makes it possible to elevate the critical pressure.

Variation of the cross-section shape of the magnetic surfaces affects the stability condition [2.15]. This leads to the natural question: how to change criterion (2.44) to take into account a noncircular shape of the magnetic surfaces? Before analyzing the effect of the shape of the magnetic surfaces on the ballooning instability, let us analyze in more detail eq. (2.44) to obtain a qualitative estimate of the primary effect. The first, stabilizing term in criterion (2.44) is associated with the shear, and the second, destabilizing term is associated with the curvature of the field lines. The third, stabilizing, term is proportional to the "geometric" part of the magnetic well which is automatically produced in the tokamak owing to the toroidal curvature ($V_0'' \sim \epsilon^2 \sim q^2$) and is not related to the plasma pressure. The criterion implies that for $q^2(\varrho) \sim 1$ (this is just the condition of the greatest practical interest) the stabilizing effect of the "geometric" magnetic well practically completely disappears, and the permissible plasma pressure can, generally, be strictly limited. The fourth term is destabilizing and related to the shear and the plasma pressure. The fifth term describes the ballooning effect weakened by the deepending of the magnetic well owing to the plasma pressure.

The depth of the magnetic well is known to be the characteristic of the magnetic configuration, which is most sensitive to the variation of the shape of the magnetic surfaces [2.9]. Therefore, in the first approximation the effect of the variation of their shape should be expected to be reflected by the third and fifth terms of criterion (2.44).

Let us consider the tokamak with noncircular magnetic surfaces which are described by the following equation in the coordinate system related to the "geometric" axis of the given magnetic surface [2.2]:

$$\psi - (1-e^2)^{-1/2}\left\{(1 - e\cos 2\omega)\varrho^2 + Q\epsilon\varrho^2 e^{\gamma/2}\left[\left(1-\frac{e}{2}\right)\cos 3\omega + \frac{3}{2}e\cos\omega\right]\right\} = \text{const} \tag{2.45}$$

Here $e = (k^2-1)/(k^2+1)$, $k = l_z/l_R$ is the parameter describing the ellipticity of the magnetic surfaces (l_z and l_R are the semiaxes of the ellipse), and Q is the parameter describing triangularity. To simplify the calculations and the resulting criterion, let us consider the case when the magnetic surfaces do not differ greatly from elliptical ones ($Q \lesssim 1$). Using the variational asymptotic method, we can obtain the following criterion of stability for the tokamak with noncircular magnetic surfaces [2.16]:

$$\frac{1}{2}s^2 + \alpha\epsilon\left[-\frac{1}{2}V_0''B_0^2R\sqrt{1-e^2} - \frac{1}{q^2}\right] - \frac{7}{4}\alpha k^{-1/2}e^{-1/|s|} - \frac{\alpha^2}{4}(3sf_1 + e^2f_2) > 0 \tag{2.46}$$

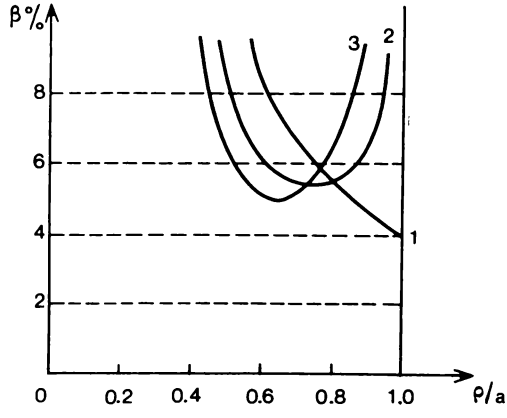

Fig. 2.9. Dependence of β^* on ϱ/a for the plasma column with the D-shaped cross section for the same parameters as in Fig. 2.8.

Here V_0'' is the "geometric" part of the magnetic well:

$$V_0'' = -\frac{2}{B_0^2 R\sqrt{1-e^2}}\left(1 - \frac{3}{2}e\frac{1+e}{2+e} + 6eQ\frac{1-e}{2+e}\right)$$

$$f_1 = 4k^{3/2}\frac{3+k^2}{(1+k^2)(1+3k^2)},$$

$$f_2 = \frac{1}{k^2(1+3k^2)}\left(\frac{1+k^2}{1+k}\right)^3 \qquad (2.47)$$

As we expected, criterion (2.46) differs from criterion (2.44) in the form of the geometric magnetic well (2.47). It can be seen from eq. (2.47) that in the absence of ellipticity ($e = 0$, $k = 1$) triangularity does not change the depth of the magnetic well. But ellipticity, even in the absence of triangularity, significantly alters the magnetic well. The case of the most practical interest is that of the combined effect of ellipticity and triangularity (D-shaped magnetic surfaces). The ellipticity also greatly changes the ballooning effect (decreases when the column is elongated along the symmetry axis of the torus) which is proportional to the shear (the function f_1). Moreover, the criterion contains a new destability term proportional to the squared ellipticity ($e^2 f_2$). This term is the difference between the ballooning effect not related to the shear and the deepening of the magnetic well owing to the plasma pressure [2.2].

Figure 2.9 presents the calculated critical plasma pressures in the tokamak with the D-shaped cross section for the same pressure and current distributions as in the tokamak with the circular cross section in Fig. 2.8. A comparison of Figs. 2.8 and 2.9 indicates that we can increase the critical β^* by a factor of 2 to 2.5 by altering the cross-section shape of the plasma column.

2.4. Thresholdless Dissipative Ballooning Modes

The flute instability of plasma in the presence of dissipation was first analyzed in [2.4]. In this study the curvature was simulated in the plane geometry by means of the effective gravity, and the inclusion of finite conductivity was shown to lead to instability in the system which had been stable within the framework of the ideal hydrodynamics. The stability of the toroidal plasma column with a finite conductivity with respect to the flute perturbations was analyzed in [2.17], where the necessary stability criterion, similar to the Mercier criterion for the ideal plasma [2.11], was derived for the low-pressure plasma. The main effect of the inclusion of finite conductivity was the disappearance of the stabilizing effect of the shear. The effect of finite pressure on the flute dissipative instability was analyzed in [2.18] and, independently, in [2.19]. The toroidal plasma column was shown to be stable for the pressure gradients below the critical value. The instability had a threshold and, when the ballooning effect exceed the stabilization due to the magnetic well, the instability started to develop with the growth rate $\gamma \sim \eta^{1/3}$, where η is the plasma resistance.

The advances in the study of the ballooning modes of the flute instability of the ideal plasma renewed the interest to the analysis of the dissipative flute instability. The reason was that the necessary criterion of stability for the ideal ballooning modes proved to be more restrictive than the Mercier criterion, owing to the presence of the new destabilizing terms related to the shear [2.14]. This had led to a paradoxical situation when the threshold of the dissipative flute instability [2.18, 2.19] proved to be higher than the threshold of the ideal ballooning modes [2.14].

The first attempt to include dissipation in the ballooning modes was made in [2.20], where it was shown that the ballooning modes with a small growth rate $\gamma \sim \eta$ exist at any pressure gradient. This result did not answer the above paradox since the threshold instability has a much higher growth rate $\gamma \sim \eta^{1/3}$.

In this section we shall find an answer to this question as we shall demonstrate that the dissipative ballooning modes have no pressure gradient threshold and develop with a high growth rate $\gamma \sim \eta^{1/3}$.

We shall analyze below the dissipative ballooning modes using the equations of one-fluid magnetohydrodynamics, including compressibility. According to the method employed in [2.5], the plasma disturbances are described by the electrostatic potential $\tilde{\varphi}$, the longitudinal component of the vector potential $\tilde{A}$ and the perturbed pressure $\tilde{p}$. The transformation suggested in [2.13] in the limit of large azimuthal numbers ($m \approx nq \gg 1$) reduces the linearized initial system of equations to two equations for the Fourier transforms φ and p [2.21]:

$$\frac{d}{dy}\frac{G}{(1+G/\Gamma)}\frac{d\varphi}{dy} - \gamma^2\tau_\theta^2(1+s^2y^2)\varphi + \frac{\alpha R B^*}{2}\left(\frac{\partial}{\partial \varrho}\frac{1}{B^*} - \frac{sy}{\varrho}\frac{\partial}{\partial y}\frac{1}{B^*}\right)p = 0 \quad (2.48)$$

$$\left(1 - \frac{1}{\gamma^2\tau_c^2}\frac{d^2}{dy^2}\right)p = \left[1 - \frac{1}{\gamma^2\tau_c^2}\frac{d}{dy}\frac{1}{(1+G/\Gamma)}\frac{d}{dy}\right]\varphi \quad (2.49)$$

Here $s = q'\varrho/q$, $\alpha = -8\pi p' Rq^2/B^2$, $\tau_\theta = Rq/c_A$, $c_A^2 = B^2/4\pi\varrho_0$, $\tau_c = Rq/c_s^2$, $c_s^2 = \gamma_0 p_0/\varrho_0$, $\tau_\perp = 4\pi\sigma a^2/c^2$, a and R are the minor and major radiuses of the torus, q is the safety factor, $\Gamma = \gamma\tau_\perp/n^2q^2$, $G = \varrho[g_{11}/\sqrt{g} + (s^2y^2/\varrho^2)(g_{22}/\sqrt{g}) - 2(sy/\varrho)(q_{12}/\sqrt{g})]$, and g_{ik} are the metric coefficients of the surface coordinate system with the straight field lines [2.10].

For the ideally conducting plasma we have $\gamma \sim 1/\tau_\theta$, then $G \ll \Gamma$ and the system of equations (2.48) and (2.49) reduces to one second-order equation for φ (see eq. (2.44)).

In the case of nonideally conducting plasma we have $\gamma \ll 1/\tau_\theta$ and eqs. (2.48) and (2.49) have two different scales, namely, $y \sim 1$ and $y \gg 1$. Hence, we can apply the van der Paul averaging method to these equations.

The ballooning modes in tokamak for $nq \gg 1$ are the perturbations localized on the column radius, which correspond to large characteristic y values in the averaged equation. For $y^2 \gg M^2/\Gamma^2$ eqs. (2.48) and (2.49) are reduced to one averaged equation. For the circular magnetic surfaces this equation has the form

$$\Gamma p'' - \left\{ \frac{\Gamma^2}{N^2}(1 + s^2y^2) + \alpha V_0 - \frac{\alpha^2(1 + s^2y^2 + M^2/\Gamma)}{2\Gamma(1 + M^2/\Gamma^2)[1 + \Gamma(1 + s^2y^2)/N]} \right\} p = 0 \qquad (2.50)$$

Here $M = \tau_\perp/\tau_0 n^2q^2$ and $N = \tau_\perp/\tau_\theta n^2q^2$ are the parameters describing the ratio of the skin time to the sound time and the Alfven time, respectively, $M^2 = \gamma_0\beta N^2$, where γ_0 is the adiabatic exponent (in the high-temperature plasma $N \gg 1$), and V_0 is the magnetic well in the tokamak [2.10].

For the reverse limiting case $\gamma^2 \ll M^2/\Gamma^2$ the instability can be shown to be significantly weakened. The condition $\gamma^2 \gg M^2/\Gamma^2$ in the conventional notation has the form $\gamma^2 \gg k_\parallel^2 c_s^2$ and implies that the averaged perturbation of the pressure does not have time to level off along the field lines.

We can see from eq. (2.50) that the form of its potential significantly depends on the ratios s/s_k (where $s_k = \alpha^{1/2}/N^{1/2}$), α/α_k (where α_k is found from the condition $\alpha/2 = V_0$), and β/β_k (where $\beta_k = \alpha^{4/3}/N^{2/3}$). For every low shears $s \leq s_k$ and pressures $\beta = \beta_k$ eq. (2.50) yields a low growth rate of the order of the inverse skin time $\Gamma = \alpha/2V_0$, as in [2.20].

Here we shall analyze the systems with the shear values in the range of practical interest, $s \sim 1$ (naturally, $s \gg s_k$). We shall solve eq. (2.50) with a variational method. Write down the functional corresponding to this equation and substitute as the test function the function of the form $p = 1/(\lambda^2 + y^2)$, where λ is the variational parameter.

After variation we obtain the following expressions for determining the growth rate and parameter λ:

$$(\Gamma^3 + \gamma_0\beta N^2\Gamma)\left[1 - N^2\left(\frac{\alpha^2}{2} - \alpha V_0\right)/2s^2\Gamma^2\lambda^2\right] = \alpha^2N^2/2 \qquad (2.51)$$

$$\alpha^2\left(\frac{\alpha^2}{2} - \alpha V_0\right)/\Gamma^2\lambda^2 + s^3\Gamma^{1/2}\lambda/N = N^2/\Gamma\lambda^4 \qquad (2.52)$$

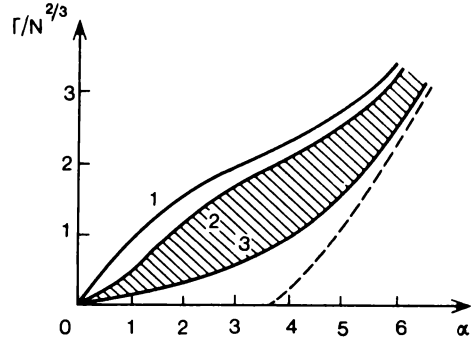

Fig. 2.10. The normalized growth rate $\Gamma/N^{2/3}$ as a function of α for various values of $\tilde{\beta} = \beta\gamma_0 N^{2/3}$; 1) $\tilde{\beta} = 0$; 2) $\tilde{\beta} = 1$; 3) $\tilde{\beta} = 10$. The shaded region corresponds to the high-temperature plasma. The dotted line represents the threshold growth rate of the nonpotential gravitational-dissipational instability.

For high pressures $\beta \gg \beta_k$, when the perturbation of the magnetic field is significant, the expression for the growth rate has the form

$$\Gamma = \begin{cases} \dfrac{N^{2/3}}{s^{2/3}} \left(\dfrac{\alpha^2}{2} - \alpha V_0 \right)^{2/3} & \text{for} \quad \alpha \geq \alpha_k \\ 0 & \text{for} \quad \alpha \leq \alpha^k \end{cases} \tag{2.53}$$

This growth rate corresponds to the nonpotential gravitational-dissipational instability [2.18, 2.19] which has a pressure gradient threshold.

For low plasma pressures, $\beta \leq \beta_k$, $\alpha \leq \alpha_k$, and eqs. (2.51) and (2.52) can be reduced to

$$\Gamma^3 + \gamma_0 \beta N^2 \Gamma = \alpha^2 N^2/2 \tag{2.54}$$

A qualitatively new result follows from eq. (2.54), namely, that the growth rate of the dissipative ballooning modes does not have a threshold in the pressure gradient. The instability starts to develop for any small pressure gradient with the growth rate $\Gamma \sim \alpha^{2/3} N^{2/3}$ [$\gamma \sim (1/\tau_s)\ (\tau_s/\tau_\theta)^{2/3}$]. This fully eliminates the paradoxical situation discussed above.

Figure 2.10 shows the growth rate of the dissipative ballooning modes as a function of the plasma pressure gradient α for various plasma pressures. Curve *1* corresponds to $\beta = 0$ or the fully compressible fluid, $\gamma_0 = 0$; curve *2* corresponds to $\tilde{\beta} = \beta\gamma_0 N^{2/3} = 1$, and curve *3* corresponds to $\tilde{\beta} = 10$. The region between curves *2* and *3* corresponds to the high-temperature plasma. The dotted line represents the threshold growth rate (2.53) which was, in fact, derived under the assumption that the sound speed was infinite. Thus, the ion sound smoothed the perturbations of pressure along the field lines and the instability did not grow for $\alpha < \alpha_k$. If the speed of ion sound is finite, we encounter an essentially different situation; the perturbations of pressure do not have time to

be smoothed along the field lines and for any pressure gradient there occurs the ballooning instability developing with the Alfven oscillations. The growth rate of these dissipative ballooning modes decreases with increasing plasma pressure, as can be seen from Fig. 2.10.

It is interesting to find the region of localization for this instability, apart from its growth rate. The characteristic size $\Delta\varrho$ of the region of localization in the real space is related to the characteristic width of localization in the y space by $\Delta\varrho = \varrho/nqs\Delta y$. Using eqs. (2.51) and (2.52), we can calculate $\Delta y \approx \lambda$ for all values of the parameters α and β. For instance, the results for two characteristic cases $\alpha \lesssim \alpha_k$, $\beta \sim \beta_k$ and $\alpha > \alpha_k$, $\beta \sim \beta_k$ are $\Delta\varrho \sim \varrho\alpha^{1/5}/nqsN^{2/5}$ and $\Delta\varrho = \varrho\alpha^{1/3}/nqsN^{1/3}$.

Using the above estimates and the well-known dimensional expression for the transfer coefficients $\chi \sim \gamma/k_\perp^2$ (in this case this is, apparently, the estimate for the turbulent heat conductivity), we can find for the low-pressure plasma $\chi \sim (a^2/\tau_s)(\alpha^{16/15}/N^{2/15})$, and for the high-pressure plasma $\chi \sim (a^2/\tau_s)\alpha^2$. In both cases the characteristic energy time is of the order of the skin time, and if these estimates are valid, then the dissipative ballooning in stability is not significant for the experiments.

Conclusion

The linear theory is just a first step in the analysis of the effect of the hydromagmetic instabilities in the experiments. Only the nonlinear treatment can definitely demonstrate that a given type of hydromagnetic instability is possible.

A fairly large number of theoretical studies have treated the nonlinear stages of the helical and tearing instabilities, resulting in improved understanding of them. However, in connection with our studies of the effect of the peripheral plasma on the column stability (Sec. 2.2), we believe that the formation and reconnection of the islands in currentless plasma should be analyzed in more detail. The nonlinear stage of the flute ballooning oscillations has not been studied at all. In particular, there is practically no understanding of the relative contributions of the ideal and dissipative ballooning modes and their effect on plasma confinement. Apparently, the nonlinear stage of the ballooning modes cannot be analyzed without taking into account dissipation. This is the field of the highest current interest in the MHD theory of plasma.

Appendix

Simplification of the variational principle

It is convenient to make use of the coordinate system with straight field lines [2.2] in which a length element has the form

$$dl^2 = g_{11}\,d\varrho^2 + g_{22}\,d\theta^2 + 2g_{12}\,d\varrho = d\theta + g_{33}\,ds^2 \qquad \text{(2.A.1a)}$$

where the coordinate ϱ characterizes the magnetic surface. Since we consider the axially symmetric torus, the metric coefficients g_{ik} are independent of the longitudinal coordinate s. In this coordinate system the ratio between the

equilibrium contravariant field components $B^\theta/B^z = B_J/\sqrt{g} = B_0/g_{33} = qR$ is independent of the angular variable θ (here $B_J = J/2na$, J is the longitudinal current, and B_0 is the longitudinal field) and this fact greatly simplifies the stability analysis.

It is well known that the equations of motion of the ideal plasma can be derived from the variational principle. The variational treatment of the stability problem in many cases proves to be more convenient than the direct use of differential equations (this is especially true for complex systems). In any case, substituting a test function into the variational principle, we obtain the necessary criterion of stability of the sufficient criterion of instability. The more accurate is the test function the closer we are to the necessary and sufficient criterion (that is, the exact solution of the problem). Moreover, the variational principle tends to improve the results; for instance, if we make an error $\delta \ll 1$ in the test function, the error in the expression for the oscillation spectrum proves to be of the order of δ^2.

The variational functional is the difference between the kinetic energy T and the potential energy W:

$$T = \frac{1}{2}\int_{V_i} \varrho_0 \left(\frac{\partial \xi}{\partial t}\right)^2 dV \tag{2.A.1}$$

$$W = \frac{1}{2}\int_{V_i} \left\{ \gamma_0 p_0 (\operatorname{div}\xi)^2 + \frac{1}{4\pi}\left(\operatorname{curl}\,[\xi \times \mathbf{B}]\right)^2 + \xi\cdot\nabla p_0 \operatorname{div}\xi \right.$$
$$\left. - \frac{1}{4\pi}[\xi \times \operatorname{curl}\mathbf{B}]\cdot\operatorname{curl}\,[\xi \times \mathbf{B}] \right\} dV + \frac{1}{8\pi}\int_{V_e} (\operatorname{curl}\mathbf{A})^2\, dV \tag{2.A.2}$$

Here ξ is the plasma displacement, V_i is the integration region in plasma, and V_e is the integration region in a vacuum. We shall transform the expression for W omitting the first term related to the plasma compressibility since it is known not to affect the boundary of stability.

Equation (2.A.2) is too complicated since the displacement vector ξ generally contains three components which are, in fact, related to each other, so that eq. (2.A.2) does not lend itself to explicit analysis.

The general method of simplification of eq. (2.A.2) suggested in [2.6] is applicable to the systems in strong longitudinal magnetic fields (the small parameters in it are the squared ratio $(B_J/B_0)^2$ between the field B_J of the current and the longitudinal field B_0 and β for the total field, $\beta = \beta_J (B_J/B_0)^2$; in modern tokamaks we have $\beta_J \sim 1$, so that these parameters are close to each other in them).

The main physical idea here is the elimination of the magneto-acoustic oscillations. Ignoring the terms of the order of $(B_J/B_0)^2$ and β in comparison with unity [2.3], we obtain the condition

$$\tilde{B}^r = 0 \tag{2.A.3}$$

where $\tilde{B}^{\alpha}$ is the contravariant component of the perturbed magnetic field. On the other hand, if we replace the displacement components with the quantities $\xi^{\varrho}_{\perp}$, $\xi^{\theta}_{\perp}$, and $\xi^{s}_{\parallel}$, which are given by

$$\xi^{\varrho} = \xi^{\varrho}_{\perp}, \quad \xi^{\theta} = \xi^{\theta}_{\perp} - \frac{B^{\theta}}{B^{s}} \xi^{s}_{\parallel}, \quad \xi^{s}_{\parallel} - \frac{B_{\theta}}{B_{s}} \xi^{\theta}_{\perp} \tag{2.A.4}$$

and have the sense of the components of the longitudinal ($\xi_{\parallel}$) and transverse ($\xi_{\perp}$) displacements, then we can write the following expressions for the components of the perturbed magnetic field, ignoring the small terms of the order of $(B_{\perp}/B_0)^2$:

$$\tilde{B}^{\varrho} = (\mathbf{B} \cdot \nabla)\, \xi^{\varrho}_{\perp}$$

$$\tilde{B}^{s} = \frac{1}{\sqrt{g}} \left(\frac{\partial}{\partial s} \sqrt{g} B^{s} \xi^{\theta}_{\perp} - \frac{\partial}{\partial \varrho} \sqrt{g} B^{s} \xi^{\varrho}_{\perp} \right) \tag{2.A.5}$$

$$\tilde{B}^{s} = \frac{(-1)}{\sqrt{g}} \left(\frac{\partial}{\partial \varrho} \sqrt{g} B^{s} \xi^{\varrho}_{\perp} + \frac{\partial}{\partial \theta} \sqrt{g} B^{s} \xi^{\theta}_{\perp} \right) \tag{2.A.5}$$

The condition $\tilde{B}^{s} = 0$ implies that the displacement components are expressed in terms of one function φ:

$$\xi^{\varrho}_{\perp} = \frac{(-1)}{\sqrt{g} B^{s}} \frac{\partial \varphi}{\partial \theta}, \qquad \xi^{\theta}_{\perp} = \frac{1}{\sqrt{g} B^{s}} \frac{\partial \varphi}{\partial \varrho} \tag{2.A.6}$$

The function φ has the sense of the electrostatic potential. Now we can rewrite the field components (2.A.5) in the symmetric form:

$$\tilde{B}^{\varrho} = -\frac{(1)}{\sqrt{g}} \frac{\partial}{\partial \theta} \frac{\mathbf{B} \cdot \nabla}{B^{s}} \varphi, \quad \tilde{B}^{\theta} = \frac{1}{\sqrt{g}} \frac{\partial}{\partial \varrho} \frac{\mathbf{B} \cdot \nabla}{B^{s}} \varphi \tag{2.A.7}$$

Substituting eq. (2.A.6) for displacements and eq. (2.A.7) for the field components into eq. (2.A.2) for the potential energy W, we can readily rewrite it in the following form [2.24]:

$$W = \frac{1}{2} \int_{V_i + V_e} \left\{ \frac{1}{4\pi} \left[g_{11} \left(\frac{1}{\sqrt{g}} \frac{\partial}{\partial \theta} \frac{\mathbf{B} \cdot \nabla}{B^{s}} \theta \right)^2 + g_{22} \left(\frac{1}{\sqrt{g}} \frac{\partial}{\partial \varrho} \frac{\mathbf{B} \cdot \nabla}{B^{s}} \varphi \right)^2 \right.\right.$$
$$\left. - \frac{2 g_{12}}{g} \frac{\partial}{\partial \theta} \frac{\mathbf{B} \cdot \nabla}{B^{s}} \varphi \cdot \frac{\partial}{\partial \varrho} \frac{\mathbf{B} \cdot \nabla}{B^{s}} \varphi \right] - \frac{dp_0/d\varrho}{\sqrt{g} B^{s}} \frac{\partial \varphi}{\partial \theta} \cdot \frac{1}{\sqrt{g}} \frac{D(\varphi, 1/B^{s})}{D(\varrho, \theta)}$$
$$\left. + \frac{j^{s}}{c \sqrt{g} B^{s}} \frac{D[\varphi, (\mathbf{B} \cdot \nabla / B^{s}) \varphi]}{D(\varrho, \theta)} \right\} \sqrt{g}\, d\varrho\, d\theta\, ds \tag{2.A.8}$$

The three terms in the brackets in eq. (2.A.8) describe the perturbed energy of the magnetic field; they vanish for the perturbations which are constant along the field line $(\mathbf{B} \cdot \nabla / B^{s}) \varphi = 0$. The second term proportional to $dp_0/d\varrho$ and to the curvature of the field lines describes the flute oscillations. The last term containing j^{s} is responsible for the helical instability.

Integration in eq. (2.A.8) is performed over the plasma and vacuum since we formally extend the displacement (and the potential φ) continuously into the vacuum region.

This description with the longitudinal component of the vector potential, A_l, and the electrostatic potential for the transverse flow of the plasma was first suggested in [2.22]. In other words, the simplified variational principle corresponds to the equations of [2.22] expanded in powers of $1/B_0$.

The variational principle (2.A.8) can be easily applied to the treatment of various specific instabilities.

For instance, taking the test function in the form

$\varphi_1 = c_1 \varrho^m$ for $\varrho < a$ and $\varphi_2 = c_2 \varrho^{-m}$ for $\varrho > a$,

we obtain the splitting of the kink instability modes described in Sec. 2.1.

Equation for small-scale oscillations

Take the perturbed potential in the form [2.13]

$$\varphi(\varrho, \theta, s) = \sum_m e^{-im\theta} \int_{-\infty}^{\infty} e^{+imy} \hat{\varphi}(\varrho, y, s)\, dy \tag{2.A.9}$$

where $\hat{\varphi}(\varrho, y, s)$ can be conveniently written in the eikonal form:

$$\hat{\varphi}(\varrho, y, s) = F(a, y)\, e^{-inq(\varrho)y + i(h/R)s} \tag{2.A.10}$$

Here the phase is constant along the magnetic field but varies very rapidly in the directions perpendicular to the field for $m \approx nq \gg 1$. The amplitude $F(\varrho, y)$ is a slow-varying function in comparison with the phase and, thus, can be expanded in powers of the small parameter $1/nq$.

Substituting eq. (2.A.9) into eq. (2.A.8) for the potential energy and retaining only the principal terms for $nq \to \infty$, we can easily obtain

$$W = \frac{1}{2} \int_0^a (nq)^2 \left(\frac{B^\theta}{B^s}\right)^2 da \int_{-\infty}^{\infty} \left\{ G(\varrho, y) \left(\frac{\partial F}{\partial y}\right)^2 + \frac{4\pi p_0' k^2 q^2}{\sqrt{g}\, B^s} \left[\frac{\partial}{\partial \varrho} \frac{p}{B^s} - \frac{sy}{\varrho} \frac{\partial}{\partial y} \left(\frac{1}{B^s}\right) \right] F^2 \right\} dy \tag{2.A.11}$$

where

$$G(\varrho, y) = \varrho \left(\frac{g_{11}}{\sqrt{g}} + \frac{g_{22}}{\sqrt{g}} \frac{s^2 y^2}{\varrho^2} - 2 \frac{g_{12}}{\sqrt{g}} \frac{sy}{\varrho} \right)$$

Variation of this functional yields the sought equation:

$$\frac{\partial}{\partial y} \left[G(\varrho, y) \frac{\partial F}{\partial y} \right] - \frac{4\pi p_0' R^2 q^2}{\sqrt{g}\, B^s} \left[\frac{\partial}{\partial \varrho} \frac{1}{B^s} - \frac{sy}{\varrho} \frac{\partial}{\partial y} \frac{1}{B^s} \right] F = 0 \tag{2.A.12}$$

Asymptotic variational method

We shall illustrate the approximate analytical method for solving equations with both periodic and nonperiodic coefficients [see eq. (2.A.12)] by applying it to the simple model equation

$$\frac{d}{dy}(1 + s^2y^2)\frac{dF}{dy} + \alpha \cos y\, F = 0 \tag{2.A.13}$$

Let us rewrite this equation eliminating the first derivative [$F = u(1 + s^2y^2)^{-1/2}$]:

$$\frac{d^2u}{dy^2} - V(y)u = 0 \tag{2.A.14}$$

where

$$V(y) = \frac{s^2}{(1 + s^2y^2)^2} - \frac{\alpha \cos y}{1 + s^2y^2}$$

For $s^2 \ll 1$ the potential $V(y)$ is a well slowly varying in the interval of the order of $1/s$ with superposed rapid oscillations; that is, eq. (2.A.13) has two scales, namely, $y \sim 1/s$ and $y \sim 1$. Therefore, we can introduce a slow variable $t = sy$, apart from the variable y, as it is typically done in the averaging method. Let us separate the slow-varying and rapid-varying parts of the potential $V(y, t)$:

$$\bar{V} = \frac{1}{2\pi}\int_0^{2\pi} V(y, t)\, dy = \frac{s^2}{(1 + t^2)^2} \tag{2.A.15}$$

$$\tilde{V} = V - \bar{V} = -\frac{\alpha \cos y}{1 + t^2} \tag{2.A.16}$$

write down the solution in the same form: $u = \bar{u} + \tilde{u}$.

The oscillating part $\tilde{u}$ is given by the equation

$$\frac{d^2\tilde{u}}{dy^2} + \frac{a \cos y}{1 + s^2y^2}\bar{u} = 0 \tag{2.A.17}$$

The solution of this equation in the lowest-order approximation in s has the form

$$\tilde{u} = \frac{\alpha \cos y}{1 + s^2y^2}\bar{u} \tag{2.A.18}$$

Now we can write down the variational functional for eq. (2.A.14) in the form

$$W = \int_{-\infty}^{\infty} \left\{\left(\frac{du}{dy}\right)^2 + V(y)u^2\right\} dy \tag{2.A.19}$$

and substitute the asymptotic solution of eq. (2.A.14) as the test function:

$$u = \bar{u}\left(1 + \frac{\alpha \cos y}{1 + s^2 y^2}\right) \tag{2.A.20}$$

We can assume that the parameter s here is not small and find the slow-varying function $\bar{u}$ with the variational method or from physical considerations.

In the analysis of the stability boundary when the slow-varying function tends to a constant [2.23], we shall assume it to be equal to unity. After substitution of eq. (2.A.20) into the functional (2.A.19) and subsequent integration we can readily find the necessary criterion of stability from the condition.

$$\frac{1}{4} s^2 - \frac{3}{8} \alpha e^{-1/|s|} - \frac{1}{2} \alpha^2 > 0 \tag{2.A.21}$$

(the terms with α^2 and s^2 are omitted since they are small in comparison with unity). This is the necessary criterion of stability for the model equation (2.A.13); it is similar to the criterion for the ballooning modes [eq. (2.44)].

References

2.1. V. D. Shafranov, *ZhTF*, **2**, 241 (1970).
2.2. V. D. Shafranov, E. I. Yurchenko, *Nucl. Fusion*, **8**, 329 (1968).
2.3. O. P. Pogutse, E. I. Yurchenko, *PPPL*-tr-122, 1977; *ORNL*/tr-4470, 1977.
2.4. H. Furth, M. Rosenbluth, J. Killen, *Phys. Fluids*, **6**, 459, (1963).
2.5. B. B. Kadomtsev, O. P. Pogutse, *Questions in Plasma Theory*, vol. 5, Atomizdat, Moscow, 1967, p. 209 (in Russian).
2.6. B. B. Kadomtsev, O. P. Pogutse, *ZhETF*, **65**, 575 (1973).
2.7. O. P. Pogutse, E. I. Yurchenko, *Fizika plazmy*, **3**, 504 (1977).
2.8. B. Saydom, *Proc. 2UN Intern. Conf. P.U.A.E.*, Geneva, vol.31, 157, 1958.
2.9. L. S. Solov'ev, V. D. Shafranov, *Questions in Plasma Theory*, vol. 5, Atomizdat, Moscow, 1967, p. 3 (in Russian).
2.10. V. D. Shafranov, E. I. Yurchenko, *ZhETF*, **53**, 1157 (1967).
2.11. C. Mercier, *Nucl. Fusion*, **1**, 47 (1960).
2.12. A. M. M. Todd, J. Manicam, et al., *PPPL*-1470, 1978.
2.13. J. W. Conner, et al., *Phys. Rev. Lett.*, **40**, 396 (1978).
2.14. O. P. Pogutse, E. I. Yurchenko, *ZhETF Pis'ma*, **28** (6), 344 (1978).
2.15. L. S. Solov'ev, V. D. Shafranov, E. I. Yurchenko, *Plasma Phys. Contr. Nucl. Fug. Res.* IAEA, Vienna, 197 (1969).
2.16. O.P. Pogutse, N.V. Chudin, E.I. Yurchenko, *Fizika plazmy*, **6**, 621 (1980).
2.17. J. L. Johnson, J. M. Greene, *Plasma Phys.*, **9**, 611 (1967).
2.18. A. H. Glasser, et al., *Phys. Fluids*, **18**, 875 (1975).
2.19. A. B. Mikhailovsky, *Nucl. Fusion*, **19**, 95 (1075).
2.20. G. Bateman, D. B. Nelson, *Phys. Rev. Lett.*, **41**, 805, (1978).
2.21. O. P. Pogutse, E. I. Yurchenko, *ZhETF Pis'ma*, **31** (8), 479 (1980).
2.22. B. B. Kadomtsev, O. P. Pogutse, *DAN SSSR*, **170**, 811 (1966).
2.23. L. D. Landau, E. M. Lifshits, *Quantum Mechanics*, Pergamon Press, Oxford, 1977.
2.24. O. P. Pogutse, E. I. Yurchenko, *Nucl. Fusion*, **181**, 1629 (1978).

3. Helical Equilibria and Helical Instabilities of Current-Carrying Plasmas

L. E. Zakharov, Cand. Sc. (Phys. and Math.)

Introduction

Some tokamaks make it now possible to obtain sufficiently stable discharges with $q(a) = aB_z/RB_\theta$ close to 2 or even smaller (here a is the minor radius and R is the major radius of the plasma column and B_z and B_θ are the longitudinal and poloidal magnetic fields). This significant progress in experimental work gives rise to a pointed question how to reconcile this fact and the theory of helical instability of a current-carrying plasma column. According to the theory of kink instability, the region $q(a) < 2$ contains a fairly wide zone in which the plasma must be unstable with respect to the kink-mode $m = 2, n = 1$ (m and n are the wave numbers for the minor and major circumferences of the torus, respectively) which is a perturbation similar to the surface wave [3.1]. According to the linear theory of stability, the instability zone becomes narrow or disappears entirely only for strongly peaked current distributions corresponding to $q(a)/q(0) \approx 3.5$ [3.2] [here $q(0)$ is the q value at the magnetic axis]. The value of $q(0)$ should be of order of 0.5, that is, it should be considerably smaller than unity. However, realization of such current profiles should be inhibited by the processes of internal disruption which prevent noticeable increase in the current density over the critical value at the centre and decrease in $q(0)$ below 1, according to the available theory [3.3].

The kink instability, which is typically related to the model of ideal magnetohydrodynamics, is widely believed to be not dangerous [3.4]. This belief springs from the studies of the dynamics of development of the kink mode [3.5–7]. As it was demonstrated by the results of numerical simulation, a noticeable rearrangement of the configuration—formation of bubbles—is observed only when shear is absent and the value of q is constant over the cross section of the plasma column. If the current distribution in the plasma is not uniform, then, according to the calculations reported in [3.6], the kink instability gives rise to the development of the helical deformation of the plasma column which, however, is stopped at the nonlinear stage. The result is a new configuration and it can be said that the equilibrium with the cylindrical symmetry unstable with respect to the kink mode converts into a new equilibrium with the helical symmetry which is stable with respect to the given mode. This nonlinear stabilization of the instability can be naturally related to shear owing to which any deformation of the cross section of the plasma column produces deformation of the internal magnetic surfaces that is prevented by the condition of frozen magnetic fluxes.

It is such interpretation of the nonlinear dynamics of the helical instability that has yielded the conclusion that, in Bateman's words [3.4, p. 182], the kink instability "is a good example of an instability which was once thought to be dangerous because of its large growth rate and broad spatial extent compared to internal interchange modes and which now appears to be relatively harmless by itself". This conclusion based on the results of numerical simulation has led to the situation when the kink instability is no longer regarded as a cause of developent of such enigmatical phenomena in tokamaks as, for instance, the disruptive instability. Moreover, this conclusion implies that the distinct instability zones given by the linear theory [3.1] lose their meaning if we take account the noninear effects revealed by nymerical simulation. For instance, this indicates that we can realize the regimes of tokamaks corresponding to the instability zones and this practically does away with limitations on the current distributions [3.2] given by the classical theory of kink instability.

This paper aims at reconsidering this viewpoint and proving that actually the transition to a new stable helical equilibrium is not possible. Then the above coclusions obtained from the results of numerical simulation of the kink instability and its accompanying limitations are upheld.

As a starting point, we shall analyze the conditions of stability of a current-carrying plasma column in configurations with helical symmetry. We shall demonstrate that in a strong longitudinal field in the presence of helical deformation the interaction between the plasma current j_{pl} and the longitudinal field B_z along the axis is of essential importance. Though this fact has been formally taken into account by the equations describing the helical equilibria the specific forces operating in configurations with helical symmetry have not been analyzed in detail yet. We shall show below that the interaction between the plasma current and the longitudinal magnetic field gives rise to a force which can disrupt the plasma column under certain conditions. This is just the force that causes the helical instabilities. Its nature clearly indicates that if the plasma is in the zone of helical instability in the Shafranov diagram [3.1] (see Fig. 3.1.) then no transition into a new helical stability can occur; depending on the current density at the column axis there can occur either total rearrangement—inversion of the plasma—or only the surface envelope should be reversed while the central kern which is in the stability zone remains unaffected.

Thus, we believe that stable tokamak regimes are feasible only in the stability zones in the Shafranov diagram and that the above conclusion on a relative harmlessness of the kink instability is incorrect. The stabilization of the kink mode found in numerical calculations is due not to the shear as it could be expected but entirely to the surface currents produced in the ideal magnetohydrodynamics employed in the model. Since the destabilizing force is a bulk one and the stabilization is due only to the surface currents, the ideal MHD model cannot gauge the extent of harmfulness of the kink instability.

This paper consists of the following material. Section 3.1 presents the solution of the equilibrium equations for the plasma column with the helical symmetry and

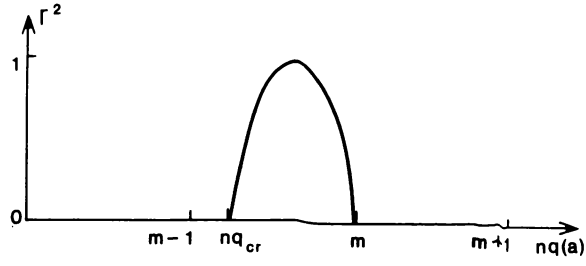

Fig. 3.1. The diagram of stability for the kink mode with the wave numbers m and n. The left-hand boundary nq_{cr} of the instability zone depends on the current distribution, position of the wall, and the shape of the column cross section; $\Gamma^2 = \gamma^2 4\pi\rho a^2/B_\theta^2(a)$.

classifies the helical equilibria both for the case of the high plasma currents and the case of the stellator with helical windings. These solutions are employed in Sec. 3.2 to analyze the forces responsible for helical deformation of the plasma column. Section 3.3 demonstrates the relationship between the theory of the helical equilibria and the linear theory of the helical instability. A stability criterion for the helical modes is also found there. Section 3.4 presents a general picture of the resistive instabilities of plasma with a free boundary. Nonlinear stabilization of the kink modes found in the above-mentioned numerical calculations is discussed in Sec. 3.5. The basic concepts of this paper are used to explain the disruptive instability in tokamaks in Sec. 3.6. Appendix 3.1 presents the method for solving the equilibrium equation for the plasma column with elliptical cross section and an arbitrary current distribution. Appendix 3.2 gives the derivation of the stability criterion given in Sec. 3.3.

3.1. Helical Equilibria of the Plasma Column with the Uniform Current Distribution

We shall consider the plasma column with the straight magnetic axis thus neglecting the toroidality effects. Let ϱ, ω, and s be the cylindrical coordinates, where $\varrho = \sqrt{x^2 + y^2}$ and s is the longitudinal coordinate along the axis of the system. In the case of helical symmetry all parameters of the system are functions of the variables ϱ and $\theta = \omega - \varkappa s$. The parameter $\varkappa$ determining the period $L = 2\pi/\varkappa$ of the system can be taken to be equal to n/mR, where R is the major radius of equivalent torus and n and m are the longitudinal and poloidal wave numbers ($s = R\zeta$, where ζ is the toroidal angle). We have $\varkappa = 1/2R$ for the mode with $m = 2$ and $n = 1$ which we shall analyze in more detail.

The geometry of a magnetic configuration with the helical symmetry is described by the helical flux function $\Psi(\varrho, \theta)$ equal to the magnetic flux across a helical surface with $\theta = \omega - \varkappa s = \text{const}$, which has the length of unity, the width of ϱ and

whose one edge is the axis of the system $\varrho = 0$ [3.8]. Written below are the main equations for the configurations with the helical symmetry [3.8, 3.5]:

$$\mathbf{B}^* \equiv B_\rho \mathbf{e}_\rho + B_\omega \mathbf{e}_\omega - x\varrho B_z \mathbf{e}_\omega \tag{3.1}$$

$$\mathbf{j}^* \equiv j_\rho \mathbf{e}_\rho + j_\omega \mathbf{e}_\omega - x\varrho j_z \mathbf{e}_\omega$$

$$\mathbf{B}^* = [\mathbf{e}_z \nabla \Psi], \qquad \frac{4\pi}{c}\mathbf{j} = [\mathbf{e}_z \nabla I] \tag{3.2}$$

$$B_z + x\varrho B_\omega = I(\Psi)$$

$$\frac{4\pi}{c}(j_z + x\varrho j_\omega) = 4\pi(1 + x^2\varrho^2)p'(\Psi) + II'(\Psi) \tag{3.3}$$

The surface function $I(\Psi)$ is, to within the factor $c/4\pi$, identical to the poloidal current across the helical surface with $\theta = \text{const}$ between $\varrho = \infty$ and the running value of ϱ.

The equation for the flux function Ψ which is related to the geometry of the magnetic surfaces with $\Psi(\varrho, \theta) = \text{const}$ has the form

$$\frac{1}{\varrho}\frac{\partial}{\partial \varrho}\frac{1}{1 + x^2\varrho^2}\frac{\partial \Psi}{\partial \varrho} + \frac{1}{\varrho^2}\frac{\partial^2 \Psi}{\partial \theta^2} =$$

$$= 4\pi^2 p'(\Psi) + \frac{II'(\Psi)}{1 + x^2\varrho^2} - \frac{2xI}{(1 + x^2\varrho^2)^2} \tag{3.4}$$

The main features of the helical equilibria are revealed even in the long-wavelength limit when we can assume $xa \ll 1$, where a is a characteristic transverse dimension of the plasma column. Then, instead of eq. (3.4), we obtain the well-known simplified equilibrium equation [3.5]

$$\triangle_{\rho,\vartheta}\Psi = \frac{4\pi}{c}[j_z(\Psi) - j_B] \tag{3.5}$$

where $j_z(\Psi) = j_{\text{pl}}$ is the density of the longitudinal plasma current, and $(4\pi/c)j_B \equiv 2xB_z = 2(n/mR)B_z$ describes the source of the longitudinal field flux across the helical surface. In a strong longitudinal field we can assume $j_B = \text{const}$. Here j_B is numerically equal to such current density for which the resonance condition $q = \varrho B_z/RB_\vartheta = m/n(\Psi = 0)$ is satisfied.

When we are solving the equilibrium problem it is natural to identify the plasma column boundary Γ with the current channel boundary. Outside plasma we have

$j_\parallel(\Psi) = 0$ and eq. (3.5) is linear. The boundary conditions for Ψ are

$$\Psi_i|_\Gamma = \Psi_e|_\Gamma = \text{const}, \quad \frac{\partial \Psi_i}{\partial n}|_\Gamma = \frac{\partial \Psi_e}{\partial n}|_\Gamma \tag{3.6}$$

If a surface current $i(\theta)$ flows along the plasma boundary, the second boundary condition is replaced with the pressure balance condition.

Equation (3.5) has a simple exact solution for a plasma column with the uniform current distribution $j_\parallel(\Psi) = \text{const}$ when the column has an elliptical cross section.

We shall make use of the elliptical coordinates

$$x = d \sinh u \cos \nu, \quad y = d \cosh u \sin \nu \tag{3.7}$$

in the poloidal cross section. If the plasma boundary Γ coincides with the coordinate surface $u = u_0$ [$j_\parallel(\Psi) = j_\parallel$ for $u < u_0$ and $j_\parallel(\Psi) = 0$ for $u > u_0$], we obtain

$$l_x = d \sinh u_0 = a, \; l_y = d \cosh u_0 \text{ and, } \lambda = l_y/l_x > 1 \tag{3.8}$$

where l_x and l_y are the semiaxes of the ellipse and

$$d^2 = l_y^2 - l_x^2, \; \sinh 2u_0 = \frac{2\lambda}{\lambda^2 - 1}, \; \cosh 2u_0 = \frac{\lambda^2+1}{\lambda^2 - 1}, \; e^{2u_0} = \frac{(\lambda+1)^2}{\lambda^2-1} \tag{3.9}$$

The equation for the flux function Ψ has the form

$$\Delta^* \Psi = \frac{2}{d^2(\cosh 2u + \cos 2\nu)} \left(\frac{\partial^2 \Psi}{\partial u^2} + \frac{\partial^2 \Psi}{\partial \nu^2} \right) = \begin{cases} \dfrac{4\pi}{c} (j_\parallel - j_B), & u < u_0 \\ -\dfrac{4\pi}{c} j_B, & u > u_0 \end{cases} \tag{3.10}$$

Its solution inside the plasma column is

$$\Psi_i = \frac{4\pi}{c} (j_\parallel - j_B) \frac{d^2}{8} \left[\cosh 2u - \cosh 2u_0 - \cos 2\nu + \frac{\cosh 2u}{\cosh 2u_0} \cos 2\nu \right] = \frac{4\pi}{c} (j_\parallel - j_B) \frac{\lambda^2 a^2}{2(\lambda^2 + 1)} \left(\frac{x^2}{a^2} + \frac{y^2}{\lambda^2 a^2} \right) \tag{3.11}$$

and the solution outside the column is

$$\Psi_e = \frac{4\pi}{c} j_\parallel \frac{d^2}{8} \left[2(u - u_0) \sinh 2u_0 + \frac{\sinh 2u_0}{\cosh 2u_0} \sinh 2(u - u_0) \cos 2\nu \right] - \frac{4\pi}{c} j_B \frac{d^2}{8} \left[\cosh 2u - \cosh 2u_0 - \cos 2\nu + \frac{\cosh 2u}{\cosh 2u_0} \cos 2\nu \right] \tag{3.12}$$

For $n = 0$ ($j_B = 0$) the solutions (3.11) and (3.12) are reduced to the well-known solutions for a straight column with elliptical cross section and translational symmetry [3.9]. An important fact for finding the solution (3.12) outside the column is that the term proportional to $(u - u_0)$, which determines the logarithmic behaviour of Ψ_e at infinity ($\sim \ln \varrho$), is related only to the real plasma current j_z rather than the fictitious current j_B.

The "current" j_B is related to the flux Ψ_B of the longitudinal field B_z across the helical surface with $\theta = \text{const}$:

$$\Psi_B = -\frac{4\pi}{c} j_B \frac{x^2 + y^2}{4} = -\frac{4\pi}{c} j_B \frac{d^2}{8} (\cosh 2u - \cos 2v) \tag{3.13}$$

This is a power function of the coordinates.

Let us make use of eq. (3.12) to analyze the magnetic configuration outside the plasma and to classify the helical equilibria. At large distances from the axis when we can neglect the field of the plasma current the magnetic field is determined by the flux

$$\Psi_{e\infty} = -\frac{\pi}{c} j_B [(x^2 + y^2) + e_\infty (x^2 - y^2)] \tag{3.14}$$

where

$$e_\infty = \frac{\lambda^2 - 1}{\lambda^2 + 1} \left[1 - \frac{2\lambda}{(\lambda + 1)^2} \frac{j_z}{j_B}\right] \tag{3.15}$$

The first term in eq. (3.14) is the flux of the longitudinal field Ψ_B and the second term is the flux Ψ_{ext} of the maintaining field which must be produced by external helical windings. The parameter ϵ_∞ can be regarded as a characteristic of the geometry of magnetic surfaces at large distances from the plasma. If $|e_\infty| > 1$, the surfaces are open and have hyperbolic cross sections, and if $|e_\infty| < 1$, the surfaces have elliptical cross sections and $e_\infty = (\lambda_\infty^2 - 1)/(\lambda_\infty^2 + 1)$, where λ_∞ is the ratio between the semiaxes.

Depending on the relationship between the plasma current j_z and the current j_B [$(4\pi/c)j_B = (2n/mR)B_z$; see eq. (3.14)] there can exist three types of configurations outside the plasma.

1. The case of strong plasma current. Then j_z is so high that $|e_\infty| > 1$. The longitudinal field makes a small contribution to the geometry of the magnetic configuration and in its poloidal cross section it is similar to the configuration of the straight plasma column with the translational symmetry (see Fig. 3.2*a*). The magnetic surfaces are closed only near the plasma column; behind a separatrix lying some distance from the column the magnetic surfaces are open.

2. The case of intermediate current, that is, when j_z is not too high so that $|\epsilon_\infty| < 1$ but, at the same time, $j_z > j_B$. The magnetic surfaces are closed everywhere (see Fig. 3.1, *b* and *c*). In the vicinity of the plasma column the magnetic field $\mathbf{B}^*$ has the same direction as the field of the plasma current. There is a closed separatrix within which two magnetic islands are formed. Beyond the separatrix the magnetic sur-

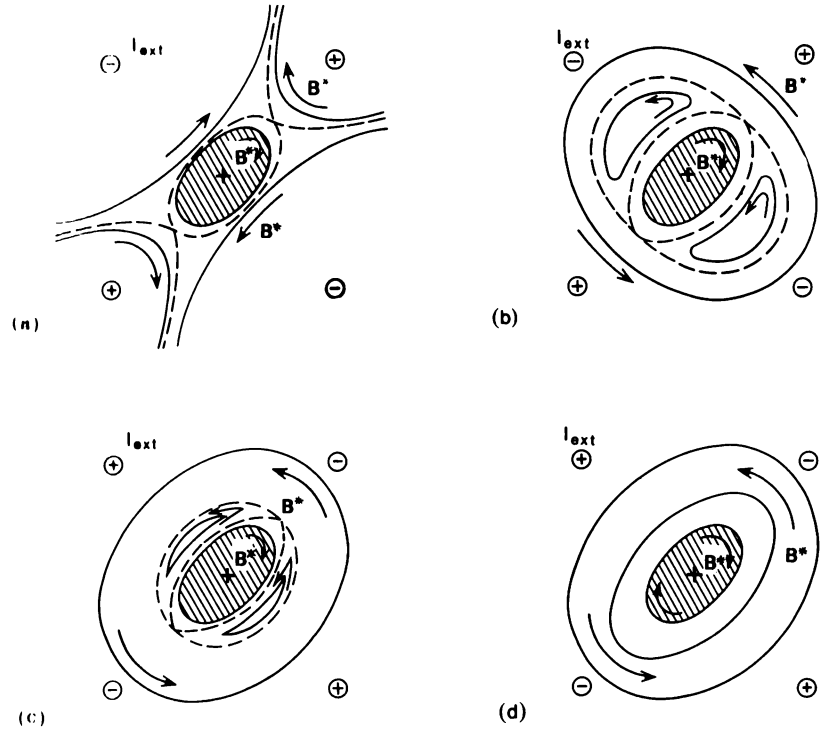

Fig. 3.2. The geometry of the magnetic configuration of the plasma column with the elliptical cross section. (*a*) Equilibrium with a high plasma current corresponding to the pinch with the current: $|e_\infty| > 1$. (*b*) Equilibrium with the intermediate current $j_s > j_B$, $-1 < e_\infty < 0$, corresponding to the tokamak parameters in the stability zone $nq(a) < nq_{cr}$. (*c*) Equilibrium with the intermediate current $j_s > j_B$, $0 < e_\infty < 1$, corresponding to the tokamak parameters in the instability zone $nq_{cr} < nq(a) < m$. (*d*) Equilibrium of the stellator type: $j_s < j_B(nq(a) > m)$.

faces also have simple shapes but the direction of the magnetic field $\mathbf{B}^*$ is changed to the opposite. In the magnetic islands q corresponds to 2 (for $m = 2$ and $n = 1$).

In this case we shall discuss the following two situations: (a) the major semiaxis of the external ellipses is perpendicular to the major semiaxis of the plasma cross section ($e_\infty < 0$) (see Fig. 3.2*b*); and (b) the major semiaxes of the external ellipses and the plasma cross section are parallel ($e_\infty > 0$) (see Fig. 3.2*c*). As it will be shown below, the transition from the case (a) to the case (b) corresponds to crossing the boundary of the kink instability.

3. The case of weak plasma current ($j_z < j_B$). The direction of the magnetic field $\mathbf{B}^*$ is always opposite to that of the plasma field $\mathbf{B}_{pl}$. The magnetic configuration has a simple structure without any separatrix. A separatrix may appear in a configuration of this type if we include the terms we have omitted in eq. (3.4), that is, if the long-wavelength approximation is violated.

We can say that the configurations of the first type correspond to high-current pinch where the plasma current makes a predominant contribution to the formation of the geometry. The configurations of the third type can be said to correspond to the stellator configuration, where the contribution of the plasma current is small and the geometry is determined by the longitudinal field and the field of the helical windings. The configurations of the second type form an intermediate class and will be shown below to correspond to the tokamak parameters.

For the higher modes ($m > 2$) we obtain a full similarity to the above-discussed case of $m = 2$. An exact solution of the equilibrium equation (3.5) for the uniform plasma current can be obtained, for instance, using the appropriate conformal transformation. However, the solution is no longer so simple as that for the plasma column with the elliptical cross section. We shall have no need for the exact solutions in the case of $m \geq 3$ and we shall only give here the solutions in the linear approximation (in deviation from the circular cylinder).

Assume that the plasma boundary is described by

$$\varrho = a + \xi \cos(m\omega - n\zeta), \qquad \xi \ll a \tag{3.16}$$

and the plasma current is uniform ($j_z = \text{const}$). The current density j_B now corresponds to $nq = m$.

For the boundary conditions

$$\Psi_i|_{\tilde{\varrho}} = \Psi_e|_{\tilde{\varrho}} = \text{const}, \qquad \left.\frac{\partial \Psi_i}{\partial \varrho}\right|_{\tilde{\varrho}} = \left.\frac{\partial \Psi_e}{\partial \varrho}\right|_{\tilde{\varrho}} \tag{3.17}$$

where $\tilde{\varrho} = a + \zeta \cos m\theta$, we obtain the following solutions of eq. (3.5):

$$\Psi_i = \frac{\pi}{c}(j_z - j_B)\left[\varrho^2 - 2a\xi\frac{\varrho^m}{a^m}\cos m\theta\right]$$

$$\Psi_e = -\frac{\pi}{c}j_B\left[\varrho^2 - 2a\xi\frac{\varrho^m}{a^m}\cos m\theta\right] + \frac{\pi}{c}j_z a^2\left[\ln\frac{\varrho^2}{a^2} - 2\frac{\xi}{a}\frac{\varrho^m}{a^m}\cos m\theta\right]$$

$$+ \frac{\pi}{c}j_z\frac{2\xi a}{m}\left[\frac{\varrho^m}{a^m} - \frac{a^m}{\varrho^m}\right]\cos m\theta \tag{3.18}$$

As in the case of $m = 2$, we can obtain three types of the magnetic configuration outside the plasma which correspond to (1) the equilibria of a straight plasma col-

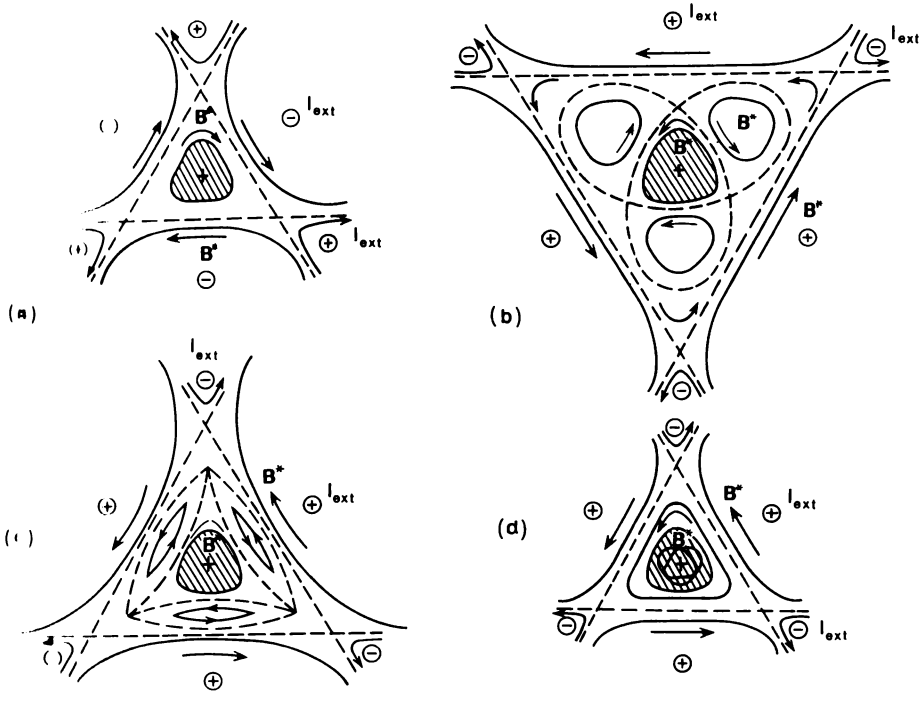

Fig. 3.3. The magnetic configuration types for the plasma column with the helical deformation and the mode with $m = 3$.

umn of a non-circular cross section with an open separatrix, (2) the equilibria with a closed separatrix and magnetic islands, and (3) the stellator equilibria with a simple topology (see Fig. 3.3).

The case of higher modes ($m \geq 3$) differs from the case of $m = 2$ in that the maintaining field has a higher multipolarity for the case of $m \geq 3$ and it depends on higher powers in the coordinates x and y than 2 (x^m, y^m). The flux Ψ_B related to the longitudinal field is proportional to $x^2 + y^2$ and, therefore, at large distances from the axis the topology of the configuration in the case of $m \geq 3$ is always determined by the maintaining field. However, if we are not interested in the region outside the external separatrix, we obtain a full similarity between the equilibria with $m \geq 3$ and the above-discussed case with $m = 2$. For instance, we can distinguish between two types of configurations in the case of moderately high current and $m \geq 3$, namely, (2a) the cusps of the column cross section and the external separatrix are oppositely directed; and (2b) the cusps of the column cross section and the external separatrix have the same direction. When we go over from (2a) to (2b), we cross the left-hand boundary of the stability diagram for the kink mode.

Appendix 3.1 presents an approximate method for solving the equilibrium equations for an arbitrary distribution of the plasma current.

3.2. Forces Determining the Equilibrium of the Plasma Column with the Helical Symmetry

To understand the nature of the forces determining the shape of the plasma column cross section we have to identify the field produced by the external windings in the total solution of the equilibrium equation. These fields are, firstly, the longitudinal field B_z and, secondly, the multipole field which should be produced by the external helical windings. The latter will be referred to as the maintaining field B_{ext} and its flux will be denoted as Ψ_{ext}.

To identify Ψ_{ext} in Ψ_e we must subtract the longitudinal field flux Ψ_B [see eq. (3.13)] from Ψ_e omit the logarithmic term $\sim \ln \varrho$ corresponding to the main part of the plasma field Ψ_{pl} and take the solutions having singularities only outside the plasma including $\varrho = \infty$. The remaining terms in Ψ_e which decline for $\varrho \to \infty$ are related to the field of the plasma current.

For the plasma column with the elliptical cross section we obtain

$$\Psi_{ext} = -\frac{4\pi}{c} j_z \frac{d^2}{8} \frac{\sinh 2u_0}{\cosh 2u_0} e^{-2u_0} \cosh 2u \cos 2v + \frac{4\pi}{c} j_B \frac{d^2}{8} \frac{1}{\cosh 2u_0} \cosh 2u \cos 2v$$

$$= \frac{4\pi}{c}(x^2 - y^2)\frac{1}{4}\frac{\lambda^2 - 1}{\lambda^2 + 1}\left[\frac{2\lambda}{(\lambda + 1)^2} j_z - j_B\right] \tag{19}$$

For instance, equation (3.19) yields the well-known expression for the column with the translational symmetry for $n = 0$ ($j_B = 0$) [3.10–12].

Before analyzing the forces in the equilibrium with the helical symmetry we shall first find what determines the translational-symmetry equilibrium of the plasma column with the elliptical cross section. The field $\Psi_{ext} = (2\pi/c)A(x^2 - y^2)$ is a purely quadrupole field corresponding to four straight conductors parallel to the plasma column (see Fig. 3.4*a*). The currents with the same direction as that in the plasma are attractive and give rise to a force disrupting the cross section of the plasma column. The balance of this force and the intrinsic contraction of the plasma current is

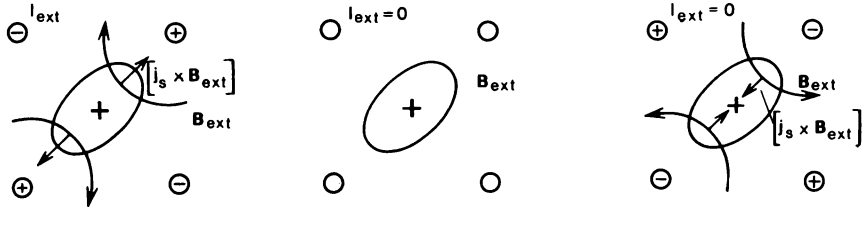

Fig. 3.4. The interaction $[\mathbf{j}_{pl} \times \mathbf{B}_{ext}]$ of the plasma current with the maintaining field. (*a*) B_z is lower than the critical value, $nq(a) < nq_{cr}$. (*b*) B_z is equal to the critical value, $nq(a) = nq_{cr}$. (*c*) B_z is higher than the critical value, $nq(a) > nq_{cr}$.

precisely the factor that determines the shape of the cross section of the plasma column.

It is well known that when the current in the quadrupole windings increased so that $A \cdot 0.15 j_z$, which corresponds to $\lambda = 2.89$, the disruptive force exceeds the force of intrinsic plasma contraction and equilibrium becomes unfeasible [3.11, 3.12].

The first mention of this effect can be found in [3.13]. For the uniform current the critical relation between j_z and A does not depend on the plasma dimensions. Therefore, if $A > 0.15 j_z$ the quadrupole confining field can fully disrupt the plasma column cross section.

Now the interaction between the quadrupole maintaining field and the plasma current with a nonuniform distribution can be easily understood. Clearly, we also have here a critical value of A for which an equilibrium with a given current distribution becomes impossible. When we are solving the equations the critical situation is formally equivalent to the separatrix getting to the boundary of the current channel. When the maintaining field is further increased, we encounter the following two cases.

1) The maintaining field exceeds the critical field, but at the centre of the plasma column $j_z(0) > A/0.15$. Under such conditions the quadrupole field will disrupt only the periphery of the column with the central part remaining unaffected.

2) The balance condition for the current density $[j_z(0) < A/0.15]$ is violated at the centre of the column, too. Under such conditions the plasma column is totally disrupted by the quadrupole field.

The existence of the critical current density $j_z = A/0.15$ below which there can be no equilibrium in the quadrupole field may explain the experimental difficulties with breakdown in a preset quadrupole field.

Below we shall see that such arguments which follow from the analysis of the equilibrium of a column with the translational symmetry can be extended by analogy to the case of the helical symmetry.

Let us now analyze the expression for the maintaining quadrupole field [see eq. (3.19)] for a column with the helical deformation. The term j_B in eq. (3.19), that decreases (in comparison with the straight column) the quadrupole maintaining field Ψ_{ext} that would be produced by the helical windings, indicates that the helical stability involves an additional force equivalent to the interaction between the plasma current and the quadrupole field. The nature of this force is readily understood—it is the interaction between the plasma current j_{pl} flowing along the helical lines and the longitudinal magnetic field B_z. It can be easily seen to be disruptive and taking some of the responsibilities of the maintaining field (see Fig. 3.5). When the field B_z is increased up to the critical value, so that

$$j_B = \frac{c}{4\pi} \frac{2n}{mR} B_z = \frac{2\lambda}{(\lambda + 1)^2} j_z \tag{3.20}$$

the confining field Ψ_{ext} becomes redundant and the stability prevails in the absence of helical windings (Fig. 3.4*b*). When B_z is increased further, the disruptive force related to the longitudinal field is higher than the force of plasma pinching by the own magnetic field of the plasma. Under such conditions a confining field Ψ_{ext} of

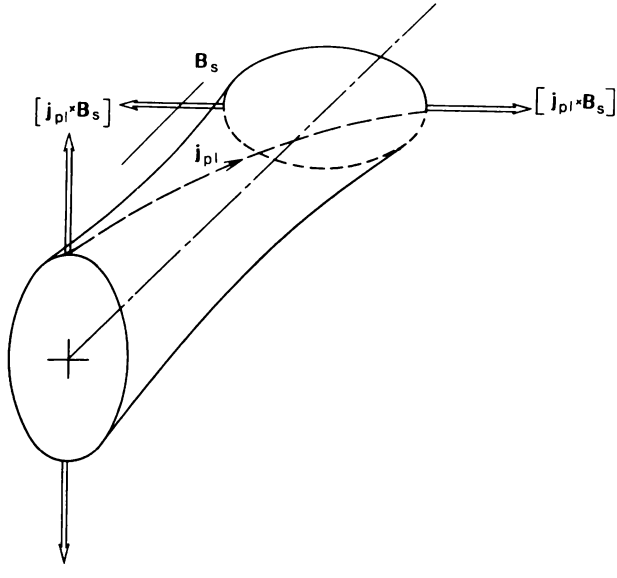

Fig. 3.5. The interaction $[\mathbf{j}_{pl} \times \mathbf{B}_s]$ of the plasma current with the longitudinal field.

the opposite sign is needed to compensate for the lack of balance of the above forces (see Fig. 3.4*b*).

Thus, in contrast to the plasma column with the translational symmetry, the stability in the cross section of the plasma column with the helical deformation is determined by the balance of the following three forces: (1) the force of plasma self-contraction (pinch effect); (2) the force of the interaction with the maintaining multipole field $\mathbf{B}_{ext}$; and (3) the force of interaction of the plasma current flowing along the helical lines with the longitudinal magnetic field B_s.

It can be readily seen that the contribution of the third force increases and the critical value of B_s [see eq. (3.20)] drops with an increase in deformation, that is, in λ. The critical value of B_s is the highest for the column with small deformation ($\lambda \to 1$). In the case of the elliptical ($m = 2$) cross section and uniform current distribution it is

$$B_s = \frac{4\pi}{c} \frac{Rj_{pl}}{2n}, \quad j_B = \frac{j_{pl}}{2} \tag{3.21}$$

For $m = 2$ and $n = 1$ it corresponds to

$$q = 1 \tag{3.22}$$

that is, to the left-hand boundary of the instability zone of this kink mode in the

Shafranov diagram [3.1].

For higher modes the expression for Ψ_{ext} in the approximation linear in ξ has the from

$$\Psi_{ext} = -\frac{\pi}{c} a^2 \frac{\varrho^m}{a^m} \cos m\theta \frac{2\xi}{a} \left[\frac{m-1}{m} j_s - j_B \right] \quad (3.23)$$

and all said above is also applicable here. Generally, the critical value of the longitudinal field B_s for the uniform current distribution corresponds to the condition

$$nq = m - 1, \quad j_s = \frac{m}{m-1} j_B \quad (3.24)$$

The conclusion that the critical longitudinal fields B_s corresponds to the left-hand point nq_{cr} in the Shafranov diagram is general and applicable to any current distribution in the plasma column (see Appendix 3.1). Indeed, if B_s exceeds the critical value, then any small helical deformation of the plasma column gives rise to a force related to the longitudinal field, which is higher than the force of pinching by the own field of plasma. Clearly, this implies the kink instability in the absence of a compensating effect of the helical windings.

Our analysis of the helical equilibria suggests that it is just the interaction between the plasma current and the longitudinal magnetic field that is responsible for all types of helical instabilities. This is evident for the kink mode with $m = 1$ and $n = 1$ [3.14, 3.15]. To show this for higher modes with $m \geq 2$ we must perform the above analysis of the helical equilibria.

The above results imply that the helical instability of a specific mode with m and n numbers is unfeasible in principle in the case of a sufficiently high, rather than low as is customary assumed, current density corresponding to the position to the left from the instability zone in the Shafranov diagram. Since the equilibrium equations describe both the ideal and the dissipative plasma, this conclusion is a general one and does not depend on the model used for describing the plasma.

We have seen from the above analysis of equilibrium that the cause of the helical instability does not disappear with an increase in the deformation. On the contrary, the interaction detween the bulk plasma current and the longitudinal field is intensified at the nonlinear stage of the instability with increasing helical deformation. In particular, this proves the unfeasibility of maintaining discharge under steady-state conditions in the zone of the helical instability since this instability will necessarily lead to a significant rearrangement of the configuration.

When the current density in the plasma is nonuniform, B_s is higher than the critical value, $nq(a) > nq_{cr}$, but the current density at the magnetic axis is sufficiently high ($nq(0) < m - 1$), the development of the mode with m and n can result only in the rearrangement of the periphery of the plasma column. If under such conditions we have $nq(0) > m - 1$ at the magnetic axis, too, then the interaction of the plasma current with the longitudinal field can, in principle, fully turn out the plasma column. In our opinion, the former case corresponds to a minor disruption in a tokamak and the latter to a major disruption.

3.3. The Link Between the Equilibrium Theory and the Theory of Stability of the Helical Modes. The Necessary Condition of Stability

At first sight, the results of Sec. 3.2 contradict the conventional opinion on the conditions of development of the kink instabilities. According to the conventional point of view, the safe zone is precisely the region of low currents, where the Kruskal-Shafranov criterion is met. But we shall demonstrate below that the results of the equilibrium theory are entirely valid and hold with the earlier developed concepts. Moreover, the equilibrium theory facilitates a unified approach to understanding of the general picture of the helical instabilities both in the ideally conductive and the dissipative plasma.

The development of the helical instability can be analyzed by writing the balance of forces for each stage, that is, determining which forces needed for the equilibrium are lacking. Since we have identified above the main forces which contribute to the helical equilibrium, we can now employ the equilibrium theory for the analysis of the stability conditions.

Let us once more treat the case of the uniform current distribution. According to the results of Sec. 3.3, the plasma must be unstable with respect to the mode with the numbers m and n for $nq > m - 1$. This result of the equilibrium theory is, clearly, not in full agreement with the theory of the kink instability [3.1] since it lacks the right-hand boundary of the instability zone. However, it should be remembered that in our equilibrium analysis we assumed a given plasma current distribution. The plasma motion due to the instability gives rise to the induced currents in the plasma, which change the current distribution and, hence, the equilibrium conditions.

The above analysis of the equilibrium with a given current distribution is fully applicable to the instability for the plasma of a very low conductivity $\sigma \to 0$, when the current distribution in the plasma column is entirely determined by the external uniform electric field E which is much greater than the induced emfs $(1/c)$ $[\mathbf{v} \times \mathbf{B}]$ due to the plasma motion:

$$\frac{1}{c}[\mathbf{v} \times \mathbf{B}] \ll E = \frac{j_z}{\sigma} \tag{3.25}$$

The motion is, clearly, purely inertial under the effect of the above-mentioned interaction between the plasma current and the longitudinal field (see Fig. 3.6). At the linear stage this gives the instability with the hydromagnetic increment scale

$$\gamma = \frac{2B_\vartheta^2(a)}{4\pi\varrho a^2}(q + 1 - m), \qquad B_\vartheta(a) = \frac{4\pi}{c} j_z \frac{a}{2} \tag{3.26}$$

which was obtained in [3.16] for the analysis of the instability of mercury jets carrying current in a longitudinal field. The instability region given by eq. (3.26) can be readily seen to be identical to that predicted by the equilibrium theory. This case is, naturally, very far from that of high-temperature plasma.

Let us now analyze the model of ideally conducting plasma with the free boundary, for which

$$\sigma = \begin{cases} \infty, & \varrho < a \\ 0, & \varrho > a \end{cases} \tag{3.27}$$

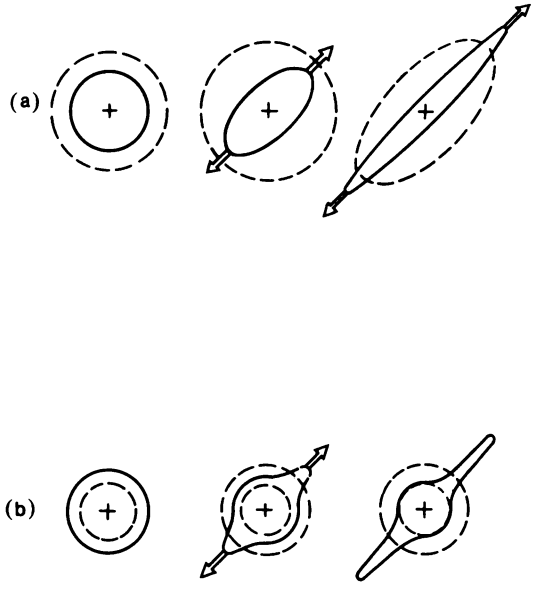

Fig. 3.6. The disruption of the plasma of low conductivity in a strong longitudinal field owing to the evolution of the helical instability of the mode with $m = 2$. (*a*) Uniform current density, $nq > 1$. (*b*) Nonuniform current density, $nq(a) > nq_{cr}$, the necessary criterion $nq(0) < m - 1$ is satisfied.

and demonstrate how the equilibrium theory yields the instability condition for the classical kink mode [3.1]:

$$m - 1 < nq < m \tag{3.28}$$

If we are not interested in the value of the instability growth rate, then the motion equations for the plasma may be replaced by the equilibrium equations for the deformed plasma column. Then only the forces acting on the plasma surface are not balanced. We can find out whether the plasma is stable or not from the direction of these forces depending on whether they tend to increase or decrease the deformation.

When we analyze the helical deformation we must take into account that the longitudinal Φ and the poloidal χ magnetic fluxes are frozen into the plasma. As it is typically done, the poloidal flux χ is defined as the magnetic flux across the torus opening formed by the given magnetic surface. In a strong longitudinal field B_z, the frozenness of Φ means that the cross-sectional area of each of the magnetic surfaces is conserved, and when χ is frozen in, the rotational transform $\mu(\Phi) = d\chi/d\Phi$ (or $q = 1/\mu$) is conserved at each surface. But if we use the approximation linear in perturbation we can employ the old approach with the given current distribution for solving the equilibrium equation. Therefore, magnetic configuration inside the plasma

will still be described by eq. (3.11) or eq. (3.18). Meanwhile, the external field Ψ_e will lack the maintaining field Ψ_{ext}. The part of the external helical windings providing for the stability of the column's interior will be played by the surface currents induced at the plasma surface. They can be easily found from the first boundary condition (3.17) and the fact that for $\varrho \to \infty$ the poloidal field component is absent: $\Psi_e|_{\varrho \to \infty} = \Psi_B$. Then we have

$$\Psi_e = -\frac{\pi}{c} j_B \varrho^2 + \frac{\pi}{c} j_* a^2 \ln \frac{\varrho^2}{a^2} - \frac{\pi}{c}(j_* - j_B) 2a\xi \frac{a^m}{\varrho^m} \cos m\theta \tag{3.29}$$

and the surface current is

$$i_*(\theta) = m\xi \cos m\theta \left[\frac{m-1}{m} j_* - j_B \right] \tag{3.30}$$

The sign of this current is, naturally, identical to those of the currents in eq. (3.23) in the external windings shown in Fig. 3.4.

Though the equilibrium inside the plasma column is provided for owing to the surface current $i_*(\theta)$, the configuration, on the whole, is unstable since a ponderomotive force is acting on these currents. The easiest way to calculate this force is by analyzing the difference in the magnetic pressures at the column surface:

$$\left.\frac{\mathbf{B}_e^2 - \mathbf{B}_i^2}{8\pi}\right|_{\tilde{\varrho}} = \frac{1}{8\pi}\left[\left(\frac{\partial \Psi_e}{\partial n}\right)^2 - \left(\frac{\partial \Psi_i}{\partial n}\right)^2\right] = \frac{2\pi}{c} ma\xi \left(\frac{m-1}{m} j_* - j_B\right)(j_* - j_B) \cos m\theta \tag{3.31}$$

We see that in the zone of the kink instability [see eq. (3.28)] with $mj_B/(m-1) > j_* > j_B$ the magnetic pressure acting on the surface currents $i_*(\theta)$ tends to increase the perturbation as it should be expected. Equation (3.31) readily illustrates the origin of the boundaries of the instability zone in the Shafranov diagram (see Fig. 3.1): the left-hand boundary corresponds to the zero of the induced current $i_*(\theta)$, and the right-hand boundary corresponds to the zero of the effective magnetic field acting on this current since $mB_\theta - (na/R)B_z = 0$. It can be generally shown that this result is valid for any current distribution in the plasma. This makes clear the well-known result that in the ideally conducting plasma for any other shape of the plasma cross section the right-hand boundary of the instability zone is given by the condition $nq(a) = m$.

We have shown the identity of the results of the theories of equilibrium and stability for the uniform current. Now let us analyze the general stability of the plasma with a nonuniform current. Plasma destabilization is due mainly to the interaction of the current flowing in the peripheral regions of the column with the longitudinal magnetic field. Pinching of the plasma under the effect of its current is the stabilizing effect. Hence, it is clear that to stabilize the helical instability we have to increase the current density at the column centre and simultaneously decrease it at the periphery. This explains the well-known fact of the stability theory that if the total currents are the same the current distribution peaked at the centre is more stable than the uniform distribution [3.1] and shows the possibility of total stabilization of the kink modes with $m \neq 1$ for a nonuniform current distribution.

Moreover, we see here that, though the shear of the magnetic field necessarily accompanies nonuniform current distribution, it does not concern the stability of the helical modes by itself. To make plasma we have just to provide for a balance of forces in favour of self-contraction of the plasma.

These results can be easily illustrated with the energy principle. The stability conditions for the kink modes are most conveniently obtained from the expression for the potential energy [3.17]:

$$W = \int_0^\infty \left[\varrho Y'^2 + \frac{m^2}{\varrho} Y^2 + \frac{\frac{4\pi}{c} j' R}{B_z \left(\mu - \frac{n}{m} \right)} Y^2 \right] d\varrho \tag{3.32}$$

where $Y = \varrho B_z(\mu - n/m)$ is a test function describing a perturbation of the longitudinal component of the vector potential which is identical to within a factor to the perturbation of the normal component of the magnetic field, and $\mu(\varrho) = 1/q(\varrho)$. We know [3.18] that eq. (3.32) yields the stability conditions for both the kink mode with the free boundary and for the tearing mode. The difference is that if the resonance surface $\mu(\varrho_s) = n/m$ is in the region of the ideally conducting plasma, then the necessary condition is $Y(\varrho_s) = 0$, while for the plasma of a finite conductivity it is allowed that $Y(\varrho_s) \neq 0$ but the integral in eq. (3.32) is taken as the principal value.

In the model of a step-wise (uniform inside the plasma) current distribution $j_z' = -j_z \delta(\varrho - a)$ eq. (3.32) readily yields the well-known instability condition (3.28). From this we can easily obtain from eq. (3.32) the sufficient condition of the kink instability for a declining current distribution:

$$nq(0) > m - 1, \qquad nq(a) < m \tag{3.33}$$

which was derived earlier from the analysis of the helical equilibria.

Now consider a monotonic current distribution $j(\varrho)$ ($j'(\varrho) \leq 0$) such that the resonance surface $\mu = n/m$ is beyond the current channel. Take for comparison the current distribution $j_1(\varrho)$ which coincides with $j(\varrho)$ for $(\varrho < d$ $(j_1(\varrho) = j(\varrho))$ and vanishes for $\varrho > d$ $(j_1(\varrho) = 0)$. Owing to the increasing weight factor $1/(\mu - n/m)$ in the third term of eq. (3.32), the column stability is better provided for by the current density dropping along a smaller distance. Therefore, the distribution $j_1(\varrho)$ is more stable than the distribution $j(\varrho)$. The more rigorous derivation is given in Appendix 3.2.

If d is small, the distribution $j_1(\varrho)$ corresponds to the column with a uniform current the instability condition for which is $nq > m - 1$. Hence, if the condition (3.33) is satisfied, the distribution $j(\varrho)$ is certainly unstable.

Thus, if the resonance surface $nq = m$ is beyond the current channel, the necessary condition of stability of the helical mode with m and n (both for the plasma with the free boundary and the tearing mode) is

$$nq(0) < m - 1 \tag{3.34}$$

The above arguments on the cause of the helical instabilities are fully reflected by the energy principle written in the form (3.32). In particular, the higher stability of the distribution $j_1(\varrho)$ in comparison with $j(\varrho)$ readily follows from the equilibrium theory since the additional wings of the current distribution just increase the disruptive force due to the helical deformation of the column.

As mentioned above, when the condition $nq(0) < m - 1$ is satisfied, the helical mode with m, n is not catastrophic even when the Kruskal-Shafranov criterion $nq(a) > m$ is violated. In this case the helical instability can rearrange only the periphery of the plasma column without affecting its centre. This implies, in particular, that when we increase the current in a tokamak and pass the kink instability zone with m, n, we must provide for a nonuniform current distribution which would provide for $nq(0) < m - 1$ at the centre of the column when at the boundary we have $nq(a) = m$. These conditions are relatively easy to satisfy for the higher values of m, n since even a small current nonuniformity is sufficient for them. This explains, in particular, why the discharge is formed without instabilities if we promote current peaking at the centre at the starting stage. Moreover, it becomes clear why experiments typically reveal no modes with $n \neq 1$. For $q \approx 2$ to 4 they correspond to higher values of m and are easily stabilized when the current distribution is nonuniform.

Condition (3.34) is most difficult to satisfy when we pass the instability zone of the mode with $m = 2$, $n = 1$ (we ignore here the mode with $m = 1$). Here a ratio of at least 2 in $q(a)/q(0)$ is needed. According to the calculations of [3.2], $q(a)/q(0) \approx 3.5$ is needed for the full stability of this mode for power-function current profiles. These conditions, clearly, contradict the results of the reconnection theory [3.3] according to which $q(0)$ increases up to 1 after each internal disruption. The stable regimes with $q(a) \approx 2$ obtained with some tokamaks suggest that the contribution of the reconnection processes for the mode with $m = 1$ was, apparently, overestimated in [3.3] and that, in fact, $q(0)$ can be lower than 1.

3.4. Resistive Helical Modes in the Current-Carrying Plasma

As can be seen from the above discussion, in the two limiting cases of $\sigma \to 0$ and $\sigma \to \infty$ the helical instability zones have a common left-hand point nq_{cr} (see Fig. 3.1) but quite different lengths to the right of this point. How does the transition from one limit to another occur? We shall give a brief answer to this question within the framework of the model of finite-conductivity plasma.

Consider the following model of the plasma column with the free boundary:

$$\sigma(\varrho) = \begin{cases} \sigma = \text{const}, & \varrho < a \\ 0, & \varrho > a \end{cases} \tag{3.35}$$

It should be borne in mind that the applicability of such a model to instability of the high-temperature plasma must be specially analyzed and we shall use it only for illustrating the results of the theory of helical equilibrium.

The exact dispersion equation for such model ($j_z \sim \sigma$) was derived earlier in [3.19, 3.16], where it was analyzed for the cases of $\sigma \to 0$ and $nq = m$. In the limit $\tau_{sk}/\tau_a \gg 1$, where $\tau_a = \sqrt{4\pi\varrho a^2/B_0^2}$ is the Alfven flight time and $\tau_{sk} = 4\pi\sigma a^2/c^2$ is the skin time this equation was solved in [3.20]. In accordance with the predictions of the theory of helical equilibrium there was found the resistive surface helical mode which is unstable when the Kruskal-Shafranov criterion is satisfied, $nq(a) > m$. The stability diagram for such a model is shown in Fig. 3.7. This helical instability is the surface flow in the layer of the width $\delta = (a^2/Rq)(2m\omega_0\tau_{sk})^{-1/3}$, where $\omega_0^2 = 4\pi\varrho a^2/B_0^2$ and it has the growth rate $\gamma = \omega_0(4m^2/\omega_0\tau_{sk})^{1/3}$ which is considerably higher than, for instance, the growth rate of the tearing mode. Physically, this mode is the principal adial mode of the current convective instability for such column model with the free boundary ($\sigma = 0$ for $\varrho > a$) and it exists for any distribution of the conductivity $\sigma(\varrho)$ in the plasma.

Such modes that appear when $nq > m$ are also known to exist when the resonance surface is inside the plasma column with a nonuniform conductivity. These potential current convective instabilities [3.21] or the rippling modes [3.22] are due to the conductivity transfer with the motion of the medium.

$$\frac{\partial\sigma}{\partial t} + \mathbf{v}\cdot\nabla\sigma = 0 \tag{3.36}$$

which gives rise to the current component along the helical perturbation. The interaction between this current and the longitudinal field B_z when $nq > m$ can be readily seen always to produce a force increasing the displacement.

Thus, the general picture of the resistive helical instabilities fully conforms to the above conclusion that the helical instability of both the ideal and the dissipative plasma cannot occur to the left of the nq_{cr} value in the Shafranov diagram (see Figs. 3.1 and 3.7). To the right of this point the helical instability manifests itself either as an instability of the ideally conducting plasma with the free boundary, or as the tearing

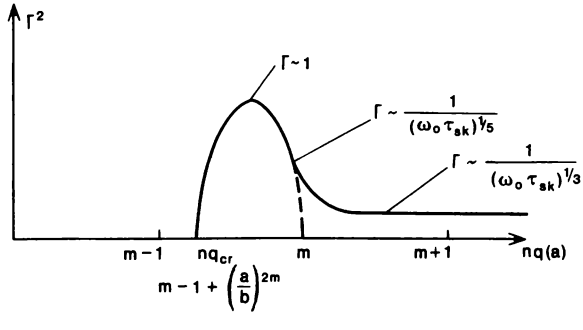

Fig. 3.7. The stability diagram for the plasma column with the free boundary for the case of finite conductivity; b is the wall radius.

mode, or as the current convective instability (including the surface helical mode [3.20]). Interestingly, when the resonance condition is satisfied in the model with the free boundary, at the column boundary there is observed the interaction between the internal rippling mode and the external surface helical mode. This leads to a sharp increase in the growth rate of the resistive helical mode up to $\gamma = \omega_0(16m^2/\omega_0\tau_{sk})^{1/5}$ (see [3.16]).

The general picture of the helical instabilities suggests that though the left-hand instability zone point nq_{cr} in the Shafranov diagram is sensitive to the current distribution, the position of the wall and the shape of the column cross section, it is not sensitive to the plasma model and is the same for the high-temperature plasma and just for a conducting fluid.

On the contrary, the right-hand instability zone point $nq(a) = m$ does not depend on the current distribution and the shape of the column cross section but it is sensitive to the model of the column. For instance, the model discussed here even for a high but finite conductivity has instabilities with high increments in the region $nq(a) > m$ (though they are much smaller than the hydromagnetic ones). Actually these instabilities do not occur in the tokamak plasma since the plasma conductivity σ is a function of the magnetic surface, $\sigma = \sigma(\Psi)$, owing to the high longitudinal electron heat conductivity equalizing the electron temperature along the field. Therefore, the model of conductivity convection with the plasma given by eq. (3.36), which determines fast instabilities, cannot be realized in the pure form. We can say that the applicability of the Kruskal-Shafranov criterion $nq(a) > m$ to the current-carrying plasma is based, in fact, not on the high electric conductivity of plasma ($\sigma = \infty$) but on the high longitudinal electron heat conductivity which provides for the dependence $\sigma = \sigma(\Psi)$.

Thus, to fully eliminate the instability of a certain mode with m, n we must be to the left of the instability zone, that is, at a higher current. Under such conditions

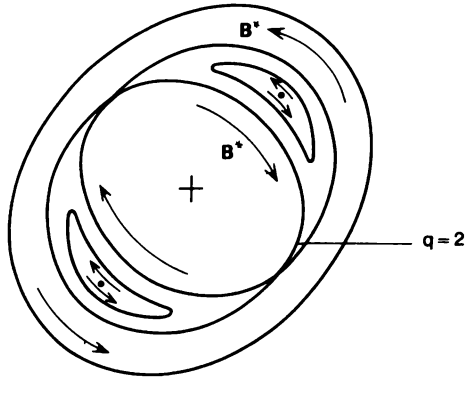

Fig. 3.8. Multiply connected equilibrium magnetic configuration with helical symmetry.

this mode can be regarded as being absolutely stabilized in a certain sense. The modes whose stability is provided for by the condition $nq(a) > m$ can be regarded as being conditionally stabilized. For instance, when the total current in the column is increased while the current density profile is conserved only the modes which were conditionally stabilized can become unstable.

In conclusion of this section we shall qualitatively analyze the possibility of obtaining the helical equilibrium for a current distribution which corresponds to a position within the instability zone for the ideal mode (see Fig. 3.1). As shown in Sec. 3.2 the equilibrium of such a column necessitates the helical currents I_{ext} which compensate the interaction between the plasma current and the longitudinal field (see Fig. 3.4 *b*). These currents can be passed along the axis of the magnetic islands. Since under such conditions $I_{ext} \parallel \mathbf{B}$ and no forces will act on the maintaining conductors, these conductors can be replaced with the current-carrying plasma. In the general case the current-carrying plasma also outside the magnetic islands will be needed to provide for equilibrium (see Fig. 3.8). Though $nq(a)$ will be greater than m at the boundary of such an equilibrium configuration, the current distribution in the central kernel corresponds to the instability zone of the mode with the free boundary. Such multiply connected equilibria can be regarded as the result of evolution of the tearing mode (see Fig. 3.8). Simply connected steady-state helical equilibria are unfeasible in the instability zone.

3.5. Nonlinear Stabilization of the Helical Instabilities of the Ideally Conducting Plasma

Here we shall discuss the cause of saturation of the helical instabilities on the nonlinear stage, found in the numerical calculations reported in [3.6, 3.25]. The above model of the uniform current in the column with the elliptical cross section contributes greatly to understanding of this cause. According to the frozenness of the fluxes, we shall assume that the cross-sectional area of the magnetic surfaces and the rotational transform $\mu(\Phi) = 1/q(\Phi)$ are conserved. For the column with the helical deformation the general expression for μ in the equivalent torus of the radius R has the following form:

$$\mu = \frac{d\chi}{d\Phi} = \frac{n}{m} + R\frac{d\Psi}{d\Phi} \tag{3.37}$$

In this expression the first term is the geometric part n/m of the rotational transform due to the rotation of the surface, $\omega - \varkappa s = \text{const}$, and the second term describes the rotational transform related to the flux Ψ across this surface. The factor R takes into account the length of the helical surface in the equivalent torus (it should be remembered that Ψ is the flux per unit length).

For the sake of simplicity, we shall assume that during the evolution of the mode with $m = 2$ and $n = 1$ the column cross section is elliptical and only the parameter λ

increases. If at the start at $\lambda = 1$ the current distribution was uniform, then μ will remain constant in the cross section with variation of λ. The column with the elliptical cross section and the uniform current proves to have the constant plasma current density j_* for a constant μ and any λ since

$$2\mu = 1 + \left(\frac{j_*}{j_B} - 1\right) \frac{2\lambda}{\lambda^2 + 1} \tag{3.38}$$

Therefore, this case illustrates some features of the nonlinear evolution of the kink mode. We can readily see that to conserve the initial value of μ with increasing λ we must increase the current density j_* since the right-hand factor in the second term of eq. (3.38) decreases with increasing λ. When the cross-sectional area is conserved, this corresponds to an increase in the bulk current of the plasma column.

Now let us show that the relationship between the tearing force leading to the instability and the self-contraction of the column is not changed with such increase in the current density. Write down the expression for Ψ_{ext} in terms of the conserved parameter μ:

$$\Psi_{ext} = \frac{2\pi}{c}(x^2 - y^2)\frac{\lambda^2 - 1}{(\lambda + 1)^2} j_B(\mu - 1) \tag{3.39}$$

This expression shows that self-maintained equilibrium corresponds to $\mu = 1$. When $\mu < 1$ ($q > 1$) and irrespective of λ the disruptive force due to the interaction between the bulk current of the plasma and the longitudinal field exceeds the force of current contraction. Therefore, despire the increase in the current density, the cause of instability does not disappear at the nonlinear stage but, on the contrary, increases owing to the factor $(\lambda^2 - 1)/(\lambda + 1)^2$.

What causes the stabilization of the helical mode, found in numerical calculations which has promoted the conclusion on the safety of the helical modes? When the cross-sectional area is conserved, the bulk plasma current increases owing to the increase in the current density. The total current in the plasma column is determined by the external circuit. In particular, in the absence of a wall the total current must be conserved and therefore the symmetric component of the negative surface current i_0 is generated on the plasma surface. It can be readily seen that the longitudinal field acts on it preventing development of the perturbation thus stabilizing the instability at the nonlinear stage at a certain value of i_0.

Similar arguments are applicable to any type of current distribution in the plasma. The cause of instability due to the bulk current increases, rather than disappears, with evolution of the mode. Stabilization is due not to the shear, as it is sometimes assumed, but exclusively to generation of the negative surface current.

In particular, the negative surface current cannot occur in the stationary case. Therefore, there is no any stable helical equilibrium to be reached by the initially unstable configuration and we can definately state that the current distribution in the stable discharges corresponds to the stability criteria for the kink mode with the free boundary.

Though we have analyzed the mode with the free boundary, note that the increase in the bulk current is a general feature of any plasma deformation conserving the

magnetic fluxes. This should be accompanied with generation of the delta-shape negative current near the boundary of the current channel. We believe that generation of this current also explains the nonlinear saturation of the pure helical mode found in the calculations of the dynamics of the resistive plasma with the fixed boundary [3.25].

3.6. Disruptive Instability in Tokamak

The disruptive instability has been related to the simultaneous evolution of the tearing modes with different m and n and their nonlinear interaction [3.25, 3.29]. We believe that the above results provide a basis for a new approach to the qualitative analysis of the disruptive instability in tokamak [3.23]. The disruptive instability is known to result in the ejection of a considerable part of the energy from the column; it is basically related to the evolution of the mode with $m = 2$, $n = 1$, which is sometimes followed with a series of modes with $m = 3, 4, \ldots$ [3.26]. The mode with $m = 2$, $n = 1$ can lead to the disruptive instability even for high values of $q(d) \approx 4$ at the limiter.

As it was noted above, at the stationary discharge state the current distribution in the plasma column must satisfy all the conditions of the theory of hydromagnetic stability of the kink modes. This means that at the stable stage the mode with $m = 2$, $n = 1$ typically leading to the disruptive instability is stabilized either owing to a sufficiently nonuniform current profile, so that $q(0) < 1$, or owing to the presence of the current-carrying plasma outside the resonance surface $q = 2$. It can be easily seen from eq. (3.32) that for $q > 2$ $(\mu - n/m < 0)$ the term with j' produces a stabilizing effect.

But, as noted above, such stabilization of the helical modes by the peripheral plasma for $nq > m$ is not absolute. The experimentally observed disruptive instabilities for the mode with $m = 2$, $n = 1$ sometimes even for high values of $q(d) \approx 4$ at the limiter imply that the contribution of the peripheral plasma to stabilization is small. Therefore, we believe that in tokamaks, at least for the regimes with $q(a) \approx 2$, stabilization of the mode with $m = 2$ and $n = 1$ is due only to a sufficiently highly peaked current distribution, so that the necessary criterion $q(0) < 1$ [see (3.34)] is definitely satisfied. This conclusion agrees with the indirect experimental data [3.24] according to which $q(0) \approx 0.5$ in the stable discharges for $q(a) \approx 2$.

Accordingly, the exitation of the helical mode with $m = 2$ and $n = 1$ is due to a drop in the current density at the centre of the column [an increase in $q(0)$], for instance, owing to internal disruption or accumulation of impurities. This leads to an increase in the effective radius of the current channel and violation of the stability conditions. If $q(a)$ in the Shafranov diagram (see Fig. 3.1) is regarded as the value of q at a certain radius characterizing the current channel, the discharge can be said to enter the zone of the helical instability from the left. If $q(a)$ is regarded, as it is typically done, as the value of $q(d)$ at the diaphragm radius (we believe that it is less appropriate), then it can be said that the instability zone appears owing to a drop in the current density at the centre. In terms of this interpretation the instability zone was absent at the stable stage owing to a sufficiently large ratio $q(d)/q(0)$.

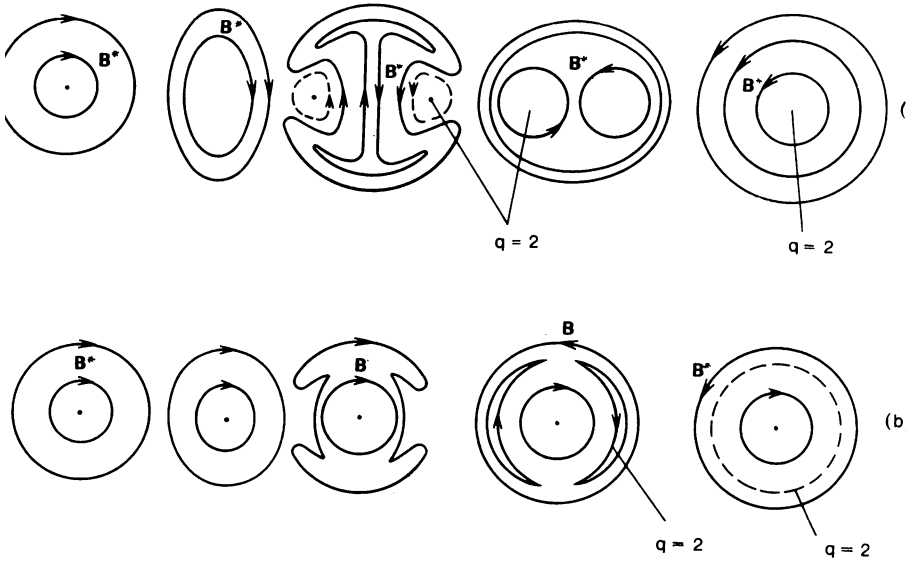

Fig. 3.9. Qualitative picture of inversion of the plasma column, $nq(a) > nq_{cr}$. *a*—Violation of the necessary criterion $nq(0) > m - 1$. *b*—The criterion $nq(0) < m - 1$ is satisfied.

In principle, the instability of the mode with $m = 2$ and $n = 1$ can be caused also by the transfer of the current from the peripheral plasma inside the surface $q = 2$. This, clearly, will have a strong destabilizing effect [see eq. (3.32)]. But under such condition disruption must be preceded with a noticeable positive spike of the voltage.

Either large or small disruption can occur depending on the value of $q(0)$ directly before the disruption. As noted above, if $q(0) > 1$, then the helical instability of the mode with $m = 2$ and $n = 1$ can, in principle, result in total rearrangement of the plasma column. If the instability conditions for this mode are violated but $q(0)$ remains below 1, then the helical instability can rearrange only the periphery of the column. Thus, we believe that large and small disruption differ only in the $q(0)$ value, and the higher this value (the wider the current distribution) the stronger the disruption.

As noted above, the cause of the helical instability, namely, the interaction of the bulk plasma current with the longitudinal magnetic field, does not disappear with the evolution of the mode. The negative surface current generated at the plasma surface serves as the stabilizing factor. It can be naturally assumed that such current appearing in the peripheral plasma sufficiently rapidly decays annihilating with a part of the bulk current. Thus stabilization of the helical mode is eliminated. According to the concepts reported in [3.5, 3.21] the evolution of the nonstabilized helical mode results in the inversion of the plasma column, so that its central part is re-

moved outwards and the peripheral part is drawn inwards (see Fig. 3.9). This process leads to an increase in the minor radius of the plasma.

We can evaluate the effect of the variation δI of the total plasma current by analyzing the condition of conservation of the total helical flux Ψ. The helical flux between the shell and the magnetic axis (or some surface with the radius a_m) prior to disruption can be taken to be equal to the helical flux between the shell and the new plasma surface, where the column core is found after the inversion:

$$\int_{a_m}^{b} \left[B_\theta(Q) - \frac{n_Q}{mR} B_z \right] dQ = \int_{d}^{b} \left[B_\theta^f(Q) - \frac{n_Q}{mR} B_z \right] dQ \tag{3.40}$$

Here B_θ and B_θ^f are the initial and final distributions of the field of the current, b is the shell radius, and d is the radius of the surface where the plasma core is found (d) can be naturally related to the radius of the diaphragm). Hence, the current jump δI is given by

$$\frac{\delta I}{I} = \frac{2l_i - \frac{n}{m} q(d) \cdot \left(1 - \frac{a_m^2}{d^2}\right)}{\ln \frac{b^2}{d^2}},$$
$$l_i = \frac{1}{d \cdot B_\theta(d)} \int_{a_m}^{d} B_\theta(Q)\, dQ \tag{3.41}$$

where l_i and $q(d)$ are the initial values of the flux internal inductance and q at the diaphragm radius. In the case of total inversion, $a_m = 0$, eq. (3.41) yields for the parabolic current distribution with $q(d) = 2$

$$\frac{\delta I}{I} = \frac{1}{2\ln (b^2/d^2)}, \qquad l_i = 3/4 \tag{3.42}$$

Typically, the current increase owing to disruption is of the order of 15%. But eq. (3.42) gives a higher value of $\delta I/I$. This implies that, apparently, even large disruption typically does not lead to the total inversion of the column.

In this case we can estimate the radius a_m and find the zone of mixing using the measured value of $\delta I/I$ and eq. (3.40). In theory a_m can be regarded as the maximum radius for which the core of the column ($Q < a_m$) for a given current distribution in it is stable if there is no current-carrying plasma at $Q > a_m$.

When the mode with $m = 2$ and $n = 1$ has been passed, the value of $q(0)$ at the centre of the column proves to be 2 if the column has been totally restructured. This provides for the development of disruption [see eq. (3.33)] for the mode with $m = 3$ and $n = 1$ and so on. In this way we can explain the sequence of appearance of the helical harmonics in the case of large disruption.

Note that when $q(0) > 1$, there can also occur the instability of the mode with $m = 3$ and $n = 2$ [see eq. (3.33)], which, in principle, can result in disruption. However, the resonance surface for it lies deeper than for the mode with $m = 2$ and

$n = 1$. The experimental observation that the disruptive instability mainly occurs just for the mode with $m = 2$ and $n = 1$ indicates that the fractional mode with $m = 3$ and $n = 2$ behaves as the tearing mode which is stabilized by the currents flowing beyond the surface $q = 1.5$.

In terms of our approach the time of evolution of the disruptive instability is determined by the decay of the surface current. Within the framework of the model of plasma with finite conductivity this time would be close to the skin time calculated for a certain peripheral conductivity of the plasma. We believe that such simplified model is insufficient for explaining the actual time of disruption and we shall have to put forward a more consistent model of the peripheral plasma.

Conclusion

In this study we have attempted to demonstrate the close links between the theories of helical equilibrium and helical instabilities of the current-carrying plasma. We have found the condition of helical equilibrium in the long-wavelength approximation and revealed the specific features of the configurations with helical symmetry due to the essential role played by the interaction between the plasma current and the longitudinal magnetic field in such configurations. We have explicitly shown the cause of the helical instabilities and estimated the extent of their influence on the plasma. In particular, we have shown that the helical instabilities can be regarded as relatively harmless if there is a sufficiently large ratio between the values of q at the axis of the column and the plasma boundary $[q(a)/q(0)]$ which plays the part of the actual safety factor of stability of the plasma column. Formally, the sufficient condition is that for $nq(a) \approx m$ we have $nq(0) < m - 1$. When these conditions are satisfied, we can pass the respective instability zones and increase the current in the plasma column. For instance, if we conserve $q(a)/q(0) \approx 4$, which is found in the regimes with $q(a) \approx 2$ according to the indirect data [3.24, 3.27], we can hope to obtain stable regimes with $q(a) \approx 1$.

The conclusion that the requirements of the linear theory of stability must be satisfied imposes some restrictions on possible current distributions in tokamaks and can prove useful for interpreting the experimental results, especially, for the regimes with low $q(a)$.

Appendix 3.1

Equilibrium of the Column with the Elliptical Cross Section and Distributed Current

The class of analytical exact solutions of the equilibrium equations is very limited. The approximate approach based on the method of moments [3.28] is more effective than the attempts to find exact solutions. We shall use it for describing the equilibrium in the column with elliptical cross section and helical symmetry.

Assume that the cross section of the magnetic surface is described by the equations

$$x = a \cos t, \qquad y = \lambda(a)\, a \sin t \tag{3.A1.1}$$

where a is the coordinate corresponding to the magnetic surfaces, and $\lambda(a)$ is the ratio between the semiaxes of the cross section. At the boundary of the column we have $\lambda(a_0) = \lambda_0$. The metric coefficients which will be used below are

$$q_{22} = \frac{a^2}{2}\left[\lambda^2 + 1 + (\lambda^2 - 1)\cos 2t\right]$$

$$\sqrt{g} = a\lambda\left[1 + \frac{a\lambda'}{\lambda} - \frac{1}{2}\frac{a\lambda'}{\lambda}\cos 2t\right] \tag{3.A1.2}$$

The effective current density $j(\Psi) = j_*(\Psi) - j_B$ is now regarded as a given function $j(a)$.

If we ignore the effects of toroidality, the equations for the moments have the form [3.30]

$$\frac{d}{da}\left\langle f_k \frac{g_{22}}{\sqrt{g}}\Psi'(a)\right\rangle = \frac{4\pi}{c}\ \langle f_k\sqrt{g}\rangle\ j(a) \tag{3.A1.3}$$

The angle brackets denote averaging over t, and f_k is the set of harmonic functions: $f_0 = 1, f_1 = \varrho\cos\theta, f_2 = \varrho^2\cos 2\theta$, and so on. In the model of nested ellipses [see eq. (3.A1.1)] only two moments corresponding to the functions f_0 and f_2 are needed. The averaged quantities entering into eq. (3.A1.3) are

$$\langle\sqrt{g}\rangle = \frac{1}{2}(a^2\lambda)',\ \langle f_2\sqrt{g}\rangle = \frac{1}{8}\left[a^4(\lambda^3 - \lambda)\right]'$$

$$\left\langle\frac{g_{22}}{\sqrt{g}}\right\rangle = \frac{a}{2\lambda}\frac{\left(\lambda^2+1\right)\left(1 + \frac{1}{2}\frac{a\lambda'}{\lambda} + \sqrt{1 + \frac{a\lambda'}{\lambda}}\right) + \left(\lambda^2 - 1\right)\frac{1}{2}\frac{a\lambda'}{\lambda}}{\sqrt{1 + \frac{a\lambda'}{\lambda}}\left(1 + \frac{1}{2}\frac{a\lambda'}{\lambda} + \sqrt{1 + \frac{a\lambda'}{\lambda}}\right)}$$

$$\left\langle f_2\frac{g_{22}}{\sqrt{g}}\right\rangle = \frac{a^3}{4\lambda}\frac{(\lambda^4 - 1)\sqrt{1 + \frac{a\lambda'}{\lambda}} - 2\lambda^2\frac{a\lambda'}{\lambda}}{\sqrt{1 + \frac{a\lambda'}{\lambda}}\left(1 + \frac{1}{2}\frac{a\lambda'}{\lambda} + \sqrt{1 + \frac{a\lambda'}{\lambda}}\right)} \tag{3.A1.4}$$

The first equation (3.A1.3) relates the flux $\Psi(a)$ to the current density $j(a)$:

$$\Psi'\left\langle\frac{g_{22}}{\sqrt{g}}\right\rangle = \frac{4\pi}{c}\int_0^a j(a)\frac{1}{2}(a^2\lambda)'\,da \tag{3.A1.5}$$

The second equation is used for determining the ellipticity of $\lambda(a)$. We shall write it

down in the form suitable for direct numerical integration:

$$\frac{a\lambda'}{\lambda}\left\{\left[\lambda^4+6\lambda^2+1-\frac{\frac{a\lambda'}{\lambda}(\lambda^4-1)}{\left(1+\sqrt{1+\frac{a\lambda'}{\lambda}}\right)^2}\right]\lambda j(a)\right.$$

$$-\left[(\lambda^2+1)\left(1+\frac{2}{1+\sqrt{1+\frac{a\lambda'}{\lambda}}}\right)+\lambda^2-1\right]\frac{1}{a^4}\int_0^a j'(a)a^4\lambda(\lambda^2-1)\,da$$

$$\left.+\left[4(\lambda^4-1)\frac{1}{1+\sqrt{1+\frac{a\lambda'}{\lambda}}}-8\lambda^2\right]\frac{1}{a^2}\int_0^a j'(a)a^2\lambda\,da\right\}$$

$$=4(\lambda^2+1)\frac{1}{a^4}\int_0^a j'(a)a^4\lambda(\lambda^2-1)\,da-4(\lambda^4-1)\frac{1}{a^2}\int_0^a j'(a)a^2\lambda\,da \tag{3.A1.6}$$

To solve eq. (3.A1.6) by the method of iterations we substitute the function $\lambda(a)$ from the previous iteration into the right-hand side and the expression in braces. This approach yields good convergence ($\lesssim 10$ iterations) for all reasonable current distributions.

The magnetic field $\mathbf{B}^*$ has the form

$$|\mathbf{B}^*|=\Psi'(a)\,|\nabla a|=\frac{\Psi'\sqrt{\lambda^2+1+(\lambda^2-1)\cos 2t}}{\lambda\sqrt{2}\,1+\frac{1}{2}\frac{a\lambda'}{\lambda}-\frac{1}{2}\frac{a\lambda'}{\lambda}\cos 2t} \tag{3.A1.7}$$

and the rotational transform has the form

$$\mu(a)=\frac{n}{m}+R\frac{d\Psi}{d\Phi}=\frac{n}{m}+\frac{4\pi R}{c B_z}\frac{j(a)a^2\lambda-\int_0^a j'(a)a^2\lambda\,da}{(a^2\lambda)'\left\langle\frac{g_{22}}{\sqrt{g}}\right\rangle} \tag{3.A1.8}$$

In this model the quadrupole component of the confining field Ψ_{ext} is

$$\Psi_{ext} = -\frac{\pi}{c}(x^2 - y^2)\left\{\frac{\lambda^2 - 1}{(\lambda+1)^2} j_B - 4\,\frac{(j_* - j_B)\lambda - \frac{1}{a_0^2}\int_0^{a_0} j_*' a^2 \lambda\, da}{(\lambda+1)^2}\right.$$

$$\left.\times \frac{\lambda^2 - 1 + \lambda^2 \frac{a\lambda'}{\lambda}}{(\lambda^2+1)\left(1 + \sqrt{1 + \frac{a\lambda'}{\lambda}}\right) + \lambda^2 \frac{a\lambda'}{\lambda}}\right\} \tag{3.A1.9}$$

All quantities in eq. (3.A1.9) are taken at the column boundary $a = a_0$.

This model demonstrates the general relationship between the equilibrium equations and the respective equations describing the stability of the helical modes. In the approximation linear in $\alpha = \lambda - 1$ eq. (3.A1.4) is directly reduced to the second-order equation

$$a^2\alpha'' + a\alpha'\left(2\frac{a\Psi''}{\Psi'} + 3\right) + \alpha\left(2\frac{a\Psi''}{\Psi'} - 2\right) = 0 \tag{3.A1.10}$$

Making the replacement $\alpha = \xi/a$ and using the fact that $\Psi' = aB_z(\mu - n/m)/R$, according to eq. (3.A1.8), we obtain for the displacement ξ the well-known equation describing the stability of the helical mode with $m = 2$ [3.1]:

$$\frac{d}{da}\left[a^3\left(\mu - \frac{n}{m}\right)^2 \frac{d\xi}{da}\right] - 3a\left(\mu - \frac{n}{m}\right)^2 \xi = 0 \tag{3.A1.11}$$

Using eq. (3.A1.9) in the approximation linear in α we see that the condition for existence of the helical equilibrium maintained only by the longitudinal field is

$$\left[\frac{4\pi}{c} j_B a_0 \alpha - \Psi'(2\alpha + a_0\alpha')\right]_{a=a_0} = 0 \tag{3.A1.12}$$

Since $(4\pi/c)j_B = (2n/mR)B_z$, $\Psi' = aB_z(\mu - n/m)/R$, and $\alpha = \xi/a$, eq. (3.A1.12) is reduced to

$$\frac{a\xi'}{\xi} + 3 - \frac{2\mu}{\mu - \frac{n}{m}} = 0 \tag{3.A1.13}$$

which exactly corresponds to the left-hand boundary of the instability zone in the Shafranov diagram [3.1].

The model of nested ellipses which we have used here for describing the helical equilibrium can, of course, be employed for describing the equilibrium with the translational symmetry ($n = 0, j_B = 0$), that is, for tokamaks with noncircular cross sections.

Appendix 3.2

Proof of the Comparison Theorem

In Sec. 3.4 we derived the necessary criterion of stability $nq(0) < m - 1$ from the energy principle by comparing the stability conditions for two current distributions $j(\varrho)$ and $j_1(\varrho)$ which differed in their behaviour at $\varrho > d$. The arguments for greater stability of the distribution $j_1(\varrho)$ given there can seem to be unfounded since they take into account only the behaviour of the destabilizing coefficient at the test function and ignore the spatial dependence of the test function. Therefore, we shall give here the rigorous proof of the theorem of comparison of the distributions $j(\varrho)$ and $j_1(\varrho)$.

Clearly, it is sufficient to demonstrate that stability is decreased by any addition to $j_1(\varrho)$ of a flat current distribution $j_2 = \text{const}$ (wings) at a certain segment $d < \varrho \leq d_1$ with an arbitrary d_1, so that $j_2 < j_1(d)$. The proof is as follows. The criterion of stability is known to be the absence of zeros of the solution $Y(\varrho)$ of the Euler equation satisfying one of the boundary conditions, for instance, for $\varrho = \infty$ [$Y(\infty) = 0$]. At the segment $d_1 < \varrho < \infty$ such solution is

$$Y_e(\varrho) = (d_1/\varrho)^m \tag{3.A2.1}$$

and at the segment $d < \varrho \leq d_1$ it is

$$Y_m = \frac{A}{1+A}\left(\frac{\varrho}{d_1}\right)^m + \frac{1}{1+A}\left(\frac{d_1}{\varrho}\right)^m \tag{3.A2.2}$$

The constant A is found from the condition of joining for $\varrho = d_1$

$$\frac{d_1 Y_e'}{Y_e} - \frac{d_1 Y_m'}{Y_m} = -\frac{2\mu_2^*}{\mu_2 - \dfrac{n}{m}} \tag{3.A2.3}$$

where $\mu_2^* = j_2 R/2B_z$ and $\mu_2 = \mu(d_1)$. Hence, we obtain

$$Y_m = \frac{\mu_2^*}{m\mu_2 - n}\left(\frac{\varrho}{d_1}\right)^m + \frac{m\mu_2 - n - \mu_2^*}{m\mu_2 - n}\left(\frac{d_1}{\varrho}\right)^m \tag{3.A2.4.}$$

Now let us find from the joining conditions for $\varrho = d$

$$\frac{d \cdot Y_m'}{Y_m} - \frac{d \cdot Y_i'}{Y_i} = -\frac{2(\mu_1^* - \mu_2^*)}{\mu_1 - \dfrac{n}{m}} \tag{3.A2.3}$$

[where $\mu_1^* = j_1(d)R/2B_z$, $\mu_1 = \mu(d)$] the logarithmic derivative of the inner solution $d \cdot Y_i'/Y_i$. Equation (3.A2.5) yields

$$\frac{d \cdot Y_i}{Y_i} = \frac{2\mu_2^*}{\mu_2^* + (m\mu_2 - n - \mu_2^*)D^m} + \frac{2(\mu_1^* - \mu_2^*)}{m\mu_1 - n} - 1 \tag{3.A2.6}$$

where $D = d_1^2/d^2 > 1$. To determine that the distribution with the additional wings ($\mu_2^* \neq 0$) is less stable than the initial distribution $j_1(\varrho)$ ($\mu_2^* = 0$) we have just to show that the contribution of the term $\sim \mu_2^*$ to $d \cdot Y_i'/Y_i$ is positive. Since

$$\mu_2 = \mu_1 \frac{1}{D} + \mu_2 \left(1 - \frac{1}{D}\right) \tag{3.A2.7}$$

direct calculations yield for this term

$$2\mu_2^* \frac{\{m\mu_1 - n + nD^m - m\mu_1 D^{m-1} - \mu_2^*(mD^m - D^m - mD^{m-1} + 1)\}}{[\mu_2^* + (m\mu_2 - n - \mu_2^*)D^m](m\mu_1 - n)} \tag{3.A2.8}$$

The terms in the numerator of eq. (3.A2.8) can be conveniently rearranged in the following way:

$$\{\ \} = (\mu_1 - \mu_2^*)(mD^m - D^m - mD^{m-1} + 1) + [n - (m-1)\mu_1](D^m - 1) \tag{3.A2.9}$$

The first term here is always positive, the second term in the instability zone of the distribution $j_1(\varrho)$ is also definately positive. Thus, instability of the above distribution with wings follows from instability of the initial distribution $j_1(\varrho)$.

Since any monotonic current distribution which coincides with $j_1(\varrho)$ for $0 < \varrho \leq d$ and has a nonzero current density for $\varrho > d$ can be obtained by overlapping appropriate layers with j_2, and this leads only to decreasing stability, we can say that we have proven the conclusion of Sec. 3.4 that $j_1(\varrho)$ has a higher stability than $j(\varrho)$, which directly yields the necessary criterion $nq(0) < m - 1$.

References

3.1. V. D. Shafranov, *ZhTF*, **40**, 241 (1970).
3.2. J. A. Wesson, *Nucl. Fusion*, **18**, 87 (1978).
3.3. B. B. Kadomtsev, *Fizika Plasmy*, **1**, 710 (1975).
3.4. G. Bateman, *MHD Instabilities*, MIT Press, Cambridge, 1978.
3.5. B. B. Kadomtsev, O. P. Pogutse, *ZhETF*, **65**, 575 (1973).
3.6. M. N. Rosenbluth, D. A. Monticello, H. R. Strauss, R. B. White, *Phys. Fluids*, **19**, 1987 (1976).
3.7. Yu. N. Dnestrovskii, L. E. Zakharov, D. P. Kostomarov, A. S. Kukushkin, *ZhETF Pis'ma*, **1**, 45 (1975).
3.8. L. S. Soloviev, V. D. Shafranov, *Questions in Plasma Theory*, vol. 5, p. 57, Atomizdat, Moscow, 1967 (in Russian).
3.9. R. Gajewski, *Phys. Fluids*, **15**, 70 (1972).
3.10. V. S. Mukhovatov, V. D. Shafranov, *Nucl. Fusion*, **11**, 605 (1971).
3.11. L. E. Zakharov, Thesis, Moscow, 1974.
3.12. H. R. Strauss, *Phys. Fluids*, **17**, 1040 (1974).
3.13. W. Feneberg, K. Lackner, *Nucl. Fusion*, **13**, 549 (1973).
3.14. J. L. Johnson, C. R. Oberman, R. M. Kulsrud, E. A. Frieman, *UN Geneva Conference*, **31**, 198 (1958).
3.15. B. B. Kadomtsev, *Questions in Plasma Theory*, vol. 2, p. 165, Atomizdat, Moscow, 1963 (in Russian).

3.16. S. N. Breus, *ZhTF*, **30**, 1030 (1960).
3.17. L. E. Zakharov, *Nucl. Fusion*, **18**, 335 (1978).
3.18. H. P. Furth, P. H. Rutherford, H. Selberg, *Phys. Fluids*, **16**, 1054 (1973).
3.19. R. J. Tayler, *Rev. Med. Phys.*, **32**, 907 (1960).
3.20. L. E. Zakharov, *ZhETF Pis'ma*, **32**, 100 (1980).
3.21. B. B. Kadomtsev, in *Plasma Phys. and Contr. Nucl. Fusion Res.* (1976, IAEA) vol. 1, p. 555, Vienna, 1977.
3.22. H. P. Furth, J. Killeen, M. N. Rosenbluth, *Phys. Fluids*, **6**, 459 (1963).
3.23. L. E. Zakharov, *ZhETF Pis'ma*, **31**, 756 (1980).
3.24. V. S. Vlasenkov, V. M. Leonov *et al.* in *Plasma Phys. and Contr. Nucl. Fusion Res.* (1978, IAEA), vol. 1, p. 211, Vienna, 1979.
3.25. B. V. Waddell, B. Carreras, H. R. Hicks, J. A. Holmes, *Phys. Fluids*, **22**, 896 (1979).
3.26. V. G. Merezhkin, *Fizika plasmy*, **4**, 275 (1978).
3.27. V. M. Leonov, V. G. Merezhkin *et al.* in Proc. VIII Conf. on Plasma Phys. and Contr. Nucl. Fusion Res. Rep. IAEA-CN-38/N-2, Brussels, 1980.
3.28. P. H. Rutherford, *Phys. Fluids*, **16**, 1903 (1973).
3.29. J. D. Callen, B. V. Waddell *et al.* in *Plasma Phys. and Contr. Nucl. Fusion Res.* (1978, IAEA), vol. 1, p. 415, Vienna, 1979.
3.30. L. E. Zhakharov, V. D. Shafranov, Kurchatov Institute IAE-3075, preprint (1978).

4. Solitary Waves and Vortexes in Plasma

V. I. Petviashvili, D. Sc. (Phys. and Math.)

Introduction

When we describe the waves in plasma we can often ignore the dissipative effects since they are slower than the effects of dispersion and nonlinearity. Dispersion, that is, the dependence of the wave group velocity on the wave vector, leads to spreading of wave packets owing to phase mixing of the harmonic waves constituting the wave packet. Nonlinearity is the dependence of the wave packet properties on the amplitude. In plasmas nonlinearity typically results in matching of the phases in the packet and displacement of the wave energy towards higher wave numbers in the space of wave numbers. This gives rise to harmonics with large wave numbers and manifests itself in breakdown (or collapse) of the wave packet. At some branches of oscillations a stable equilibrium can set in between the effects of nonlinearity and dispersion and then a part of the initial perturbation is converted into a series of solitons, that is, the stationary solitary waves (see, for instance, [4.1-4]). It is not easy to trace the onset of such an equilibrium in time but nevertheless some equations have been solved with the inverse method of scattering [4.3]. If this cannot be done but soliton can be proved to be stable, we can assume that the initial perturbation will convert into a series of such solitons. However, even stability is far from easy to prove essentially in multidimensional and other complicated cases. Then we shall limit ourselves to finding soliton solutions with numerical method [4.5] and producing indirect evidence of possible realization of solitons. For instance, if the energy density in soliton increases with increase of energy, it is, probably, stable.

In a weakly unstable medium wnere solitons can be realized, small disturbances will grow converting into solitons. The higher the amplitude of a stable soliton the greater the volume it occupies in the wave number space. The soliton will grow until its volume reaches the absorption region at high wave numbers. Then an equilibrium will be established between pumping at low wave numbers and absorption at high wave numbers with a stationary energy flux between them. We shall refer to such solitons as the dissipative ones. For instance, such are the solitons on the flowing down film of viscous liquid [4.6] (see Fig. 4.1).

It has been found that the character of evolution of waves in an unstable medium depends on the relationship between the signs of the dispersion and nonlinearity corrections which can either lead to localization and synchronization of waves into individual wave packets, giving rise to a random series of solitons (soliton turbulence) and sharply reducing the number of the degrees of freedom of the system, or mainly result in exchage of energy between the degrees of freedom each of which remains independent of the others (wave turbulence). The statistical approach is ful-

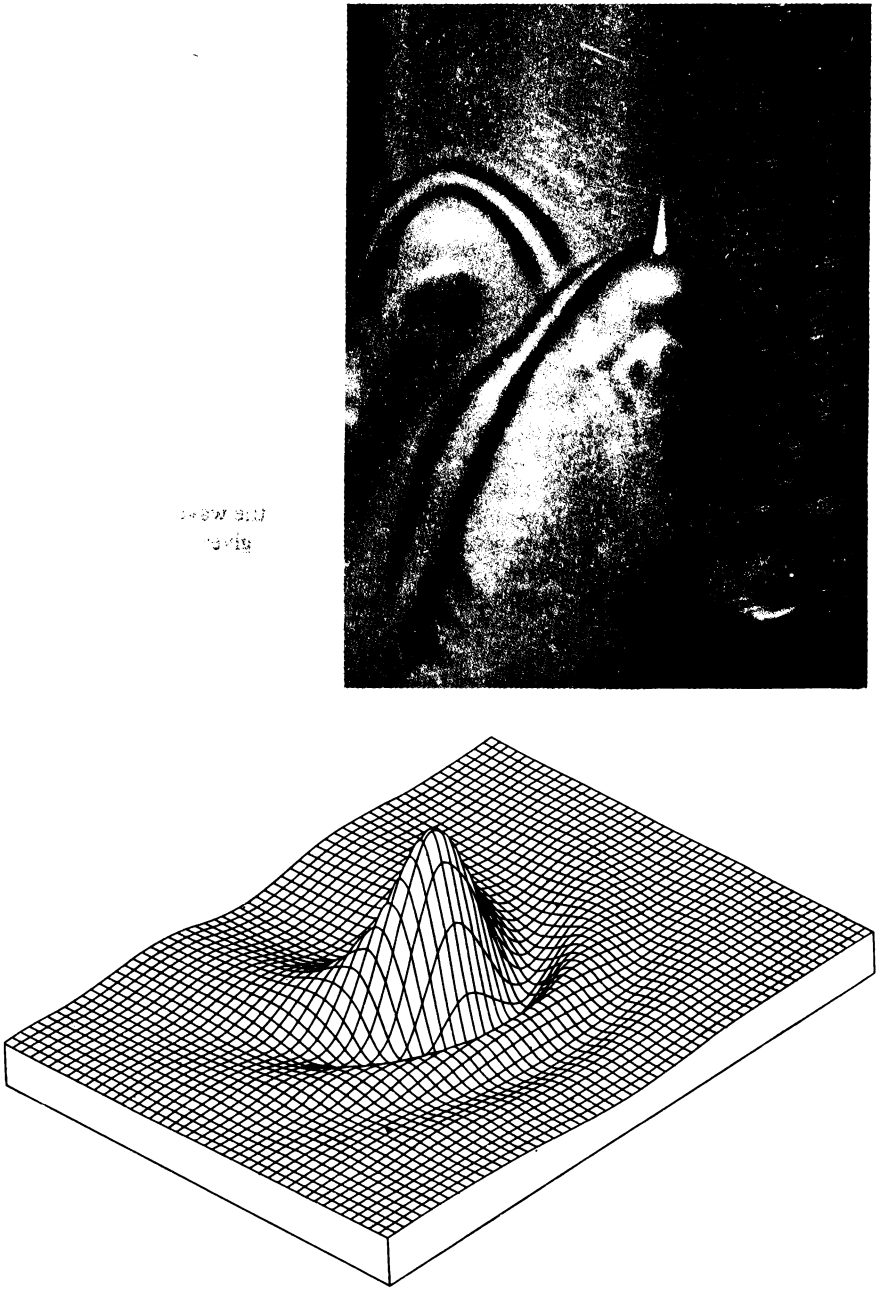

Fig. 4.1. Soliton turbulence on flowing down film of viscous liquid; (*a*) photograph; (*b*) computational realization of solution.

ly applicable to the latter state. In the case of soliton turbulence we can apply the statistical approach to solitons as weakly-interacting particles [4.4] but it is unclear how to do this in a sufficiently general case. The situation is simplified by the fact that the soliton growth ends with saturation and all solitons become the same (dissipative) solitons. The parameters of the dissipative soliton can be found fairly easily with the perturbation theory or the stabilizing factor method [4.5]. We encounter great difficulties if we have to take into account the collisions between solitons. Figure 4.1 gives a clear illustration of the soliton turbulence. Another possibility is that instability in the medium gives rise to a multidimensional periodic wave in the form of one-dimensional, two-dimensional or three-dimensional lattice.

The theory of nonlinear waves in dispersive media is based on the idea put forward by Korteweg and de Vries (KdV). According to this idea, for the sake of simplification, we should regard the parameters of nonlinearity and dispersion as being of the same order of smallness when we expand the wave equations of the general form into the series in powers of small parameters. When we take into account these opposite effects on an equal basis, we can reveal essential features of the phenomena under consideration and obtain a foundation for explicit classification of them. Owing to this idea, such concepts as soliton, self-focussing, collapse, etc. became general in character.

For a long time this idea was not popular owing to the apparent difficulties involved in the analysis of the resulting simplified equations. One of the first instances of its application was in the theory of plasma waves [4.1, 4.2].

We shall conditionally divide the simplified nonlinear equations into following two arbitrary groups; equations of the first group are obtained from the equations for the acoustic branch of oscillations, for instance, the KdV equations; those of the second group are obtained from the equations for the optical branch, for instance, the NSE equation. The methods of analysis of the stability discussed below and the procedure for finding multidimensional soliton solutions are common for both groups of equations.

4.1. Multidimensional KdV Equation

Let us treat the branch of the potential acoustic oscillations. The equation for this branch contains, apart from amplitude, two characteristic parameters, namely, the characteristic dispersion length D and the viscosity coefficient. We shall limit ourselves to treating the isotropic medium and such disturbances whose characteristic size is much greater than D, the velocity amplitude is much smaller than the velocity of sound and for which viscosity can be ignored. Then the equation of acoustic oscillations is

$$\frac{\partial^2 \mu}{\partial t^2} - c^2 \Delta \mu = -\alpha \Delta \Delta \mu - \frac{\partial}{\partial t} (\nabla \mu)^2 \tag{4.1}$$

Here μ is, for instance, the velocity potential, c is the sound velocity in the medium, and the dispersion constant $\alpha \propto (cD)^2$ can be either positive or negative. Dispersion is referred to as positive or negative according to the sign of α. The right-hand side

of eq. (4.1) including dispersion and nonlinearity is assumed to be small. Therefore, we can further simplify eq. (4.1) still retaining its fundamental properties. If the energy density is small, the waves in medium can be regarded as a series of individual packets weakly interacting with each other and propagating with the velocity close to c. It is well known from hydrodynamics that nonlinearity results in steepening of wave packet in the direction of motion, so that the packet dimension in the direction of motion is, typically, much smaller than its transverse dimension. If we treat an individual packet, we can take

$$\mu = \mu(z - ct, \mathbf{r}_\perp, t) \tag{4.2}$$

where the z axis is parallel to the direction of propagation of the wave packet. In such a packet the dependence on the last two arguments is assumed to be weak and the derivatives with respect to these arguments are assumed to be of the order of smallness of nonlinearity and dispersion. Substitution of eq. (4.2) into eq. (4.1) yields

$$2c\frac{\partial^2\mu}{\partial z \partial t} + c^2\Delta_\perp\mu = \alpha\frac{\partial^4\mu}{\partial z^4} - c\frac{\partial}{\partial z}\left(\frac{\partial\mu}{\partial z}\right)^2 \tag{4.3}$$

We have retained here only the terms of the first order of smallness, and the terms of higher orders of smallness have been omitted (such as $\partial^2\mu/\partial t^2$, and $\alpha\Delta\Delta_\perp\mu$).

Equation (4.3) conserves the following integrals of motion:

$$N = \int \left(\frac{\partial\mu}{\partial z}\right)^2 d\mathbf{r} \tag{4.4}$$

$$H = \int \left\{\frac{\alpha}{4c}\left(\frac{\partial^2\mu}{\partial z^2}\right)^2 + \frac{c}{4}\left(\Delta_\perp\mu\right)^2 + \frac{1}{6}\left(\frac{\partial\mu}{\partial z}\right)^3\right\} d\mathbf{r} \tag{4.5}$$

Conservation of the integral (4.5) can be especially well demonstrated if we rewrite eq. (4.3) in the variational form:

$$\partial^2\mu/\partial z\,\partial t = \delta H/\delta\mu \tag{4.6}$$

The KdV equation was generalized for the weakly nonlinear case and written in the form (see [4.1, 4.7])

$$\frac{\partial}{\partial z}\left(\frac{\partial u}{\partial t} + u\frac{\partial u}{\partial z} - \frac{\alpha}{2c}\frac{\partial^3 u}{\partial z^3}\right) = -\frac{c}{2}\Delta_\perp u \tag{4.7}$$

which coincides with eq. (4.3) if we take

$$u = \partial\mu/\partial z \tag{4.8}$$

Equation (4.7) was used in [4.7] to study the stability of the solution in the form of one-dimensional soliton and the relationship between stability and the sign of dispersion was found there. The solution in the form of one-dimensional soliton

propagating with the velocity $-\alpha k_0^2/2c$ is

$$u = -\frac{3\alpha k_0^{-2}}{2c}\cosh^{-2}\left[\frac{k_0}{2}\left(z + \frac{\alpha k_0^2}{2c}t\right)\right] \tag{4.9}$$

where $1/k_0$ is the characteristic soliton width, and the condition of applicability of eqs. (4.1), (4.3) and (4.7) leads to $|\alpha| k_0^2 \ll c^2$. Since eq. (4.7) describes the wave in the reference frame travelling along the z axis with the speed c, we see from eq. (4.9) that in the case of positive dispersion ($\alpha > 0$) the soliton has a negative amplitude and travels with a subsonic speed. In the case of negative dispersion the soliton has a positive amplitude and travels with a supersonic speed. But according to eq. (4.7), the phase velocity of infinitely small disturbances with the wave vector $\mathbf{k}$ along the z axis is $(c/2)(k_\perp/k_z)^2 + \alpha k_z^2/2c$. Thus, in a medium with positive dispersion the speed of infinitely small disturbances is always higher than the soliton speed. In a medium with negative dispersion there exist such infinitely small disturbances whose phase velocity along the z axis is equal to the soliton velocity. This difference should determine the stability of one-dimensional soliton. Indeed, as it was shown in [4.7] with the perturbation theory and in [4.3, 4.8] with the method of the inverse scattering problem, the solution in the form of one-dimensional soliton is stable in the medium with negative dispersion and unstable in the medium with positive dispersion.

According to the numerical calculations [4.5], eqs. (4.3) and (4.7) have the solution in the form of multidimensional soliton in the case of positive dispersion. Let us find such a solution in the three-dimensional case. We shall seek the solution of eq. (4.7) for $\alpha > 0$ in the form of smooth axially symmetric stationary wave propagating with the velocity $-c_1$:

$$u = -2c_1 f(\zeta, \varrho); \qquad 0 < c_1 \ll c \tag{4.10}$$

$$\zeta = \sqrt{2cc_1/\alpha}\,(z + c_1 t); \qquad \varrho = 2c_1 r_\perp \alpha^{-1/2} \tag{4.11}$$

Equations (4.7) and (4.10) yield

$$\frac{\partial^2 f}{\partial \zeta^2} + \frac{1}{\varrho}\frac{\partial}{\partial \varrho}\varrho\frac{\partial f}{\partial \varrho} - \frac{\partial^4 f}{\partial \zeta^4} = \frac{\partial^2 f^2}{\partial \zeta^2} \tag{4.12}$$

Assume that eq. (4.12) has such a solution that the integral $\int f^2 \varrho\, d\varrho\, d\zeta$ is finite. Write down f in the form of the Fourier-Bessel integral

$$f = \int\int F(p, q)\cos(q\zeta)\, J_0(p\varrho)\, p\, dp\, dq \tag{4.13}$$

$$F = \frac{2}{\pi}\int\int f(\zeta, \varrho)\cos(q\zeta)\, J_0(p\varrho)\varrho\, d\varrho\, d\zeta \tag{4.14}$$

Here J_0 is the zero-order Bessel function; here and below integrals are taken between zero and infinity. Using the Fourier transformation, we obtain from eq. (4.12)

$$F = GN, \quad G \equiv q^2/(q^2 + p^2 + q^4) \tag{4.15}$$

where N is the Fourier transform of the nonlinear term:

$$N(p, q) = \frac{2}{\pi}\int\int f^2 \cos(q\zeta)\, J_0(p\varrho)\varrho\, d\varrho\, d\zeta \tag{4.16}$$

Thus, eq. (4.12) is reduced to the nonlinear integral equation (4.15).

Equation (4.15) cannot be solved by the conventional iterative method since it yields a divergent sequence owing to strong computational instability. This instability can be suppressed as follows. Introduce the constants

$$s_1 = \int\int F^2 p\, dp\, dq \tag{4.17}$$

$$s_2 = \int\int FGNp\, dp\, dq \tag{4.18}$$

Clearly, if F satisfies eq. (4.15), then $s_1 = s_2$. Instead of eq. (4.15) we shall solve the following integral equation:

$$F = (s_1/s_2)^\gamma GN, \quad 1 < \gamma < 3 \tag{4.19}$$

The principal qualitative difference of this equation from eq. (4.15) is that the degree of nonlinearity of eq. (4.15) is 2 while that of eq. (4.19) is $2 - \gamma$. Using the iterative method for the system of equations (4.13), (4.16)-(4.19), we obtain a rapidly converging series, and simultaneously $s_1 \to s_2$. This means that by formally decreasing the degree of nonlinearity with the stabilizing factor $(s_1/s_2)^\gamma$ we suppress the computational instability. It can be verified empirically that the most rapid convergence is obtained when γ is equal or close to 2 when the degree of nonlinearity is zero. For $\gamma \leq 1$ or $\gamma \geq 3$ the instability is not suppressed. Equation (4.15) indicates that F has a finite singularity of the form $p^2/(q^2 + p^2)$ at the origin of the coordinates. As can be seen directly from eq. (4.12), this leads to f declining at infinity not as an exponential function but as a power function $|f| \sim r^{-n}$, where r is the distance to the centre of the soliton and n is the space dimension.

The iterative procedure is performed in the following way: take the initial test function F, then find f from eq. (4.13), and successively find N, s_1 and s_2 from eqs. (4.16), (4.17) and (4.18). Substituting them into eq. (4.19), we obtain a corrected F which we again substitute into eq. (4.13), and so on. The initial test function has a weak effect on the convergence of the iterative process. Recently, an exact analytical expression was found for the two-dimensional soliton solution of eq. (4.7) [4.9].

If the dimensionless equation for the two-dimensional soliton is written in the form

$$\frac{\partial^2 f}{\partial z^2} + \frac{\partial^2 f}{\partial y^2} - \frac{\partial^4 f}{\partial z^4} = \frac{\partial^2 f^2}{\partial z^2} \tag{4.20}$$

then, according to [4.9], the solution of eq. (4.20) is

$$f = 12(3 + y^2 - z^2)(3 + y^2 + z^2)^{-2} \tag{4.21}$$

The results of numerical solution of eq. (4.20) by means of the stabilizing factor method (see [4.5]) agree with expression (4.21).

4.2. Stability of Multidimensional Solitons and the Langmuir Soliton

The simplified equations typically have more integrals of motion than the initial equations. Therefore, if a stationary solution is weakly unstable in the general case, then it can prove to be stable within the framework of the simplified equation.

The stability of three-dimensional soliton solutions was analyzed in [4.10, 4.11] for the simplified equations conserving the number N and the energy H of the quasiparticles. If for constant N the soliton solution gives the minimum H, then any perturbation conserving N results in an increase in the energy of the solution, and therefore the soliton is stable. It was shown in [4.11] that the presence of such conventional minimum of H can be found by using the Holder inequality and the comparatively little-known inequality [4.12]

$$\left(\int |\psi|^4 d\mathbf{r}\right)^2 \leq 16 \int |\psi|^2 d\mathbf{r} \cdot \left(\int |\nabla\psi|^2 d\mathbf{r}\right)^3 \tag{4.22}$$

where the integrals are three-dimensional and ψ is any integrable function.

For instance, let us treat the nonlinear Schrödinger equation

$$i\frac{\partial\psi}{\partial t} + \Delta\psi + f(\varphi)\psi = 0, \quad \varphi \equiv |\psi|^2 \tag{4.23}$$

which conserves the integrals

$$H = \int [|\nabla\psi|^2 - F(\varphi)] d\mathbf{r}, \tag{4.24}$$

$$N = \int |\psi|^2 d\mathbf{r}, \quad F \equiv \int f\, d\varphi \tag{4.25}$$

Using inequality (4.22), we obtain from eq. (4.24)

$$H \geq [(\int |\psi|^4 d\mathbf{r})^2/16N]^{1/3} - \int F d\mathbf{r} \tag{4.26}$$

Hence, if $f = \varphi^k$, the Holder inequality readily shows that for $k < 2/3$ the right-hand side of inequality (4.26) has a lower limit, so that H has a conditional minimum dependent on N. This shows that with this condition the three-dimensional soliton solutions are stable, and for $k > 2/3$ they are unstable.

A more exact criterion of instability was obtained in [4.10] by means of variational analysis of the spectrum of the perturbation eigenfrequencies for the soliton solution of eq. (4.23).

If the soliton solution has the form

$$\psi = u(r)e^{i\Omega t}, \qquad \Omega = \text{const} > 0 \tag{4.27}$$

then the integrals (4.24) and (4.25) are the functions of Ω. Then, according to [4.10], soliton is stable if

$$\partial N/\partial\Omega > 0 \tag{4.28}$$

Otherwise, small initial perturbations of soliton grow exponentially with time. This condition is valid for spaces of any dimension. Figure 4.2 shows the dependence of N on Ω numerically calculated for the case of spherically symmetric nodeless soliton solution and $f = \varphi/(1+\varphi)$ in the three-dimensional space, which directly indicates that soliton is stable for $\Omega > 0.08$. This illustrates the importance of inclusion of the additional nonlinear corrections of higher orders. If we had assumed simply that $f = \varphi = |\psi|^2$, then all soliton solutions of eq. (4.23) would be unstable, according to the criterion (4.28), since in that case N is proportional to Ω^{-2}.

The criterion (4.28) seems to be more general than we can infer from the above analysis. According to this criterion, the soliton solution of multidimensional KdV equation (4.7) is stable in the one-dimensional and two-dimensional cases and

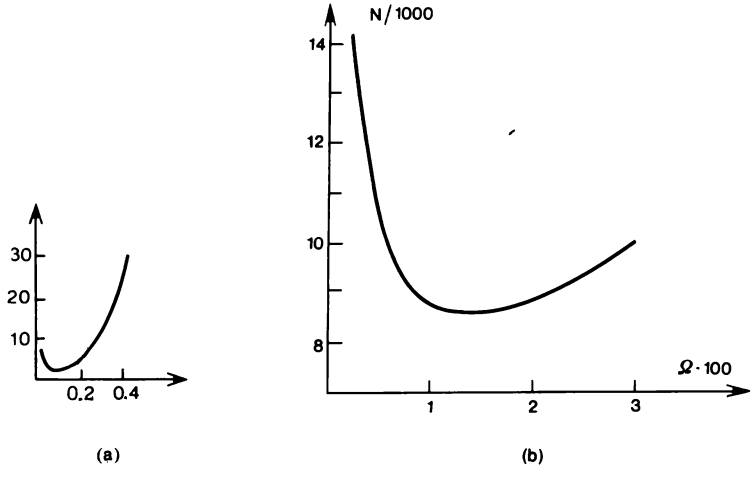

Fig. 4.2. The "number of particles" as a function of frequency for the soliton solutions of the nonlinear Schrödinger equation with "saturating" nonlinearity (*a*). The same dependence for the soliton solutions of the equation (2.12) for the Langmuir waves (*b*).

unstable in the three-dimensional case, though this criterion has not been proven to be applicable to the equations of the type of eq. (4.7).

Let us now analyze the stability of the Langmuir solitons.

As noted in [4.4, 4.13], the most important nonlinear effect of the Langmuir waves is the variation of the plasma density under the influence of the ponderomotive force in the region where the wave packet is localized. For the second, third and other harmonics the nonlinearity effect is smaller than the above effect by a factor of $(v_T/v_{ph})^n$, where v_T is the thermal velocity of electrons, v_{ph} is characteristic phase velocity of the wave and n is the numbe of harmonics. In [4.4, 4.13] this variation was found in the first nonvanishing order of approximation to within the squared field amplitude. In this approximation the three-dimensional Langmuir soliton is unstable. As noted in Sec. 4.1, higher-order nonlinear corrections can play a stabilizing part even for small packet amplitudes. Therefore, these corrections may be useful. They are most easily found in the kinetic treatment with quasilinear approximation, when we assume that the packet is in the soliton state, that is, it is stationary and has only one total frequency ω.

Then the oscillating part of the distribution function f_1 is described by the equation

$$\frac{\partial f_1}{\partial t} + \mathbf{v}\cdot\nabla f_1 = -\frac{e}{m}\nabla\varphi\frac{\partial f_0}{\partial \mathbf{v}}\cos\omega t \tag{4.29}$$

where f_0 is the distribution function averaged over time. In the quasilinear approximation f_0 is given by the equation

$$\mathbf{v}\cdot\nabla f_0 = -\frac{e}{m}\frac{\partial}{\partial \mathbf{v}}\langle\nabla\varphi f_1\cos\omega t\rangle \tag{4.30}$$

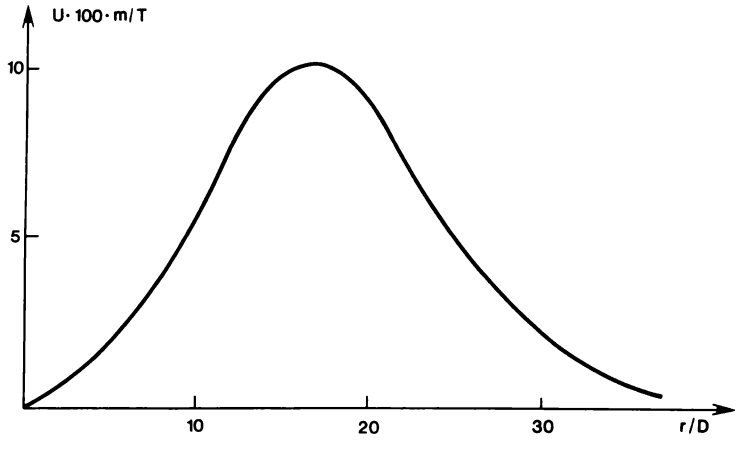

Fig. 4.3. The dimensionless high-frequency potential in the Langmuir soliton as a function of the radius in the case of indifferent stability.

For the sake of simplicity we shall treat the one-dimensional case with $\nabla = \partial/\partial x$. Using f_1 from eq. (4.29) and performing averaging, we obtain approximately

$$\frac{\partial f_0}{\partial x} = \frac{2}{\nu} U \frac{\partial}{\partial \nu} \nu \frac{\partial^2 f}{\partial x \partial \nu} + \frac{\partial U}{\partial x} \frac{1}{\nu} \frac{\partial}{\partial \nu} \nu \frac{\partial f_0}{\partial \nu}$$

$$U \equiv \frac{e^2}{4m^2\omega^2} |E|^2, \qquad E = -\partial\varphi/\partial x \tag{4.31}$$

Take $f_0 = \int_0^\infty G_\varepsilon(x) J_0(q\nu) q dq$. Then using the Fourier-Bessel transformation over ν we can reduce eq. (4.31) to the ordinary differential equation in G and find

$$n = \int f_0 d\nu = n_0 \sqrt{\frac{2T}{\pi m}} \int_0^\infty \exp(-Tq^2/2m) \frac{dq}{\sqrt{1+2Uq^2}}$$

$$\approx n_0 \left[1 - \frac{mU}{T} + \frac{9}{2} \left(\frac{mU}{T} \right)^2 + \dots \right] \tag{4.32}$$

Equation (4.32) is applicable to the three-dimensional case, too, when we have to take $\mathbf{E} = -\nabla\varphi$. When we derived eq. (4.32), we assumed that the ion density follows the electron density which is the case if $T_i \ll T_e$. If this condition is not satisfied, the corrections to eq. (4.31) of the order of U^2 can be readily found with the perturbation theory. We shall assume that the electron density in the stationary Langmuir wave packet has the form (4.32).

Then in the spherically symmetric case this packet satisfies the equation

$$-\Omega E + 3D^2 \frac{\partial}{\partial r} \frac{1}{r^2} \frac{\partial}{\partial r} r^2 E = \left[-\frac{mU}{T} + \frac{9}{2}\left(\frac{mU}{T}\right)^2 \right] E$$

$$\Omega \equiv (\omega^2 - \omega_p^2)\omega_p^{-2}, \quad \omega_p^2 = 4\pi e^2 n_0/m, \quad D^2 = \frac{T}{m\omega_p^2} \tag{4.33}$$

In contrast to the Zakharov equation [4.13], this equation includes the term of the second order in U, which has a stabilizing effect in the sense of the criterion (4.28). On the other hand, the inclusion of higher-order corrections deteriorates the conditions for conservation of the integrals N and H. Figure 4.2 shows the dependence of $N = (m/T)\int U d\mathbf{r}$ on Ω found by soling eq. (4.33), and Fig. 4.3 presents the dimensionless high-frequency potential mU/T in the soliton as a function of the radius (in the Debye radius units) for the value of Ω corresponding to the minimum of N. These plots show that the Langmuir wave packet could convert to the stable soliton state with increasing amplitude and decreasing size just when the packet size exceeds the Debye radius.

The parameters of the dissipative Langmuir soliton were calculated in [4.14], where only the first nonlinear term in the right-hand side of eq. (4.33) was taken into consideration. The Landau damping at high wave numbers and energy pumping at low wave numbers were included, and the solution was found with the stabilizing factor method [4.5]. It has been shown that the Landau damping can be compensated with a relatively weak energy pumping, for instance, in the form of parametric instability.

These calculations were stimulated by the experiments on the interaction between plasma and high-intensity laser radiations. In the regions where the local Langmuir frequency was close to the frequency or half-frequency of the electromagnetic wave the experiments revealed the formation of cavitons (depressions of the density of the plasma) whose characteristic size was of the order of several Debye radiuses. The lifetime of cavitons was considerably greater than the collapse time. Apparently the electron density in cavitons oscillated with one frequency close to the Langmuir frequency. This can explain the discrete character of the Raman spectrum of the electromagnetic wave scattered in the region where the cavitons were formed.

4.3. Simplified Equation for Langmuir Waves in Magnetic Fields

An equation for the Langmuir waves in the absence of a magnetic field including the primary nonlinear effect, namely, the ponderomotive force, was derived in [4.13]. The characteristic dispersion length in this case is known to be equal to the Debye radius. The presence of a weak magnetic field greatly increases this length in the direction perpendicular to the field. Let us analyze the effect on the equation for the Langmuir waves [4.15].

The dispersive equation for the potential waves with the frequency close to ω_r and the wave vector direction close to that of a magnetic field can be written as

$$\omega^2 = \omega_p^2(1 + 3k_z^2 r_D^2 + \alpha k_\perp^2 k_z^{-2})$$

$$\alpha k_\perp^2 \ll k_z^2, \qquad k^2 r_D^2 \ll 1, \qquad \alpha \equiv \frac{\omega_B^2}{\omega_p^2 - \omega_B^2} \tag{4.34}$$

where ω_p and ω_B are the Langmuir and electron cyclotron frequencies. If the frequency of the packet is close to ω_p, the potential in it can be written in the form

$$\Phi = \frac{1}{2}[\psi(\mathbf{r}, t)\exp(-i\omega_p t) + \text{c.c.}] \tag{4.35}$$

Here the dependence of the "amplitude" ψ on time and $\mathbf{r}_\perp$ is weak and, for the sake of simplicity, we assume that the packet speed is much lower than that of the ion sound. Then the variation of the plasma density under the effect of the high-frequency force is described by

$$n_1 = -1/[16\pi(T_e + T_i)]\left|\frac{\partial\psi}{\partial z}\right|^2 \tag{4.36}$$

In eq. (4.36) we can ignore the electric field perpendicular to the magnetic field owing to the assumed weak dependence of ψ on $\mathbf{r}_\perp$. Hence we can find the local variation of the Langmuir frequency and eqs. (4.34)-(4.36) yield

$$\frac{\partial^2}{\partial z^2}\left(\frac{2i}{\omega_t}\frac{\partial\psi}{\partial t} + 3r_D^2\frac{\partial^2\psi}{\partial z^2}\right) - \frac{\partial}{\partial z}\frac{n_1}{n_0}\frac{\partial\psi}{\partial z} = \alpha\Delta_\perp\psi, \qquad \Delta_\perp \equiv \frac{\partial^2}{\partial x^2} + \frac{\partial^2}{\partial y^2} \tag{4.37}$$

where n_0 is the mean plasma density. Equation (4.37) gives different signs of dispersion perpendicular to the magnetic field, depending on the sign of α. For a wave packet of a finite size eq. (4.37) conserves the number N of the particles and the energy H given by

$$N = \int\left|\frac{\partial\psi}{\partial z}\right|^2 d\mathbf{r}, \tag{4.38}$$

$$H = \int\left(3r_D^2\left|\frac{\partial^2\psi}{\partial z^2}\right|^2 + \alpha|\nabla_\perp\psi|^2 - \frac{|\partial\psi/\partial z|^4}{32\pi n_0(T_e + T_i)^2}\right)d\mathbf{r} \tag{4.39}$$

Note that the total energy of the wave packet is $N + H$. According to the sign of α given by eq. (4.34), eq. (4.37) can have a stationary three-dimensional solution if the plasma frequency is higher than the cyclotron frequency, when the contribution of the transverse electric field to the energy (4.39) is positive. We shall seek the stationary solution of eq. (4.37) in the form

$$\frac{\partial\psi}{\partial z} = \sqrt{32\pi n_0(T_e + T_i)}Af(\varrho, \zeta)\exp(i\omega_p A^2 t/2) \tag{4.40}$$

Here we have introduced the dimensionless coordinates

$$\zeta = \frac{A}{\sqrt{3}r_D}z, \qquad \varrho = \frac{A^2}{\sqrt{3\alpha}r_D}\mathbf{r}_\perp \tag{4.41}$$

Now we obtain the following equation for the dimensionless real function f:

$$\frac{\partial^2}{\partial\zeta^2}\left(\frac{\partial^2 f}{\partial\zeta^2}-f+f^3\right)=\Delta_\varrho f \tag{4.42}$$

Equation (4.42) has the soliton solution, that is, a smooth solution tending to zero at infinity. This solution was found numerically in [4.15] with the stabilizing factor method described in Sec. 4.1. It can be readily shown that the soliton energy (4.39) is positive and the number of the particles is proportional to A^{-3}, and therefore we have $\partial N/\partial A<0$ and such a soliton is unstable according to the stability criterion (4.28). In the presence of a small perturbation the soliton will either spread out or collapse. In the case of collapse it will convert into the dissipative soliton described in Sec. 4.2. Since the Larmor radius is greater than the Debye radius, the effect of magnetic field on such a soliton can be neglected.

It has been observed recently that high-frequency radio waves are strongly scattered by the regions of the ionosphere irradiated with high-intensity radio waves with a frequency close to the Langmuir plasma frequency in the scattering range. The frequency of the scattered wave proves to be strongly modulated by a frequency close to the frequency of the scattering wave. This modulation and, possibly, the scattering itself can be explained by formation of a cluster of Langmuir solitons pumped by the high-intensity radio wave. The pumping is due to the parametric instability of the dissipative type occurring at low wave numbers in the fields of the high-intensity radio wave.

Thus, the stationary three-dimensional Langmuir solitons described in Sec. 4.2 can be formed in the ionosphere under the effect of a high-intensity radio wave at the final stage of evolution of the parametric instability. The solitons tend to form large-size clusters extended along **B**. Intense heating of electrons occurs in the cluster, resulting in a decrease in the plasma density in it. But the greatest decrease in the plasma density occurs inside the soliton. It is due to the ponderomotive force (high-frequency pressure) with which the Langmuir oscillations trapped in the soliton act on the plasma. The amplitude of these vibrations can be much greater than the amplitude of the pumping radio wave. The high amplitude of the vibrations in the soliton cluster can strongly modulate the waves scattered by the cluster. The modulation frequency is equal to the soliton frequency which is markedly lower than the Langmuir frequency of the surrounding plasma.

4.4. Solitons of the Electromagnetic Waves with Ordinary Polarization

The electromagnetic wave with ordinary polarization in the vicinity of the Langmuir frequency has the anisotropic spatial dispersion:

$$\omega^2=\omega_p^2+c^2k_\perp^2+c^4k_z^2k_\perp^2\omega_p^{-2} \tag{4.43}$$

$$c^2k^2\ll\omega_p^2,\ \omega_B^2$$

Here the axis z is parallel to the magnetic field.

Let us analyze the conditions of existence of the ordinary wave in the form of nonspreading wave packet—soliton. The soliton exerts the high-frequency pressure on the plasma, so that the plasma density in the region of the packet is changed by

$$n_1 = -|E|^2/[16\pi(T_e + T_i)] \tag{4.44}$$

We shall see from the discussion below that the soliton is flattened across the z axis so that $k_z \gg k_\perp$. Under these conditions the electric field in the ordinary wave is almost parallel to the z axis, so that we can include in eq. (4.44) only E_z, that is, the field component parallel to **B**. Write down for E_z:

$$E_z = \frac{1}{2}[E(\mathbf{r}, t)\exp(-i\omega_p t) + \text{c.c.}] \tag{4.45}$$

The characteristic frequency of the dependence of E on time is assumed to be much lower than ω_p. Then eqs. (4.43)-(4.45) yield

$$\frac{2i}{\omega_p}\frac{\partial E}{\partial t} + \frac{c^2}{\omega_p^2}\left(1 - \frac{c^2}{\omega_p^2}\frac{\partial^2}{\partial z^2}\right)\Delta_\perp E + |E|^2 E/[16\pi n_0(T_e + T_i)] = 0 \tag{4.46}$$

When we derived eq. (4.46), we made use of the fact that the packet is elongated along the axis z. Equation (4.46) conserves the number of particles

$$N = \int |E|^2 \, d\mathbf{r} \tag{4.47}$$

and the packet energy

$$H = \int \left\{ \frac{c^2}{\omega_p^2}|\nabla_\perp E|^2 + \frac{c^4}{\omega_p^4}\left|\nabla_\perp \frac{\partial E}{\partial z}\right|^2 - |E|^4/[32\pi n_0 (T_e + T_i)] \right\} d\mathbf{r} \tag{4.48}$$

Now let us find the stationary soliton-like solution of eq. (4.46). To do this take

$$E = \sqrt{16\pi n_0(T_e + T_i)}\, A f(\varrho, \zeta) e^{iA^2\omega_p t/2} \tag{4.49}$$

$$\zeta = \omega_p z/c, \qquad \varrho = A\omega_p r_\perp/c \tag{4.50}$$

where f is a real function. Substitution of eq. (4.7) into eq. (4.46) yields

$$\left(1 - \frac{\partial^2}{\partial \zeta^2}\right)\Delta_\varrho f = f - f^3 \tag{4.51}$$

To satisfy the conditions of applicability of our treatment, that is, $c^2k^2 \ll \omega_p^2, \omega_B^2$, the constant A (the dimensionless amplitude of the soliton) must be much smaller than unity. Equation (4.51) can be solved by the stabilizing factor method described in Sec. 4.1 [4.5]. We can see from eqs. (4.48) and (4.51) that the soliton of the ordinary wave differs from the soliton of the NSE in the second dispersive term in the square brackets in eq. (4.48) and in the left-hand side of eq. (4.51). It can be seen that this term has a stabilizing effect, since owing to it the wave packet energy (4.48) is limited from below for a fixed N.

Such lower energy limit is sufficient for stability of the soliton. However, this stability can exist only for small A values. When the total soliton energy grows, A increases and the soliton dimensions decrease; this is equivalent to an increase in the effective wave number, so that the terms of higher orders of smallness must be in-

cluded in the frequency expansion (4.43). Thus, we must add to eq. (4.43) the term

$$\frac{c^6 k_z^4 k_\perp^2}{\omega_p^4}\left(1+\frac{\omega_p^2}{\omega_B^2}-\frac{k_\perp^2}{k_z^2}\right) \tag{4.52}$$

For large A values the last term in the parentheses in eq. (4.52) included in eq. (4.46) leads to the loss of the soliton stability resulting in collapse, that is further growth of the effective wave number in the soliton. Under the effect of a magnetic field the wave number leads to the build-up of the transverse curl component of the electric field of the ordinary wave and weakening of the dependence of the frequency on ω_p. As a result, the wave is no longer locked by the depression of the plasma density and is emitted from the plasma. The I type bursts of the radiation in radio-frequency range of the solar corona [4.17] can be attributed to such a loss of stability simultaneously by a large cluster of solitons of the ordinary wave.

4.5. Two-Dimensional Langmuir Solitons in the Strong Magnetic Field Without Density Well

High-intensity beams of runaway electrons are observed in tokamaks and stellators in low-density regimes ($\omega_p < \omega_B$). They, apparently, are generated in regions of reconnection of the magnetic field lines, where a constant electric field appears along the magnetic field. To explain the reconnection and formation of the electric field we must assume that the electric resistance in the reconnection region is much greater than the resistance due to binary collisions of electrons. Probe measurements in the cross section of the plasma column revealed regions of localization of high-intensity Langmuir noises with the monochromatic frequency spectrum. Simultaneously, electromagnetic radiation with the same frequency was emitted from the plasma [4.18]. Apparently, the observed Langmuir waves give rise to the anomalous resistance needed for reconnection. The waves themselves are due to the instability of the runaway electrons generating waves with frequencies lower than the electron cyclotron frequency [4.19, 4.20].

Since the increment is not large and is localized in a small region, the condition of maintaining the anomalous resistance is that the Langmuir waves that are generated in this region do not spread over the whole plasma.

In this section we are noting the possibility of self-localization of the Langmuir waves around a magnetic field line or at a magnetic surface, which is accompanied with a narrowing of the frequency spectrum of the turbulent noises. Both these effects have been observed in the experiments with the stellator Uragan-2 [4.18]. A peculiar feature of these strongly nonlinear effects is the absence of plasma density wells. The phases of the oscillations are self-correlated via the higher harmonics of the fundamental oscillating modes. The modulation instability is stabilized with damping at the Doppler resonance.

A simplified nonlinear equation for the Langmuir waves in the magnetic field was derived in Sec. 4.3, where, as in [4.13] in which the magnetic field was ignored, the nonlinearity mechanism was the formation of the plasma density well under the ef-

fect of the high-frequency pressure. In this equation for $\omega_p < \omega_B$ the dispersion correction perpendicular to the magnetic field reverses its sign, so that the one-dimensional soliton solutions become stable.

Such solitons were observed in [4.21]. They were produced owing to the instability of the electron beam with a small spread in the velocity space. Such solitons were clearly absent in the experiment [4.18] discussed above. The oscillations were observed to be localized perpendicular to the magnetic field, rather than parallel to it, and no plasma density wells were found in the localization region. This can be explained by the fact that, instead of a narrow beam, in tokamaks and stellators we have a long tail of runaway electrons to the velocity distribution f of electrons, which has only one peak. Such a distribution function is unstable with respect to amplification of the potential waves with the frequencies $\omega < \omega_B$ [4.19, 4.20]. The waves propagating towards the tail are intensified owing to the "anomalous" Doppler resonance with the electrons whose velocity along the magnetic field is $v_z = (1 + \omega_B/|\omega|)\omega/k_z$. The interaction at the Čerenkov resonance for $v_z = \omega/k_z$ here must be small as is the case owing to the smallness of the derivative $\partial f/\partial v_z$ at this point.

The waves propagating in the direction opposite to the tail are damped at the "normal" Doppler resonance for $v_z = (1 - \omega_B/|\omega|)\omega/k_z$. An order-of-magnitude estimate of the Doppler resonance increment or decrement is $\alpha\omega(\omega_p/\omega_B)^2$, where α is the ratio of the densities of the particles in the tail and the thermal particles. Therefore, if the electron distribution function has a tail, we obtain only the waves propagating along the tail and no plasma density depressions. The one-dimensional solitons observed in [4.21] contain a standing Langmuir wave in the density depression. The standing wave component propagating in the direction opposite to that of the electron distribution tail is not damped at the normal Doppler resonance since owing to the narrowness of the electron beam in the veiocity space there are no electrons having the appropriate resonance velocity.

This explanation is substantiated by the following fact observed in [4.21]. When the electron beam had a large velocity spread, that is, when damping at the normal Doppler resonance became possible, the density depressions were observed much less often than in the case of the electron beam with a small velocity spread, though these beams exhibited a negligible difference in the Langmuir noise levels.

Now, let us demonstrate for $\omega_p < \omega_B$ the possibility of realization of the propagating Langmuir soliton without a density depression localized on a magnetic surface or around a magnetic field line. Such a soliton is easily intensified by the tail of the electron distribution function, and if there appears the component propagating in the opposite direction, this component is damped, so that we do not observe a density well due to this component in the presence of the tail of accelerated electrons.

Assuming that ω_B is sufficiently high, we can regard the electron motion as one-dimensional in the hydrodynamic approximation and obtain

$$\frac{\partial v}{\partial t} + v\frac{\partial v}{\partial z} = -\frac{v_T^2}{n}\frac{\partial n}{\partial z} + \frac{e}{m}\frac{\partial \varphi}{\partial z} \tag{4.53}$$

$$\frac{\partial n}{\partial z} + \frac{\partial}{\partial z}(nv) = 0 \tag{4.54}$$

$$\Delta\varphi = 4\pi e(n_e - n_0) \tag{4.55}$$

Here v is the electron velocity along the magnetic field which is parallel to the z axis. We shall look for the stationary solution propagating along z with a constant velocity u, so that all the quantities depend on $z - ut \equiv \zeta$ and $\mathbf{r}_\perp$. We assume that the velocity u is much higher than the thermal velocity v_T, and hence we can ignore the pressure in eq. (4.53). Then after integration over z eqs. (4.53) and (4.54) yield

$$v = u(1 - \sqrt{1 + \psi}), \qquad \psi \equiv 2e\varphi/mu^2 \tag{4.56}$$

$$n = n_0[1 + N(\mathbf{r}_\perp)](1 + \psi)^{-1/2}, \quad n_0 = \text{const} \tag{4.57}$$

Here N is the integration constant which differs from zero only in the region of localization of the wave and is found from the following condition for the electron density averaged over z: owing to their frozenness in the magnetic field the thermal electrons are not displaced perpendicular to the magnetic field despite the high-frequency pressure, so that the electron density averaged over z cannot depend on $\mathbf{r}_\perp$. Therefore, we have $\langle n \rangle = n_0$, where the angle brackets denote averaging over z. Using eq. (4.57), we obtain now

$$N(\mathbf{r}_\perp) = \langle (1 + \psi)^{1/2} \rangle^{-1} - 1 < 0 \tag{4.58}$$

But then we obtain that the mean flux of electrons along the magnetic field in the soliton differs from zero, that is, the wave entrains the electrons:

$$\langle nv \rangle = -n_0 u N(\mathbf{r}_\perp) \tag{4.59}$$

Owing to conservation of the mean charge in the soliton the mean electric field perpendicular to the magnetic field is zero:

$$\langle \nabla_\perp \psi \rangle = 0, \qquad \langle \psi \rangle = 0 \tag{4.60}$$

Finally, substitution of eq. (4.57) into the Poisson equation (4.55) yields the soliton equation

$$\Delta\psi = 2k_0^2[(1 + N)(1 + \psi)^{-1/2} - 1], \quad k_0 \equiv \omega_p/u \tag{4.61}$$

Let us analyze the system of equations (4.58) and (4.61) for small amplitudes $|\psi| \ll 1$. Assume that the soliton is localized on the magnetic surface which approximately coincides with the plane $x = 0$, and it declines exponentially with increasing distance from this plane. Write down ψ as the series

$$\psi = \sum_{m=1}^{\infty} \psi_m(x) \cos m(k_z\zeta + k_y y), \quad \zeta \equiv z - ut \tag{4.62}$$

For small amplitudes our system of equations can be written as

$$\Delta\psi = k_0^2\left[-(1 + N)\psi + \frac{3}{4}\psi^2 - \frac{5}{8}\psi^3 + 2N\right]$$

$$N(x) = -\frac{3}{8}\langle \psi^2 \rangle \tag{4.63}$$

Assume that $0 > k - k_0 \ll k_0$, where $k = (k_x^2 + k_y^2)^{1/2}$. Substituting eq. (4.62) into eq. (4.63) and eliminating ψ_2, we obtain from the perturbation theory for the first harmonic ψ_1

$$k_0^{-2} \frac{\partial^2 \psi_1}{\partial x^2} = A^2 \psi_1 - \frac{3}{8} \psi_1^3,$$
$$A^2 \equiv (k^2 - k_0^2) k_0^{-2} \ll 1 \tag{4.64}$$

Amplitudes of the higher harmonics are much smaller than that of the first harmonic and are of the order of $\psi_m \sim A^m$.

Equation (4.64) has the soliton solution localized in the vicinity of the plane $x = 0$:

$$\psi_1 = 2.3A/\cosh(Ak_0 x) \tag{4.65}$$

This solution is unstable with respect to modulation over y. Therefore, we must look for axially symmetric soliton solutions of the system of equations (4.58) and (4.61), which are periodic in z, namely, $\psi = \psi(\zeta, r_\perp)$, $N = N(r_\perp)$, where the principal wave number k_z satisfies the condition $0 < k_z - k_0 \leq k_0$. Since the theory of perturbations is not applicable here, we shall find the solution with the stabilizing factor method [4.5]. Owing to high magnetic pressure the plasma density averaged over oscillations is independent of the coordinates even if the high-frequency pressure is comparable to the plasma pressure.

Thus, we obtain the axially symmetric two-dimensional soliton without plasma density depression, which oscillates along z with the principal wave number k_z and propagates with the velocity u. The fundamental soliton frequency is $\omega = k_z u > \omega_p$, the oscilations of the dimensionless potential ψ are such that for $A^2 \equiv (k_z^2 - k_0^2) k_0^{-2} \leq 1$ the transverse wave number is of the order of Ak_z and, hence, the soliton radius is of the order of $1/Ak_z$ [4.18].

According to the quasilinear or weak-turbulence theory, the waves with different wave vectors have different frequencies owing to spatial dispersion, and therefore the turbulence spectrum is wide and the wave packet always spreads out. Build-up of the Langmuir waves by the tail of fast particles was analyzed within the framework of the quasilinear theory in [4.22].

This approach is valid if the noise level is low. Over a certain energy density threshold nonlinear self-matching of the wave phases is started which is typically, evidenced by narrowing of the frequency spectrum and self-localization of the wave packets. While in the case of weak turbulence the predicted spectrum width is of the order of the fundamental frequency itself, in the case of strong nonlinearity this width is much smaller. Therefore, the phenomena observed with Uragan-2 are not explained by the weak-turbulence theory. A considerable proportion of the accelerated electrons are produced only at individual resonance magnetic surfaces or field lines, where the electrons are accelerated owing to the development of the MHD helical instability. Owing to the anomalous Doppler effect these electrons amplify the Langmuir waves which would spread all over the plasma but for the self-localization effect which gives rise to solitons localized in the instability region. The energy density in such solitons can be compared to the plasma pressure; this facilitates effective pumping of the longitudinal energy of the escaping electrons to

the transverse mode. There are many trapped electrons for such a high energy density in the soliton. This indicates a need for a nonlinear theory of instability for the anomalous Doppler resonance, which can be developed by analogy to the theory of trapped electrons in the monochromatic Langmuir wave. Such a theory will yield estimates of the anomalous resistance and give a more complete picture of reconnection of the field lines.

The tail of the electron distribution function in the magnetized plasma is a much more natural and frequent phenomenon than the electron beam which is, typically, produced with a special device. Usually, the tail is responsible for a considerable part of the electric current with the anomalously low resistance, thus strongly affecting the hydrodynamic properties of the plasma. Therefore, further efforts are needed to study the interaction between the runaway electorns of the tail with the solitons analyzed above, which occurs also at the resonances with multiple cyclotron frequencies, apart from the resonance discussed above.

4.6. Solitary Vortex in Nonuniform Plasma

Drift waves can propagate in the plasma which is nonuniform in the direction perpendicular to a constant magnetic field. These waves can be easily amplified by either a current or an electron beam, or an ion temperature gradient, or dissipative effects [4.20]. It has been shown in [4.23] that at the nonlinear stage of evolution of this branch there appear two-dimensional solitary vortices localized perpendicular to the magnetic field. These vortices strongly increase the heat conductivity of the plasma as the convective cells in a liquid do. The vortex radius decreases with increasing amplitude and tends to the Larmor ion radius r_B. Therefore, the finite-amplitude vortexes are insensitive to the magnetic field shear, and we can describe them assuming that the magnetic field is constant.

The waves in plasma with the frequencies below ω_{B_e} and the phase velocity along the magnetic field lower than both the thermal velocity of electorns and the Alfven velocity are described by the electric potential φ in which electrons have the Boltzmann distribution. In a plasma of a sufficiently high density the electron density is equal to the ion density and given by

$$n = N\exp(e\varphi/T_e) \tag{4.66}$$

Here N and T_e are assumed to depend on the coordinate x perpendicular to the magnetic field.

The phase velocity of the wave is assumed to be higher than the thermal velocity of ions. Then the ions are described by the hydrodynamic equation

$$\frac{d\mathbf{v}}{dt} = -\frac{e}{m}\nabla\varphi + [\mathbf{v} \times \omega_{B_i}] - \frac{1}{nM}\nabla nT_i \tag{4.67}$$

We shall assume that the wave frequency is much lower than ω_{B_i} and that the ion velocity along the magnetic field parallel to the z axis is negligibly small. Then we can obtain a solution of eq. (4.67) in the form of a series in powers of $(1/\omega_{B_i})(d/dt)$. The first terms of the series give the following expression for the ion velocity com-

ponent perpendicular to the magnetic field:

$$\mathbf{v}_\perp = r_B^2\left\{\left[\omega_{B_i} + \nabla\psi\right] - \left(\frac{\partial}{\partial t} + \mathbf{r}_B^2\left[\omega_{B_i} \times \nabla\psi\right]\cdot\nabla\right)\nabla_\perp\psi\right\} + \ldots$$

$$T_i \ll T_e \tag{4.68}$$

Here $r_B^2 \equiv T_0/m\omega_{B_i}^2$, $\psi = e\varphi/T_0$, and T_0 is the electron temperature in the plane of propagation of the axis of the sought vortex, which is given by the equation $x = 0$.

The system of equations (4.66) and (4.68) is closed with the continuity equation which can be written in the form

$$\frac{d\ln n}{dt} + \operatorname{div}\mathbf{v}_\perp = 0 \tag{4.69}$$

Here we again ignore the ion velocity along the magnetic field. Substitution of eqs. (4.66) and (4.68) into eq. (4.69) yields the following equation for ψ:

$$\frac{1}{\omega_{B_i}}\frac{\partial}{\partial t}\left(r_B^2\Delta\psi - \psi\right) + r_B^2\left[\nabla\psi \times \nabla\left(r_B^2\Delta\psi - \ln N - \frac{T_0}{T_e}\psi\right)\right]_z = 0$$

$$\Delta = \frac{\partial^2}{\partial x^2} + \frac{\partial^2}{\partial y^2}, \qquad T_0 = T_e(0) \tag{4.70}$$

This equation was derived and analyzed in [4.24] for the drift waves with a statistical method for $T_e = \text{const}$. The equation describes in the linear approximation the drift waves propagating along y with the drift velocity

$$v_* = -\omega_{B_i} r_B^2 \partial(\ln N)/\partial x \tag{4.71}$$

If T_e and N are independent of the coordinates, eq. (4.70) has a stationary solution

$$\Delta\psi = F(\psi), \qquad \partial\psi/\partial t = 0 \tag{4.72}$$

where F is an arbitrary function. This indeterminacy typical of ideal liquid is eliminated for $v_* \neq 0$. Then, if we take $\partial/\partial t = -u\partial/\partial y$, where u is the constant velocity of propagation of the vortex, we obtain from eq. (4.70) after integration over y

$$r_B^2\Delta\psi = A^2\psi - g\psi^2, \qquad A^2 \equiv 1 - v_*/u$$

$$g \equiv -\omega_{B_i} r_B^2 \frac{\partial T_e/\partial x}{2T_0 u} \approx \partial(\ln T)/\partial(\ln N^2) \tag{4.73}$$

Equation (4.73) has the following soliton solution depending on the radius r:

$$\psi = \frac{A^2}{g} f(\varrho), \qquad \varrho \equiv Ar/r_B, \qquad r^2 \equiv x^2 + (y - ut)^2 \tag{4.74}$$

Equations (4.73) and (4.74) indicate that f satisfies the soliton equation

$$\frac{1}{\varrho}\frac{\partial}{\partial\varrho}\varrho\frac{\partial f}{\partial\varrho} = f - f^2 \tag{4.75}$$

whose solution is given in Fig. 4.4.

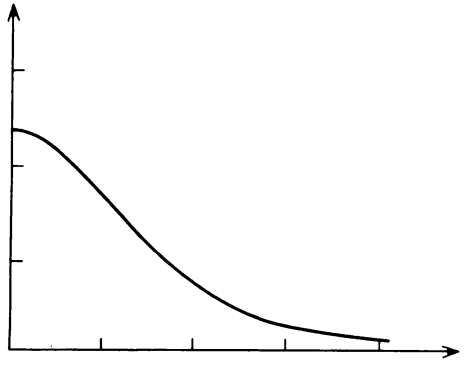

Fig. 4.4. The drift soliton.

The motion of ions along the z axis was analyzed in [4.23] and it was shown to result in a small slope of the soliton solution (4.74) to the magnetic field in the plane (y, z). It was also shown that the one-dimensional soliton solution of eq. (4.70) is unstable.

The fact that the drift soliton appears only in the presence of a temperature gradient and that, according to eq. (4.68), the plasma in it rotates as in a vortex implies that this soliton is a convective vortex. It can exist in the presence of only a gradient of T_e without a density gradient if $T_i \ll T_e$.

The kinetic treatment would yield an equation for the dependence of the vortex amplitude A on time and the instability increment with respect to amplification of the drift wave.

Note a recently derived equation [4.25] describing the vortexes in a shallow rotating atmosphere, and in particular, the Great Red Spot of Jupiter. This equation is very similar to the drift vortex equation given here.

References

4.1. B. B. Kadomtsev, *Collective Phenomena in Plasma*, Nauka, Moscow, 1976 (in Russian).

4.2. L. A. Artsimovich, R. Z. Sagdeev, *Plasma Physics for Physicists*, Atomizdat, Moscow, 1979 (in Russian).

4.3. V. E. Zakharov, S. V. Minakov, S. P. Novikov, L. P. Pitaevsky, *Theory of Solitons*, Nauka, Moscow, 1980 (in Russian).

4.4. L. I. Rudakov, *DAN SSSR*, **207**, 821, 1972.

4.5. V. I. Petviashvili, *Fizika plazmy*, **2**, 469, 1976.

4.6. V. I. Petviashvili, O. Yu. Tsvelodub, *DAN SSSR*, **238**, 1321, 1978.

4.7. B. B. Kadomtsev, V. I. Petviashvili, *DAN SSSR*, **192**, 753, 1970.

4.8. V. E. Zakharov, *ZhETF Pis'ma*, **22**, 364, 1975.

4.9. L. A. Bordag, A. R. Its, et al., *Physics, Lett.*, **63A**, 205, 1977.

4.10. N. G. Vakhitov, A. A. Kolokolov, *Izv. VUZov*—Radiofizika, **16**, 1020, 1973.
4.11. V. E. Zakharov, E. A. Kuznetsov, *ZhETF*, **66**, **594**, 1974.
4.12. O. A. Ladyzhenskaya, *Mathematical Problems of Dynamics of Viscous Incompressible Liquid*, Fizmatgiz, Moscow, 1961 (in Russian).
4.13. V. E. Zakharov, *ZhETF*, **62**, 1745, 1972.
4.14. V. I. Petviashvili, O. Yu. Tsvelodub, *Fizika plazmy*, **6**, 467, 1980.
4.15. V. I. Petviashvili, *Fizika plazmy*, **1**, 28, 1975.
4.16. I. J. Kantor, *JGR*, **79**, 199, 1974.
4.17. V. I. Petviashvili, O. S. Korolev, *Fizika plazmy*, **1**, 436, 1975.
4.18. V. I. Petviashvili, N. F. Perepelkin et al., *ZhETF*, **79**, 828, 1980.
4.19. B. B. Kadomtsev, O. P. Pogutse, *ZhETF*, **53**, 2025, 1967.
4.20. A. B. Mikhailovsky, *Theory of Plasma Instabilities*, Atomizdat, Moscow, 1975 (in Russian).
4.21. S. V. Antipov, M. V. Nezlin, E. I. Snezhkin, A. S. Trubnikov, *ZhETF*, **76**, 1571, 1979.
4.22. V. V. Parail, O. P. Pogutse, *Yadernyi sintez*, **18**, 303, 1978.
4.23. V. I. Petviashvili, *Fizika plazmy*, **3**, 270, 1977.
4.24. A. Hazegawa, C. G. McLennan, Y. Kodama, *Physics Fluids*, **22**, 2122, 1979.
4.25. V. I. Petviashvili, *ZhETF Pis'ma*, **32**, 632, 1980.

5. Observation of Langmuir Solitons

M. V. Nezlin, D. Sc. (Phys. and Math.)

Introduction

In the recent years physicists became deeply interested in the fascinating nonlinear wave structures, known as *solitary waves* or *solitons*. A soliton is a wave packet in which the wave field is localized in a limited (generally propagating) spatial region and is absent outside this region. Soliton, however, differs fundamentally from the classical wave packet which, being a linear formation, is known to spread out rapidly owing to the variation of the group velocity in the whole wavelenth range of the packet. Soliton is essentially nonlinear; the (linear) dispersion of the group velocity in it is exactly compensated by the reverse phenomenon, namely, nonlinear self-compression of the wave packet, and therefore the soliton propagates without spreading out and conserving its shape.

Thus, the soliton is a nonspreading, nonlinear wave packet in which the phases and amplitudes of the waves are appropriately self-consistent [5.1–3].

It would seem natural to regard exact mutual compensation of dispersion and nonlinearity as being hardly probable and soliton as being a product of the theorists' imagination, rather than a real phenomenon. But, strange as it may seem, numerous theoretical studies and calculations and some (as yet few) experiments definitely demonstrate the existence and wide occurrence of solitons. Moreover, physicists are increasingly coming to the belief that solitons may play an essential part in such different fields as physics of elementary particles, solid state physics, hydrodynamics, astrophysics, nonlinear optics, plasma physics, and even biology [5.3–6]. The soliton is a fundamental part of the system of concepts of a new science known as "synergetics" [5.7]; special conferences on the soliton have been held [5.4b, 5.6, 5.8]. Sometimes it can be heard [5.4b] that in physics of nonlinear waves the soliton has the same position as the linear oscillator in classical physics (such extreme opinions are, possibly, inspired by the current fashion).

The history of solitons starts about 150 years ago with the famous Scott-Russel's observation in an English canal in 1834 [5.3, 5.4]. Korteweg and deVries were the first to introduce solitons into theory in 1895 [5.9]. A vivid example of solitons in nonlinear optics is the observed transformation of a laser beam in a dispersive medium into a sequence of wave bunches, that is, solitons [5.10, 5.11].

Solitons were first introduced into plasma physics, apparently, in [5.12]. Now we can identify a number of areas in plasma physics which definitely involve or can involve solitons. They include plasma turbulence, relaxation of beams of chared particles and laser beams in plasma, formation of energy distribution of particles which are optimal for plasma chemistry, anomalous plasma resistance, self-compression of high-intensity waves, namely, the Langmuir, lower hybrid,

drift and other waves (and, respectively, heating of plasma with these waves and anomalous diffusion of plasma in the magnetic field), nonlinear phenomena in space plasma, and so on. Even this brief list demonstrates that experimental studies of solitons in plasma are not only of fundamental scientific interest but have also a considerable practical significance, particularly, for development of the plasma thermonuclear reactors of the tokamak or stellator type in the immediate future.

Here we shall discuss the experimental results on the solitons produced from the Langmuir waves and the so-called oblique Langmuir waves with large amplitudes in plasma in a strong magnetic field. But first we shall present the main theoretical concepts which will be needed for interpreting the experimental data.

5.1. Langmuir Solitons (Review of Theoretical Results)

The Langmuir solitons are produced owing to self-compression of the Langmuir waves, that is, in the process which is the reverse of the spreading of the linear wave packet. This self-compression is a kind of instability known as the *modulational instability* [5.13–15]. We shall illustrate the physical meaning of the modulational instability by the case of one-dimensional wave packet whose length L is large in comparison with the wavelength, $L \gg \lambda = 2\pi/k$. If the packet were linear (that is, had a small amplitude), the rate of its spreading would be determined by the dependence of the group velocity v_g on the wave number k: $\partial L/\partial t = |\partial v_g/\partial k|\, 2\varkappa$, where $2\varkappa \simeq 4\pi/L \ll k$ is the interval of the wave numbers of the packet. The characteristic time of spreading is $\tau \simeq L/(\partial L/\partial t) \simeq \pi/(\partial v_g/\partial k)\varkappa^2$. If the dispersive wave packet is nonlinear (that is, if the wave frequency depends on the wave amplitude E_0), then under certain conditions the packet stops spreading and even undergoes self-compression or collapse [5.14]. The mechanism of this effect is related to the *ponderomotive force of the dynamic pressure* pushing plasma out of the region with an increased strength of the high-frequency field of the wave. If such a region appears as a result of fluctuation, it partially traps the wave and the field strength in this region is increased still further; this leads to further pushing out of plasma, that is, to deepening of the *"well"* of the plasma density, an so. Thus, if fluctuation of the field occurs in a region whose spatial scale corresponds to the characteristic wave number $\varkappa$, the wave proves to be modulated with the spatial period $2\pi/\varkappa$. In other words, under certain conditions conversion of monochromatic wave into a spatially modulated wave proves to be energetically favourable. This effect is known as the modulational instability or self-compression of the wave packet. After appearance of this instability the wave field may develop in two directions. If self-compression of the wave at a certain stage is balanced with dispersion, the soliton is formed; if it is not balanced, the wave will *collapse* until it is absorbed by the plasma particles or converted into other waves [5.1, 5.2, 5.14]. The direction of the wave evolution depends on the geometry of the system, and the characters of dispersion and nonlinearity. In the

discussion below we shall always assume that the system has the plane geometry, (linear) dispersion of waves is expressed by

$$\omega_k = \omega_p + \frac{3}{2}(kr_D)^2\omega_p \tag{5.1}$$

and nonlinearity [5.1] by

$$\omega = \omega_k \alpha E_0^2 \tag{5.2}$$

where α is a coefficient, k is the wave number, $\omega_p = (4\pi n_0 e^2/m)^{1/2}$ is the Langmuir frequency, $r_D = (T_e/4\pi n_0 e^2)^{1/2}$ is the electron Debye radius, n_0 is the plasma density, T_e is the electron temperature, and E_0 is the amplitude of the electric field of the wave. Under the given conditions the Langmuir wave field which was initially spatially uniform will break down into a series of Langmuir solitons under the effect of the modulational instability [5.15]. The conditions of the modulational instability have the form [5.1, 5.2]

$$\alpha \frac{\partial v_g}{\partial k} < 0 \tag{5.3}$$

and

$$\left| \frac{\partial v_g}{\partial k} \right| \varkappa^2 < 4|\alpha| E_0^2 \tag{5.4}$$

The first of these conditions (the Lighthill criterion) is satisfied for the Langmuir waves with any amplitude since the nonlinear addition to the Langmuir wave frequency [see eq. (5.2)] due to the ponderomotive force of the high-frequency dynamic pressure is $\alpha E_0^2 = -\omega_p E_0^2/32\pi n_0 T_e < 0$, while the derivative $\partial v_g/\partial k = 3\omega_p r_D^2 > 0$. The Lighthill criterion (5.3) follows from the so-called nonlinear parabolic equation [5.1] which is used to analyze the stability of wave packets. This criterion is applicable only if the concept of the wave packet is applicable, that is, if the size L of the wave formation is much greater than the initial wavelength λ or if $\varkappa \ll k$; the condition for the wavelength has the form $kr_D < (1/3)(m/M)^{1/2}$.

Condition (5.4) implies that in the wave the electric energy density $W_0 E_0^2/16\pi$ should be higher than a certain threshold value:

$$W_0/n_0 T_0 > 3(\varkappa r_D)^2/2 \tag{5.5}$$

In the Langmuir soliton due to the modulational instability the high-frequency dynamic pressure force pushing out plasma from the density well is counterbalanced by the excess thermal pressure of plasma due to formation of the density well; therefore, the depth of the well is given by

$$\delta n/n_0 \simeq W/nT_e \tag{5.6}$$

The distributions of the electric field $E(x)$, the wave electric energy density $W(x) \sim E^2(x)$ and the plasma density perturbation $\delta n(x)$ along the soliton have

the form of a bell-like curve close to the Gaussian distribution:

$$E(x) = E_0 \cosh^{-1}(k_0 x)$$
$$W(x) \sim E^2(x) = E_0^2 \cosh^{-2}(k_0 x)$$
$$\delta n(x) = \delta n \cosh^{-2}(k_0 x) \sim E^2(x)$$

Here x is the longitudinal coordinate. The characteristic width of this distribution at the level of $1/e$ of the amplitudes of E_0, E_0^2 and δn, known as the soliton width Δ, is [5.1, 5.15, 5.24]

$$\Delta_E \approx \frac{3.3}{k_0} \approx r_D \left(\frac{60nT}{W}\right)^{1/2} = r_D \left(\frac{60n}{\delta n}\right)^{1/2}$$

$$\Delta_n = \Delta_{E^2} \approx \frac{2.2}{K_0} \approx r_D \left(\frac{30_{nT}}{W}\right)^{1/2} = r_D \left(\frac{30n}{\delta n}\right)^{1/2} \tag{5.7}$$

In constrast to [5.1], we have assumed here that $T_e \equiv T \gg T_i$, where T_i is the ion temperature (in [5.1] it was assumed that $T_e = T_i = T$, so that $\delta n/n = W/(2nT)$, and the soliton width in this model was greater than the width found from eqs. (5.7) by a factor of $2^{1/2}$). The width Δ characterizes the packet size at which the nonlinear self-compression of the packet is counterbalanced with dispersive spreading.

When comparing theoretical predictions with experimental results, we shall use both expressions (7) for the soliton width depending on what parameter is measured in the experiment: the width Δ_E will be determined from the oscillogram of the field E indicator (the high-frequency probe), and the width Δ_n will be determined from the oscillogram of the plasma density indicator (the diagnostic resonator).

The Langmuir soliton discussed above, that is, the self-compressed wave packet whose size is greater than the wavelength,

$$\Delta > \lambda = 2\pi/k \tag{5.8}$$

appears owing to the long-wave modulational instability ($\varkappa < k$) and is known as the *envelope soliton*. This soliton is characterized by a relatively large size and low intensity of oscillations:

$$\frac{W}{nT} \approx \frac{\delta n}{n} \gtrsim (\varkappa r_D)^2 < (k r_D)^2 < \frac{m}{M} \tag{5.9}$$

Here m and M are the masses of the electron and the ion. A considerably more interesting phenomenon is the *large-amplitude Langmuir soliton* which appears when

$$W/nT > (kr_D)^2 \tag{5.10}$$

that is, in the case of *short-wave modulational instability*, known in Americal literature as the *oscillating two-stream instability (OTSI)* ($\varkappa > k$). The size of this soliton is smaller than the initial wavelength:

$$\Delta < \lambda \tag{5.11}$$

Everything that was said about the envelope soliton is applicable to this soliton, apart from the Lighthill criterion (5.3) which is not applicable to the large-amplitude soliton.

The following facts should be noted for the velocity of the Langmuir soliton. Firstly, according to the theory [5.1, 5.2, 5.15], the soliton velocity cannot exceed the ion sound speed c_s. Secondly, the mechanism of formation of the Langmuir soliton is related to formation of a *standing wave* and its localization in plasma [5.16, 5.17, 5.22]. Thirdly, a propagating soliton must be rapidly stopped by plasma particles [5.18, 5.19]. Therefore, experimental studies of solitons which are at rest or stopped moving in plasma are of the greatest interest. We shall bear this in mind when describing the experimental results. Incidentally, eq. (5.6) is valid only for slow solitons whose velocity is much lower than the ion sound speed.

Thus, we can formulate the following (conventional) definition of the Langmuir soliton: it is *plasma density well "filled" with the Langmuir oscillations* or, simpler, *a density well with a "Langmuir filling"*.

5.2. Langmuir Solitons (Experimental)

The experiments on Langmuir solitons can be classified into two groups. The first group includes the experiments with the following essential features [5.20–23]: firstly, no magnetic field is applied, and secondly, the plasma in the experimental installation exists in a medium with a relatively high concentration of neutral atoms (argon, the pressure $p_0 \approx 1$ to 2×10^{-4} mm Hg) and therefore is highly collisional. The first of the above features provides for certain procedural advantages (for instance, makes it possible to measure the soliton parameters by means of "probing" of plasma with an electron beam) but does not allow us to study the properties (stability) of solitons in *magnetized* plasma. Owing to the second feature, the time of scattering τ_e of the plasma electrons with respect to the loss of momentum in collisions with neutral atoms proves to be negligibly small in comparison with the "time of flight" of the soliton and even the passage time of the ion sound in the system ($\tau_s = L/c_s$). Under such conditions the Langmuir soliton (whose velocity is always lower than c_s or even close to zero, as noted above) travels a very short distance during the time τ_e. Therefore, after external "pumping" of the Langmuir waves (external pumping by high-frequency field

[5.20, 5.21] or electron beam [5.22, 5.23]) has been discontinued, the soliton just have no time to move during the time of collisional decay of the waves (approximately τ_e of the order of several microseconds), that is, it proves to be practically unobservable. Under such experimental conditions the question about the properties (stability) of a *free* soliton (existing without "pumping") remains open.

The second group includes the experimental studies [5.24–26] distinguished by the collisionless regime of a strongly magnetized plasma [$\tau_e \gg \tau_s$; $\omega_H \gg \omega_p$, where $\omega_H = eH/mc$, and $\omega_p = (4\pi ne^2/m)^{1/2}$ are the Larmor and Langmuir frequencies, respectively]. Another distinguishing feature of these experiments is that they are performed in *moving* plasma in order to make possible the recording with stationary devices of the "most interesting" solitons, that is, those that are not moving or are stopped with respect to the plasma. Two techniques were used in these experiments for generation of the Langmuir solitons: either with the external high-frequency electric field (produced with a "pumping resonator") [5.24] or with the electron beam [5.24–26].

Here we shall review the main results obtained in the experiments of the second group [5.24–26]. Two modifications of the experimental installation were used in these studies. One of them was used for the excitation of the Langmuir waves by the external high-frequency electric field and by the electron beam.

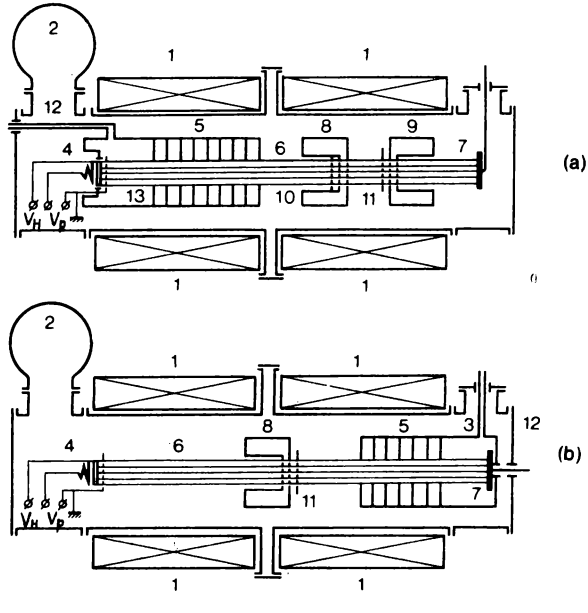

Fig. 5.1. Experimental setup: (*a*) first modification; (*b*) second modification.

The first modification (see Fig. 5.1*a*) comprised the following components: the solenoid *9* 250-cm long which produced in the experiments approximately uniform magnetic field $H = 2 \times 10^3$ Oe, the vacuum chamber with the diffusion pump *1*, the discharge chamber *12* in which plasma was produced by passing an electron beam from the electron gun through the gas (hydrogen) fed into the chamber, a series of diaphragms comprising the so-called gas delay unit *3* with the length of 80 cm, in which the plasma moving along the magnetic field (with the velocity about c_s) is freed of the neutral gas for a time sufficient for conducting the experiment [5.24], the plasma column *11* with the diameter of 3–4 cm, the beam collector *8*, the working volume with the length $L \approx 100$ cm, which contains two quarter-wave resonators—the pumping resonator *4* and the diagnostic resonator *5* (the working openings of the resonators are covered with mesh grid of 95% transparency), two high-frequency generators connected to these resonators, a pair of "modulating" grids *6*, the high-frequency probe *7* and the selective tunable receiver P5-20 for recording the Langmuir oscillations, and three pulsed power sources—two (independent) for controlling the electron gun and one for controlling the pulsed valve for feeding gas to the discharge chamber. The plasma was produced in the discharge chamber with pulsed hydrogen feeding by means of the pulsed (10–20 μs) electron beam with the electron energy of 0.5 to 2 keV and the current of tens to hundreds of milliamperes. The plasma flowed from the discharge chamber along the magnetic field and about 50 μs after the end of the electron beam pulse, having passed the gas delay unit, it got into the working volume where it continued to travel with (approximately) the ion sound velocity $c_s \approx 2 \times 10^6$ cm/s. The gas pressure in the working volume (in the flowing plasma regime) was about 3×10^{-6} mmHg (and remained at this level for about 10 ms after plasma had flowed). The electron temperature (measured with the Langmuir probe) was $T_e \approx 10$ eV, the typical plasma density was $n \approx 3 \times 10^9$ cm^{-3}, $r_D \approx 3 \times 10^{-2}$ cm.

The electron beam used for generating the Langmuir waves in the plasma was operated independently from the electron beam which produced the plasma; its parameters were independent and the pulse duration was approximately equal to the plasma pulse duration, the beam diameter was 3 cm, and the electron number density in the beam was $n_1 \approx (1 \text{ to } 3) \times 10^7$ cm$^{-3} \leq 10^{-2}\, n$. In this experimental series, when the plasma wave excitation by the electron beam was used, the pumping resonator was still placed in the way of the plasma flow though the pumping generator was not operational; the resonator just provided for self-modulation of the beam at the fixed frequency $f = 500$ MHz $\approx f_p$, which facilitated recording of solitons with the P5-20 receiver which was tuned to this frequency. This resonator determined the beginning of the working volume. The plasma with the above parameters was magnetized ($\omega_H \gg \omega_p$) and collisionless ($\tau_e \gg \tau_s = L/c_s$) [5.24]. The absence of collisions was an absolutely necessary condition of the experiments [5.24] with generation of the Langmuir solitons with the external high-frequency field, because the pumping resonator operated with single pulses of short duration (about 1–3 μs), which was much shorter than the time of subsequenty observation of solitons.

The second modification of the installation (see Fig. 5.1*b*) differed from the first primarily in the character of the velocity distribution of the electrons in the beam. In the first modification of the installation (Fig. 5.1*a*) the electron beam entered the working volume after having passed the plasma column and (therefore) the electron velocity distribution was strongly spread out. In the second modification the discharge chamber of the plasma source was at the end of the installation opposite to the electron gun. In this case the plasma flowed toward the beam and the electrons entering the plasma when it had reached the working volume could be regarded as monoenergetic. This change of the experimental conditions proved to be essential and greatly facilitated observation of the Langmuir solitons. Another useful alteration was made in this modification of the installation, namely, the diameter of the beam and the plasma was increased approximately twice (up to 6 cm), owing to the decrease in the magnetic field in the working volume by a factor of 3.5 with the same cathode diameter of the electron gun. The duration of the electron beam pulse was 500 μs and all measurements were performed during the pulse. The energy of the electrons in the beam was $W_1 = 200$ to 1000 eV, the current was $I = 50$ to 80 mA, the electron number density was $n_1 \approx (1 \text{ to } 2) \times 10^7 \text{ cm}^{-3} \lesssim 10^{-2}\, n$, and the magnetic field was $H = 500$ to 1000 Oe. The plasma speed v in these experiments was as low as 4×10^5 cm/s, that is, it was just a fraction of the ion sound speed c_s in contrast to the first modification of the installation where the plasma speed $v \approx c_s$.

Now let us briefly discuss the diagnostics and experimental procedures. The plasma density, its variation with time and the density wells associated with solitons were determined with the resonator technique [5.24–26]. We shall not go into the details of the technique. Note only that the diagnostic resonator serving as the plasma density indicator (*5* in Fig. 5.1) had the Q factor value of about 250, the width of the resonance curve was about 5 MHz, and the operating frequency was about 750 MHz, which was considerably higher than the fundamental frequency of the pumping resonator and the frequency $f_p = \omega_p/2\pi \approx 500$ MHz of the Langmuir plasma oscillations under consideration; there was no coupling between the resonators, which could result in their influencing each other.

A high-frequency probe was used for determining the relative strength of the electric field of the Langmuir oscillations. The working surface of the probe was the 0.1 mm tungsten wire grid with the diameter 6 cm and the mesh size 2×2 mm^2. The probe (Fig. 5.1) was placed into the plasma flow with its surface perpendicular to the magnetic field H. Therefore, the probe primarily detected the waves with a large electric field components parallel to $\mathbf{H}$, that is, the Langmuir waves in this case. The signal from the probe was measured by means of two independent techniques. In the first technique the signal was fed via a coaxial cable to the 75-Ohm input of the selective tunable receiver (P5-19 or P5-20 type), the detected signal from the output of the receiver was fed to an S1-42 storage oscillograph and then photographed. The receivers made it possible to identify a fixed frequency within the 0.8 MHz band in the 250–1000 MHz range. In the second technique the signal was fed to a detector with the 50–1000 MHz working frequency range and then to an U3-7A wide-band amplifier, we shall refer to such a signal as the integral signal since it comprises

practically all high-frequency oscillations, rather than those at one selected frequency. In both techniques the oscillogram of the signal from the high-frequency probe represented the time dependence of the envelope of the oscillation amplitudes.

No absolute measurements of the electric field of the Langmuir waves were performed in this study. In principle, they are not necessary since the quantity $E_0^2/16\pi$ in the soliton is determined by the density well $\delta n/n$ as can be seen from eq. (5.6). In the experiments of the first group discussed above [5.20–23] where no external magnetic field was applied, the absolute measurements of the electric field were done with the electron beam perpendicular to the magnetic field. In the experiments described here [5.24–26] this method was inapplicable owing to the presence of a strong magnetic field.

Excitation of the Langmuir waves with the high-frequency field was performed by means of the quarter-wave pumping resonator (*4* in Fig. 5.1). This resonator is similar in the design to the diagnostic resonator but its fundamental frequency is much lower. It was excited by a pulse generator of decimetre waves with the frequency $f_E = 495$ MHz; the plasma density was chosen for the field frequency f_E to be sufficiently close to the Langmuir electron frequency. The resonator was excited by means of a loop placed at the antinode of the magnetic field in the resonator. The excited electric field had the maximum strength in the resonator gap and its direction was parallel to the external constant magnetic field **H**. The generator pulse duration was 1 μs, and the pumping intensity was several watts.

To trap the oscillations at the pumping frequency in the plasma, the initial density of plasma was chosen so that $f_E \lesssim f_p$. The nonlinear wave packet (soliton) generated in this way passed with flowing plasma by the high-frequency probe (*7* in Fig. 5.1) and the diagnostic resonator *5*; the probe and the resonator were fixed to each other (with the spacing of 3 cm) and could be shifted together along the installation. This arrangement was convenient for observing the solitons localized in the plasma, as the soliton travelling with the plasma was easily detected by the electric field pulse from the high-frequency probe and the respective signal from the diagnostic resonator which indicated the plasma density. Since we knew the plasma speed we could easily convert the time characteristics of the soliton localized in the plasma into the spatial parameters.

We shall start the discussion of the experimental results from the experiments on pumping of the plasma waves with the external high-frequency electric field. First, the following fact should be noted. Clearly, it is very difficult to make the pumping frequency to coincide with the frequency of the excited Langmuir wave which, according to eq. (5.2), strongly depends on the wave amplitude. Therefore in the experiments with external pumping of the high-frequency waves in plasma there was made an artificial density well, that is, a local density nonuniformity (by means of two grids *6* in Fig. 5.1). When such a well region flowed together with plasma through the pumping resonator, the high-frequency field pulse was applied. At the moment, on the varying plasma density profile there were two points of resonance between the pumping field frequency and the plasma oscillations frequency; one such point was at the leading front of the artificial plasma density well and the second one was at its back front. Since the

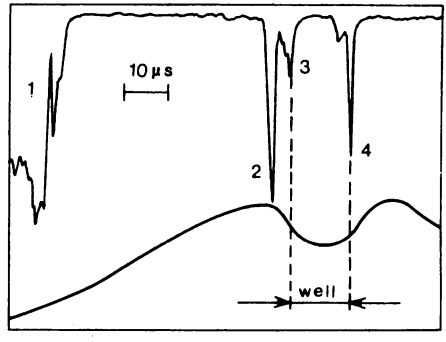

Fig. 5.2. Oscillogram of the signal from the high-frequency probe (at the top, downward deflection) and schematic of plasma density variation with time (10 μs per interval).

density well was spreading with the motion of the plasma, the speeds of these points relative to the installation were different—the leading front of the well had a higher speed than the entire plasma, and the back front had a considerably lower speed.

Figures 5.2 and 5.3 present the results of the experiments on pumping of the plasma waves by the external high-frequency fields. In Fig. 5.2 the lower curve is the schematic of the oscillogram of the signal from the diagnostic resonator (we do not present here the actual oscillogram so that not to be distracted by the purely diagnostic details the discussion of which can be found in [5.24]); it shows the variation with time of the dinsity of the flowing plasma (upward trace deflection). The upper curve (downward trace deflection) is the oscillogram of the detected signal from the high-frequency probe at the Langmuir electron frequency $f = 492$ MHz $\approx f_p$ (the plasma density $n \approx 3 \times 10^9$ cm^{-3}). Pulse *1* presents the Langmuir oscillations at the end of the pulse of the primary beam producing the plasma, *2* is the pulse of the pumping resonator at the frequency $f_E = 495$ MHz $\approx f_p$, and *3* and *4* are the pulses of the high-frequency probe at the distance $\Delta z = 15$ cm from the point of pumping. It can be seen that pulses *3* and *4* are localized at the leading front and back front of the moving artificial density well. Under different conditions [5.24] pulse *4* corresponding to the back front of the well is also observed in the absence of pulse *3*. Therefore, field bunches *3* and *4* are *independent* solitary Langmuir waves which exist for a long time without noticeable spreading. For instance, field bunch *4* exists for more than 20 μs in the plasma after high-frequency pumping has been discontinued; this time is more than 10^4 periods of the Langmuir oscillations and the bunch travels in this time not less than several tens of centimetres with the plasma (with the local speed of the back front of the density well). But the width of field bunch *4* (the product of the pulse duration by the speed of the plasma at the back front of the well $v \approx 1 \times 10^6$ cm/s) is not more than 0.7 cm ($\Delta_E \approx 20 r_D$). This wave formation

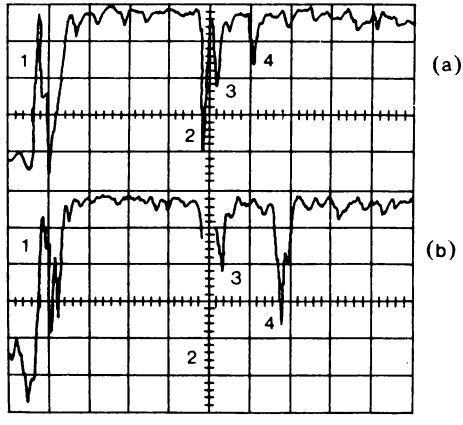

Fig. 5.3. Oscillogram of the signal of the high-frequency probe for $\Delta z = 5$ cm (*a*) and $\Delta z = 10$ cm (*b*). Figures denote mutually corresponding plasma density wells and high-frequency field bunches (10 μs per interval).

cannot be a linear wave packet; otherwise, as noted in Sec. 5.1, it would spread out at distances of the order of its own width [5.24]. The duration of pulses *3* and *4* is of the order of 10^3 periods of the Langmuir oscillations; hence, they are the envelope of the amplitudes of the Langmuir waves, that is, *the solitary waves with the "Langmuir filling"*.

Proceeding from the above discussion, we can regard field bunches *3* and *4* as the Langmuir solitons. The width of the soliton localized at the back front of the density well is smaller than the plasma column diameter by a factor of 5 to 6, that is, the soliton can be regarded as being approximately one-dimensional.

Figure 5.3 illustrates the character of soliton evolution during the passage along the installation (*a* for the distance between the pumping resonator and the observation point $\Delta z = 5$ cm, and *b* for $\Delta z = 10$ cm). It can be seen that the field bunch localized at the back front of the density well grows and is observed proportionately later with increasing distance from the pumping resonator. This implies that the characteristic length of soliton formation from the Langmuir waves is of the order of 10 cm, and the characteristic time of soliton formation is of the order of several thousand Langmuir periods (The uneven shape of pulse *4* in Fig. 5.3 indicates that it represents, most probably, 2 to 3 solitons, rather than one.)

Another experiment was performed with the use of modulating grids *6* (Fig. 5.1) which produced the plasma density well in the above experimental series. The voltage pulse fed to these grids allows us to obtain a short-duration electron beam in the plasma. Under certain conditions this beam produces the Langmuir solitons. Moving the high-frequency probe away from modulating grids *6*, we can analyze the character of soliton propagation along the magnetic field. The

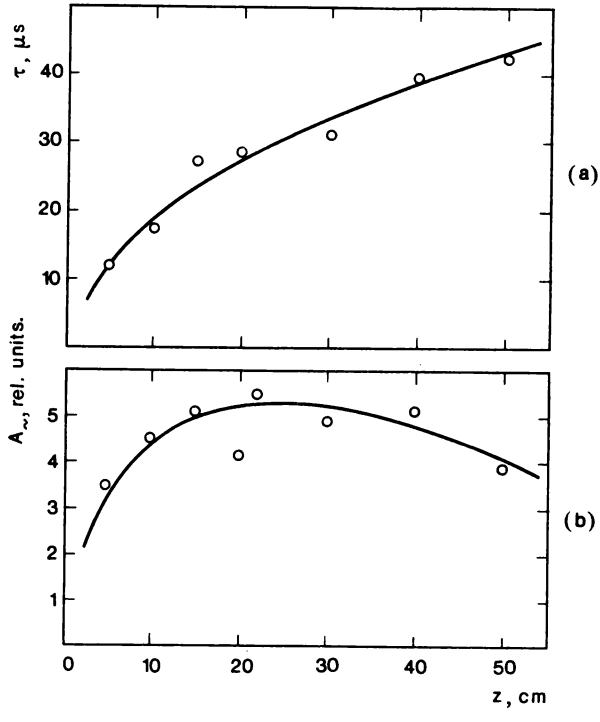

Fig. 5.4. (*a*) The delay τ in the appearance of a high-frequency field bunch at the probe as a function of the displacement of the probe along the installation. (*b*) The electric field amplitude of the bunch as a function of the distance it has travelled, $z \equiv \Delta z$.

results are shown in Fig. 5.4 which presents the delay in the appearance of the high-frequency field pulse at the probe as a function of the displacement of the probe along the working volume. It can be seen that the field bunches freely travel not less than 50 cm in the installation in about 40 μs. In other words, the lifetime of the field bunches amounts to at least 2×10^4 periods of the electron plasma oscillations. The field bunches observed at large distances form the entry to the working volume typically have higher magnitudes and smaller width than those observed at small distances. Figure 5.4*b* shows the amplitude $A_{\sim}$ of the electric field in the field bunches (relative units) as a function of the distance it has travelled in the system.

It should be stressed that in the experiments with high-frequency pumping of the plasma waves discussed above the plasma density wells corresponding to the Langmuir solitons were not identified in the oscillograms of the variation of the plasma density with time owing to the procedural reasons [5.24]. The presence of

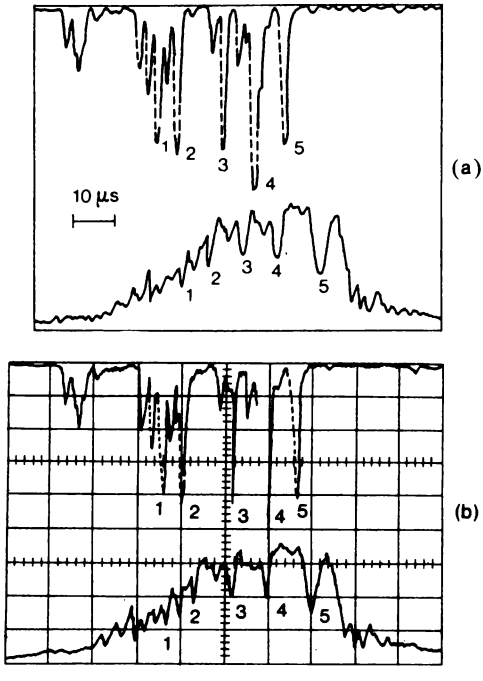

Fig. 5.5. (*a*) Oscillograms of the integral signal of the high-frequency probe (upper, downward trace deflection) and the signal of the diagnostic resonator (lower, upward trace deflection); 10 μs per interval. The plasma density $n = 1.8 \times 10^9$ cm^{-3}, the observed oscillation frequency $f = 350$ MHz, the energy of the beam electrons $W_1 = 900$ eV. (*b*) Correspondence between the field bunches and the density wells after the displacement of the lower oscillogram in Fig. 5.5(*a*) by 6 μs to the left (the approximate transit time of the plasma).

both attributes of the Langmuir soliton, namely, the plasma density well and its high-frequency filling, was demonstrated in the experiments on excitation of solitons by the electron beam, which are discussed below.

The most interesting results on the beam excitation of solitons were obtained with the experimental installation of the second modification (see Fig. 5.1*b*); the monoenergetic electron beam proved to be an incomparably more reliable source of Langmuir solitons with distinct and sufficiently deep density wells that the beam with a spread-out velocity distribution [5.25]. Therefore, we shall first discuss the experimental results obtained with the installation shown in Fig. 5.1*b*. These results show that the Langmuir waves excited by the electron beam in plasma are a series of solitons, that is, the Langmuir wave field bunches associated with deep plasma density wells ($\delta n/n = (3 \text{ to } 30) \times 10^{-2}$). The solitons

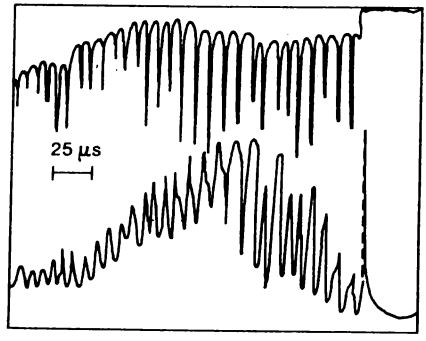

Fig. 5.6. Oscillograms of the integral signal of the high-frequency probe (upper) and the signal of the diagnostic resonator (25 μs per interval). The plasma density $n = 1 \times 10^9$ cm^{-3}, $W_i = 900$ eV. The intensity peak in the oscillation spectrum is at the frequency 300 to 350 MHz. For the deepest density wells we have $\delta n/n = 0.3$. The signal cut-off at the end of the oscillograms is due to discontinuation of the beam. The density wells in the lower oscillogram correspond to downward deflections up to the smooth peak and to upward deflections beyond the peak.

are localized in the plasma, that is, they are at rest (in the first approximation) with respect to the plasma; if they are moving relative to the plasma, their speeds are much lower than the ion sound speed c_s. These results are illustrated with Figs. 5.5–7 which show and compare the simultaneous oscillograms for the signals of the plasma density indicator (the lower one) and for the envelope of the electric field amplitude of the Langmuir waves. Sharp deviations, both upward and downward, can be seen in the oscillograms for the plasma density indicator. These deviations correspond to rarefaction ("density wells") and compression of plasma ("density bunches"). Ignoring the details of operation of the diagnostic resonator (they are discussed in [5.24, 5.25]), we shall note the following general rule: in the rising part of its oscillogram and in the plateau region of the (smooth) maximum the downward deviations correspond to the density wells and the upward deviations correspond to density bunches; in the declining part of the oscillogram (following the signal maximum), on the contrary, the upward deviations correspond to density wells and the downward deviations correspond to density bunches. To establish the correspondence between a specific plasma density well and a specific high-frequency field pulse for the sought Langmuir soliton we should take into account the fact that the indicators of the field and the plasma density were at the distance of 2 cm from each other (see Fig. 5.1); the plasma travelled this distance in 5 to 6 μs. Therefore, if the soliton is localized in the plasma, then the signal of its density well should appear in the oscillogram 5 to 6 μs later than the signal of the high-frequency field of the soliton. The data in Figs. 5.5*a* and *b* confirm this delay. Indeed, if, for instance,

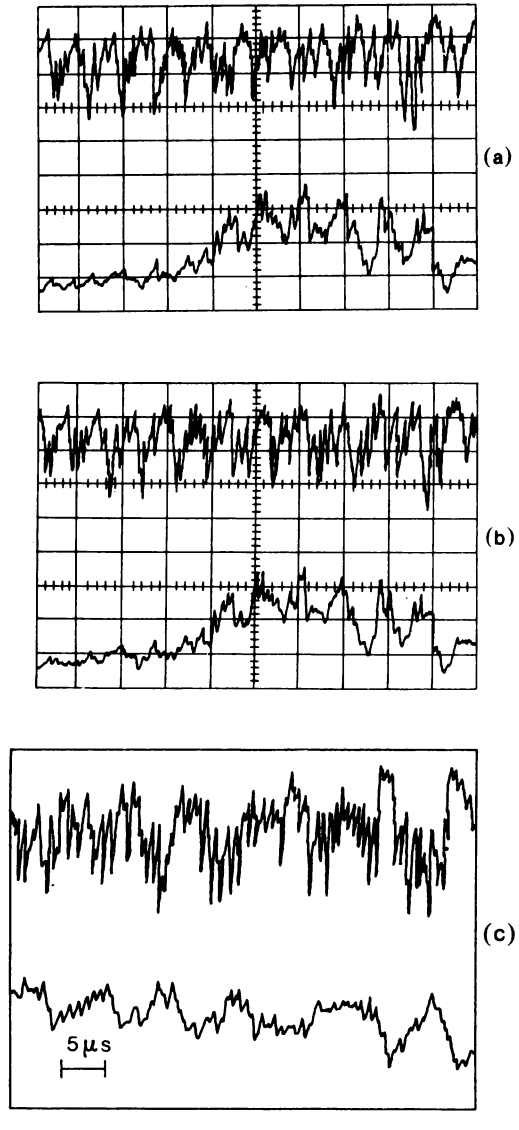

Fig. 5.7. Oscillograms of the same signals as in Fig. 5.6. (*a*), (*b*) 10 μs per interval, $n = 4.2 \times 10^9$ cm^{-3}, $f = 550$ MHz, $W_1 = 900$ eV. (*b*) Comparison of the above oscillograms after displacement of the lower one by 5 μs to the left. (*c*) 5 μs per interval, $W_1 = 900$ eV, no displacements of the oscillograms.

in Fig. 5.5*a* we shift the lower ("delay") oscillogram to the left by the indicated time of flight of plasma, that is, by approximately 6 μs, then the high-frequency field pulses with the numbers *1*, *2*, *3*, *4*, *5* and *6* will practically coincide in time with the respective plasma density wells (Fig. 5.5*b*). A similar phenomenon can be seen in Fig. 5.7. These results suggest that the observed field bunches of the Langmuir waves travel with the speed of the plasma relative to the installation, that is, that they are at rest relative to the plasma.

The oscillations whose oscillograms are shown in Figs. 5.5–5.7 are, indeed, the Langmuir oscillations—their frequency is given by $f \approx (ne^2/\pi m)^{1/2} \approx 10^4 n^{1/2}$. These oscillations form bunches. The characteristic period of the bunches, that is, the period of modulation of the amplitude of the high-frequency field (a few microseconds), is about 10^3 times the period of the Langmuir oscillations. Therefore, these field bunches are solitary waves with the "Langmuir filling". The number of the field bunches is approximately (Fig. 5.5) or exactly (Fig. 5.6) equal to the number of the density wells. Figures 5.5–5.7 suggest that the Langmuir field bunches are localized at the plasma density wells.

Thus, the above experimental data can be reliably interpreted as follows: the wave formations under study are Langmuir solitons travelling together with plasma (or resting in the system of the plasma).

Interestingly, Fig. 5.6 seems to illustrate the existence of a more or less regular *"lattice" of the large-amplitude Langmuir solitons* with the spatial period $\lambda_M \approx \approx \lambda/2 = u_0/2f_p$, where u_0 is the velocity of the electrons in the beam. According to theoretical predictions [5.16, 5.27], such a lattice can be comparatively stable.

Under certain conditions (for instance, those in Fig. 5.6) the integral signal from the indicator of the Langmuir wave field is modulated in time in the same way as the signal at the given frequency (in Fig. 5.6 this is the frequency $f \approx p_p = 300$ MHz). This means that the waves of *all* the frequencies in the high-frequency spectrum are localized in the plasma density wells and are practically absent outside of these wells. Under these conditions the modulational instability of the Langmuir waves is manifested particularly clearly.

It should be noted that under various experimental conditions two cases of wave modulation are observed: in one case there is one soliton per (each) modulation wavelength (Fig. 5.6), in the other case a whole series of solitons is observed per modulation wavelength (Fig. 5.7). Not only wave bunches but also plasma density wells are observed in such series (Fig. 5.7). The period of the envelope of these series varies from 5 to 20 μs, that is, for the plasma speed $v \approx 0.4 \times 10^6$ cm/s the spatial period varies from 2 to 8 cm.

When a correspondence can be found between field bunches and specific density wells higher-intensity bunches prove to correspond to deeper and more narrow wells (see, for instance, Figs. 5.5 and 5.6).

The depth of modulation of the plasma density (the depth of plasma wells) varies between 10 and 30%. The deepest density wells are illustrated in Fig. 5.6, where $\delta n/n \approx 30\%$. If $\delta n/n \lesssim 1$ to 2%, the density well cannot be recorded owing to the background of the intrinsic fluctuations of the plasma density. The width of the density well (the duration of the well pulse multiplied by the plasma speed $v \approx 0.4 \times \times 10^6$ cm/s) is typically of the order of 0.5 to 1 cm. Figure 6 shows the most narrow

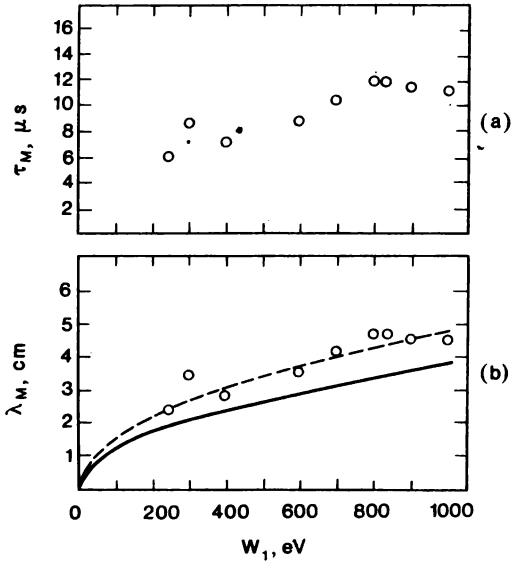

Fig. 5.8.(*a*) The period τ_M of modulation of the electric field pulses of the nonlinear Langmuir waves as a function of the electron energy in the "pumping beam". (*b*) The experimental points give the modulation length $\lambda_M = \tau_M v$, where $v = 0.4 \times 10^8$ cm/s; the solid curve gives the wavelength of the linear Langmuir wave excited by the electron beam, $\lambda = u_0/f_p$, as a function of the electron energy in the beam, $W_1 = mu_0^2/2$.

wells whose width is not more than approximately 0.3 cm (that is, about $10r_D$, where r_D is the electron Debye radius). This width is practically equal to the gap width of the diagnostic resonator which is 2.5 mm, while the grid mesh width is 2 to 2.5 mm. This implies that the actual width of these wells can be even smaller.

Under some (fairly typical) experimental conditions there is not detailed correlation between the field bunches and the plasma density wells though their general characters of variation are qualitatively similar [5.25]. These cases can, apparently, be regarded as soliton turbulences [5.28–31].

The period of modulation τ_M of the Langmuir waves and the respective modulation length $\lambda_M = v\tau_M$ (where $v \approx 0.4 \times 10^8$ cm/s is the plasma speed) increase with increasing speed of the electrons of the beam. This increase is illustrated by the data of Fig. 5.8, which were averaged over many pulses of the beam for each electron energy W_1. Figure 5.8 also presents the length of the linear Langmuir wave excited by the electron beam in the plasma as a function of W_1;

$$\lambda = u_0/f_p \tag{5.12}$$

Here u_0 is the speed of the electrons of the beam ($u_0 \approx 6 \times 10^7 \times (W_{1(eV)})^{1/2}$ cm/s.

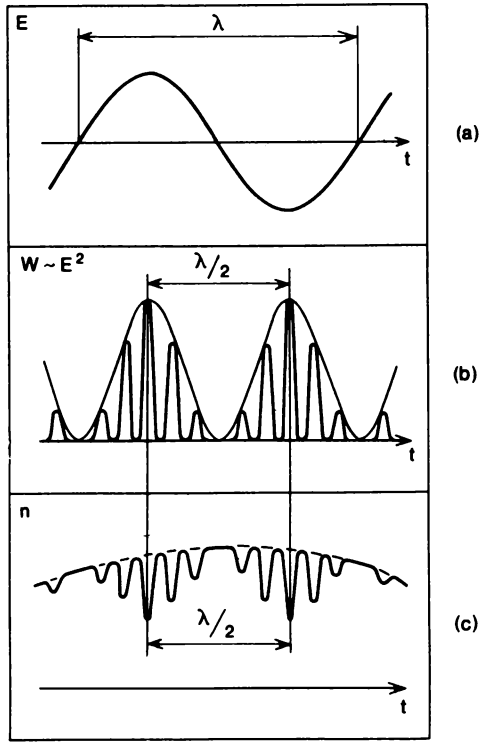

Fig. 5.9. Spatial profiles of the standing Langmuir wave (schematic): (*a*) field strength E; (*b*) field energy density $W \sim E^2$; (*c*) plasma density. Self-compression of the waves and their division into several solitons occur in the interval of the length $\lambda/2$; this figure corresponds to oscillograms of the type of those in Fig. 5.6.

We can see that the values of λ_M and λ are close and their dependences on W_1 are similar. Conditions of two types were observed in the experiments: either $\lambda_M \approx \lambda$ (as in Fig. 5.8) or $\lambda_M \approx \lambda/2$ (as Figs. 5.6, 5.7 and 5.9).

In these experiments the modulational instability of the Langmuir waves with distinct field bunches and respective plasma density wells (standing out against the background of intrinsic plasma noise) was observed starting from a certain threshold energy of oscillations, and this threshold tended noticeably to decrease with increasing electron energy W_1 in the beam [5.25].

To analyze the spectrum of oscillations the signal from the high-frequency probe was measured with two receivers (P5–19 and P5–20) tuned to different frequencies and connected in parallel. The results have shown that if at the Langmuir frequency $f_p \approx 500$ MHz, the frequency difference Δf between the receivers is not more than

5 MHz, the oscillograms of their output signals are practically identical. When $\Delta f =$ $= 15$ MHz the pulses from the receivers coincide in approximately half of the cases; and when $\Delta f = 25$ MHz, coincidence of the pulses is rather rare. However, the oscillograms for $\Delta f = 50$ MHz are sometimes very similar. These results imply that the width of the frequency spectrum of the Langmuir waves in the regime of soliton formation is $\Delta f = 15$ MHz for the fundamental frequency $f = f_p \approx 500$ MHz.

As for the "mean free path" of solitons, we can see from Fig. 5.6 that is seems to correspond to the soliton lifetime of no less than 100 μs, that is, its lowest estimate is more than about 50 cm. This estimate was also obtained in the independent experiments described above, in which the Langmuir solitons were observed after the external pumping (by electron beam or pumping resonator) of the waves had been discontinued; the lifetime of the Langmuir solitons was found to exceed several tens of thousands of the periods of the Langmuir oscillations (see Figs. 5.2–4).

5.3 Comparison of Theoretical Predictions with Experimental Results

We shall make the following comparisons between the theoretical predictions and experimental results for the Langmuir solitons: (1) the relationship between the longitudinal size (width) Δ_n of the soliton and the depth of the plasma density well, $\delta n/n$; (2) the relationship between the characteristic dimension of the modulational instability of the Langmuir waves (the modulation length λ_M) and the parameters of the electron beam and the plasma; (3) the threshold of the observed modulational instability and its dependence on the energy of the electrons of the beam; (4) the frequency spectrum of oscillations in the Langmuir soliton, and (5) the relationship between the observed degree of self-compression of the Langmuir wave and the "coefficient of amplification" of its electric field. Let us now analyze the above experimental data in this sequence.

1. To compare the soliton width and the depth of the density well let us consider the data in Fig. 5.10, where the density well corresponding to the soliton (pulse *3*) is $\delta n/n = 0.1$, and the soliton width (at the level of $1/e$ of the maximum) is $\Delta_n = 0.25$ cm $\approx 6r_D$. On the other hand, according to the theory of Sec. 1 [see eq. (5.7)], the soliton width is determined by the depth of the density well:

$$\Delta_{n.\text{theor}} \approx r_D\left(30\frac{n}{\delta n}\right)^{1/2} = r_D\left(30\frac{nT}{W}\right)^{1/2}$$

For the case shown in Fig. 5.10 this equation yields for the soliton width: $\Delta_{n.\text{theor}} \approx$ $\approx 18r_D$. Hence, $\Delta_{n.\text{exper}}/\Delta_{n.\text{theor}} \approx 1/3$. At the present stage of development of the physics of solitons this ratio between the predicted and observed values should, apparently, be regarded as a not bad agreement, rather than a disagreement.

2. According to the experimental results discussed above and shown, for instance, in Figs. 5.8 and 5.9, the modulation length for the nonlinear Langmuir waves satisfies the condition $\lambda_M \approx \lambda$ or $\lambda_M \approx \lambda/2$, where $\lambda = u_0/f_p$ [see eq. (5.12)]. This implies that the starting (linear) Langmuir wave is the envelope for shorter-wavelength field modulation due to the modulational instability. This behaviour of

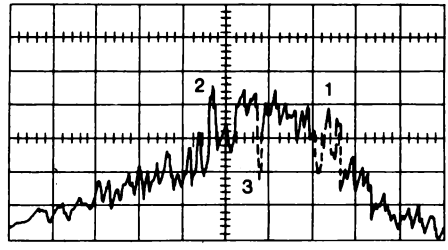

Fig. 5.10. Oscillogram of the output signal from the diagnostic resonator serving as the indicator of the plasma density (5 μs per interval). Pulses *1* and *3* correspond to the density wells with the duration $\tau < 1$ μs, pulse *2* corresponds to a plasma bunch; $n = (3 \text{ to } 3.5) \times 10^9$ cm^{-3}, $f = 500$ MHz, $W_1 = 300$ eV. Pulse *3* corresponds to the relative depth of the density well $\delta n/n = 0.1$.

the nonlinear waves also agrees with the theoretical predictions; it is typical of the *oscillating two stream instability* (*OTSI*) discussed in Sec. 5.1. This type of modulational instability must develop at a sufficiently high density of the oscillation energy; according to eq. (5.10), we have

$$W/nT \approx \delta n/n \approx (kr_D)^2$$

where k is the wave number of the oscillations modulated by the starting Langmuir wave with the wavelength λ (that is, $k > 2\pi/\lambda$). If the oscillation energy is lower, modulational instability of another type can occur, when the modulation length of the oscillations is larger than the wavelength of the starting (linear) Langmuir wave. The resulting solitons are known as the *envelope solitons* (see Sec.5.1). In contrast to this, the case illustrated by Figs. 5.7 and 5.9 can be described by the term the "*soliton envelope*".

As it was shown above, the observed Langmuir solitons in the first approximation are resting with respect to the plasma, that is, in the system of moving plasma they can be regarded as bunches of standing nonlinear waves. The simplest picture of the standing waves is obtained when (see Figs. 5.6 and 5.9) the spatial period of wave modulation is equal to the half-wavelength of the starting wave, that is, coincides with the spatial period of the wave intensity, $\lambda_M/2$. Under such conditions the wave forms a regular series of the plasma density wells with the period $\lambda_M/2 \approx u_0/2f_p$ and is localized in these wells, making up a quasistable "*soliton lattice*" treated theoretically in [5.16].

The process of formation of the standing nonlinear wave and, in particular, of the wave with the wavelength half that of the starting pumping wave, was observed in the experiments [5.23] with highly collisional nonmagnetized plasma (and in numerical simulations [5.28, 5.31, 5.17]). The further turbulence of the standing wave was calculated numerically in [5.28].

3. The threshold (critical) energy density of the Langmuir waves corresponding to the beginning of the oscillating two-stream instability is given by the theoretical

relationship (5.10):

$$(W/nT)_{cr} \approx (kr_D)^2$$

Since, as shown above.

$$k^2 > (2\pi/\lambda)^2 = 4\pi^2 f_p^2/u_0^2 = 2\pi ne^2/W_1$$

and

$$r_D^2 = T_e/4\pi ne^2$$

then we have $(kr_D)^2 \geq T_e/2W_1$ and therefore the threshold is

$$(W/nT)_{cr} \gtrsim T_e/2W_1 \tag{5.13}$$

For instance, for $W_1 = 800$ eV and $T_e = 10$ eV the instability threshold is

$$(W/nT)_{cr} \gtrsim 0.6 \times 10^{-2} \tag{5.14}$$

Equation (5.13) implies that the threshold of the oscillating two-stream instability is largely dependent on the energy of the electrons in the beam exciting the waves.

In this connection, the experiments reported in [5.25] have demonstrated that for a relatively low energy of the electrons in the beam ($W_1 = 400$ eV) the modulational instability is relatively near the threshold and therefore no sufficiently deep plasma density wells are produced, which would be noticeable against the background of the intrinsic plasma noise. According to eq. (5.13), an increase in the electron energy up to 800 eV should considerably lower the threshold of instability; as shown by the experimental results of [5.25], this is, indeed, accompanied with the formation of distinct density wells where the field bunches which produced them are localized. The depth of the wells $\delta n/n$ is about (4 to 5) $\times 10^{-2}$, that is, higher than the threshold (5.14) almost by an order of magnitude. We can assume that in this case the instability threshold was considerably surpassed and the wells were significantly deepened. The width Δ_n of the resulting solitons can be estimated as 0.8 cm $\approx 20r_D$. The characteristic wave number of solitons is $k_0 \approx 2/\Delta_n \approx 1/10r_D$, that is, $(k_0 r_D)^2 \approx 10^{-2}$. According to eq. (5.7), now we should have $W/nT \approx \delta n/n \approx 6(k_0 r_D)^2 \approx 6 \times 10^{-2}$, while the experimental results yield $\delta n/n \approx$ (4 to 5) $\times 10^{-2}$. The comparison of these results shows that there is a good agreement between the theoretical and experimental values of the threshold.

Since we have a qualitative agreement between experimental results and theoretical predictions, we can use the theoretical relationship

$$E_0^2/(16\pi) \approx (\delta n/n)(nT_e)$$

for estimating the electric field in the observed Langmuir solitons. When $\delta n/n = 3 \times 10^{-1}$ and $n = 1 \times 10^9$ cm^{-3} (the conditions as in Fig. 5.6) or $\delta n/n = 1 \times 10^{-1}$ and $n = 3 \times 10^9$ cm^{-3} (the conditions as in Fig. 5.10) and for $T_e = 10$ eV we have $E_0 \approx 150$ V/cm.

4. The frequency spectrum of the nonlinear Langmuir waves due to the modulational instability proves to be sufficiently narrow. The characteristic width of the spectrum is $\Delta f_{nonlin} = 10$ to 15 MHz $\approx f_i$, where $f_i = f_p(m/M)^{1/2}$ is the Langmuir frequency of the molecular hydrogen ions (where M is the ion mass) for the plasma density $n = 3 \times 10^9$ cm^{-3}, which was typical for our experiments.

As can be seen from Figs. 5.8 and 5.9, the Langmuir soliton concentrates the energy of the waves which was initially contained in the volume of the length $\lambda_M = (1/2 \text{ to } 1)\lambda$, that is, the wave energy density W is higher by the factor of approximately λ/Δ_n than the initial energy density W_0. For instance, for $\lambda = 4$ cm (Fig. 5.8) and $\Delta_n = 0.2$ cm we obtain $W \approx 20W_0$. If we take $W_0/nT \approx$ (1 to 2)% (which seems to be reasonable), we obtain $W/nT \approx$ (20 to 40)%, which agrees quite well with the observed $\delta n/n \approx 1/3$ (see Fig. 5.6).

Now we can make the following conclusions. (1) No significant disagreement has yet been found between the experimental data and the theoretical predictions of Sec. 5.1 (in the first approximation) both in qualitative and quantitative estimates. (2) In magnetized collisionless plasma the Langmuir solitons are quite real and sufficiently stable, and their parameters and other properties are close to the theoretical predictions. This result is by no means trivial; at the starting stage of this experimental series many theorists were fairly sceptical about the feasibility of producing the quasistable Langmuir solitons in radially confined magnetized plasma.

5.4 The Oblique Langmuir Solitons

In this section we shall continue describing the search for plasma wave solitons but, in contrast to the preceding sections, we shall deal with the electron waves in the magnetized plasma column of a limited diameter, in contrast to the Langmuir waves. The frequencies of these waves are lower than f_p. Dispersion of these waves (known as the Trivelpiece-Gould waves) is described by

$$f = f_p \cos\theta = f_p \frac{k_z}{(k_z^2 + k_\perp^2)^{1/2}} \tag{5.15}$$

where $k_z = 2\pi/\lambda_z$ and $k_\perp \approx 1/a$ are the longitudinal and transverse wave numbers, and a is the radius of the plasma column.

These waves can be referred to as the oblique Langmuir waves in the finite plasma. In contrast to the oblique Langmuir waves in the finite plasma (which are, in principle, conceivable), the transverse wave number $k_\perp$ of the waves described by eq. (5.15) is determined by the plasma column radius a; for instance, if the plasma column is separated from the (far) walls, then $k_\perp \approx 1/a$.

Another interesting aspect of the modulational instability of these waves is that the Lighthill criterion (5.3) is not satisfied for these waves (see Sec. 5.1), and we can verify experimentally how this fact affects the possibility of soliton formation.

The oblique Langmuir solitons were studied experimentally in [5.26] which was a continuation of the studies [5.25, 5.24]. These experiments were performed with the same installation but *after* the pumping with the electron beam had been discontinued, that is, under the conditions of "afterglow" of the beam-treated plasma. This study was possible owing to the fact that plasma was collisionless [5.24] (see Sec. 5.2) and that, in particular, the pressure of the neutral gas (hydrogen) in the analyzed plasma was sufficiently low ($p \lesssim 5 \times 10^{-6}$ mmHg). It was just the high concentration of the neutral gas (the argon pressure $p \gtrsim$ (1 to 2) $\times 10^{-4}$ mmHg) that did not allow the American experimenters [5.22, 5.23] to observe the Langmuir

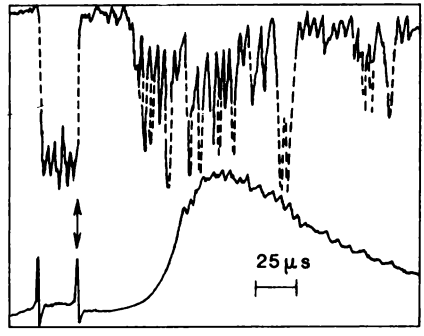

Fig. 5.11. Oscillograms from the indicators of the plasma density (the lower one—upward trace deflection) and for the envelope of the amplitudes of the high-frequency electric field of the waves (the upper one—downward trace deflection); 25 μs per interval. The indicators are at the end of the plasma column at the distance $L = 140$ cm from the discharge chamber of the plasma source. As in all other oscillograms in [5.26], the density wells correspond to downward deflection in the lower oscillogram; the arrow indicates the switching-off of pumping by the electron beam.

solitons *after* the electron beam pumping had been discontinued; owing to the electron-atom collisions the Langmuir oscillations decayed during a fraction of a microsecond, that is, they were unobservable in the scale of the characteristic times of the problem.

To obtain the waves described by eq. (5.15) the plasma column diameter was taken to be 3 cm, that is, half that used in the experiments [5.25]. In this case the column diameter is smaller than the wavelength $\lambda = u_0/f$ of the electron oscillations generated in the plasma by the electron beam (see below) and the observed oscillations correspond to the sought oscillation mode described by eq. (5.15). The general experimental conditions and techniques were the same as in [5.25]. The plasma density was $n = (3 \text{ to } 4) \times 10^9$ cm^{-3}, the longitudinal magnetic field $H = 2 \times 10^3$ Oe, the electron temperature $T_e = (10 \text{ to } 20)$ eV, the plasma column length about 200 cm, and the plasma speed $v = (2 \text{ to } 6) \times 10^8$ cm/s. The electron beam had the following typical parameters: the electron beam energy $W_1 = 2$ to 2.5 keV, the current $I = 2$ to 2.5 A, the electron density in the beam $n_1 = (0.1 \text{ to } 0.2)n$, and the beam pulse duration about 20 μs. Under such conditions we had the plasma frequency $f_p = 500$ to 600 MHz, the velocity of the electrons of the beam $u_0 = (2.5 \text{ to } 3) \times 10^9$ cm/s, and the length of the Čerenkov wave excited by the electron beam in the plasma $\lambda_0 = u_0/f_p \approx 5 \text{ cm} > 2a$. The plasma speed was measured from the shift with time of the ion saturation current at mesh probes (with 95% transparency) placed along the plasma column. The wave velocity was also measured with these probes which were connected to two independent receivers P5-19 and P5-2 tuned to the same frequency. This experimental procedure made it possible to observe wave evolution for one beam "shot". As in [5.24, 5.25], the indicators of the electric field

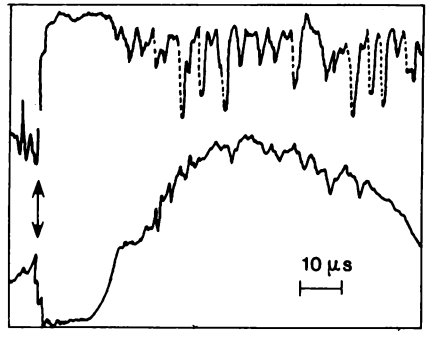

Fig. 5.12. Oscillograms similar to those in Fig. 5.11; 10 μs per interval, $L = 110$ cm, $v = 2 \times 10^6$ cm/s. The distance between the field bunches is 5 to 10 cm, the characteristic size of the bunches is about 4 cm.

were mesh high-frequency probes with the surface perpendicular to the magnetic field. Therefore, the probes detected only the waves with considerable electric field component parallel to the magnetic field, among all the waves in the plasma column. Thus, either purely longitudinal (Langmuir) waves or the oblique Langmuir waves were primarily identified among all the high-frequency waves propagating along the magnetic field.

The following experimental results have been obtained.

1. The oblique Langmuir waves with the frequencies $f = 150$ to 350 MHz $< f_p$ corresponding to the dispersion mode (5.15) are found for a very long time (up to 100–200 μs) in the "afterglow" plasma, that is, after the pumping electron beam has been cut off. This lifetime of the waves should be regarded as sufficiently long since the oscillation period is just a few nanoseconds. Figures 5.11–5.15 illustrate the waves in the afterglow plasma and show the variation of the plasma density with time (the lower oscillograms in Figs. 5.11, 5.12, and 5.13b; upward trace deflections) and the oscillograms for the detected envelope of the amplitudes of the high-frequency waves (the upper oscillograms, downward trace deflections).

2. The figures show that the waves are concentrated into bunches in which the characteristic time of variation of time envelope of the oscillation amplitudes is a few microseconds, that is, it is of the order of thousands of oscillation periods. Therefore, as in the experiments [5.24, 5.25], these wave bunches are solitary waves with the high-frequency filling.

3. The oscillograms readily yield an estimate of the speeds of the wave bunches and the plasma itself as the ratio of the distance L of the indicators of the high-frequency field and the plasma density from the discharge chamber of the plasma source to the time of flight which is approximately equal to the time interval between cut-off of the electron beam and the moment of recording of the wave bunches and the plasma (of a given density). It can be seen that the wave bunches travel together with the plasma with the velocity v of the order of 10^6 cm/s. The

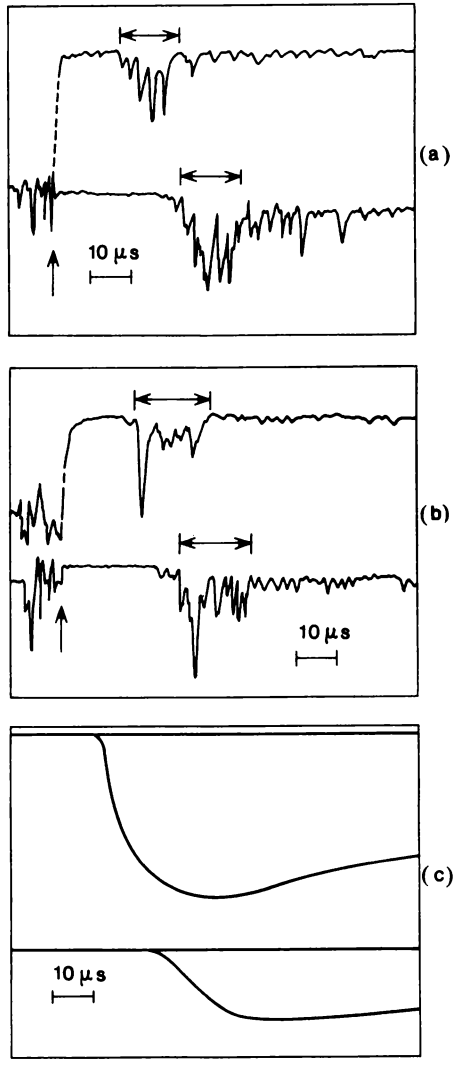

Fig. 5.13. Oscillograms (*a*, *b*) from two identical indicators of the electric field of the waves which are at the distance of 94 cm from each other and tuned to the same frequency $f = 250$ MHz; 10 μs per interval. (*c*) The variation of the plasma density with time in two cross sections of the plasma column at the distance of 94 cm from each other. The time differences between the oscillograms from the field and density indicators due to the 94-cm separation of them are approximately equal.

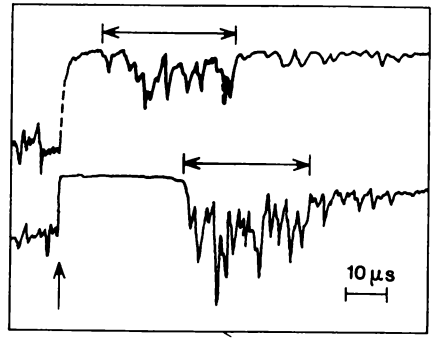

Fig. 5.14. Oscillograms of two indicators of the wave field at the distance of 94 cm from each other; 10 μs per interval. The total length of the wave packet does not increase during the time of plasma passage and some of its components become more distinct and narrow (self-compression).

characteristic sizes of the wave bunches and the distances between them can be found by multiplying this velocity (which is different under different conditions) by the duration of the wave pulses and the intervals between them (as it was done in [5.24, 5.25]).

4. The observed waves evidence a sharp modulation of their amplitude (see Figs. 5.11–5.15) with the distinct spatial periods $\lambda_M = 5$ to 6 cm $\approx \lambda_0/2$ and $\lambda_M \approx 10$ to 12 cm $\approx \lambda_0$, where $\lambda_0 = u_0/f$ is the initial wavelength of the wave generated by the electron beam in the plasma (for $u_0 = 2.5 \times 10^9$ cm/s and $f = 2.5 \times 10^8$ s^{-1} we have $\lambda_0 = 10$ cm). The characteristic longitudinal size of the wave bunches is about 4 cm, that is, of the order of the plasma column diameter.

5. During afterglow of the beam-treated plasma there is observed modulation of the plasma density in the form of density wells and bunches, which approximately correlate with the wave bunches (see Fig. 5.12). Therefore, according to the discussion in Item 2 and the results of [5.20–25], we can regard the observed wave formations as the oblique Langmuir solitons with high-frequency filling.

6. The wave bunches propagate along the installation without spreading. This can be seen, for instance, from Figs. 5.13–5.15 which present oscillograms of the signals from two probes which are at different distances from the plasma source, the distance between the probes is 94 and 78 cm. The data shown in Figs. 5.13–5.15 were obtained in one beam shot with two independent receivers tuned to the same frequency. We see from the figures that the observed wave bunches travel the distance about 100 cm along the magnetic field in approximately 15 μs without spreading; the width of the individual pulses comprising a wave packet, the distance between them and the total width of the wave packet (shown in the figures by arrows) do not vary as the packet propagates along the installation. Hence, the observed wave packets are essentially nonlinear since a linear wave packet rapidly spreads out at distances of the order of its width (see Sec. 5.1).

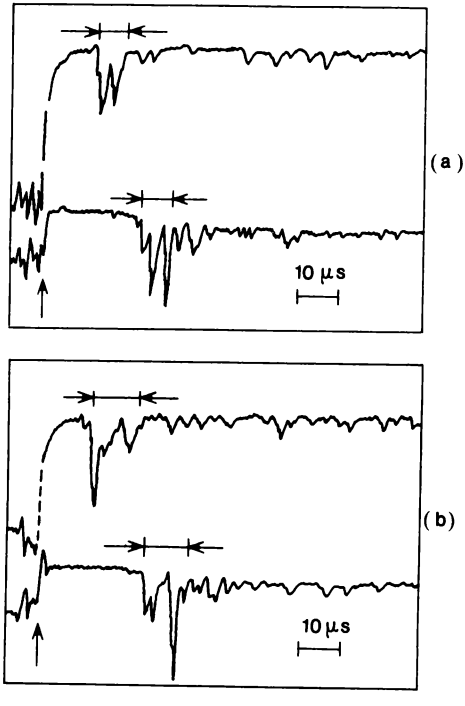

Fig. 5.15. Same as in Fig. 5.14. Illustrations of self-compression of the nonlinear waves, 10 μs per interval.

7. The wave bunches are localized in the plasma; they are approximately at rest relative to the plasma and travel relative to the installation together with the plasma. The speed of wave bunches and the plasma is close to the ion sound speed in atomic hydrogen, c_s = (2 to 5) $\times$ 10^6 cm/s (the higher value corresponds to T_e = 20 eV). The conclusion that the observed nonlinear waves are localized in the plasma follows from the comparison of their speed relative to the installation and the speed of the plasma, as can be seen from Figs. 5.13*a* and *b*. These figures compare the shifts with time of the oscillograms for two high-frequency probes which are at a distance of 94 cm from each other and the shifts with time of the oscillograms for two plasma density indicators which are at the same distance. It can be seen that both the wave bunches and the plasma travel the distance of 94 cm in about 15 μs; the speed of the waves and the plasma (on the average) is $v \approx 6 \times 10^6$ cm/s.

Similar time differences in recording of the wave bunches travelling with plasma were observed in another experiment in which the high-frequency probe (the signal from it was fed to an P5-19 receiver) was moved in the direction of the plasma motion with each "shot" of the electron beam; the plasma speed was (2 to 3) $\times$ 10^6 cm/s. The experimental results are shown in Fig. 5.16. It can be seen that the wave bunches travel along the magnetic field without changing their shape. As in Figs. 5.13–5.15, the wave bunches are "frozen" into the plasma.

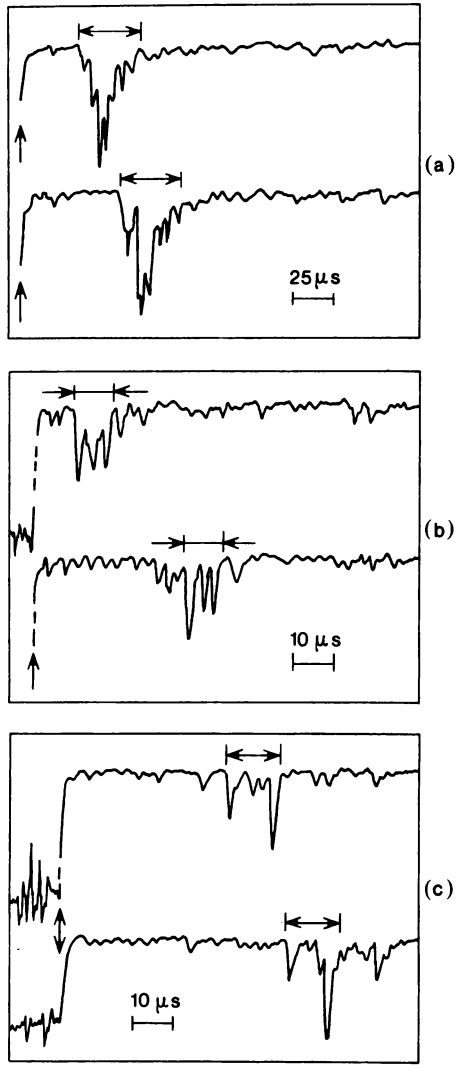

Fig. 5.16. Oscillograms of the same wave field indicator displaced from the initial position in the direction of plasma motion: (*a*) displacement 30 cm, (*b*) 60 cm, (*c*) 20 cm; 25, 10 and 10 μs per interval respectively.

Thus, the observed wave bunches are either at rest relative to the plasma or travel relative to it with a speed which is definitely not higher than the ion sound speed c_s. But under the given experimental conditions this speed is lower by three orders of magnitude than the characteristic speed of the linear Trivelpiece-Gould waves with dispersion described by eq. (5.15). This fact provides further evidence that the oblique Langmuir waves under study are essentially nonlinear.

8. Figures 5.14–5.15 illustrate the evolution with time of the observed nonspreading wave bunches. For instance, the upper oscillogram in Fig. 5.14 reveals only some "embryos" of the electric field peaks but the lower oscillogram shows in the same plasma regions (displaced by 94 cm along the magnetic field) distinct field bunches with noticeably higher amplitude, which formed after 15–20 μs. A considerably larger number of distinct field bunches is seen on the lower oscillograms than on the upper ones. The total length of the series of the wave bunches (shown by arrows) is the same in the upper and lower oscillograms in Fig. 5.14 (as is the case in Figs. 5.13 and 5.15, too).

Figures 5.15*a* and *b* also clearly illustrate self-compression of the waves as they travel (together with the plasma) along the installation. We see that the field bunches become much more narrow and distinct with time; in particular, in Fig. 5.15 the width of the field bunches at the end of the plasma column is so small that they are represented by points, rather than a line, on the cathode-ray tube screen. Thus, Figs. 5.13–15 illustrate the modulational instability (self-compression) of the waves under study; in Figs. 5.14 and 5.15 the growth rate of this instability is $\gamma \approx 10^3\ s^{-1} \approx mf_p/M$, where m and M are the masses of the electron and the proton.

9. The lifetime τ of the observed packets of the oblique Langmuir waves (solitons) in free motion (that is, in the absence of excitation) is clearly longer than 20 to 30 μs, that is, 10^4 oscillation periods. During this time solitons travel along a greater part of the installation without noticeable spreading.

10. The experimental results suggest the following mechanism of self-compression of the nonlinear oblique Langmuir waves giving rise to solitons. Since, as shown above, the characteristic length of wave modulation λ_M is smaller than or of the order of the initial wavelength (that is, modulation results in sharp "tearing" of the high-frequency filling) the mechanism of self-compression seems to have the same nature as in the experiments [5.22, 5.25], where it was due to the oscillating two-stream instability discussed in Sec. 5.1. This mechanism apparently is not related to the well-known Lighthill criterion (5.3) which is associated with formation of the envelope soliton ($\lambda_M \gg \lambda_0$), that is, the situation when the high-frequency filling of the wave packet varies adiabatically.

11. The frequency spectrum band of the observed solitons (synchronous at lower frequency) is about 40 MHz wide though the total spectrum width is more than 200 MHz. There is a distinct difference in time between appearances of the wave bunches in various regions of the frequency spectrum; the lower-frequency oscillations appear at the distant high-frequency probe considerably later. For instance, at the probe which is at the distance of 100 cm from the plasma source the waves with the frequency 150 MHz appear by about 10 to 12 μs later than the waves with the frequency 200 MHz, about 20 μs later than the waves with the frequency 250 MHz, and so on [5.26]. This observation suggests cascade amplification of the waves in the plasma owing to collective processes of their scattering and decay [5.1, 5.2].

Thus, the study [5.26] for the first time revealed the slow (approximately standing with respect to plasma) long-lived oblique Langmuir solitons due to the modulational instability of the Trivelpiece-Gould waves. Further experimental and theoretical work is needed to compare their properties with theoretical predictions.

The oblique Langmuir soliton discussed here should be distinguished from the other soliton of the same wave branch described by eq. (5.15), which has an entirely different nature and generation mechanism. This soliton (*nonlinear solitary space-charge wave*), described by the Korteweg-de Vries (KdV) equation, exists under the conditions of (linear) dispersion of the waves described by eq. (5.15) as well as ion-acoustic waves or "shallow-water" waves. The KdV solitons are the propagating nonspreading pulses due to the equilibrium established between the nonlinear steepening of the wave front and its dispersive spreading [5.1, 5.2]. In contrast to the solitons due to the modulational instability, these solitons do not have high-frequency filling.

The speed of the KdV soliton depends on its amplitude. It is close by the order of magnitude to the phase velocity v_{ph} of the *linear* wave in that range of the wave numbers k in which the dependence of v_{ph} on k is the strongest, that is, at the maximum curvature of the dispersion dependence $\omega(k)$ [5.1, 5.2]. For instance, the speed of the ion-acoustic soliton is not much higher than the ion sound speed, and the speed of the Trivelpiece-Gould space-charge solitary wave is also not much higher than the characteristic "plasma-waveguide" velocity $v_{ph} \approx \omega_p a$, where a is the plasma column radius. The longitudinal soliton size also corresponds to the wave number in the region of the highest dispersion of the phase velocity [5.1, 5.2]. In particular, the space-charge KdV soliton in the magnetized plasma waveguide has the longitudinal size of the order of a; the space-charge solitons in radially restricted magnetized plasma column were observed in the experiments [5.32–35].

Table 5.1 compares the properties of two types of the Trivelpiece-Gould solitons, namely, the oblique Langmuir soliton and the KdV soliton formed by the space-charge wave. The velocity of the KdV soliton given in the table corresponds to the specific conditions of the experiments [5.26]. It can be seen from the table that the properties of these two types of solitons differ greatly.

TABLE 5.1

Soliton type	Speed relative to plasma	Structure	Mechanism of excitation
Oblique Langmuir ("slow") soliton [5.26]	$v \ll c_s$	Plasma density well with the Langmuir "filling"	Modulational instability
Trivelpiece–Gould space–charge soliton ("fast soliton") [see eq. (5.15)] [5.32–35]	$v \approx 10^3 c_s$	Without filling	KdV mechanism

Conclusion

The experimental results discussed in this review suggest that solitons are the most characteristic state of the strong Langmuir turbulence of the magnetized collisionless plasma. They are sufficiently stable and are not strongly affected by all numerous deviations from the perfect system geometry, which are unavoidable under real experimental conditions.

The solitons are produced owing to the modulational instability (self-compression) of large-amplitude electron waves. Their size decreases with increasing wave energy density. The minimal observed size of the Langmuir solitons is 5 to 6 Debye radiuses; this value, apparently, corresponds to the boundary of strong absorption by the plasma particles (the Landau damping, etc.).

When it was possible to compare the experimental results with theoretical predictions, we found a certain qualitative agreement. However, some problems were identified that definitely need further theoretical analysis, such as the following.

1. The detailed mechanism of the modulational instability with the modulation wave length shorter than the starting oscillation wavelength, $\lambda_M \lesssim \lambda$, that is, the phenomenon when the starting wave (or its half) is the soliton envelope (see Figs. 5.6–5.9).

2. The spatial structure and the frequency spectrum of the Langmuir soliton in the radially nonuniform plasma column.

3. The spatial structure, the frequency spectrum and the mechanism of formation of the "oblique Langmuir "soliton.

References

5.1. B. B. Kadomtsev, *Collective Phenomena in Plasmas,* Pergamon Press, Oxford, 1980.

5.2. a) L. A. Artsimovich, R. Z. Sagdeev, *Plasma Physics for Physicists,* Atomizdat, Moscow, 1979 (in Russian).
b) A. A. Galeev, R. Z. Sagdeev, *Nonlinear Theory of Plasma,* in "Questions in Plasma Theory", vol. 7, Atomizdat, Moscow, 1973 (in Russian).

5.3. A. C. Scott, F. Y. E. Chu, D. W. Mclaughlin, *Proc. IEEE,* **61**, 1443, 1973.

5.4. a) K. Rebbi, *Sci. Amer.,* **240**, 76, 1979.
b) *Solitons and Condensed Matter Physics* (Symposium proceedings), ed. A. R. Bishop, Springer, N.–Y., 1978.

5.5. V. I. Petviashvili, *ZhETF* Pis'ma, **32**, 632, 1980.

5.6. a) *Solitons in Physics* (Conf. proceedings), Phys. Scripta, **20**, Nos. 3, 4, 1979.
b) A. S. Davydov, *ibid,* p. 387.
c) A. C. Scott, *ibid,* p. 395.

5.7. N. Haken, *Synergetics: an Introduction,* Springer, Berlin, 1978.

5.8. *Sov.–Amer. Symposium on Soliton Theory,* Kiev, 1979; Physica, D, 1981, Special Issue.

5.9. D. J. Korteweg, G. de Vries, *Phil. Mag.,* **39**, 422, 1895.

5.10. G. A. Askaryan, *UFN,* **111**, 249, 1973.

5.11. R. J. Chiao, F. Gardmire, C. H. Townes, *Phys. Rev. Lett.,* **13**, 479, 1964.

5.12. A. A. Vedenov, E. P. Velikhov, R. Z. Sagdeev, *Nucl. Fusion,* **1**, 82, 1961.
5.13. A. A. Vedenov, L. I. Rudakov, *DAN SSSR*, **159**, 767, 1964.
5.14. V. E. Zakharov, *ZhETF*, **62**, 1745, 1972.
5.15. L. I. Rudakov, *DAN SSSR,* **207**, 821, 1972.
5.16. a) A. G. Litvak, V. A. Mironov, G. M. Fraiman, *ZhETF Pis'ma,* **22**, 368, 1975.
b) A. G. Litvak, V. I. Trakhtengerts, T. N. Fedoseeva, G. M. Fraiman, *ZhETF Pis'ma,* **20**, 544, 1974.
5.17. N. S. Buchelnikova, E. P. Matochkin, *Journ. de Phys.,* **40**, C-7, 621, 1979.
5.18. V. V. Gorev, A. S. Kingsep, L. I. Rudakov, *Izv. vuzov,* Radiofizika, **19**, 691, 1976.
5.19. L. I. Rudakov, V. N. Tsytovich, *Phys. Reports,* **40**, 1, 1978.
5.20. H. C. Kim, R. Stenzel, A. Y. Wong, *Phys. Rev. Lett.,* **33**, 886, 1974.
5.21. H. Ikezi, K. Nishikawa, K. Mima, *Journ. Phys. Soc. Japan,* **37**, 766, 1974.
5.22. A. Y. Wong. B. H. Qoun, *Phys. Rev. Lett.,* **34**, 1499, 1975.
5.23. H. Ikezi, R. P. H. Chang, R. A. Stern, *Phys. Rev. Lett.,* **36**, 1047, 1976.
5.24. S. V. Antipov, M. V. Nezlin, E. N. Snezhkin, A. S. Trubnikov, *ZhETF*, **74**, 965, 1978 (see also *ZhETF Pis'ma*, **23**, 613, 1976; **25**, 158, 1977).
5.25. S. V. Antipov, M. V. Nezlin, E. N. Snezhkin, A. S. Trubnikov, *ZhETF*, **76**, 1571, 1979.
5.26. S. V. Antipov, M. V. Nezlin, A. S. Trubnikov, *ZhETF*, **78**, 1743, 1980.
5.27. V. P. Pavlenko, V. I. Petviashvili, *Journ. de Phys.,* **40**, C-7, 621, 1979.
5.28. G. I. Morales, Y.C. Lee. *Phys. Fluids*, **19**, 690, 1976.
5.29. B. A. Al'terkop, A. S. Volokitin, V. P. Tarakanov, *DAN SSSR*, **234**, 806, 1977; *Fizika plazmy*, **3**, 59, 1977.
5.30. Yu. S. Sigov, Yu. V. Khodyrev, *DAN SSSR*, **229**, 833, 1976; Preprint IPM AN SSSR, No. 11, 1976.
5.31. T. A. Gorbushina, L. M. Degtyarev, R. Z. Sagdeev, V. D. Shapiro, V. I. Shevchenko, Preprint IPM AN SSSR No. 17, 1978.
5.32. H. Ikezi, P. J. Barrett, R. B. White, A. Y. Wong, *Phys. Fluids*, **14**, 1997, 1971.
5.33. S. M. Krivoruchko, Ya. B. Fainberg, V. D. Shapiro, V. I. Shevchenko, *ZhETF*, **67**, 2092, 1974.
5.34. V. D. Fedorchenko, Yu. P. Mazalov, A. S. Bakai, A. V. Pashchenko, B. N. Rutkevich, *ZhETF*, **70**, 1768, 1976.
5.35. J. P. Lynov, R. Michelsen, H. L. Pecseli, J. H. Rasmussen, K. Saeki, V. A. Turikov, *Phys. Scripta*, **20**, Nos. 3–4, 328, 1979.

6. Measurement of the Electron Temperature and the Plasma Density from Cyclotron Absorption in Open Traps

G. N. Chulkov, A. A. Skovoroda, Cand. Sc. (Phys. and Math), *A. V. Timofeev,* D. Sc. (Phys. and Math), *and V. A. Zhil'tsov*

Introduction

The plasma dynamics in open traps is to a considerable extent determined by the electron temperature T_e. For instance, T_e determines the potential to which the plasma is charged (the ambipolar potential); T_e determines also the time of cooling of the ions (typically, in open traps the mean energy of the ions is considerably higher than T_e).

Up till now the electron temperature in open traps was measured mainly from the Thomson scattering of the laser radiation. However, continuous determination of the spatial profile of T_e during one working cycle entails considerable technical difficulties. Moreover, such measurements are practically unfeasible in low-density plasmas ($n_0 < 10^{12}$ cm^{-3}). Estimates of T_e from the ambipolar potential are rather inaccurate and are, actually, just order-of-magnitudeestimates.

Multibeam microwave interferometry typically yields reliable results for the plasma density distribution n_0. But interferometric data require complicate mathematical treatment and the use of *a priori* assumptions on the form of the distribution.

Diagnostics based on the electron cyclotron resonance (ecr) often makes possible fast *local* measurements of n_0 and T_e. The most widely used diagnostic makes use of the absolute measurements of the radiation spectrum for the harmonics of the electron cyclotron frequency in tokamaks. When we record the "black" harmonics of the electron cyclotron radiation whose intensity is proportional to T_e, according to the Kirchoff's law, and the frequency corresponds to the position of the cyclotron resonance point in space, we, thus, measure continuously in space and time the electron temperature in tokamaks. Clearly, this method is applicable to the high-density plasma of open traps, too. We shall not discuss such methods in detail here since there is wide selection of literature on them (see, for instance [6.1]).

In this review we shall analyze the diagnostic methods based on measurements of the absorption coefficient for a probe beam of electromagnetic waves with the frequency ω close to the electron cyclotron frequency ω_e or its harmonics $n\omega_e$. In open traps the dependence of the magnetic field on the coordinates is fairly complicated (see Fig. 6.1) and this makes the calculations of the absorption coefficient η more

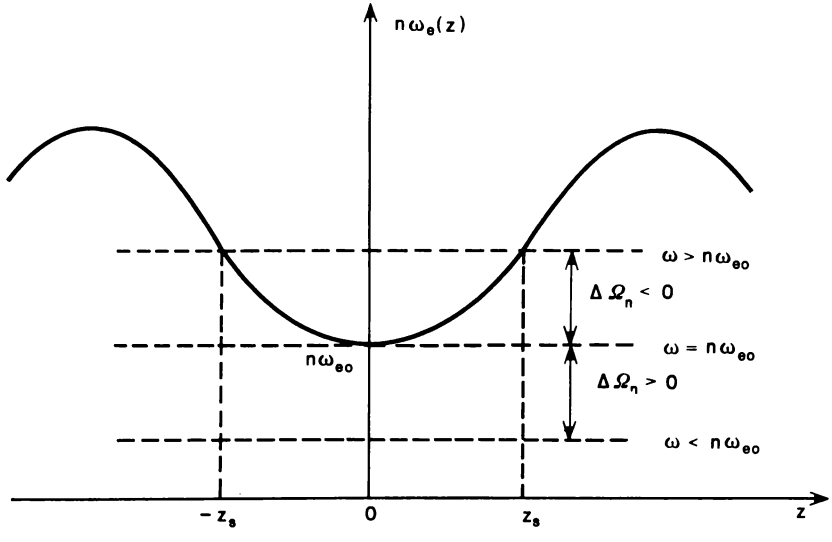

Fig. 6.1. The magnetic field as a function of the distance along the axis of the open magnetic trap. The condition $n\omega_e(z_s) = \omega$ determines the positions of the resonance points.

difficult. However, it is precisely this fact, as noted in [6.2], that makes the measurement of T_e relatively simple.

When we calculate the absorption coefficient for the cyclotron oscillations, we must bear in mind that the region of the resonance interaction in which electron's exchange energy with oscillations occupies just a small part of the trap. Electrons leave this region moving along the magnetic field. However, they retain a "memory" of the resonance interaction even after considerable displacement. This results in a nonlocal relationship between the electric current and the wave field producing it, so that the wave equation acquires the integral form. This is quite natural since this problem belongs to the class of problems on propagation of oscillations in nonuniform dispersing media. Such problems, typically, can be solved only with significant approximating assumptions. We shall assume that the absorption coefficient is small ($\eta \ll 1$). This assumption will allow us to calculate the absorption coefficient using the method of successive approximations assuming in the zero-order approximation that the electromagnetic oscillations do not exchange energy with electrons.

In the first section of this paper we shall calculate the absorption coefficient for the first harmonic of the electron cyclotron frequency when the wave propagates along the magnetic field of the open trap. We shall consider the oscillations with the frequency $\omega < \omega_{e0}$, where ω_{e0} is the minimum cyclotron frequency in the trap. This case illustrates the main physical features of ecr in open traps.

In the second section we shall calculate the absorption coefficient for the higher harmonics of the cyclotron frequency ($\omega \approx n\omega_{e0}$, $n \geq 2$) making more general assumptions on the direction of wave propagation and the relationship between ω and $n\omega_{e0}$.

In the third section we shall discuss various modifications of this diagnostic technique and some results of its experimental application.

Note that in this paper, though we are analyzing the ecr diagnostics for open traps, its modifications can be applicable to arbitrary systems with nonuniform magnetic field, including toroidal systems.

6.1. Resonance Absorption of Oscillations with $\omega \simeq \omega_e$

6.1.1. Resonance cyclotron interaction in nonuniform magnetic field

Let us analyze the resonance cyclotron interaction at an oscillation frequency close to ω_{e0}. Assume that in the vicinity of the magnetic field minimum the cyclotron frequency varies parabolically: $\omega_e(z) = \omega_{e0}(1 + z^2/L^2)$. Consider the oscillations propagating along the magnetic field. These oscillations have the most intense interaction with electrons and therefore these oscillations should be useful for diagnostics of a low-density plasma, where the absorption coefficient is, generally, small.

If the conditions $\omega - \omega_{e0} \gg \omega_{e0}(\varrho_e/L)^{2/3}$, where ϱ_e is the mean Larmor radius, is satisfied, then the absorption coefficient η is determined by the plasma density and by the derivative $d\omega_e/dz$ at the cyclotron resonance point [6.3] but it is independent of the electron temperature. In this case, as shown in [6.4], the kinetic effects due to thermal motion of electrons determine the fine structure of the resonance layer in which absorption occurs, rather than the absorption coefficient. This makes it possible to find the local density values from the absorption coefficient.

When $|\omega - \omega_{e0}| < \omega_{e0}(\varrho_e/L)^{2/3}$ the absorption coefficient must, apparently, depend on the temperature but an exact expression for it has not been derived yet owing to mathematical difficulties involved.

If the electrons were cold, there would be no resonance interaction for $\omega < \omega_{e0}$. When we take into account the thermal motion, the resonance condition has the form $\omega = \omega_e + k_\parallel v_\parallel$ due to the Doppler effect, where the subscript $\parallel$ denotes parallel orientation with respect to the main magnetic field. The resonance condition implies that the electrons that travel towards the wave must have the resonance interaction with it for $\omega < \omega_{e0}$.

In the frequency range $\omega < \omega_{e0}$ the absorption coefficient is proportional to the number of electrons with the resonance velocity $v_\parallel = (\omega_{e0} - \omega)/k_\parallel$. Hence, when we find the ecr line broadening in the frequency range $\omega < \omega_{e0}$, we can determine the electron temperature, and if the velocity distribution of electrons differs from the Maxwellian distribution, then we can determine the form of the velocity distribution, too.

With decreasing electron temperature and increasing difference $\omega_{e0} - \omega$ the so-called effect of finite time of the resonance interaction (eft) starts to manifest itself. This effect, as the Doppler effect, results in the broadening of the ecr line in the frequency range $\omega < \omega_{e0}$. The effect is due to the nonumiformity of the magnetic field, owing to which any individual electron is in resonance with the wave only for a finite time Δt which can be estimated from the condition

$$\Phi(\Delta t) = \int_0^{\Delta t} [\omega_e(z(t')) - \omega] dt' \sim 1 \tag{6.1}$$

Here $\Phi(\Delta t)$ is the phase difference between the Larmor electron rotation and the electromagnetic oscillations, where the moment when the electron passes the minimum of the magnetic field is taken as the starting moment; for the sake of simplicity the Doppler effect is ignored and the oscillations with $\omega < \omega_{e0}$ are taken into consideration. Assuming that the electron moves along $\mathbf{B}_0$ with constant velocity we can find the resonance interaction time $\Delta t \sim \omega_{e0}^{-1}(L/\varrho_e)^{2/3}$ from eq. (6.1). Owing to the uncertainty relation $\Delta\omega\Delta t \sim 1$ the electrons cannot distinguish between the oscillations the difference between whose frequencies is $\Delta\omega \leq (\Delta t)^{-1}$. Hence, the ecr lines must broaden up to the frequency $\omega < \omega_{e0}$ and the order-of-magnitude estimate of the characteristic eft broadening is $\omega_{e0}^{-1}(L/\varrho_e)^{2/3}$.

6.1.2. The absorption coefficient

The electric field of the oscillations propagating along the magnetic field $\mathbf{B}_0$ is perpendicular to the vector $\mathbf{B}_0$ and has a circular polarization, rotating in the same sense as electrons or ions. We shall deal with the oscillations of the first type, which alone can exchange energy with electrons. In the approximation of cold electrons the wave equation describing propagation of such oscillations has the form

$$\frac{d^2E_-}{dz^2} + \frac{\omega^2}{c^2}\left(1 + \frac{\omega_p^2}{\omega[\omega_e(z) - \omega]}\right)E_- = 0 \tag{6.2}$$

We employ here the right-handed Cartesian system of coordinates with the axis Oz parallel to the magnetic field. The quantity $E_- = E_x - iE_y$. The time dependence of the oscillations is written as $\exp(-i\omega t)$, so that for the electric vector rotating in the same direction as electrons we have $E_y = E_x i$. Since the wavelength of the cyclotron oscillations typically satisfies the condition $\lambda \ll L$, the dependence of the electric field of the oscillations on the coordinate z can be taken in the quasiclassical form:

$$E_-(z) = E(0)\left(\frac{k_0}{k(z)}\right)^{1/2} \exp\left\{i\int_0^z k(z')dz'\right\} \tag{6.3}$$

where

$$k(z) = \frac{\omega}{c}\left(1 + \frac{\omega_p^2}{\omega(\omega_e(t) - \omega)}\right)^{1/2}, \qquad k_0 = k(0)$$

Using the method of successive approximations, we can calculate the energy obtained by electrons from the electric field of a given form. The energy of an individual electron varies under the effect of oscillations according to the equation

$$\dot{e} = -\frac{e}{2}\,\mathrm{Re}(E_- v_-^*)$$

Here E_- is taken along the unperturbed trajectory of the electron and $v_- = v_x - iv_y$ is found from the unperturbed motion equation which yeilds

$$v_-(t) = v_-(0)\exp\left\{-i\int_0^t \omega_e(z(t'))dt'\right\}$$

When the electron passes the magnetic field minimum, where the cyclotron frequency is close to the frequency of the oscillations under considerations, the electric field vector and the vector of the transverse electron velocity rotate synchronously for some time. It is precisely this region that determines the variation of the electron energy:

$$\Delta\epsilon \approx -\frac{e}{2} v_\perp(0) E_-(0) J \exp(i\Phi_0)$$

$$J = \int_{-\omega}^{\omega} dt \exp\left\{i\Phi(t)\right\}$$

$$\Phi(t) = -\omega t + \int_0^t \omega_e(z(t'))dt' + v_\parallel \int_0^{z(t)} k(z(t'))dt'$$

Here Φ_0 is the phase difference at the moment when the electron passes the magnetic field minimum.

We shall assume that the phase Φ_0 varies randomly in successive passages. The phase randomization can be caused by the fact that the spectrum of the probe beam has the finite width $\delta\omega \gtrsim \omega_b$, where $\omega_b \sim v_\parallel/L'$ is the frequency of oscillations of electrons along the trap, and L' is the trap length. The phase randomization can also be the result of the Coulomb collisions, if their frequency ν is higher than $\omega_e(\rho_e/L)^3$, and of the nonlinear effects for $E_- \gtrsim (B_0 v/c)(\rho_e/L)^3$ (see [6.5]). Note that the conditions under which phase randomization occurs are usually satisfied.

If the phase variation in successive passages through the resonance is random, the energy variation Δe due to the resonance interaction also must be random. This will result in the energy diffusion of electrons with the diffusion coefficient $D = |\Delta e|^2 \omega_b$. The total energy absorbed per unit time by the electrons in the field tube with the unit cross-sectional area is

$$\dot{W} = -N_0 \int dv D \frac{\partial f_0}{\partial \epsilon} = n_0 \int dv |v_\parallel| \frac{1}{T_e} |\Delta\epsilon|^2 f_0 \qquad (6.4)$$

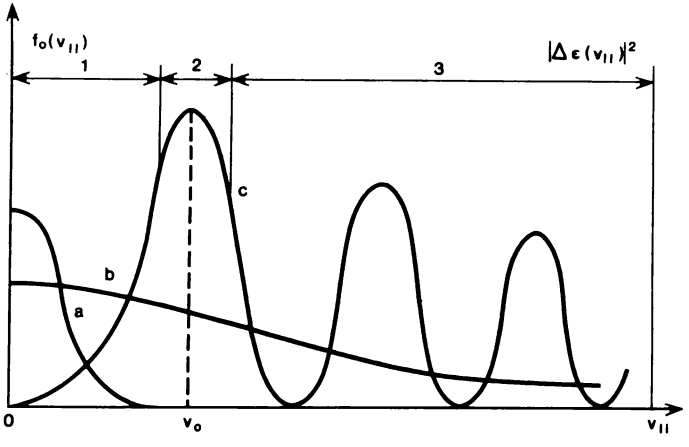

Fig. 6.2. The distribution function $f_0(v_\parallel)$ for low (curve *a*) and high (curve *b*) temperatures and the function $|\Delta\epsilon(v_\parallel)|^2 = (ev_\perp/2)^2|EJ|^2$ (curve *c*), where: region $1 - |y|^2 \approx 2\pi|\Phi_s|^{-1}\exp(-2|\Phi_s|)$; region $2 - |y|^2 \approx 2^{2/3}3^{-1/3}\Gamma^2(1/3)|\Phi_s|^{-2/3}$; region $3 - |y|^2 \approx 8\pi|\Phi_s|^{-1}\cos^2\left(\Phi_s + \frac{\pi}{4}\right)$; $\Phi_s = \Phi(t_s)$; $t_s = t(z_s)$.

where $N_0 = n_0 L'$ is the number of electrons in the given field tube, and f_0 is the Maxwellian distribution. The absorption coefficient is given by $\eta = \dot{W}/S$, where $S = c^2k|E_-|^2/4\pi\omega$ is the energy flux density of the oscillations.

The absorption coefficient and the character of its frequency dependence are significantly affected by the relationship between the thermal velocity of electrons v_T and the characteristic scale of variation of the function $|\Delta\epsilon(v_\parallel)|$ giving the increment of the electron energy due to a passage through the magnetic field minimum. A schematic of this function is shown in Fig. 6.2. The function has the absolute maximum for $|v_\parallel| = v_0 = (\omega_{c0} - \omega)/k_0$. In this case the resonance condition is satisfied at the magnetic field minimum and the electron is in resonance with the oscillations for the longest possible time $\Delta t \approx \omega_{c0}^{-1}(L/\varrho_e)^{2/3}$; see Sec. 6.1.1. For $|v_\parallel| > v_0$ there are two symmetric resonance points $z = \pm z_s$ found from the condition $\omega = \omega_c(z_s) - k_\parallel(z_s)|v|_\parallel$. Their contributions to $|\Delta\epsilon|$ can amplify or attenuate each other. This results in oscillations of $|\Delta\epsilon(v_\parallel)|$; see Fig. 6.2. When $\omega - \omega_{c0} \gg \omega_{c0}(\varrho_e/L)^{2/3}$, an order-of-magnitude estimate of the resonance interaction time is $\Delta t \approx \omega_{c0}^{-1}L/(z_s\rho_e)^{1/2}$. Finally, if $|v_\parallel| < v_0$, the resonance condition is not satisfied for any coordinate z, and the resonance interaction is due to the eft effect discussed above. Figure 6.1 illustrates the three cases we have analyzed. If we take into account the Doppler effect, we should plot $n\omega_c(z) - k_\parallel(z)/|v_\parallel|$ on the axis of ordinates.

The eft effect determines the broadening of the ecr line in the frequency range $\omega < \omega_{e0}$ at low T_e, when the number of electrons with $|v_\parallel| > v_0$ is low (see Fig. 6.2, curve *a*), while the Doppler effect determines broadening at high T_e, when the number of such electrons is high. In both limiting cases simple analytical expressions can be derived for the absorption coefficient. When the condition

$$v_T = (T_e/m_e)^{1/2} \ll c^{3/2}/(\omega L)^{1/2}(\Delta\Omega)^{3/2}/(\Delta\Omega + q)^{3/4}$$

where $\Delta\Omega = (\omega_{e0} - \omega)/\omega_{e0}$ and $q = (\omega_p/\omega_{e0})^2$, is satisfied, the integral (6.4) is determined by the region *1* in Fig. 6.2 and can be calculated exactly by using the saddle-point method:

$$\eta \approx \frac{\pi}{2 \cdot 3^{1/2}} q \frac{\omega L}{c} \frac{1}{(\Delta\Omega + q)^{1/2}} \exp\left\{ - 12^{1/3} \left(\frac{\omega L}{c_T} \right)^{2/3} \Delta\Omega \right\} \tag{6.5}$$

Equation (6.5) implies that the cyclotron absorption line is broadened in the frequency range ω/ω_{e0} exponentially and the characteristic broadening value is proportional to $T_e^{1/3}$.

If we have

$$v_T \gg c^{3/2}/(\omega L)^{1/2}(\Delta\Omega)^{3/2}/(\Delta\Omega + q)^{3/4}$$

$$c^{5/3}/(\omega L)^{2/3}(\Delta\Omega)^{3/2}/(\Delta\Omega + q)^{2/3}$$

a considerable number of electrons have the velocity $|v_\parallel| > v_0$ and the scale of variation of $f_0(v_\parallel)$ is significantly greater than the period of oscillations of $|\Delta\epsilon(v_\parallel)|^2$ (see Fig. 6.2, curve *b*). Under such conditions we can calculate the absorption coefficient by averaging $|\Delta\epsilon|^2$ over the rapid oscillations using the expression $|\Delta\epsilon|^2 \approx \pi e^2 v_\perp^2 |E_-|^2 (d^2\Phi/dt^2)|^{-1} \theta(|v_\parallel| - v_0)$, where $\theta(x)$ is a step function defined as

$$\theta(x) = \begin{cases} 1 \text{ for } x > 0 \\ 0 \text{ for } x < 0 \end{cases}$$

and $d^2\Phi/dt^2$ is calculated for the point $t = t(z_s(v_\parallel))$. Then we obtain

$$\eta \simeq \frac{\pi}{2} q \frac{\omega L}{c} \left(\frac{2\Delta\Omega + 3q}{\Delta\Omega + 2q} \right)^{1/2} \exp\left\{ - \left(\frac{c}{v_T} \right)^2 \frac{(\Delta\Omega)^3}{\Delta\Omega + q} \right\} \tag{6.6}$$

Note that the absorption coefficient (6.6) is proportional to the number of electrons for which the cyclotron resonance condition is satisfied at the magnetic field minimum: $\eta \sim f_0(v_0) \propto \exp\left[- (v_0/v_T)^2 \right]$, where $v_0 = \Delta\Omega/k_0\omega$, and $k_0 = (\omega/c)(1 + q/\Delta\Omega)^{1/2}$.

The detaining $\Delta\Omega$ enters into eqs. (6.5) and (6.6). Therefore, at small $\Delta\Omega$ values the absorption coefficient η can prove to be given by eq. (6.6) and for large $\Delta\Omega$ values, by eq. (6.5).

The adiabatic traps do not confine electrons with sufficiently high longitudinal velocity, so that the tail of the distribution is cut off at $|v_\parallel| = v_1 = (2e\varphi_0/m_e)^{1/2}$, where φ_0 is the ambipolar potential. The lack of electrons with $|v_\parallel| > v_1$

manifests itself at high electron temperatures if $\nu_1 < \nu_0$ and at low electron temperatures if $\nu_1 < (2/3)^{1/3}(\omega L)^{1/3}\nu_T^{2/3}(\Delta\Omega)^{1/2}$. In both cases the following approximate expression must be used for the absorption coefficient:

$$\eta \approx \frac{3\pi^{1/2}}{4} q \frac{\nu_1^2}{c\nu_T} \frac{1}{(\Delta\Omega)^{3/2}(\Delta\Omega + q)^{1/2}} \exp\left\{ -\left(\frac{\nu_1}{\nu_T}\right)^2 - \frac{4}{3}\frac{\omega L}{\nu_1}(\Delta\Omega)^{3/2} \right\} \tag{6.7}$$

6.2. Resonance Absorption of Oscillations with $\omega \simeq n\omega_{e0} (n \gtrsim 2)$

The intensity of the interaction between electrons and the oscillations discussed in Sec. 6.1 ($\omega \approx \omega_e$, $\theta = \mathrm{kB}_0 = 0$) is very high. For the higher harmonics of the electron cyclotron frequency the intensity of the resonance interaction is sharply reduced. In particular, this is manifested by the fact that even cold electrons absorb the oscillations with $n = 1$, $\theta = 0$ if the resonance conditions $\omega = n\omega_e$ is satisfied, while absorption for the higher harmonics of the cyclotron frequency is due to the effects related to the finite Larmor radius of electrons ($\eta \lesssim (k_\perp \varrho_e)^{2(n-1)}$, where $k_\perp$ is the component of $\mathbf{k}$ normal to $\mathbf{B}_0$; see, for instance, [6.6]). Therefore, the oscillations of the first type are more convenient for diagnostics of cold low-density plasma. But the absorption coefficient increases with the density and reaches the maximum $\eta = 1$ for $\omega_p^2 L/\omega c \gg 1$ (even if $T_e = 0$). The absorption coefficient differs from unity only for very large detuning $\Delta\Omega$ when the resonance interaction is due to the far tail of the energy distribution of electrons. Thus, we see that higher harmonics of the electron cyclotron frequency should be used for diagnostics of high-density plasma.

The wave vector of the oscillations with $\omega \approx n\omega_e$ ($n \geq 2$) practically does not vary within the resonance region ($E \sim \exp(-i\omega t + i\mathbf{k}\cdot\mathbf{r})$). This fact facilitates the calculation of the energy absorbed by electrons.

As it was done in Sec. 6.1, we shall assume that the absorption coefficient is small. It can be given by the following self-evident expression (compare with eq. (6.5)):

$$\eta = \frac{2\pi}{P} \int_{-\infty}^{\infty} dz \int_0^{\infty} d\varrho\, \varrho \exp\left(-\frac{\varrho^2}{a^2}\right) \mathrm{Re}(E^* j) \tag{6.8}$$

We employ here the same coordinate system as in Sec. 6.1; the axis Ox lies in the plane of the vectors $\mathbf{k}$ and $\mathbf{B}_0$ and $\varrho = (x^2 + y^2)^{1/2}$. The finite transverse dimensions of the probe beam are taken into account. For $\theta \neq 0$ this leads to the dependence of the oscillation amplitude on the coordinates ϱ and z. The dependence on the coordinate ϱ is included in a model form ($|E| \propto \exp(-(\varrho/a)^2)$, where E is the maximum amplitude in eq. (6.8)). The dependence on the coordinate z becomes insignificant if the beam size along the axis Oz is considerably greater than the size of the resonance zone ($\tan\theta L^{2/3}\varrho_e^{1/3} \ll a$). We shall assume that this condition is satisfied. The total flux

of energy in the beam is $P = a^2c^2kG|E_y|^2/8\omega$, where $G = (1 + \alpha_x^2)\cos\theta - \alpha_x\alpha_z\sin\theta$ and $\alpha_{x,z} = E_{x,y}/E_y$ (see [6.6]).

In the min-B traps, which are principally employed in thermonuclear research, the magnetic field increases in all directions from the centre. We shall assume that in the vicinity of the minimum $B_0(\mathbf{r})$ the field $B_0(\mathbf{r}) = B_0(1 + (z/L)^2 + (\varrho/L_1)^2)$. The electric current j due to the probe wave can be calculated by the well-known method of integration along trajectories, taking into account not more than one passage through the magnetic field minimum. This approach is valid if the phase of the cyclotron rotation is randomized during one oscillation of the electron between the magnetic mirrors of the trap (see Sec. 6.1). The velocity distribution of electrons is assumed to have the Maxwellian form.

Equation (6.8) takes into account not only the Doppler and eft effects (see Sec. 6.1) but also the relativistic dependence of the cyclotron frequency on the electron energy ($\omega_e(v) \approx \omega_e(1 - v^2/2c^2)$), as well as the effect of the finite dimensions (fde) of the probe beam and collisions*. We have included the contribution of only one nth resonance. If the width of the cyclotron absorption line exceeds the distance between the neighbouring resonances, we must sum over n in eq. (6.8). It should be remembered that we derived eq. (6.8) assuming that the absorption coefficient is small, $\eta \ll 1$. Owing to the relative "weakness" of the resonance interaction for the higher harmonics of the cyclotron frequency the condition $\eta \ll 1$ is satisfied not only for $\omega < n\omega_{e0}$ but also for $\omega \geq n\omega_{e0}$. Therefore, in contrast to the equations of Sec. 6.1, eq. (6.8) allows us to treat the entire cyclotron absorption line and not just its tail.

Broadening of the cyclotron absorption line in the frequency range $\omega < n\omega_{e0}$ ($\Delta\Omega_n = (n\omega_{e0} - \omega)/n\omega_{e0} > 0$) is determined by one of the above effects. The characteristic broadening values are as follows: Doppler effect—$\delta\Omega_n^D \sim \varkappa_z = k_z\rho_e/n$; eft—$\delta\Omega_n^{eft} \sim \lambda^{-1} = (12L^2n^2/\rho_c^2)^{-1/3}$; relativistic effect—$\delta\Omega_n^o \sim \beta^2 = (v_T/c)^2$; and collisions—$\delta\Omega_n^c \sim \nu/(n\omega_{e0})$. The first expression follows from the results of Sec. 6.1 and other expressions are self-evident.

Let us analyze how these effects influence the shape of the cyclotron absorption line in the frequency range $\omega \leq n\omega_{e0}$.

First, assume that the *Doppler effect* plays the decisive part (the characteristic broadening due to the Doppler effect is greater than all other types of broadening). Then we have

$$\eta_n(\Delta\Omega_n) \approx \frac{1}{2^{1/2}}\gamma_n(\Delta\Omega_n)(A - \tan\theta\Delta\Omega_n)^2 \exp\left\{-\left(\frac{\Delta\Omega_n}{\varkappa_z}\right)^2\right\} \tag{6.9}$$

where $A = (\alpha_x - 1)/\alpha_z$, $\gamma_n(\xi) = \pi\omega_p^2L\alpha_z^2/2cNG\omega_{e0}\xi^{1/2}I_{n-1}(\mu)$, $\mu = (k_\perp\rho_e)^2/2$, I_n is the Bessel function of the imaginary argument, and N is the index of refraction.

---

* In the case of longitudinal propagation of electromagnetic waves these effects are negligibly small in comparison with the Doppler effect.

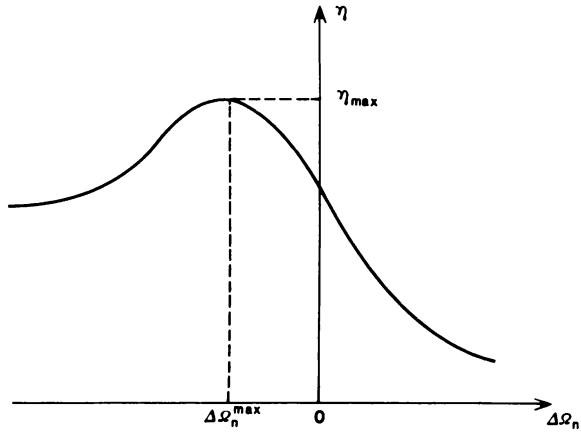

Fig. 6.3. The absorption coefficient as a function of $\Delta\Omega_n$.

As it should be expected, the Doppler effect results in the Gaussian broadening of the absorption line.

Equation (6.8) makes it possible to determine the position of the maximum of the absorption coefficient, so that we can measure the magnetic field at the centre of the trap (see below). Calculations give the following maximum of the absorption coefficient:

$$\eta_{n,\,\max} \approx 1.2\gamma_n(x_s)A^2$$

This value is reached when

$$\Delta\Omega_n \approx -\frac{\pi}{2^{1/2}}x_s$$

Figure 6.3 presents the absorption coefficient as a function of $\Delta\Omega_n$.

Note that other effects discussed above (eft, relativistic, collisional) do not change the general character of the function $\eta_n(\Delta\Omega_n)$.

Now let us discuss the influence of the *eft effect* and simultaneously take into account finiteness of the transverse dimension of the probe beam. Assuming that $x_s\lambda \ll 1$ (so that $l = \lambda(a/L_1)^2 \gg 1$), we obtain from eq. (6.8)

$$\eta_n(\Delta\Omega_n) \approx \frac{1}{6^{1/2}}\gamma_n(\Delta\Omega_n)\frac{A^2}{1+l}\exp\{-\Delta\Omega_n\lambda\} \tag{6.10}$$

Equations (6.5) and (6.10) indicate that if broadening is due to the eft effect, the main exponential factor in the expression for $\eta_n(\Delta\Omega_n)$ remains the same irrespective of the number of the harmonic and the direction of propagation of the vibrations.

The absorption coefficient has the maximum for

$$\Delta\Omega_n \approx -0.85(a/L_1)^2 \tag{6.11}$$

which is

$$\eta_{n,\max} \approx 0.54\gamma_n(l/\lambda)A^2$$

Equation (6.11) shows that the maximum of the absorption line is shifted towards higher frequencies with increasing transverse dimension of the beam. This is quite natural since the minimum cyclotron frequency along the beam trajectory averaged over the beam cross section increases with increasing a.

If the frequency of *collisions* is low, as is typical for the thermonuclear plasma, they determine only the far tail of the ecr line, which is described by

$$\eta_n(\Delta\Omega_n) \approx \gamma_n\left\{\left[\left(\frac{\nu}{n\omega_{c0}}\right)^2 + (\Delta\Omega_n)^2\right]^{1/2}\right\} A^2 \times \cos\left(\frac{1}{2}\arctan\left(\frac{n\omega_{c0}}{\nu}\Delta\Omega_n\right) + \frac{\pi}{4}\right) \tag{6.12}$$

For $\Delta\Omega_n \gg \nu/n\omega_{c0}$ eq. (6.12) yields the Lorentz line broadening which is typical for collisional broadening.

The *relativistic effects* have a decisive influence when $\theta \to \pi/2$. If the conditions $\varkappa_z \ll \beta^2$, $b = \lambda\beta^2/2 \gg 1$, and $\Delta\Omega_n \gg \beta^2(1 + n/2)$ are satisfied, the absorption coefficient is

$$\eta_n(\Delta\Omega_n) \approx \frac{1}{2^{1/2}}\gamma_n(\beta^2)\, A^2\left(\frac{2\Delta\Omega_n/\beta^2 + l_1}{n + 3/2}\right)^{n+1} \times (2\Delta\Omega_n/\beta^2 + l_1 - (n + 3/2))^{1/2} \exp(-2\Delta\Omega_n/\beta^2) \tag{6.13}$$

where $l_1 = l/b = 2a^2/L_1^2\beta^2$.

As we can see from eq. (6.8), the maximum of tne absorption coefficient is obtained for

$$\Delta\Omega_n \approx 2\beta^2\left[n + \frac{3}{2} - l_1 - \frac{\pi}{4}\left(n + \frac{3}{2}\right)^{1/2}\right]$$

and is equal to

$$\eta_{n,\max} \approx \gamma_n\left[2\beta^2\left(n + \frac{3}{2}\right)^{1/2}\right] A^2$$

The relative width of the absorption line in the vicinity of the maximum is

$$\Delta\Omega_n \approx \beta^2(n + 3/2)^{1/2}$$

In contrast to the effect of the finite beam dimension [see eq. (6.11)], the relativistic effects shift the position of the maximum $\eta_{n,\max}$ towards lower frequencies owing to relativistic decrease in the cyclotron frequency.

Note that we have analyzed eq. (6.8) assuming that $|A| \gg \varkappa_\perp$. This condition is satisfied for the extraordinary wave but can be violated for the ordinary wave if

$\theta \to \pi/2$. Then the order of smallness of the absorption coefficient in the parameter $\mu = (k_\perp \varrho_*)^2/2$ increases.

To summarize, note that, generally, the ecr line profile is shaped by all the above effects: the line centre is determined by the Doppler effect (Gaussian profile), the slope is determined by the eft and relativistic effects (exponential profile) and the tail is determined by the collisional effects (Lorentz profile).

The line maximum can be shifted with respect to $n\omega_{c0}$ by $\delta\omega$ which is of the order of the characteristic broadening scale. Note that the effect of the finiteness of the beam dimension does not change the ecr line shape but can result in a shift of its centre [see eq. (6.11)].

We have also analyzed eq. (6.8) for large negative values of $\Delta\Omega_n$ when the approximation of the linearly varying magnetic field ($|\nabla \widehat{B_0/B_0}|^{-1} = L_2$ for $r = r_s$) is applicable (see Fig. 6.1). A convenient approach is to rotate the coordinate system used above about the axis Oz so that the vector ∇B_0 lies in the plane xOz. In this case, as noted in Sec. 1 (see also [6.4]), the absorption coefficient value does not depend on which of the kinetic effects (Doppler, relativistic, etc.) determines the resonance cyclotron interaction with individual electrons, and we have

$$\eta_n = \frac{\pi}{2} \frac{\omega_p^2 L_2 n}{\omega c N G_1} \alpha_z^2 \left[A^2 I_{n-1}(\mu) + \frac{2}{n} I_n(\mu) \right] \tag{6.14}$$

Here $G_1 = B(N^2 - 1 - q)/N_\perp^2 N_z^2$, where $B = (N_\perp^2 + N^2 + 2q - 3) \sin\theta \cos\varphi \sin\psi + (N_\perp^2 - q + 2) \cos\theta \cos\psi$, $\psi = \widehat{B_0 \nabla B_0}$, and $\varphi = \widehat{k_\perp (\nabla B_0)_\perp}$ (see [6.7]).

Note that for longitudinal propagation of the wave and $n = 1$ (see [6.3]) the absorption coefficient coincides with that found from eq. (6.14).

6.3. Diagnostic Techniques Based on the ECR

6.3.1 Determination of the ecr line profile in the vicinity of the extremums of the cyclotron frequency

The profile of the ecr line is given by the expressions derived in Secs. 6.1 and 6.2. We can find the *absolute* T_e from the *relative* measurements of the line profile by analyzing the frequency dependence of the exponential functions in these expressions. This fact significantly facilitates measurement since it eliminates the need for indirect absolute calibration (for instance, by the Thomson light scattering of the blackbody radiation). Moreover, the line profile measurements themselves can be used for calibration of the absolute measurements of the electron cyclotron radiation. The ecr line profile can be obtained both by a passive method from the electron cyclotron radiation data and by the active method from the measurements of attenuation of the probe beam in plasma. The choice of the harmonic number and the angles of observation (probing) depends on the specific experimental conditions.

Note that if the energy distribution of electrons is anisotropic ($T_{e\perp} \neq T_{e\parallel}$), then these diagnostic techniques allow us to find the magnitude of anisotropy. Indeed, the temperature found from the ecr line profile corresponds to the Maxwellian longitudinal energy distribution and the temperature found from the absolute measurements of the electron cyclotron radiation corresponds to the transverse energy distribution.

The longitudinal energy distribution of electrons can also be determined from the ecr line profile. Such measurements yield the plasma potential in open traps. Indeed, the electrons with the energies exceeding the plasma potential do not make a contribution to the distribution function and this fact must affect the line profile [see eq. (6.7)].

We have assumed in the above discussion that the frequency of the oscillations used for diagnostics is close to $n\omega_{e0}$. However, the same information can be obtained from the measurements of the absorption coefficient for the waves whose frequency is close to the maximum cyclotron frequency. It should be remembered that the magnetic field in open traps has local maximums in the regions of the magnetic mirrors.

In conclusion, note that practically for any installation with a nonuniform magnetic field we can identify a direction of probing in which there is an extremum of the magnetic field. This is true, in particular, for tokamaks.

6.3.2 Measurements of the position of the absorption coefficient maximum

As shown by the above calculations, the absorption maximum occurs at the frequencies $\omega \approx n\omega_{e0}$ (see Sec. 6.2). When we find its position, we can find the magnetic field at the centre of the plasma to a high accuracy. Such measurements are needed in the experiments with high-pressure plasmas, when the magnetic field in the plasma differs considerably from the field in vacuum. The results can yield information on the diamagnetic properties of the plasma.

6.3.3 Measurements of the absorption coefficient at the frequencies $\omega > \omega_{e0}$

By measuring the absorption of the probe beam with $\omega > \omega_{e0}$ we can make local measurements of the temperature and density of electrons. The best way to find the plasma density is to use the first harmonic and longitudinal probing since under such conditions the absorption coefficient is independent of the temperature (see [6.3]). In high-density plasmas total absorption on the first harmonic occurs, and the higher ecr harmonics should be used for diagnostics. The absorption coefficient for such oscillations is proportional to $n_0 T^x$ [see eq. (6.13)], where the exponent depends on the harmonic number of and the type of the waves employed in diagnostics. Various modifications of this diagnostic method involve simultaneous use of the ordinary and extraordinary waves, several harmonics or several directions of probing.

6.3.4. Experimental applications

The physical concepts of the above diagnostic methods have been experimentally verified in weakly ionized low-density gas-discharge plasma with $n_0 < 10^{11}$ cm^{-3}. The equations for the absorption coefficient derived in [6.3] for the resonance in a linearly varying magnetic field ($\omega = \omega_*$, $\theta = 0$) have been verified in [6.8]. The authors of [6.2] have measured the plasma temperature in various gas discharges with magnetic field geometry similar to the fields in the open traps. The temperature has been determined from the ecr line profile and compared with the data obtained by other methods.

The ecr diagnostics was most widely used in the experiments with the min-B open trap Ogra-3B [6.9, 6.10]. The installation had the following parameters: a superconducting magnetic coil of the "baseball" type produced the minimum field 2 T with the mirror ratio 2.06 and the distance between the mirrors of 69 cm; the injector of neutral hydrogen atoms with the energy 20 keV, the current 0.5 A and the injection time 1-3s produced plasma with the density of up to 2×10^{10}cm^{-3} and the electron temperature of up to 300 eV. Owing to low plasma density probing along the trap axis with the first harmonic of the cyclotron frequency was used. Figure 6.4 illustrates the process of accumulation of the electron density during injection as measured by ecr absorption. Figure 6.5 shows the distribution of electrons over the longitudinal energies found from the ecr line profile which was determined by the Doppler effect. The experiment revealed an anomalous ambipolar potential ($\varphi \approx 10T_e$), so that the energy distribution of electrons had the Maxwellian form up

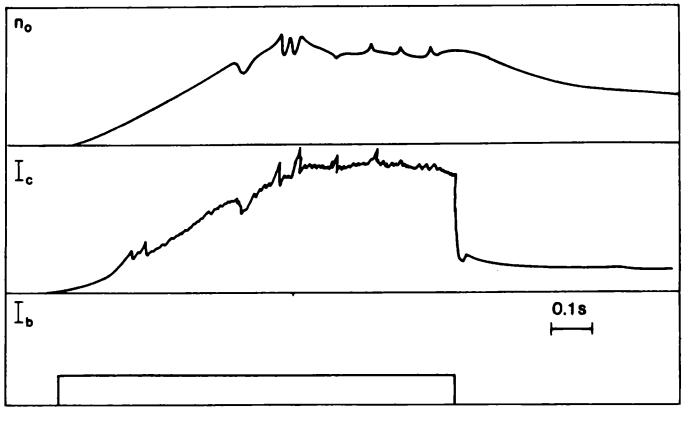

Fig. 6.4. The process of plasma accumulation in Ogra-3B: n_0 is the electron density measured by the ecr technique; I_c is the flux of the cold charge-exchange ions from the trap, and I_b is the injection beam current.

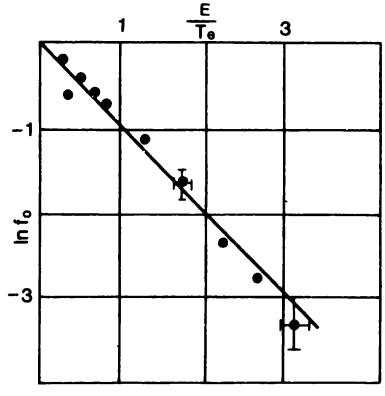

Fig. 6.5. Distribution of electrons over the longitudinal energy ϵ.

to the energies which were considerably higher than the sensitivity limits of the instruments used in the experiments.

The applicability of the ecr diagnostic method can be illustrated by the brief list of results obtained in the Ogra-3B experiments:

1) continuous measurements of the plasma density profile along the trap axis made it possible to determine the ion velocity distribution over angles, to find the longitudinal plasma size and its variation, to analyze the dynamics of accumulation and decay of plasma, and to measure the lifetime, the vacuum conditions in the installation, and the local spectra of oscillations of the plasma density;

2) continuous measurements of T_e gave information on the dynamics of heating and cooling of electrons, on the mutual effect of the cyclotron instabilities on the electron temperature, and on the energy distribution of electrons;

3) the position of the absorption maximum corresponded to the minimum of the magnetic field.

References

6.1. J. Hosea, V. Arunasalam, R. Cano, *Phys. Rev. Lett.*, **39**, 408, 1977; I. H. Hutchinson, D. S. Komm, *Nucl. Fusion*, **17**, 1077, 1977; D. K. Akulina, Yu. V. Knol'nov, *Fizika plasmy*, **4**, 1015, 1978; R. Cano, A. A. Bagdasarov, A. B. Berlizon, E. P. Gorbunov, G. E. Notkin, *Nucl. Fusion*, **19**, 1415, 1979.

6.2. A. A. Skovoroda, A. V. Timofeev, B. N. Shvilkin, *ZhETF*, **73**, 526, 1977.

6.3. K. G. Budden, *Radio Waves in the Ionosphere*, Cambridge Univ. Press, Cambridge, 1961.

6.4. A. V. Timofeev, A. K. Nekrasov, *Nucl. Fusion*, **10**, 337, 1970.

6.5. A. V. Timofeev, *Fizika plasmy*, **1**, 88, 1975.

6.6. A. I. Akhiezer, I. A. Akhiezer, R. V. Polovin, A. G. Sitenko, K. N. Stepanov, *Plasma Electrodynamics*, Nauka, Moscow, 1974, Chapter 5 (in Russian).

6.7. A. V. Timofeev, G. N. Chulkov, *Fizika plasmy*, **5**, 1271, 1979.
6.8. A. A. Skovoroda, B. N. Shvilkin, *ZhETF*, **70**, 1779, 1976.
6.9. A. A. Skovoroda, V. A. Zhiltsov, *J. de Physique*, **40**, C 7-665, 1979.
6.10 V. A. Zhiltsov, P. M. Kosarev, V. Kh. Likhtenstein, D. A. Panov, A. A. Skovoroda, A. G. Scherbakov, *Plasma Phys. and Contr. Nucl. Fusion Res.*, IAEA, Vienna, 1979, vol. 2, p. 469; V. A. Zhiltsov, P. M. Kosarev, D. A. Panov, A. A. Skovoroda, A. G. Scherbakov, *9th European Conf. on Contr. Fusion and Plasma Physics*, Oxford, 1979, p.40.

Plasma Physics
Ed. by B. Kadomtsev, Mem. USSR Acad. Sc.

This collection contains articles both original and already published in the Soviet Union in 1979-80, written by well-known Soviet scientists and devoted to the most important findings and achievements of research into the fundamental problems of plasma physics and controlled thermonuclear synthesis. The book is intended for researchers and specialists in the fields of plasma physics and thermonuclear reactions, and for anyone interested in the achievements of the Soviet Union in these areas.

Mir Publishers